



A University of Sussex PhD thesis

Available online via Sussex Research Online:

<http://sro.sussex.ac.uk/>

This thesis is protected by copyright which belongs to the author.

This thesis cannot be reproduced or quoted extensively from without first obtaining permission in writing from the Author

The content must not be changed in any way or sold commercially in any format or medium without the formal permission of the Author

When referring to this work, full bibliographic details including the author, title, awarding institution and date of the thesis must be given

Please visit Sussex Research Online for more information and further details

**Metabolic dysfunction and impairments in
the DNA Damage Response: dissecting a
pathomechanistic link between
Microcephalic Primordial Dwarfisms and
cancer cachexia**

Annie Macpherson

*A thesis submitted to the University of Sussex for the degree of Doctor
of Philosophy (DPhil)*

August 2017

DECLARATION

I hereby declare that this thesis has not been and will not be submitted in whole or in part to another University for the award of any other degree.

Signed

Annie Macpherson

ACKNOWLEDGEMENTS

Professor Mark O'Driscoll has been the driving force behind my academic development. I am filled with gratitude, for the time and energy he has invested is above and beyond what I could ever have expected from a supervisor. Thank you for your limitless support and enduring enthusiasm, for the development of both this project and myself.

To be superfluous (as is convention in a thesis acknowledgements), I am in fact incredibly grateful to everyone, and everything, that has influenced my growth and development. To all, past and present, that have taught, guided, counselled and empowered me; to those that have embraced me and helped me choose the right path. I never could have made it this far without so much positive influence.

This thesis is dedicated to my Mum and my Dad, and to my partner through it all, Tom.

University of Sussex

Annie Macpherson

DPhil Genome Stability

**Metabolic dysfunction and impairments in the DNA
Damage Response: dissecting a pathomechanistic
link between Microcephalic Primordial Dwarfisms
and cancer cachexia**

SUMMARY

ATR (ataxia telangiectasia and Rad3-related) encodes master regulator of the DNA damage response ATR. Hypomorphic mutations in *ATR* result in microcephalic primordial dwarfism disorder Seckel Syndrome (SS). *ATR*-SS also presents with an apparent lack of subcutaneous fat. This potentially suggests *ATR* deficiency impairs lipogenic function. This is concerning considering the proposed use of small molecule kinase inhibitors of *ATR* (ATRi) as cancer chemotherapeutics. ATRi is a highly selective anti-cancer agent due to synthetic lethality in ATM- or p53-deficient cells. An invariant feature of cancer is metabolic dysregulation, aggressive cancers can enforce systemic metabolic reprogramming resulting in drastic weight loss. Several screens have identified putative substrates for *ATR* in insulin signalling and metabolic pathways, indicating uncharacterised roles for *ATR* may exist here. Using several clinically relevant ATRi, I dissected the metabolic consequences of impaired *ATR* functionality on adipogenesis and lipogenic function of the 3T3-L1 cell line - widely utilised to investigate adipogenic differentiation. Acute ATRi treatment attenuated transcription of key adipogenic factors in differentiating preadipocytes, resulting in a failure to complete adipogenesis. I treated mature adipocytes chronically with ATRi, observing a striking transdifferentiation process known as browning – fat-storing white adipocytes underwent transcriptional reprogramming towards a thermogenic, brown adipocyte-like status. *ATR* deficiency generated this phenomenon by impinging on multiple pathways associated with metabolic regulation. I also observed striking cytoplasmic vacuolation and a disrupted autophagy response in every cell line treated with ATRi. I discovered *ATR* at the ER membrane, where ATRi-induced vacuolisation was derived from swollen endoplasmic reticulum (ER) concomitant with ER stress. I have characterised novel effects of *ATR* deficiency in adipocyte differentiation and metabolism, and ER and autophagic functionality. Autophagy and lipid metabolism are consistently deregulated in cancers, suggesting these results could lead to the generation of novel synthetic lethality approaches utilising ATRi and compounds targeting metabolic or autophagic pathways.

CONTENTS

CHAPTER ONE.....	1
1.1. The DNA Damage Response (DDR).....	2
1.2. The PIKK family.....	3
1.3. DNA damage recognition and ATR activation.....	7
1.3.1. ATRIP.....	8
1.3.2. Replication protein A (RPA).....	8
1.3.3. RAD9-HUS1-RAD1 complex.....	9
1.3.4. TOPBP1.....	9
1.3.5. MRE11-RAD50-NBS1 (MRN) complex.....	11
1.4. ATR downstream signalling.....	11
1.4.1. CHK1.....	11
1.4.2. MLL (Myeloid/Lymphoid Leukaemia 1).....	12
1.4.3. MCM2.....	13
1.4.4. dNTP synthesis.....	13
1.5. Modulators of ATR activity.....	13
1.5.1. TEL2.....	13
1.5.2. Fanconi Anemia group M/FA-associated protein 24 (FANCM/FAAP24).....	14
1.5.3. ATM and TOPBP1.....	14
1.5.4. mTOR signalling axis.....	15
1.6. ATR protein structure.....	16
1.6.1. HEAT repeats.....	16
1.6.2. FAT and FATC.....	18
1.6.3. PRD (PIKK regulatory domain) and PI3K domain.....	18
1.6.4. BH3-like domains.....	18
1.7. Putative ATR/ATM substrate screens.....	19
1.7.1. Matsuoka et al.....	19
1.7.2. Stokes et al.....	20
1.7.3. Cara et al.....	21
1.8. Established non-canonical activation of ATR.....	21
1.8.1. VAMP2.....	21
1.8.2. Cell metabolism - Mitochondria and Autophagy.....	22
1.8.3. Viral genome replication.....	23
1.8.4. Primary cilia.....	24
1.8.5. ATM.....	24
1.9. Disorders of ATM and ATR.....	25
1.9.1. Ataxia Telangiectasia (AT).....	25
1.9.2. Seckel Syndrome.....	26
1.10. Mouse models of ATR deficiency.....	30
1.10.1. Atr ^{-/-} mouse.....	30
1.10.2. Inducible Atr deletion mouse.....	30
1.10.3. Humanised ATR ^{S/S} mouse.....	32
1.10.4. p53 ^{-/-} /ATR ^{S/S} mouse.....	33
1.10.5. p53 ^{-/-} /Atr ^{mKO} mouse.....	33
1.11. Cancer and the DDR.....	34
1.11.1. Oncogenes.....	34
1.11.2. ATR haploinsufficiency.....	35

1.11.3. Synthetic lethality.....	36
1.11.4. Development of ATR inhibitors (ATRIs) and ATRi Clinical trials.....	38
1.11.4.1. Vertex Pharmaceuticals	39
1.11.4.2. AstraZeneca.....	40
1.11.4.3. Clinical Trials.....	40
1.12. Metabolic consequences of ATR deficiency.....	41
1.12.1. Cancer Cachexia	41
CHAPTER TWO.....	45
2.1. Cell culture.....	46
2.2. Adipogenic differentiation of 3T3-L1 preadipocytes.....	47
2.3. Extract preparation	47
2.3.1. Urea-based whole cell extract.....	47
2.3.2. IP extracts.....	47
2.4. Cell fractionations	48
2.4.1. Endoplasmic Reticulum (ER) fractionation	48
2.4.2. Nuclear/Cytoplasmic fractionation.....	48
2.5. siRNA knockdowns	49
2.6. cDNA overexpression.....	49
2.6.1. METAFECTINE PRO.....	49
2.6.2. Calcium Phosphate.....	49
2.6.3. Lipofectamine® 3000 Transfection	50
2.7. FLAG-Immunoprecipitation.....	50
2.8. 3X FLAG peptide elution.....	50
2.9. SDS-PAGE/Western blotting.....	51
2.10. Site directed mutagenesis	51
2.10.1. Agarose gel electrophoresis.....	52
2.11. Triglyceride and Free Fatty Acid Quantification	53
2.11.1. Oil Red O	53
2.11.2. Media Triglyceride Quantification	53
2.11.3. Media Free Fatty Acid (FFA) Quantification.....	53
2.12. Cell Viability Assays.....	54
2.13. Immunofluorescence	54
2.14. Fluorescent Probes	55
2.15. Reagents.....	55
CHAPTER THREE.....	58
3.1. Introduction	59
3.1.1. Overview of Adipogenesis.....	61
3.1.2. Mesenchymal Stem Cell (MSC) Commitment	62
3.1.3. Terminal Differentiation of Preadipocytes.....	63
3.1.4. Regulators of PPAR γ	65
3.1.4.1. Chromatin remodelling	65
3.1.4.2. Pre-Lamin A	66
3.1.4.3. NAD ⁺ /SIRT1 (Sirtuin 1).....	67
3.1.4.4. Calcineurin/NFAT (nuclear factor of activated T cells).....	68
3.1.4.5. p38 MAPK signalling.....	68
3.1.4.6. Free Fatty Acids	69
3.1.4.7. mTOR (mechanistic target of rapamycin)	70

3.1.5. 3T3-L1 Adipogenesis	70
3.2. Results	73
3.2.1. Small molecule inhibition of ATR decreases adipogenic differentiation of 3T3-L1 preadipocytes.....	73
3.2.2. ATRi has limited effects on viability and S-phase kinetics of Mitotic clonal expansion (MCE)	75
3.2.3. ATRi does not induce consistent defects in the early adipogenic cascade	78
3.2.4. p38 MAPK pathway is activated following ATR inhibition throughout adipogenesis ..	80
3.2.5. ATRi treatment does not block adipogenesis through increased Calcineurin activity..	83
3.2.6. ATRi does not block adipogenesis through defective pre-Lamin A processing	84
3.2.7. ATRi reduces insulin sensitivity in a primary cilia-independent manner, resulting in reduced mTORC1 activity.....	86
3.2.8. Atr siRNA induces PPAR γ 2 expression.....	89
3.3. Summary.....	91
3.4. Discussion	92
 CHAPTER FOUR	 96
4.1. Introduction	97
4.1.1. Adipocyte and adipose tissue overview	97
4.1.2. The lipid droplet	98
4.1.2.1. Lipid Synthesis.....	100
4.1.2.2. Lipolysis	101
4.1.3. Adipocyte browning	102
4.1.3.1. 4E-BP1	104
4.2. Results	106
4.2.1. Chronic ATRi treatment does not affect adipocyte viability or induce the DDR.....	106
4.2.2. Acute ATRi treatment results in decreased lipid droplet (LD) integrity.....	107
4.2.3. ATRi induces adipocyte 'browning'	112
4.2.4. ATRi induces Ca ²⁺ -p38 MAPK-ATF2 signalling in adipocytes.....	116
4.3. Summary.....	118
4.4. Discussion	119
 CHAPTER FIVE	 123
5.1. Introduction	124
5.1.1. Phagophore formation and nucleation	127
5.1.2. Transport and lysosomal fusion	129
5.1.3. Starvation-induced autophagy.....	132
5.1.4. Receptor-mediated autophagy	133
5.1.5. Interpreting LC3-I/LC3-II western blotting	135
5.2. Results	137
5.2.1. ATRi results in defective autophagy and p62 accumulation	137
5.2.2. Genetic approaches to compromise ATR phenocopy ATRi-induced defects in autophagy and p62 accumulation.....	140
5.2.3. ATRi-induced p62 accumulation is autophagy- and DDR- independent	142
5.2.4. ATRi induces TFEB translocation and lysosomal biogenesis	143
5.2.5. Altering cellular Ca ²⁺ status affects ATRi-induced p62 accumulation.....	145
5.3. Summary.....	147

5.4. Discussion	148
CHAPTER SIX	151
6.1. Introduction	152
6.1.1. <i>The endomembrane system</i>	153
6.1.2. <i>Intracellular Ca²⁺ Homeostasis</i>	154
6.1.2.1. <i>Ca²⁺ sequestration</i>	155
6.1.2.2. <i>Ca²⁺ channels/pumps</i>	155
6.1.3. <i>The BCL-2 family</i>	156
6.1.4. <i>Protein folding and quality control</i>	159
6.1.5. <i>The ER stress response</i>	161
6.1.5.1. <i>ER-Associated Degradation (ERAD)</i>	161
6.1.5.2. <i>The UPR</i>	162
6.1.5.3. <i>PERK</i>	162
6.1.5.4. <i>ATF6</i>	163
6.1.5.5. <i>IRE1α</i>	164
6.2. Results	166
6.2.1. <i>ATR inhibition and Atr siRNA induce conspicuous cytoplasmic vacuolisation</i>	166
6.2.2. <i>Contents of ATRi-induced vacuoles are pH neutral</i>	168
6.2.3. <i>ATRi induces mitochondrial fission</i>	171
6.2.4. <i>ATRi-induced vacuoles are swollen ER</i>	173
6.2.5. <i>ATRi-induced vacuolisation is attenuated by Ca²⁺-free media</i>	177
6.2.6. <i>ATRi treatment induces ER stress</i>	178
6.2.7. <i>ATR is localised to the ER</i>	180
6.2.8. <i>ATR kinase-dependently immunoprecipitates with CANX</i>	184
6.2.9. <i>ATRi-induced vacuolisation is rescued by Obatoclax</i>	185
6.3. Summary	189
6.4. Discussion	190
CHAPTER SEVEN	195
7.1 Summary	196
7.1.1 <i>Chapter 3</i>	196
7.1.2 <i>Chapter 4</i>	197
7.1.3 <i>Chapter 5</i>	197
7.1.4 <i>Chapter 6</i>	197
7.2 Discussion	198
7.2.1 <i>ER stress and adipogenesis</i>	198
7.2.2 <i>ER stress, autophagy and lipid metabolism</i>	199
7.2.3 <i>Lysosomal transport, mTOR signalling and autophagy</i>	200
7.3 Concluding remarks	204
REFERENCES	206

ABBREVIATIONS

ATM	Ataxia-telangiectasia mutated
ATMi	ATM inhibitor
ATR	Ataxia-telangiectasia mutated and Rad3-related
ATRi	ATR inhibitor
BAT	Brown adipose tissue
BCL-2	B-cell lymphoma 2
BSA	Bovine serum albumin
CANX	Calnexin
CHK1	Checkpoint kinase 1
CHK1i/UCN01	CHK1 inhibitor
DAPI	4`6-diamino-2-phenylindole
DDR	DNA damage response
DMEM	Dulbecco's Modified Eagle's medium
DMSO	Dimethyl Sulfoxide
ER	Endoplasmic reticulum
ERAD	ER-assisted degradation
FACS	Fluorescence-activated cell sorting
FFA	Free fatty acid
GA	Golgi apparatus
Hrs	Hours
IF	Immunofluorescence
KD	Kinase dead
LC3-I	Microtubule-associated protein 1A/1B-light chain 3
LC3-II	LC3-phosphatidylethanolamine (LC3-PE)
LD	Lipid droplet
MCE	Mitotic clonal expansion
mTOR	Mechanistic target of rapamycin
PBS	Phosphate buffered saline
PIKK	Phosphatidylinositol 3-kinase like kinase
PPAR γ	Peroxisome proliferator-activated receptor γ
siRNA	Short-interfering RNA
SS	Seckel Syndrome
TFEB	Transcription factor EB
TG	Triglyceride
UNT	Untreated
UPR	Unfolded protein response
VPS4b	Vacuolar protein sorting-associated protein 4b
WAT	White adipose tissue
WCE	Whole cell extract

List of Figures

Figure 1.2.1. The PIKK family.....	3
Figure 1.2.2. Simplified schematic of mTOR signalling.....	5
Figure 1.2.3. DNA damage response signalling through PIKK family members ATM and ATR.....	6
Figure 1.3. RPA facilitates stalled fork stabilisation.....	8
Figure 1.3.4 Canonical ATR activation.....	10
Figure 1.6. ATR protein structure.....	16
Figure 1.6.1. HEAT repeats can bind DNA.....	17
Figure 1.6.4. Alignment of BH3-like consensus sites within ATR with BCL2 family Members.....	19
Figure 1.7.1. Network of putative ATR/ATM substrates involved in cell metabolism identified by Matsuoka et al.	20
Figure 1.9.1. Loss of function mutations in ATM generate Ataxia Telangiectasia.....	26
Figure 1.9.2. Seckel Syndrome generated by mutations in ATRIP and ATR.....	27
Figure 1.10.2. Abnormalities of subcutaneous fat and accelerated ageing after induced knockdown of <i>Atr</i> in adult mouse.....	31
Figure 1.10.3. Humanised <i>Atr</i> ^{S/S} mouse exhibiting severe microcephaly, low birth weight and dwarfism, characteristic of ATR-SS.....	32
Figure 1.11.3. Synthetic lethality concept of PARPi on BRCA-defective tumours.....	37
Figure 1.12.1. Cancer Cachexia.....	42
Figure 1.12.2. Simplified schematic of lipid-metabolic reprogramming in cancer	43
Figure 3.1. ATR-SS has the clinical feature of lipodystrophy.....	59
Figure 3.2. <i>Atr</i> deletion in adult mice results in disproportionate wasting of adipose tissue.....	60
Figure 3.1.2. Schematic of mesenchymal stem cell commitment.....	62
Figure 3.1.3. Temporal schematic of adipogenic differentiation in vitro.....	63
Figure 3.1.5. 3T3-L1 adipogenesis overview.....	71
Figure 3.2.1. Adipogenesis of 3T3-L1 cells co-treated with or without small molecule kinase inhibitors of ATR.....	74
Figure 3.2.2. Effects of ATRi on viability and S-phase kinetics of mitotic clonal expansion.....	77
Figure 3.2.3. Assessment of early adipogenic cascade.....	79
Figure 3.2.4. p38 MAPK is activated throughout adipogenesis following ATR inhibition.....	81
Figure 3.2.5. ATRi does not block adipogenesis in a Calcineurin-dependent manner.....	83

Figure 3.2.6. ATRi does not block adipogenesis through defective pre-Lamin A processing.....	85
Figure 3.2.7. Acute ATRi treatment and Atr siRNA reduces insulin sensitivity and mTORC1 activity in 3T3-L1 preadipocytes.....	88
Figure 3.2.8. <i>Atr</i> siRNA induces PPAR γ 2 expression in the absence of adipogenic inducers.....	90
Figure 3.4.1. Schematisation of postulated mechanisms of reduced adipogenesis following ATRi, and enhanced adipogenesis following <i>Atr</i> siRNA.....	94
Figure 4.1.2. Sub-types of adipocyte.....	99
Figure 4.1.2.1. Schematic of lipid synthesis pathways.....	100
Figure 4.1.2.2. Schematic of lipolysis.....	101
Figure 4.1.3. Schematic of adipocyte browning.....	103
Figure 4.1.3.1. Mechanism of eIF4E-BP1 (4E-BP1) inactivation-induced browning.....	104
Figure 4.2.1. Chronic ATRi treatment of mature 3T3-L1 adipocytes does not affect viability or induce the DNA damage response.....	106
Figure 4.2.2.1 Chronic ATRi treatment reduces TG content of mature 3T3-L1 adipocytes.....	108
Figure 4.2.2.2. Chronic ATRi treatment decreases lipid droplet integrity of 3T3-L1 adipocytes.....	110
Figure 4.2.2.3. Chronic ATRi treatment induces FFA and TG release.....	111
Figure 4.2.3. ATRi treatment induces markers of adipocyte 'browning'.....	114
Figure 4.2.4. ATRi treatment activates the Ca ²⁺ -p38 MAPK-ATF2 signalling axis in mature adipocytes.....	116
Figure 4.3. Schematic of pathways associated with ATRi-induced adipocyte browning.....	120
Figure 5.1. Autophagy complexes - initiation to lysosomal fusion.....	126
Figure 5.1.1.1. Phagophore formation and nucleation complexes.....	127
Figure 5.1.1.2. ATG12-ATG5-ATG16 complex formation and LC3-I conjugation.....	128
Figure 5.1.2. RAB7 and FYCO1- or RILP-ORP1L-mediated transport of late autophagosomes across the microtubule.....	131
Figure 5.1.4. Role of p62 in receptor-mediated autophagy.....	134
Figure 5.1.5. Assessing autophagy with western blotting of LC3.....	135
Figure 5.2.1.1. ATRi induces aberrant autophagic processing.....	138
Figure 5.2.1.2. ATRi induces aberrant autophagic-dependent LC3 processing.....	139
Figure 5.2.2. Over expression of WT and KD-ATR constructs and Atr siRNA results in enhanced p62 and autophagic block.....	141
Figure 5.2.3. Increased p62 expression following ATRi is independent of autophagy and DNA damage induction and signalling.....	142

Figure 5.2.4. ATRi induces TFEB translocation and expression of lysosomal markers.....	144
Figure 5.2.5. Depleting extracellular Ca^{2+} inhibits ATRi-induced p62 accumulation.....	146
Figure 6.1.1. The endomembrane system.....	153
Figure 6.1.3.1 Structure of BCL-2 family members.....	157
Figure 6.1.3.2. Simplified schematic of BCL-2 family mechanisms of action.....	158
Figure 6.1.5.2. The three arms of the UPR.....	162
Figure 6.2.1.1. ATRis and <i>Atr</i> siRNA induce mass cytoplasmic vacuolisation.....	166
Figure 6.2.1.2. ATR deficiency-induced vacuolisation phenotypes exist in literature.....	168
Figure 6.2.2. ATRi-induced vacuoles are pH neutral.....	170
Figure 6.2.3. ATRi treatment induces profound changes in mitochondrial dynamics.....	172
Figure 6.2.4.1. ATRi-induced vacuoles are not swollen Golgi Apparatus (GA).....	174
Figure 6.2.4.2. VPS4b overexpression attenuates ATRi-induced vacuolisation.....	175
Figure 6.2.4.3. ATRi-induced vacuoles arise from swollen ER.....	177
Figure 6.2.5. Treatment with Ca^{2+} -free medium reduces the appearance of ATRi-induced vacuoles.....	178
Figure 6.2.6. Acute ATRi treatment affects markers of ER stress	179
Figure 6.2.7. ATR is active at the ER.....	182
Figure 6.2.8. ATR co-precipitates with CANX.....	185
Figure 6.2.9. Obatoclox rescues ATRi-induced vacuolisation.....	187
Figure 6.4.1. Structural similarities between VPS4b and p97/VCP.....	192
Figure 6.4.2. Schematic of putative mechanisms of ATRi-induced ER swelling.....	194
Figure 7.2.3.1. Network of putative ATR/ATM substrates involved in cell metabolism.....	200
Figure 7.2.3.2. ATR coprecipitates with dynein.....	202
Figure 7.2.3.3. mTOR localisation is affected by ATRi.....	202
Figure 7.2.1.4. Lipid droplets re-localise to cell periphery following ATRi treatment.....	204

List of Tables

Table 1.2.1. PIKK family binding partners and activators.....	4
Table 1.9.2. Documented ATR mutations that generate Seckel Syndrome.....	28
Table 1.11.4.1. ATR inhibitor molecular structures.....	39
Table 1.11.4.3. Clinical trials ongoing for ATRis VE-822 and AZD6738 (August 2017).....	40
Table 2.1. Cell lines utilised in this thesis.....	46
Table 2.5. siRNA oligonucleotides utilised in this thesis.....	49
Table 2.6.3. cDNA constructs utilised in this thesis.....	50
Table 2.10.1. Mutagenic PCR reaction mix per sample.....	51
Table 2.10.2. Mutagenic PCR reaction conditions.....	52
Table 2.10.3. Mutagenic PCR primers.....	52
Table 2.14. Fluorescent probes utilised in this thesis.....	54
Table 2.15.1. Reagents utilised in this thesis.....	55
Table 2.15.2. Antibodies utilised in this thesis.....	56
Table 6.2.1. Cell types where ATRi treatment induced conspicuous cytoplasmic vacuolisation.....	167

Chapter One

Introduction

1.1. The DNA Damage Response (DDR)

Tissues are required to constantly replenish worn-out cells and remodel, to preserve optimum function and maintain homeostasis. Reliable and accurate replication of genomic DNA is essential for the production of functional cells to maintain tissue homeostasis. Yet, throughout existence, cells face incalculable encounters with both exogenous and endogenous DNA damage, which can result in compromised genomic integrity. Exposure to UV-B light results in the generation of cyclobutane pyrimidine dimers, bulky lesions which perturb normal replication, requiring nucleotide excision repair (NER) ([Guintini et al., 2015](#)). UV-A light exposure results in the generation of reactive oxygen species (ROS), which induces oxidative base damage (e.g. 8-oxo-guanine), ribose-sugar modification, abasic sites and single and double stranded DNA breaks (SSBs; DSBs). ROS are also produced endogenously, as a by-product of oxidative phosphorylation ([Rahman, 2007](#)). Ionising radiation induces SSBs and DSBs ([Vignard et al., 2013](#)). To maintain genomic integrity, DNA damage must be detected, cell cycle checkpoints activated, and DNA repaired before continuation of the cell cycle. Where attempts to repair damaged DNA are unsuccessful, the fate of the cell can include apoptosis, cellular senescence or malignant transformation.

Intricate and highly regulated signalling pathways are essential to ensure stringent cell cycle parameters and DNA synthesis, effective repair of damaged DNA, and the programmed senescence or death of deleterious cells. Collectively known as the DNA damage response (DDR), this signalling axis further functions to protect and maintain effective stem cell populations from DNA damage-induced senescence throughout early development and adulthood. Controlled cell division is intimately linked to the determination of cell fate and induction into various differentiative programmes, denoting functional significance to the DDR in tissue development and homeostasis ([Errol et al., 2006](#)). A functional DDR ensures genomic stability – when the DDR is compromised, cells can experience elevated levels of mutagenesis, uncontrolled replication and malignant transformation.

Cells are equipped with multiple systems for the effective decision-making required to maintain genomic integrity - high levels of functional redundancy exist within the DDR to achieve this exceptional stability of genomic maintenance and repair

required to confront constant assault ([Errol et al., 2006](#)). The DDR is the coordinated cellular response that orchestrates appropriate DNA repair after genomic injury, principally regulated by the serine/threonine (S/T) protein kinases of the phosphatidylinositol 3-kinase (PI3K)-like kinase (PIKK) family.

1.2. The PIKK family

DDR-related PIKK family members include DNA-dependent protein kinase catalytic subunit (DNA-PKcs), Ataxia Telangiectasia-Mutated (ATM), and ATM and Rad3-related (ATR) ([Sirbu and Cortez, 2013](#)). Members of the PIKK family also include: Mechanistic Target of Rapamycin (mTOR), a kinase activated by multiple metabolic cues to control global cell metabolism and growth, Suppressor of Morphogenesis in Genitalia 1 (SMG1), a critical component of the mRNA surveillance complex mediating nonsense-mediated RNA decay, and transcription factor co-activator TRRAP (transformation/transcription domain associated protein).

PIKK family members are large proteins classified by the presence of a conserved protein S/T kinase domain ([Lempiäinen and Halazonetis, 2009](#)). Although PIKKs do not phosphorylate lipids, their kinase domains share significant sequence similarity to the PI3K family. PIKKs also contain large, highly conserved regions that generally lack sequence similarity between family members ([Cimprich and Cortez, 2008](#)). Considering the conservation, yet striking variability between each PIKK, these largely

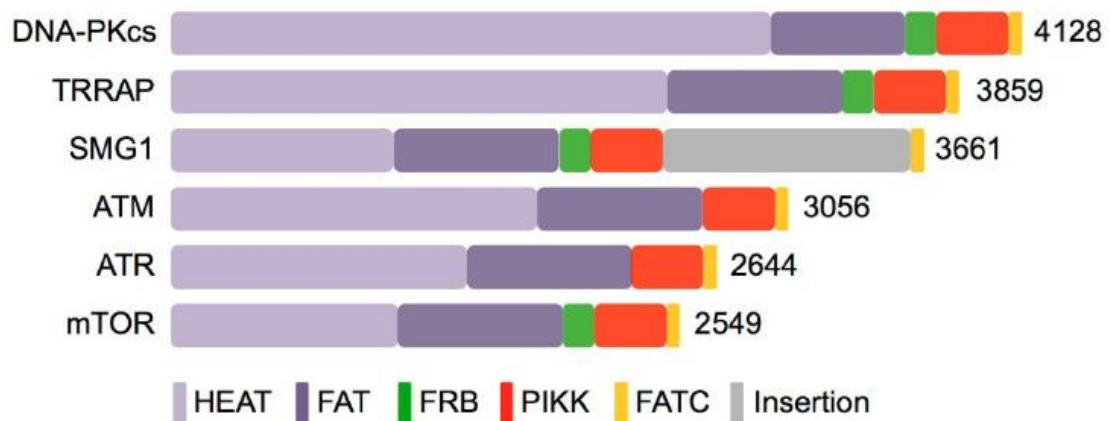


Figure 1.2.1. The PIKK family. HEAT - Huntingtin, elongation factor 3, subunit of protein phosphatase 2A, PI3-kinase target of rapamycin 1; FAT - FRAP-ATM-TRRAP domain; FRB - FKBP-rapamycin-binding domain; PIKK - PI3K-like kinase domain; FATC - FAT-C-terminal domain. Taken from ([Rivera-Calzada et al., 2015](#))

uncharacterised regions may provide future opportunity to investigate unique and non-canonical activities of each kinase.

PIKK family members share similar domain organisation – C-terminal kinase domains flanked by conserved FAT (FRAP-ATM-TRAP) and FAT C-terminus (FATC) domains, with vast N-terminal HEAT repeats expanding the majority of each protein (Fig 1.2.1) ([Perry and Kleckner, 2003](#)). Many common themes appear in the regulation and activation of each member of the PIKK family – structural homology, recruitment to sites of activation via interacting partners, and unique secondary activator components that associate with conserved PIKK Regulatory Domains (PRDs) (Table 1.2.1) ([Mordes and Cortez, 2008](#)).

Kinase	Binding Partner	Activator	Nucleic Acid
ATR	ATRIP	TOPBP1	ssDNA
ATM	NBS1	MRE11	DSB
DNA-PKcs	KU70-KU80	KU70-KU80	DSB
mTOR	Raptor/Rictor	LST8/RHEB-GTP	-

Table 1.2.1. PIKK family binding partners and activators.

Dependent on the availability of a sister chromatid for HR strand exchange, DSB repair consists of homologous recombination (HR) or the non-homologous end joining pathway (NHEJ), the latter instigated by DNA-PKcs ([Kakarougkas and Jeggo, 2014](#); [Krejci et al., 2012](#)). Comparatively to ATR and ATM, DNA-PKcs regulates a small number of targets as the catalytic subunit of DNA-dependent S/T kinase DNA-PK. DNA-PKcs relies on heterodimeric KU70-KU80 to trigger its kinase activity and mediate localisation at DNA DSB ends ([Walker et al., 2001](#)). DNA-PKcs is also required for V(D)J recombination – the process utilising programmed NHEJ to promote immune system diversity – evidenced by the severe combined immunodeficiency (SCID) observed in DNA-PKcs knockout mice ([Taccioli et al., 1998](#)).

The mTOR complexes (mTORC1/2) are key effectors and regulators of nutrient status within the cell. Incoming glucose, amino acids, growth factors and cytokines act as potent metabolic cues, where signals are transduced through multiple signalling cascades resulting in differential, threshold-based activation of the mTOR complexes. mTORC1/2 regulate autophagy, protein, lipid and nucleotide synthesis, as well as glycolysis and cytoskeletal reorganisation ([Laplante and Sabatini, 2012](#)). Generally,

mTORC1 promotes protein and lipid synthesis, fuelling proliferation when energy conditions are favourable and autophagy when they are not, and mTORC2 promotes cell survival by activating protein kinase B (AKT). Together, the vast signalling networks engaged in the activation and suppression of the mTORCs, and the multiple levels of cross talk between mTORC1 and 2 at differing nodes allows input from almost every effector of cellular metabolism, and tailored responses to small changes in nutrient status ([Laplante and Sabatini, 2012](#)).

Briefly, following stimulation by insulin, a rapid signal transduction response cascades through the cell, via the mTOR signalling axes. Insulin Receptor (IR) is rapidly autophosphorylated on the cytoplasmic β -subunit, resulting in multiple phosphorylations on IR adaptor protein insulin receptor substrate 1 (IRS1), including at Y989. P-IRS1 induces activation of PI3K, resulting in the generation of PI(3, 4, 5)P₃, which recruits AKT to the plasma membrane where it becomes phosphorylated at S473 by multiple proteins, including the mTORC2 complex (Fig 1.2.2). AKT is also phosphorylated at the plasma membrane at T308 by PI3-dependent kinase PDK1 ([Yu and Cui, 2016](#)).

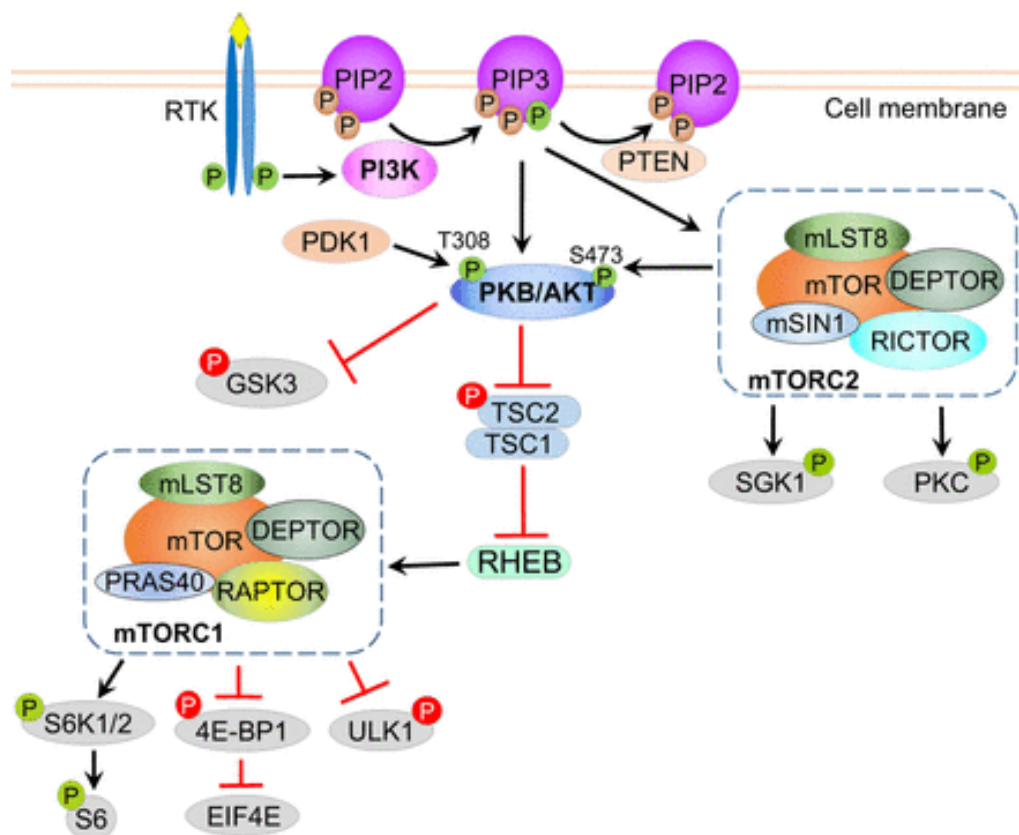


Figure 1.2.2. Simplified schematic of mTOR signalling. Taken from ([Yu and Cui, 2016](#))

Activated AKT inhibits Tuberous Sclerosis Complex 2 (TSC2) via phosphorylation, rendering it unable to bind to RAS homolog enriched in brain (RHEB), enabling activation of mTORC1.

ATM shares multiple DDR-dependent substrates with ATR and appears to phosphorylate hundreds of proteins at Ser/Thr-Glu (S/TQ) motifs after DNA damage ([Matsuoka et al., 2007](#)). Together, ATR and ATM appear to be the master regulators of the DDR, transducing signals to a large network of cellular processes ([Maréchal and Zou, 2013](#)). Whereas ATR is recruited to DNA-SSBs via Replication Protein A (RPA), ATM is recruited to DNA-DSBs via the MRE11-RAD50-NBS1 (MRN) complex, where it directly phosphorylates histone variant H2AX allowing adaptor proteins to bind and recruit effector proteins including checkpoint kinase 2 (CHK2) and p53 (Fig 1.2.3). This signal is

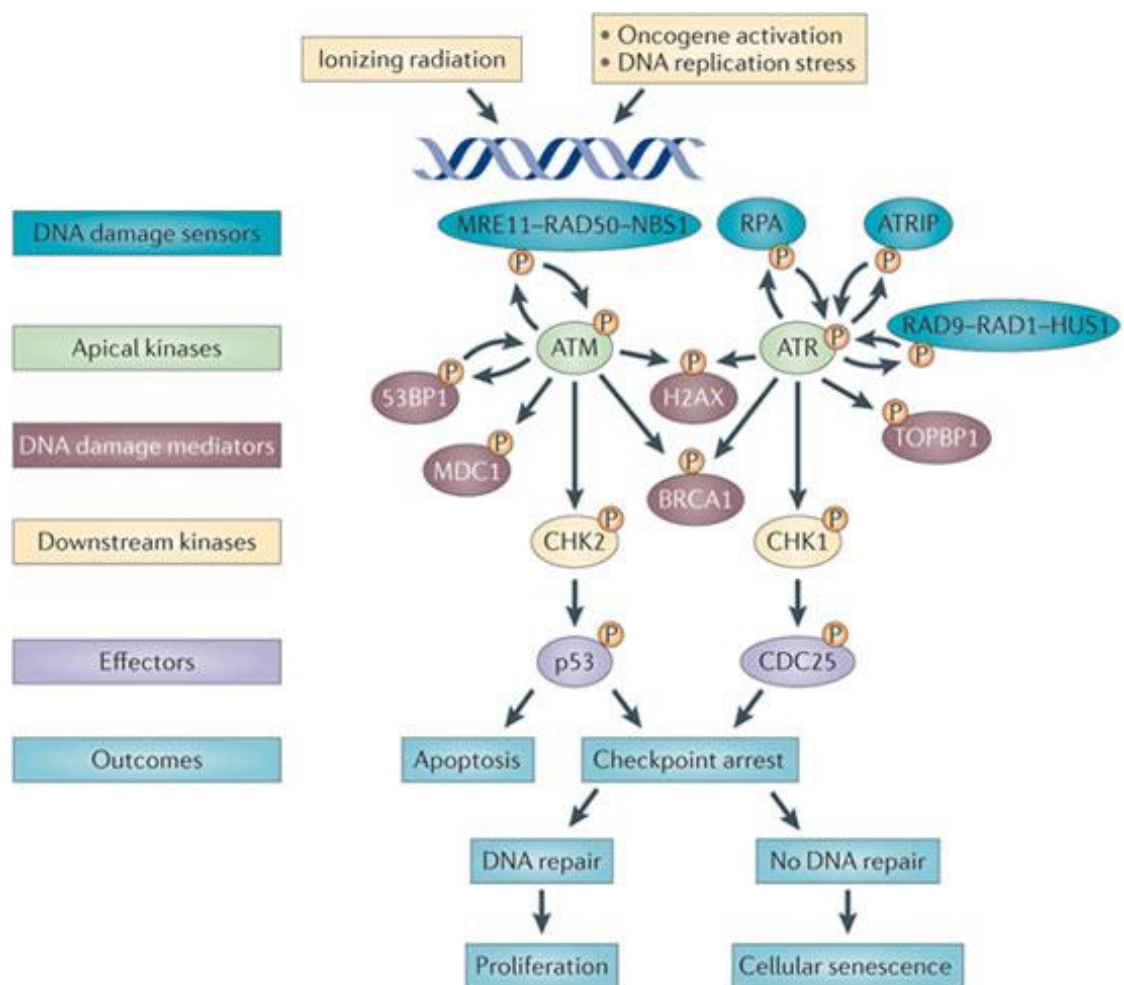


Figure 1.2.3. DNA damage response signalling through PIKK family members ATM and ATR.
Taken from ([Sulli et al., 2012](#))

propagated across the flanking chromatin, increasing the recruitment of DDR proteins to the site of damage ([Fernandez-Capetillo et al., 2004](#)). ATM primarily acts upon sites of DSBs, whereas ATR is activated after a variety of insults that expose regions of single-stranded DNA (ssDNA), frequently formed at replication forks, collectively termed 'replicative stress' ([Cimprich and Cortez, 2008](#)). ATR exists within a stable heterodimer with ATR-interacting protein (ATRIP) ([Cortez et al., 2001](#)), whereas ATM exists as a homodimer, dissociating into monomers following activation and autophosphorylation at S1981 ([Bakkenist and Kastan, 2003](#)).

1.3. DNA damage recognition and ATR activation

The widely established method of ATR activation is via DNA damage that induces regions of single-stranded DNA (ssDNA). RPA heterotrimers bind to exposed regions of ssDNA with high affinity. A common intermediate DNA structure, RPA-coated ssDNA allows activation of ATR in response to a wide variety of cues, including end-resected DSBs at the S- and G2-M phase checkpoints, nucleotide excision repair (NER) intermediates, replication fork restart and telomere erosion. Most notable of these is the canonical activator of ATR at the intra-S-phase checkpoint – replication stress ([Cimprich and Cortez, 2008](#)). Replication stress induced by fork stalling throughout S-phase is perceived as the most common activator of ATR. Replication fork stalling can occur due to a number of reasons, amongst these; DNA polymerase encountering a DNA lesion or adduct; common fragile sites (CFS); and interstrand cross-links (ICLs). At the stalled fork, the uncoupled MCM2-7 (minichromosome maintenance complex) helicase continues, generating long stretches of ssDNA through its DNA unwinding activity, allowing RPA and other DNA damage sensors to bind, recruit and activate ATR (Fig 1.3.1) ([Berti and Vindigni, 2016](#)). Most notable is Topoisomerase II Binding Protein 1 (TOPBP1), which functions to hyperactivate the ATR-ATRIP complex ([Kumagai et al., 2006](#)).

CFS are large, non-randomly distributed genomic regions that prove particularly difficult for replication machinery to copy. CFSs are exceptionally sensitive to genomic instability, where enhanced replicative stress results in gaps and breaks at CFS loci in metaphase chromosomes ([Glover et al., 1984](#)). Replication fork stalling at CFSs appears to be a common event throughout S-phase, hence accurate reproduction of these loci hinges on the ATR-dependent intra-S-phase checkpoint. ATR activity has been shown to

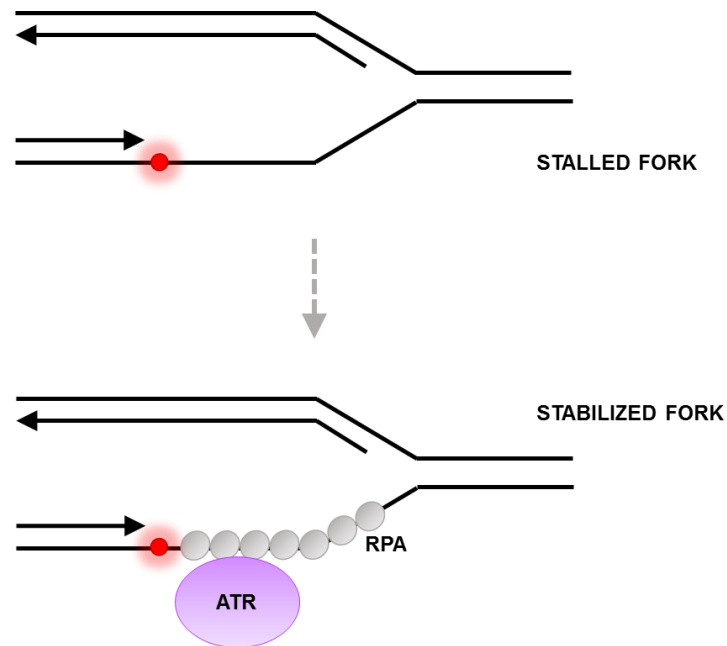


Figure 1.3.1. RPA facilitates stalled fork stabilisation. RPA binds to ssDNA at stalled replication forks to recruit ATR.

be vital for CFS maintenance - ATR deficiency results in high levels of fragile site breakage ([Casper et al., 2002](#)).

Here I will summarise the key mediators required in the activation of ATR.

1.3.1. ATRIP

ATRIP is the obligate binding partner of ATR. Interacting via a region within the N-terminal HEAT repeats of ATR, ATRIP is essential for the stability, and canonical localisation and activation of ATR at sites of DNA damage ([Ball et al., 2005](#); [Nam and Cortez, 2011](#)). Small interfering RNA (siRNA) directed against ATRIP causes loss of ATR expression, demonstrating the stability of ATR is dependent on ATRIP ([Cortez et al., 2001](#)). ATR is localised to regions of ssDNA via a direct interaction between ATRIP and stretches of RPA-coated ssDNA (coined RPA nucleofilaments) ([Zou and Elledge, 2003](#)). ATRIP also appears essential for the association and subsequent hyperactivation of ATR by TOPBP1 through a functionally conserved domain ([Mordes et al., 2008](#)).

1.3.2. Replication protein A (RPA)

RPA exists as a heterotrimeric protein complex, consisting of RPA70, RPA32 and RPA14 ([Zou et al., 2006](#)). RPA binds to ssDNA with avidity, in a sequential manner in the 5' to 3' direction ([de Laat et al., 1998](#)). Whilst all RPA subunits contain DNA-binding domains

(DBDs), binding and association with ssDNA appears to mostly occur within the tandem DBDs of RPA70, where cooperative binding of all four DBDs occludes roughly 30 nucleotides of ssDNA ([Zou et al., 2006](#)). RPA32 contains an unstructured N-terminal phosphorylation domain, which is hyperphosphorylated by PIKK family members in an ssDNA- and replication-dependent manner following DNA damage. It has been suggested that hyperphosphorylation of RPA occurs following damage to limit the use of RPA in DNA replication, whilst shifting small fractions of nuclear RPA into DNA repair actions only ([Patrick et al., 2005](#)). Whilst RPA14 has no binding affinity for ssDNA, it is required for RPA heterotrimer formation and stability ([Wold, 1997](#)).

RPA nucleofilaments are involved in almost all processes concerning DNA replication and repair, and are widely established as the common intermediate unifying the variety of disparate and genotoxic DNA structures that are capable of inducing ATR activation ([Zou and Elledge, 2003](#)).

1.3.3. RAD9-HUS1-RAD1 complex

The DNA damage-specific RAD9-RAD1-HUS1 (9-1-1) clamp complex preferentially binds to DNA substrates possessing 5' recessed ends, and is loaded onto the ssDNA-dsDNA junction by the alternative clamp loader RAD17-RFC complex (RAD17 and replication factor C) ([Ellison and Stillman, 2003](#)). RPA nucleofilaments are an important intermediate structure here, recognised by the RAD17-RFC complex ([Zou and Elledge, 2003](#)). RPA also interacts with the 9-1-1 complex via the RAD9 subunit ([Maréchal and Zou, 2013](#)).

The 9-1-1 complex has similar structure and substrate specificities to the promiscuous, homotrimeric sliding clamp protein proliferating cell nuclear antigen (PCNA), besides from the presence of an unstructured, highly phosphorylated tail on the C-terminus of RAD9, which enables it to activate the essential ATR activator TOPBP1.

1.3.4. TOPBP1

TOPBP1 hyperactivates ATR through DNA-dependent and DNA-independent mechanisms ([Kumagai et al., 2006](#)). 9-1-1-dependent activation of TOPBP1 is required for ATR activation. TOPBP1 contains several BRCA1 C-terminus (BRCT) domains which can function as phospho-peptide binding sites, allowing interaction with the highly

phosphorylated C-terminus of RAD9, in a phosphorylation-dependent manner ([Delacroix et al., 2007](#)). Recently, human protein 9-1-1 interacting nuclear orphan (RHINO) has been identified as a novel factor capable of facilitating 9-1-1-TOPBP1 complex formation in a phosphorylation-independent manner ([Cotta-Ramusino et al., 2011](#)). Association with RAD9 tethers TOPBP1 at sites of DNA damage, allowing it to effectively stimulate ATR through association with the FATC domain whilst concomitantly acting as a scaffold that facilitates ATR kinase-substrate interactions. Activation-inducing *trans*-autophosphorylation of ATR at T1989 in the FAT domain appears to be independent of TOPBP1 activity ([Ellison and Stillman, 2003](#); [Nam et al., 2011](#)).

RPA nucleofilaments appear to serve as the common intermediate structure required for the assembly and recruitment of the two independent checkpoint

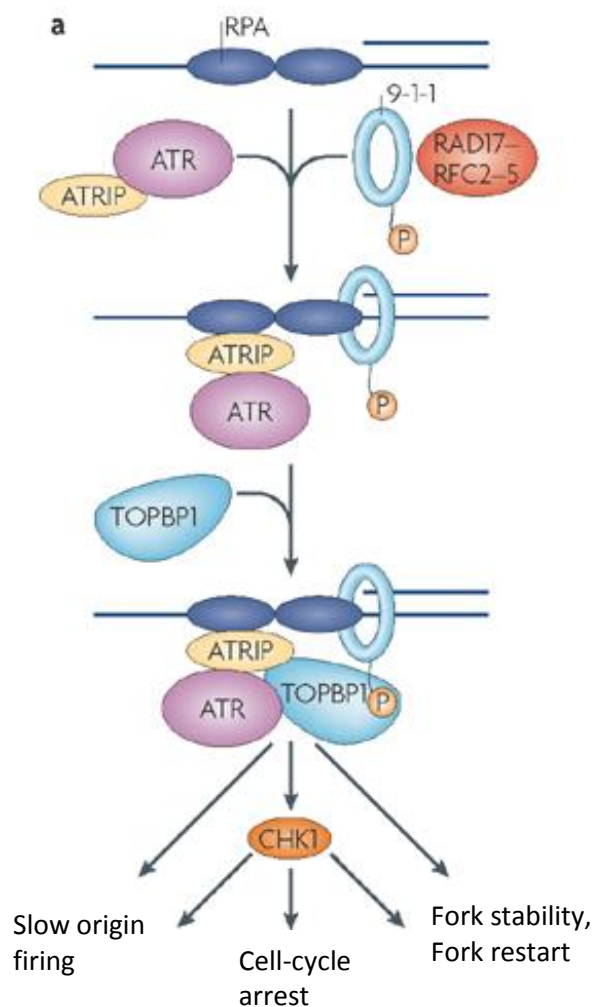


Figure 1.3.2 Canonical ATR activation. Taken from ([Cimprich and Cortez, 2008](#))

complexes for ATR activation – the 9-1-1-TOBP1 complex and ATR-ATRIP. Furthermore, the specificity of the 9-1-1-clamp complex to ssDNA-dsDNA junctions, and this requirement of RPA-ssDNA for ATR activation, together may provide a mechanism to ensure ATR is only activated at sites of DNA damage, rather than regions of ssDNA alone.

1.3.5. MRE11-RAD50-NBS1 (MRN) complex

The Nijmegen breakage syndrome 1 (NBS1) subunit of the MRN complex also directly activates ATR independently of TOPBP1, via its N-terminal BRCT2 domain ([Kobayashi et al., 2013](#)). Cells deficient in NBS1 are unable to retain or activate ATR at RPA nucleofilaments ([Stiff et al., 2005](#)). The MRN complex also appears essential for appropriate recruitment, but not activation, of TOPBP1 to the ssDNA-dsDNA junction ([Duursma et al., 2013](#)). Both TOPBP1 and NBS1 appear essential for effective ATR activation.

1.4. ATR downstream signalling

Following DNA damage recognition and activation, ATR and ATM phosphorylate hundreds of substrates at S/TQ motifs, transducing the signal to downstream targets resulting in a multitude of cellular outcomes. Here I will give a brief overview of some of the key mediators of ATR-DDR signalling.

1.4.1. CHK1

CHK1 is activated by ATR via phosphorylation on S317 and S345 in response to DNA damage, as well as in undisturbed cell cycles. Unlike other DDR protein kinases, which act at the site of DNA damage, CHK1 propagates the DNA damage signal to the rest of the nucleoplasm - the association of CHK1 with sites of DNA damage appears to be transient ([González Besteiro and Gottifredi, 2015](#)). As a multifaceted and versatile signalling kinase, CHK1 mediates a vast array of ATR-specific signalling in response to DNA damage. Chromatin association and activation of CHK1 requires ATR-ATRIP-dependent phosphorylation of RAD17 and BRCA1 ([Bao et al., 2001](#)). This also appears to be mediated by adaptor protein CLASPIN ([Kumagai and Dunphy, 2000](#)), which interacts with CHK1 in a damage-dependent manner. CLASPIN binds to the phosphorylated 9-1-1 complex subunit RAD17 at the ssDNA-dsDNA junction – an interaction important for

sustaining CHK1 phosphorylation ([Wang et al., 2006](#)). CLASPIN-mediated CHK1 activation is also mediated by the multifunctional TIMELESS protein and TIMELESS-interacting protein TIPIN. TIMELESS exists in a tightly bound complex with TIPIN. Following UV irradiation or hydroxyurea (HU) treatment, TIMELESS-TIPIN binds to RPA nucleofilaments, stabilising CLASPIN and facilitating CHK1 phosphorylation by ATR at sites of DNA damage ([Kemp et al., 2010](#)).

Following activation, CHK1 is released from the site of damage to localise to activate downstream targets within the nucleoplasm and at the centrosome ([Niida et al., 2007](#)). The most well characterised CHK1 substrate is the dual-specificity Cell division cycle 25 (CDC25) phosphatase ([Furnari et al., 1997](#)). ATR activation induces cell cycle arrest via CHK1-dependent phosphorylation of critical phosphatase CDC25A (T504). CDC25A-dependent dephosphorylation the cyclin-dependent kinase (CDK)-cyclin complexes is essential for their activity and cell cycle progression. Phosphorylation of CDC25A causes inhibition and degradation, preventing CDC25A-dependent dephosphorylation of CDK2-Cyclin A. Inhibition of CDK2-Cyclin A reduces association of CDC45 with replication origin complexes, resulting in a global inhibition of DNA synthesis due to decreased initiation of replication ([Falck et al., 2001](#)). CHK1 also phosphorylates DBF4, which may contribute to inhibition of origin firing via the regulation of CDC7 ([Heffernan et al., 2007](#)).

Much like the intra-S phase checkpoint, ATR acts upon the G2/M phase checkpoint through activation of CHK1 following ATM-dependent DNA DSB end resection, resulting degradation or cytoplasmic sequestration of the CDC25 homologues. The resulting lack of phosphatase activity increases inhibition of the Cyclin B1-CDK1 complex by maintaining inhibitory phosphorylations on CDK1, conferring G2/M phase arrest ([Furnari et al., 1997](#)).

1.4.2. MLL (Myeloid/Lymphoid Leukaemia 1)

ATR-induced S-phase arrest is instigated via several further mechanisms resulting in the inactivity of the CDC25 phosphatase and CDC45. Specifically, ATR phosphorylates lysine methyltransferase MLL in response to DNA damage, preventing MLL degradation by the S-phase kinase-associated protein 2 (SKP2) complex ([Liu et al., 2007](#)). Increased MLL

expression results in increased histone H3 methylation at replication origins, resulting in reduced loading of replication initiation factor CDC45 – required for origin firing. CDC45 binds directly to H3, an interaction blocked by H3K4 methylation. Hence, in response to DNA damage in S-phase, ATR activity intercepts S-phase progression through the stabilisation of MLL and blocking of CDC45. CHK1 also phosphorylates TRESLIN, further inhibiting CDC45 loading at replication origins ([Guo et al., 2015](#)).

1.4.3. MCM2

MCM2 is a component of the MCM2-7 helicase that functions to unwind dsDNA during DNA synthesis. Following replicative stress, ATR phosphorylates MCM2 at S108 at the replication fork, creating a docking site for Polo-Like Kinase 1 (PLK1) ([Trenz et al., 2008](#); [Yoo et al., 2004](#)). PLK1 is then capable of binding to chromatin, facilitating CDC45 loading onto local replication origins, in a manner that appears contradictory to the ATR-CHK1 generated global repression of origin firing ([Trenz et al., 2008](#)). However, by promoting dormant origin firing within existing factories local to the stalled replication fork through MCM2-PLK1, whilst inhibiting the activation of new replication complexes via CHK1, ATR redirects origin firing away from unreplicated parts of the genome, minimising the damaging consequences of replication stress whilst promoting the completion of replication within problematic areas ([Ge and Blow, 2010](#)).

1.4.4. dNTP synthesis

Several mechanisms supporting a role for ATR-CHK1 in regulating deoxynucleotide triphosphate (dNTP) synthesis after damage have been characterised ([Anacker et al., 2016](#); [Moss et al., 2010](#); [Zhang et al., 2009](#)). One established pathway describes the ATR- and CHK1-dependent downregulation of Cyclin F and CDK2 activity after DNA damage. Ribonucleotide Reductase (RNR) activity peaks in S-phase, when dNTP synthesis for DNA replication is most highly required. RNR subunit RRM2 (ribonucleotide reductase family member 2) is subject to targeted degradation in G2-M phase in a Cyclin F- and CDK2-dependent manner, as cells prepare to enter mitosis. Following ATR activation, Cyclin F and CDK2 activity is decreased, alleviating the degradation of RRM2 allowing production of dNTPs to continue ([D'Angiolella et al.](#)). These mechanisms ensure adequate production in times of genotoxic stress, where dNTPs are required for DNA synthesis and repair.

1.5. Modulators of ATR activity

Multiple proteins regulate ATR expression, signalling and activation. I will review some key modulators of ATR function in this section.

1.5.1. TEL2

PIKK family members are exceptionally large. During synthesis, these >250 kDa proteins require chaperone-assisted folding to acquire correct conformational maturation and protein stability. Telomere Length Regulation Protein 2 (TEL2) forms a chaperone complex with TELO2 interacting protein 1 (TTI1) and TTI2, coined the Triple T complex (TTT), which further contains the chaperone Heat Shock Protein 90 (HSP90), to promote the proper folding of the vast HEAT repeats contained in PIKK family members ([Takai et al., 2007](#)). The TTT/HSP90 complex acts as a PIKK-specific chaperone, interacting with the large α -helical HEAT repeats of each protein and preferentially associating within 1 hour of synthesis and not after ([Hořejší et al., 2010](#); [Hurov et al., 2010](#)). When TEL2 is absent, ATR is not appropriately folded, resulting in checkpoint defects and reduced association with ATRIP ([Hurov et al., 2010](#)).

1.5.2. Fanconi Anemia group M/FA-associated protein 24 (FANCM/FAAP24)

Interstrand cross-links (ICLs) induce replication fork stalling. However, in the case of ICL-induced fork stalling, the replication machinery remains coupled, due to the ICL acting as a physical obstruction to both helicase and polymerase. With no uncoupling of the replication machinery to generate the regions of RPA-ssDNA required for ATR activation, restructuring must occur before the lesion can be repaired. FAAP24 possesses the ability to associate with fork-structures and can form a complex with the highly conserved helicase FANCM, which possesses DNA translocase activity. As FANCM is required for effective checkpoint activation following ICLs, it is postulated that FANCM/FAAP24 is required to expose regions of ssDNA at ICLs to mediate ATR activation in response to these lesions ([Huang et al., 2010](#)). However, it appears FAAP24 is the only crucial mediator in the generation of ssDNA-RPA; hence, the level at which FANCM/FAAP24 mediates ATR activation at ICLs remains unclear ([Nam and Cortez, 2011](#)). FANCM/FAAP24-mediated activation of ATR demonstrates one of many pathways that facilitate ATR activation in response to a wide variety of DNA structures.

1.5.3. ATM and TOPBP1

Trans-autophosphorylation of ATR at T1989 generates a docking site for TOPBP1 via its BRCT domains. Phosphorylation of TOPBP1 on S1131 by ATM further promotes TOPBP1 binding to and activation of ATR, in an RPA-independent manner, suggesting ATM facilitates ATR activation at DSBs via TOPBP1 ([Yoo et al., 2007](#)). TOPBP1 is also phosphorylated by ATR at S1131 following replication stress, suggesting a positive feedback mechanism in which ATR- or ATM- dependent TOPBP1 phosphorylation enhances ATR activity. TOPBP1 also interacts with ATRIP via its ATR-activation domain, hypothesised to generate conformational changes in ATR increasing kinase activity or substrate binding ([Mordes et al., 2008](#)). ATM-induced, RPA-independent ATR activation demonstrates one of multiple means of activating ATR without all of the established ATR signalling components.

1.5.4. mTOR signalling axis

Protein kinase A (PKA) and the IGF-1 signalling axis have recently been implicated as a regulator of ATR in response to UV-induced DNA damage ([Jarrett et al., 2014](#); [Jarrett et al., 2016](#); [Kemp et al., 2017a](#)). PKA is a cAMP-dependent kinase with roles in regulation of many different cellular metabolic and signalling processes ([Del Gobbo et al., 2016](#)). In 2014, Jarrett et al. characterised a direct PKA-dependent phosphorylation on S435 of ATR, which enhanced recruitment of NER protein XPA following UV-induced DNA damage. They further characterised this event as mediated by A-kinase-anchoring protein 12 (AKAP12), which associates and is phosphorylated by ATR following damage ([Jarrett et al., 2016](#)). This work provides a mechanistic link between PKA-dependent transcription and activation of metabolic proteins, and ATR-dependent DNA repair pathways. Reduced or defective IGF-1 signalling, precursors to PKA activation, have also recently been implicated as a negative effector of ATR-CHEK1 kinase signalling axis ([Kemp et al., 2017b](#)).

Mechanisms placing mTOR effector AKT in checkpoint activation and DNA repair pathways have also been widely discussed, where increased AKT activity appears to suppress DNA damage-induced RPA foci formation and CHEK1 activation. Inhibition of AKT restores DNA-damage induced recruitment and activation of these factors ([Xu et al., 2010](#)). AKT phosphorylates TOPBP1 at a conserved S1159 residue, inducing TOPBP1

oligomerisation, which may prevent association with ATR following damage ([Liu et al., 2006](#)).

1.6. ATR protein structure

I will further discuss existing and postulated non-canonical roles of ATR in another section – prior to this, it is important to consider the protein structure of ATR.

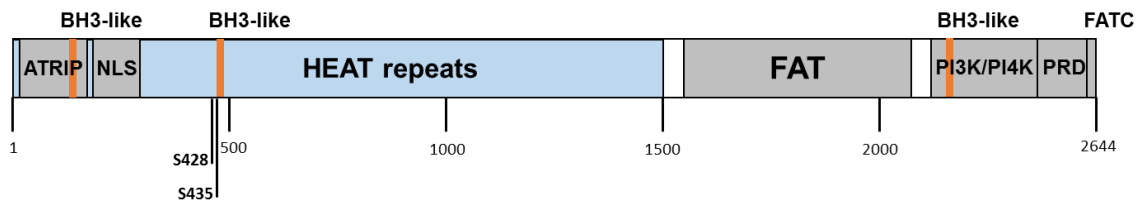


Figure 1.6. Primary ATR protein structure. ATRIP – ATRIP binding site; NLS – Nuclear localisation signal; FAT - FRAP-ATM-TRAP; PRD – PIKK regulatory domain; FATC – FAT C terminus domain. S428 – PIN1 isomerisation site; S435 – PKA-dependent phospho-site.

1.6.1. HEAT repeats

A single HEAT repeat is a structural motif consisting of two alpha helices linked by a small loop ([Yoshimura and Hirano, 2016](#)). Over half of ATR's protein structure consists of HEAT repeat units, the biological relevance of which is not fully understood ([Perry and Kleckner, 2003](#)). PIKK family members contain high levels of 'α-helicity', which only appears to differ in the arrangement and number of specific HEAT repeat units. Of the 45 HEAT repeats observed within ATR, 10 are unique and not observed in other PIKKs ([Perry and Kleckner, 2003](#)). ATM is known to interact with NBS1 via specific internal HEAT repeats ([You et al., 2005](#)), and ATRIP binds to ATR at within an N-terminal HEAT repeat domain, indicating functional relevance of the HEAT repeat domain.

Research is emerging on this structural component of the PIKK family members, where the prospective role of HEAT repeats in non-canonical activation of ATR is considered. Interestingly, FLAG-ATR purified from mammalian cells has been reported to directly interact with DNA, preferentially following UV-damage ([Ünsal-Kaçmaz et al., 2002](#)). Linearised DNA plasmids activate ATR *in vitro* in a TOPBP1-dependent manner, where stimulation of ATR again increases when the DNA is damaged by UV ([Choi et al., 2009](#)). The binding of ATR to DNA appears to be independent of RPA-ssDNA complexes. To date, the DNA-binding activity of ATR has not been isolated to a specific region. This

information gains relevance when considering two further discoveries; 1) In 2010, Sibanda *et al.* utilised X-Ray crystallography to determine the 3D structure of DNA-PK, clearly demonstrating the α -helical HEAT repeats generate a flexible cradle structure, which most likely binds to DNA ([Sibanda et al., 2010](#)); and 2) Robinson *et al.* reported in 2008 the bacterial DNA glycosylase AlkD utilises its HEAT-like repeats to bind to DNA, allowing the recognition of helical distortion induced by damage bases (Fig 1.6.1) ([Robinson et al., 2008](#)). This data opens the possibility that ATR may bind to DNA via its HEAT repeats, providing explanation of how multiple types of DNA lesions are recognised by ATR ([Nam and Cortez, 2011](#)).

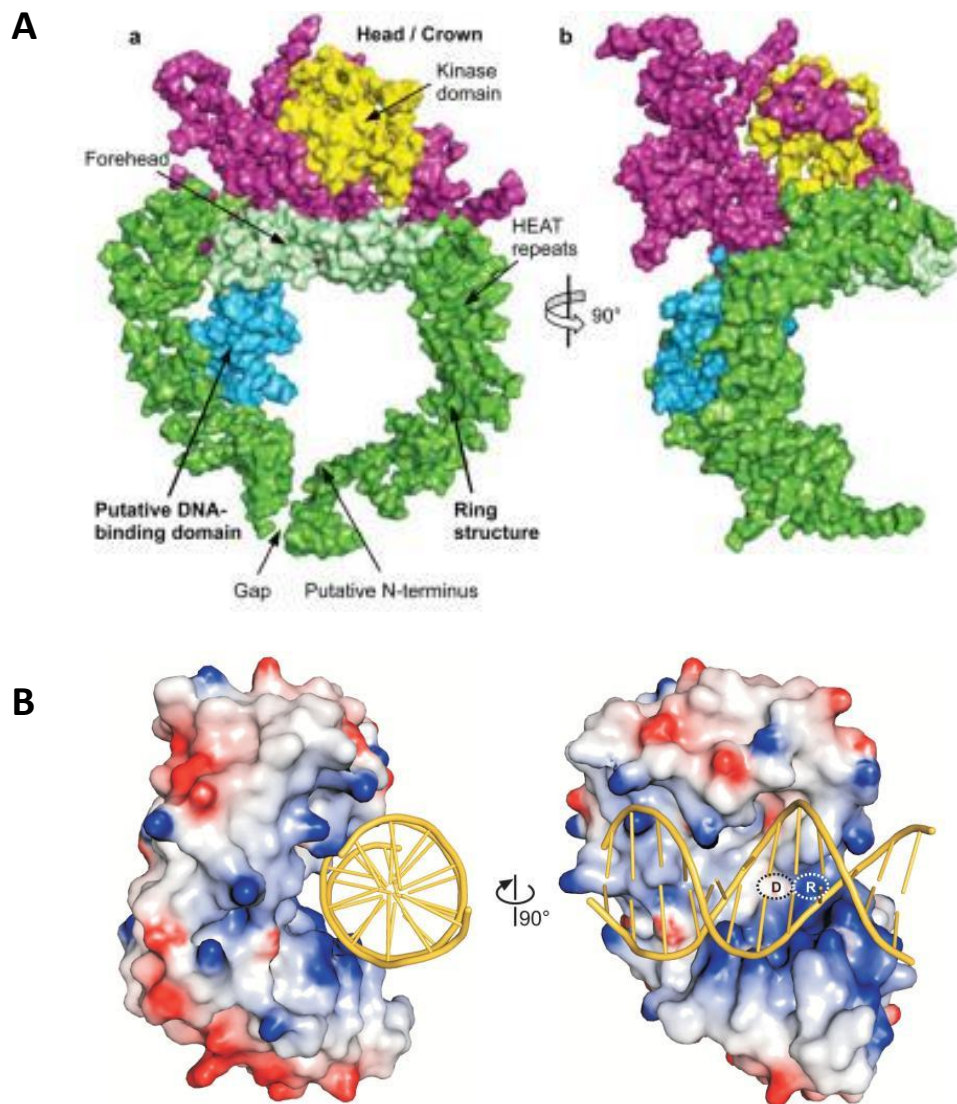


Figure 1.6.1. HEAT repeats can bind DNA. A) Crystal structure of DNA-PKcs. Taken from ([Sibanda et al., 2010](#)) **B)** Theoretical Binding of AlkD to DNA. Taken from ([Robinson et al., 2008](#))

Further to this, In 2014, Kumar et al. characterised a role for ATR HEAT repeats as a sensor of mechanical stress at the nuclear envelope ([Kumar et al., 2014](#)). Following osmotic and mechanical stress, independently of RPA and the DDR, ATR localised to the inner and outer nuclear membranes, and appeared to modulate chromatin and nuclear envelope association. The authors comment on the properties of N-terminal HEAT repeats, suggesting they could behave as ‘elastic connectors’, allowing mechanical forces influence on ATR activity.

Additionally, Mori et al. described cell death preluded by a cytoplasmic vacuolisation phenotype with moderate overexpression of ATR ([Mori et al., 2013](#)). Through expression analysis of variously sized tagged ATR-deletion constructs, they identified the N-terminus heat repeats as sufficient to induce vacuolisation, suggesting a role for ATR-HEAT repeats in cellular vacuolisation.

1.6.2. FAT and FATC

PIKKs exhibit strong sequence homology in the S/T kinase-flanking FAT and FATC regions ([Mordes and Cortez, 2008](#)). The FATC domain is required in all PIKKs for kinase activity and target protein recognition, and as FAT and FATC domains only exist together, this could be due to interaction between the two domains promoting proper folding of the kinase domain ([Jiang et al., 2006](#)). The ATR FAT domain is also the site of its activating *trans*-autophosphorylation on T1989.

1.6.3. PRD (PIKK regulatory domain) and PI3K domain

TOPBP1 activates ATR through binding to ATRIP and ATR’s PRD domain, located between the FATC and PI3K domains. Mutations in this domain result in loss of TOPBP1-induced ATR activation ([Kumagai et al., 2006](#); [Mordes and Cortez, 2008](#)). Large variations in sequence within the PRDs of different PIKK family members may allow individual responses to different regulators – ATR, ATM and mTOR are all regulated by PRD interactants ([Kumagai et al., 2006](#); [Sekulić et al., 2000](#); [Sun et al., 2007](#)). The PRD of ATM is acetylated by TIP60 inducing activation, and mutations in the PRD of DNA-PKcs interfere with function ([Mordes et al., 2008](#); [Sun et al., 2007](#)). The PI3K domain supplies ATR with its apical kinase activity – allowing the phosphorylation of substrates specifically at S/TQ motifs.

1.6.4. BH3-like domains

Three 'BH3-like' (BCL-2 homology domain 3-like) domains have recently been discovered within ATR (Fig 1.6.4). Evidence has validated the functional significance of at least one of these domains - conferring cytoplasmic ATR the ability to interact with BCL-2 family members at the mitochondria in an anti-apoptotic manner ([Hilton et al., 2015](#)). The functional relevance of these novel, BH3-like domains in relation to ATR activity is yet to be fully acknowledged, however their recognition provides further opportunity for the characterisation of previously unconsidered, non-canonical ATR interactants. Interestingly, one BH3-like domain of ATR (462-474) appears proximal to a collection of N-terminal residues that are regulated by an array of cytoplasmic enzymes (Fig 1.6). ATR-S428/P429 is a prolyl isomerase 1 (PIN1) isomerisation site ([Hilton et al., 2015](#)); ATR-S435 confers a PKA-dependent phosphorylation ([Jarrett et al., 2014](#)); ATR-S438 has been identified as a putative AKT-dependent phospho-site following insulin treatment in adipocytes ([Humphrey et al., 2013](#)). The significance on ATR function of this 'hub' of cytoplasmic interactants is yet to be fully ascertained.

	Consensus	D	X	X	X	D	K/R	X	D	A/G	D/E	Z	D	X
ATR(175-187)		M	S	R	F	L	S	Q	L	D	E	H	M	G
ATR(462-474)		L	W	S	A	L	K	Q	K	A	E	S	L	Q
ATR(2345-2357)		I	N	K	C	L	R	K	D	A	E	S	R	R
BCL2		V	H	L	T	L	R	Q	A	G	D	D	F	S
BCL-XL		V	K	Q	A	L	R	E	A	G	D	E	F	E
BCL-W		L	H	Q	A	M	R	A	A	G	D	E	F	E
MCL-1		A	L	E	T	L	R	R	V	G	D	G	V	Q
BAX		L	S	E	C	L	K	R	I	G	D	E	L	D
BAK		V	G	R	Q	L	A	I	I	G	D	D	I	N
PUMA		I	G	A	Q	L	R	R	M	A	D	D	L	N
BID		I	A	R	H	L	A	Q	V	G	D	S	M	D

Figure 1.6.4. Alignment of BH3-like consensus sites within ATR with BCL2 family members. Taken from ([Hilton et al., 2015](#))

1.7. Putative ATR/ATM substrate screens

In the last decade, several publications utilising a variety of screening approaches have identified putative, novel ATM/ATR substrates. Investigating changes in proteomic S/TQ phospho-status following DNA damage generated excellent candidates for follow-up, hypothesis-driven studies to validate novel roles for ATR and ATM. Very few of these putative, novel ATR/ATM targets have been investigated further following publication.

Of those that have, the functional significance has been validated, as novel *bona fide* ATR/ATM substrates in vivo.

1.7.1. Matsuoka *et al.*

In 2007, Matsuoka *et al.* identified over 700 putative ATM/ATR substrates, using a stable isotope labelling with amino acids in cell culture (SILAC) mass spectrometry approach (Matsuoka *et al.*, 2007). Heavy- and light-labelled samples were treated with or without IR and immunoprecipitated using a variety of phospho-SQ or phospho-TQ antibodies - bound peptides were then analysed by mass spectrometry. Peptides demonstrating a four-fold change in phospho-status after damage were considered putative substrates.

Matsuoka *et al.* utilised this approach to acquire a dataset of unbiased, putative ATR/ATM substrates in vitro. The group validated a small subset of the putative targets

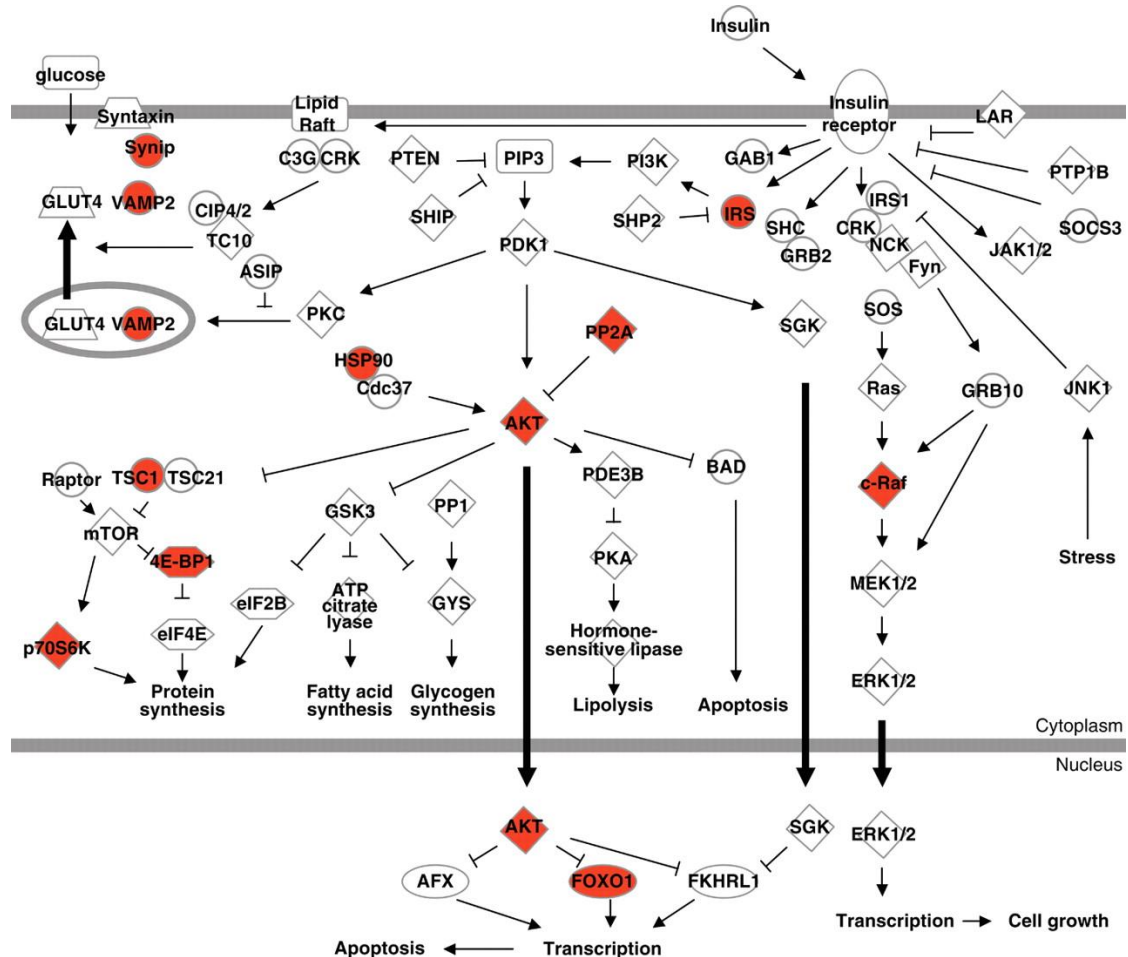


Figure 1.7.1. Network of putative ATR/ATM substrates involved in cell metabolism identified by Matsuoka *et al.* Red shading indicates putative ATR/ATM substrates after ionising radiation. FOXO1 - forkhead box protein O1; 4E-BP1 - Eukaryotic translation initiation factor 4E-binding protein 1; p70S6K - Ribosomal protein S6 kinase beta-1; VAMP2 - vesicle associated membrane protein 2; PP2A - protein phosphatase 2A. Taken from (Matsuoka *et al.*, 2007)

identified in their screen. The majority of the targets identified had roles in nucleotide metabolism and DNA repair/cell cycle checkpoints – pathways with which ATR is well established. Further from this, unexpectedly, many putative cytoplasmic targets were identified, particularly enriched in this subset were those with roles in vesicle and membrane transport, and insulin signalling and metabolism (Fig 1.7.1).

1.7.2. Stokes et al.

Stokes *et al.* also identified large numbers of novel ATR/ATM substrates in 2007, using immunoaffinity phosphopeptide isolation and mass spectrometry, but in this case, after UV damage ([Stokes et al., 2007](#)). Peptides with a 2-fold increase in intensity were considered putative ATM/ATR substrates - of 192 previously undescribed substrates recognised in this screen, roughly half were also found by Matsuoka *et al.*,. UV-induced DNA damage induces bulky lesions resulting primarily in ATR activation, suggesting the putative substrates Stokes *et al.* identified could have higher relevance within the ATR signalling axis over that of ATM.

1.7.3. Cara et al.

Established ATM and ATR substrates commonly contain clusters of highly conserved S/TQ motifs that constitute an SQ/TQ cluster domain (SCD) ([Cara et al., 2016](#)). Using a bioinformatics approach to identify SCD-containing proteins, Cara *et al.* identified over 800 putative ATM/ATR targets conserved across differing vertebrate proteomes. Interestingly, they discovered significant enrichment of SCD-containing proteins in vesicle trafficking, neural development and metabolic pathways, hinting at broad, uncharacterised cytoplasmic roles for ATM and ATR.

1.8. Established non-canonical activation of ATR

The recognition of an influence of metabolic signalling on the ATR-Chk1 axis, and the volume of putative ATM/ATR substrates identified by Matsuoka *et al.* and Stokes *et al.* in their proteomics screens has encouraged a re-approach to how ATR signalling is considered. Cytoplasmic, non-DDR roles for ATR and ATM are gaining increased recognition ([Li et al., 2009](#); [Mori et al., 2013](#); [Postigo et al., 2017](#)). Whilst cytoplasmic localisation of these proteins has been established for some time ([Cuadrado et al., 2006](#)), the implications of such have not been addressed, with the majority of ATR/ATM

research focused on DDR functions. Here I will provide a brief overview of several non-canonical roles of ATR – demonstrating how current perspectives on a metabolic role for ATR are steadily developing.

1.8.1. VAMP2

In 2009, Li *et al.* validated two novel ATM/ATR targets – VAMP2 and synapsin-I. VAMP2 (vesicle associated membrane protein 2) is a member of the synaptobrevin/VAMP family and is required for effective vesicle docking and membrane fusion of synaptic vesicles with the presynaptic membrane. Li *et al.* reported ATR and ATM within neuronal cytoplasm at levels comparable to that of the nucleus, where canonical ATM-activating DNA damage had no effect on activity of cytoplasmic ATM. They further noted defects in synaptic vesicle recycling in ATM-deficient brains. Utilising evidence from the 2007 Matsuoka *et al.* substrate screen and a site-directed mutagenesis approach, Li *et al.* validated VAMP2 and synapsin-I as a novel ATR and ATM substrates, respectively ([Li et al., 2009](#)).

Interestingly, in insulin-sensitive tissues VAMP2 is required for a similar membrane fusion process – the translocation of the vesicle-bound glucose transporter GLUT4 to the plasma membrane in response to insulin ([Ramm et al., 2000](#)). The functional relevance of impaired ATR activity on the requirement of VAMP2 in insulin-sensitive glucose uptake is yet to be ascertained – although Li *et al.* did not observe cytoplasmic ATR in insulin-sensitive NIH3T3 cells.

1.8.2. Cell metabolism - Mitochondria and Autophagy

Hilton *et al.* recently characterised an anti-apoptotic role for ATR at the mitochondria ([Hilton et al., 2015](#)). They reported *cis*- and *trans*-isomers of cytoplasmic ATR, where basal levels of *trans*-ATR were maintained by prolyl isomerase PIN1, and *cis*-ATR had unique pro-survival activity at the mitochondria following UV damage. PIN1 isomerised ATR from *cis*- to *trans*- at the phosphorylated Ser428-Pro429 motif, downregulating ATR mitochondrial activity. UV damage induced inhibition of PIN1, allowing stabilisation and interaction of pro-survival, *cis*-ATR with pro-apoptotic truncated BH3 interacting-domain (tBID) at the mitochondria, via a specific ATR BH3-like domain, exposed only in *cis*- formation. ATR-tBID binding blocked mitochondrial recruitment of pro-apoptotic

BCL2 associated X (BAX), required for initiation of apoptosis. The stabilisation of *cis*-ATR following UV appeared to be specific to cytoplasmic ATR, where nuclear *trans*-ATR remained unaffected following UV.

The group further described the mitochondrial activity of ATR as independent of ATR-kinase activity and ATRIP, suggesting a novel, non-canonical activity of cytoplasmic ATR. It is notable that ATR also interacts with BID in a canonical manner following DNA damage. BID is directly phosphorylated by ATR following DNA damage, and is required for appropriate regulation of the intra-S-phase checkpoint ([Zinkel et al., 2005](#)). Helix-4 of BID also interacts with the coiled-coil domain of ATRIP, facilitating chromatin localisation of ATR-ATRIP during replicative stress ([Liu et al., 2011](#)). Hence, it appears ATR can interact with BID in a highly context-specific manner, where immediate conditions induce differing consequences, dependent on the kinase activity and protein structure of ATR.

Another group has characterised a role for ATR and the mitochondria in yeast. In 2017, Yi et al. described a role for Mec1 (ATR) in the regulation of mitochondrial respiration following starvation-induced autophagy ([Yi et al., 2017](#)). They described Snf1 (AMPK)-dependent phosphorylation events of Mec1 at the mitochondria following glucose deprivation, resulting in recruitment of Atg1 (ULK1). The formation of a Snf1-Mec1-Atg1 complex appeared essential for the maintenance of mitochondrial respiration and subsequent autophagic induction throughout glucose starvation. Active mitochondrial respiration has recently been characterised as a prerequisite for glucose deprivation-induced autophagy ([Okamoto, 2011](#)), hence, a novel role for Mec1 in starvation-induced autophagy has been characterised here.

Mori *et al* also documented that overexpression of ATR, but not ATM, mTOR or SMG-1 resulted in autophagic cell death, suggesting tight regulation of ATR expression is crucial for cell viability ([Mori et al., 2013](#)). Taken together, these papers suggest further characterisation is required to elucidate the full influence of ATR on autophagic processing, mitochondrial maintenance and cell metabolism.

1.8.3. Viral genome replication

In 2017, Postigo et al. suggested that canonical ATR activation was possible within the cytoplasm, to promote replication of viral genomes ([Postigo et al., 2017](#)). In contrast to long-held beliefs ([Moss, 2013](#)), the group reported that smallpox virus family member *Vaccinia* recruited conserved DNA replication and repair components of the ATR signalling axis to facilitate amplification of its genome within the host cytoplasm. Using phospho-S/TQ specific antibodies and ATR/ATM inhibitors, the group noted CHK1- and ATR-dependent, cytoplasmic increases in pS/TQ status following viral infection. This increase was not due to nuclear DNA damage, as it only occurred within the cytoplasm. Although their specific conclusions are controversial in the recruitment of eukaryotic factors to the viral genome, their data further appears to reinforce the existence of multiple cytoplasmic substrates of ATR. Human Papilloma Virus 31 (HPV31) has also been reported to activate ATR-CHK1 signalling, to elevate RRM2 levels providing the dNTPs necessary for viral replication ([Anacker et al., 2016](#)).

1.8.4. Primary cilia

A functional genomic screen searching for proteins that interact with the coiled-coil domain of ATRIP identified CINP (CDK2 interacting protein) as a transient interactor, where CINP silencing induced modest defects in ATR-dependent CHK1 phosphorylation and HU sensitivity ([Lovejoy et al., 2009](#)). The function of CINP in ATR signalling remains unclear. Nam and Cortez [2011] postulated that the interaction of CINP with CEP152 (centrosomal protein 152 kDa) provided some evidence for a role of ATR and CINP in centrosomal regulation, due to mutations in both ATR and CEP152 generating the microcephalic primordial dwarfism disorder Seckel Syndrome (SS) ([Nam and Cortez, 2011](#)). Further to this, centriole appendage protein CEP164 has a role in ATR-dependent CHK1 phosphorylation following UV damage. CEP164 is also phosphorylated by and exists in complex with ATR and ATM in a DNA-damage-independent manner ([Sivasubramaniam et al., 2008](#)).

ATR localisation to the primary cilia and cilia dysfunction with ATR deficiency has been reported ([Valdés-Sánchez et al., 2013](#)). Primary cilia are chemo- and mechano-sensory organelles that transduce signals from the surrounding microenvironment into the cytoplasm ([Satir et al., 2010](#)). In 2016, Stiff et al. characterised a novel, TOPBP1-

dependent role for ATR at the primary cilia ([Stiff et al., 2016](#)). ATR-inhibited and ATR-SS cells displayed dramatically impaired cilia-dependent signalling when treated with smoothened (SMO) agonist SAG, a phenotype rescued by *ATR* overexpression. Zebrafish embryos depleted of *Atr* displayed a SS-like morphology and developmental defects typically conferred by cilia dysfunction, suggesting the observed cellular defects in cilia signalling had developmental consequences. The group conclude that defective cilia signalling may contribute to the clinical manifestation of ATR-SS.

1.8.5. *ATM*

Cytoplasmic roles of ATM are more widely established than those of ATR ([Yang et al., 2011](#)). Roles for ATM in mTORC1 suppression and pexophagy, insulin-dependent protein translation and GLUT4 translocation, endocytosis, synaptic vesicle transport and neurotransmitter release, and regulation of mitochondrial homeostasis have all been reported ([Barlow et al., 2000](#); [Halaby et al., 2008](#); [Li et al., 2009](#); [Lim et al., 1998](#); [Vail et al., 2016](#); [Yang and Kastan, 2000b](#); [Zhang et al., 2015](#)).

The clinical significance of these functions of ATR and ATM are yet to be fully understood. Insight to the essential functions of ATR can be gained through examining the congenital disorder caused by hypomorphic mutations in *ATR*, ATR-SS.

1.9. Disorders of *ATM* and *ATR*

1.9.1. Ataxia Telangiectasia (*AT*)

ATR shares a vast set of substrates with its homologue ATM ([Matsuoka et al., 2007](#)). However, ATM is non-essential – *Atm*^{-/-} mice are viable ([Kuljis et al., 1997](#)). Loss of function mutations in *ATM* generate the progressive neurodegenerative disorder Ataxia Telangiectasia (*AT*). *AT* is characterised by coordination and movement difficulties (ataxia), insulin resistance, telangiectasias (capillary dilation generating visible ‘spider-like’ clusters), predisposition to leukaemia/lymphomas and radiosensitivity ([Lavin and Shiloh, 1997](#)). The neurological features of *AT* increase in severity throughout development, where complete immobilisation often occurs towards the end of the first decade of life ([Boder and Sedgwick, 1987](#)). Ataxia appears to manifest as the affected child becomes ambulatory, whereas telangiectasias have a slightly later onset (2-8 years) ([Lavin, 2008](#)). Degenerative changes can be observed throughout the CNS and

predominantly within the cerebellum – cerebellar Purkinje cell loss appears to underlie the progressive neurodegeneration observed in AT. Interestingly, neuronal cells have high levels of cytoplasmic ATM – where cytoplasmic roles for ATM in neurotransmitter release, pexophagy and lysosomal clearance have been characterised ([Barlow et al., 2000](#); [Li et al., 2009](#); [Lim et al., 1998](#); [Yang et al., 2011](#)). However, loss of these cytoplasmic functions of ATM does not appear to generate the Purkinje cell loss observed in AT. Hypomorphic mutations in the gene encoding MRN complex member MRE11 generates AT-Like disorder (ATLD) – characterised by similar neurodegeneration to AT ([Taylor et al., 2004](#)). MRE11 enables ATM activation at sites of DNA DSBs, indicating that deficits in ATM-dependent DSB repair are more likely to generate this aspect of the syndrome.

Furthermore, AT patients are immunocompromised. ATM appears to stabilise DNA-DSB complexes during V(D)J recombination, as well as having a role in immunoglobulin class switch recombination ([Bredemeyer et al., 2006](#); [Lumsden et al., 2004](#)). Loss of ATM here results in increased instability of these DSB-dependent processes, generating lymphopenia and increased oncogenic translocations at antigen receptor loci. Increased translocations at T-cell receptor (TCR) loci have the pathological consequence of lymphoma predisposition, also observed in AT.

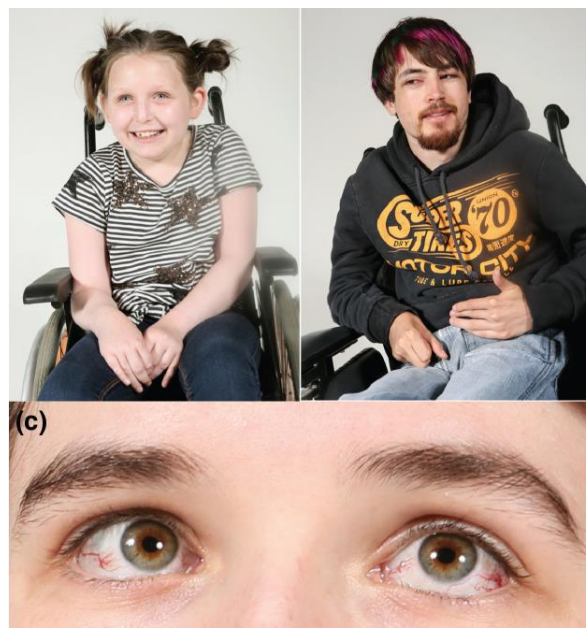


Figure 1.9.1. Loss of function mutations in *ATM* generate Ataxia Telangiectasia. Patients at 10 years (top left) and 22 years (top right). Bottom panel shows ocular telangiectasia observed in AT. Taken from ([Taylor et al., 2015](#))

Additionally, AT is characterised by insulin resistance and diabetes - ATM appears to have a role in insulin signalling – where insulin-induced ATM-dependent phosphorylation of eIF-4E-binding protein 1 (4EBP1) at S111 is required for insulin-dependent initiation of translation ([Yang and Kastan, 2000a](#)). It is postulated that through this mechanism, ATM deficiency generates the metabolic aspects of AT.

1.9.2. Seckel Syndrome

Hypomorphic mutations in *ATR* cause the severe disorder ATR-Seckel Syndrome (ATR-SS - OMIM 210600) ([O'Driscoll et al., 2003](#)). Seckel Syndrome (SS) describes many unspecified and diverse forms of microcephalic primordial dwarfism. Clinically and genetically heterogeneous, SS is characterised by intrauterine and postnatal growth retardation, atypical facial features, mental retardation and failure to thrive ([Majewski et al., 1982](#)). Among these striking clinical features, ATR-SS patients also display a marked reduction in subcutaneous fat ([O'Driscoll et al., 2004](#)), which is more often clinically associated with metabolic dysfunction (Fig 1.9.2).



Figure 1.9.2. Seckel Syndrome generated by mutations in *ATRIP* and *ATR*. A) ATR-SS generated by compound heterozygous mutations in *ATR*. Patient shows lipodystrophy of the face and marked reduction in ATR expression from B-cell lymphoblastoid samples (LBLs). Taken from ([Mokrani-Benhelli et al., 2013](#)) B) SS generated through compound heterozygous mutations in *ATRIP*. Facial lipodystrophy is apparent, and reduced ATRIP and ATR are shown in patient LBLs. Modified from ([Ogi et al., 2012](#))

A single 2101A-G transition in *ATR* represents the first mutation associated with ATR-SS. This mutation was shown to affect splicing efficiency, resulting in almost undetectable expression levels of ATR. However, this splicing defect appears 'leaky', where a fraction of ATR sufficient for viability is expressed ([O'Driscoll et al., 2003](#)). Additional compound heterozygous mutations in *ATR* have also been identified as underlying SS (Fig 1.9.2.A) ([Mokrani-Benhelli et al., 2013](#); [Ogi et al., 2012](#)). Compound heterozygous mutations in *ATRIP*, generating a C-terminal truncation and splicing defects of ATRIP have also been identified in patients with SS, phenocopying ATR-SS, exhibiting reduced ATR expression and an impaired ATR-DDR signalling axis (Fig 1.9.2.B) ([Ogi et al., 2012](#)).

To date, over 100 disease-causing mutations in *ATR* have been discovered (Table 1.9.2). Interestingly, other SS-causing mutations have been characterised in several genes encoding proteins associated with mitotic spindle formation and centrosome and kinetochore function, including centromere protein J (CENPJ), centrosomal protein 152 (CEP152), ninein, and CTBP-interacting protein (CtIP) ([Alcantara and O'Driscoll, 2014](#)). CENPJ has roles in centrosomal biogenesis, spindle assembly and disassembly, as well as controlling centriole length and duplication ([Chen et al., 2006](#); [Schmidt et al., 2009](#)). CEP152 is a centrosomal scaffold protein, controlling centriole duplication via interaction with CENPJ ([Guernsey et al., 2010](#)). Ninein is essential for asymmetric division – required for centriole organisation and microtubule anchoring ([Dauber et al., 2012](#)). CtIP has an essential role in homologous recombination DSB repair (HRR) – without functional CtIP, DSB end resection is impaired, preventing the generation of RPA-ssDNA, suppressing ATR activation ([Qvist et al., 2011](#)). Centrosome and spindle pole orientation have essential roles in asymmetrical cell division during brain development. A failure to maintain centrosome stability and function during development is ascribed as a potential contributor severe microcephaly observed in SS ([Alderton et al., 2004](#)). Interestingly, SS generated by mutations in genes encoding centrosomal proteins does not appear to have equivalent lipodystrophy to SS generated by hypomorphisms in *ATR/ATRIP*, although ciliopathies are commonly associated with metabolic syndrome ([Waters and Beales, 2011](#)).

Location on ATR	VariationID	Location on ATR	VariationID
c.7875G>A (p.Gln2625=)	93669	c.4218G>A (p.Ala1406=)	343607
c.7725G>A (p.Ala2575=)	158004	c.4002G>A (p.Gln1334=)	157981
c.7667C>G (p.Thr2556Ser)	343581	c.3945+2dupT	343608
c.7471G>A (p.Val2491Ile)	343582	c.3799G>A (p.Val1267Ile)	157980
c.7359_7361dupTAG (p.Ser2453_Arg2454insSer)	343583	c.3497A>C (p.His1166Pro)	343610
c.7300C>G (p.Pro2434Ala)	158003	c.3477G>T (p.Met1159Ile)	156536
c.7274G>A (p.Arg2425Gln)	136470	c.3424A>G (p.Ser1142Gly)	157977
c.7041+4G>C	158002	c.3120G>A (p.Leu1040=)	157975
c.6961T>C (p.Phe2321Leu)	158001	c.2875G>A (p.Val959Met)	157974
c.6960G>A (p.Lys2320=)	343584	c.2844A>C (p.Ala948=)	157973
c.6897+464C>G	156537	c.2776T>C (p.Phe926Leu)	343612
c.6896T>C (p.Met2299Thr)	343585	c.2688G>A (p.Leu896=)	157972
c.6339A>G (p.Val2113=)	157999	c.2653G>A (p.Val885Ile)	343613
c.6259A>G (p.Met2087Val)	343586	c.2532+4G>A	343614
c.6226C>G (p.Leu2076Val)	343587	c.2503T>C (p.Leu835=)	343615
c.6221+3G>A	343592	c.2442A>G (p.Glu814=)	157971
c.6197G>A (p.Arg2066Gln)	343593	c.2226T>C (p.Cys742=)	343616
c.6090G>A (p.Ala2030=)	343594	c.2022A>G (p.Gly674=)	8307
c.6079-14G>A	343595	c.1950G>A (p.Glu650=)	157968
c.6078+10T>C	343596	c.1885+7G>A	343617
c.5987T>C (p.Met1996Thr)	343597	c.1815T>C (p.Asp605=)	157966
c.5899-8delT	343598	c.1784C>T (p.Ser595Leu)	343618
c.5868C>T (p.Tyr1956=)	157996	c.1776T>A (p.Gly592=)	157965
c.5739-14_5739-6delGTTACTTCCinsT	343599	c.1350-3T>C	157964
c.5739-14G>T	157995	c.1326A>G (p.Lys442=)	157962
c.5732A>G (p.Asn1911Ser)	157994	c.1318C>T (p.Pro440Ser)	343619
c.5635G>T (p.Asp1879Tyr)	41901	c.1006C>T (p.Arg336Trp)	343620
c.5572T>C (p.Cys1858Arg)	343600	c.946G>A (p.Val316Ile)	158006
c.5460T>C (p.Tyr1820=)	136471	c.632T>C (p.Met211Thr)	93668
c.5349G>T (p.Gln1783His)	343601	c.489T>C (p.Asn163=)	343621
c.5208T>C (p.Tyr1736=)	157992	c.483A>G (p.Arg161=)	157990
c.5052T>C (p.His1684=)	343602	c.436A>G (p.Thr146Ala)	343622
c.4835A>G (p.Asn1612Ser)	157989	c.431T>G (p.Val144Gly)	343623
c.4820G>A (p.Ser1607Asn)	343603	c.423T>C (p.Ile141=)	157983
c.4764C>T (p.Leu1588=)	210490	c.325C>T (p.Arg109Trp)	343624
c.4677C>T (p.Asp1559=)	210489	c.292+15T>G	343625
c.4641+15C>T	157987	c.268C>T (p.His90Tyr)	235760
c.4641+1G>T	210488	c.260G>T (p.Ser87Ile)	343626
c.4407C>T (p.Thr1469=)	343604	c.225C>T (p.Ile75=)	343627
c.4382+6T>C	343605	c.190A>G (p.Thr64Ala)	343628
c.4351C>T (p.Arg1451Trp)	157985	c.152-9T>C	343629
c.4323A>G (p.Gln1441=)	343606	c.-46_-9del38insT	343631
c.4306A>G (p.Asn1436Asp)	157984	c.-91C>G	343632

Table 1.9.2. Documented ATR mutations that generate Seckel Syndrome. ‘=’ indicates no change.

Sourced from <https://www.ncbi.nlm.nih.gov/clinvar> (August 2017)

Nuclear fragmentation, micronuclei formation, impaired phosphorylation of ATR-dependent substrates, increased centrosome number and defective G2/M arrest are common features of SS patient cell lines ([Alderton et al., 2004](#)). This indicates that as well as enhanced replicative stress, defective mitotic checkpoint function can underlie the clinical features associated with SS. More recently, ATR-SS has been

characterised as a ciliopathy disorder, where impaired cilia function is postulated as a contributor to the clinical manifestation ([Stiff et al., 2016](#)). Appropriate centrosome functionality is required for the formation of primary cilia, and ATR-SS cells display modest defects in cilia function and formation (described in more detail in section 1.7.4).

Considering ATM and ATR have significant homology and vastly overlapping substrate sets following DNA damage, striking contrast exists between the clinical presentations of the congenital disorder of each protein. Currently, the underlying basis of this distinction is unknown. Why centrosomal proteins and ATR converge, where mutations in either result in the clinical manifestation of SS is also unclear, although roles for ATR in the spindle assembly checkpoint and centrosome function are postulated ([Brown and Costanzo, 2009](#); [Katsura et al., 2009](#)). In the context of impaired prenatal neuronal development, SS does share similarities with a variety of other DDR syndromes ([O'Driscoll and Jeggo, 2003](#)); mutations in genes encoding DNA repair pathway proteins often generate disorders characterised by cancer predisposition and neurological deficits ([Kerzendorfer and O'Driscoll, 2009](#)). It is likely that the underlying cause of the neurological deficits observed within ATR-SS and other congenital DDR disorders is due to a striking sensitivity of neuronal tissue to unrepaired DNA lesions and replicative stress.

The development of several functionally distinct mouse models of ATR deficiency has allowed further investigation into the impacts of reduced ATR function.

1.10. Mouse models of ATR deficiency

1.10.1. Atr^{-/+} mouse

Brown and Baltimore (2000) demonstrated that *Atr*^{-/-} mice are embryonic lethal due to the requirement of ATR for early embryonic cellular proliferation ([Brown and Baltimore, 2000](#)). In this study, heterozygosity of *Atr* led to increased tumour incidence. However, they were unfortunately unable to confirm if tumours from the *Atr*^{-/+} mice had lost heterozygosity of *Atr*.

1.10.2. Inducible Atr deletion mouse

A study investigating the conditional deletion of *Atr* in adult mice confirmed that the most marked clinical features of SS originate from reduced *Atr* expression during

embryonic development ([Ruzankina et al., 2007](#)). Using the tamoxifen-inducible CRE-ERT2 promoter system in adult mice to selectively delete *Atr*, the group circumvented the early embryonic lethality related to deficiencies in ATR during development. However, successful recombination and deletion of the *Atr^{flox}* allele was not achieved in a significant minority of cells, rendering the cellular phenotype of this transgenic mouse closer to a mosaic of *Atr^{flox}*- and *Atr^Δ* expression. Interestingly, 3 months after inducing *Atr^{mKO}* (*Atr* mosaic knockout) in adult mice, animals displayed a 70% decrease in their subcutaneous adipose layer, leading to a 20% lower body weight compared to control mice after 1 year (Fig 1.10.2) ([Ruzankina et al., 2007](#)). The group reported this phenotype as the result of a depletion of the cycling sub-population of stem progenitors (required to sustain and replenish the adipocyte population), due to the inherent toxicity of ATR deficiency in cycling cells. However, they did not characterise further whether the sharp decrease in subcutaneous fat tissue was due to cell death, or reduced intracellular lipid content, hence the potential for a role of ATR in maintaining appropriate lipid metabolism remains unchallenged.

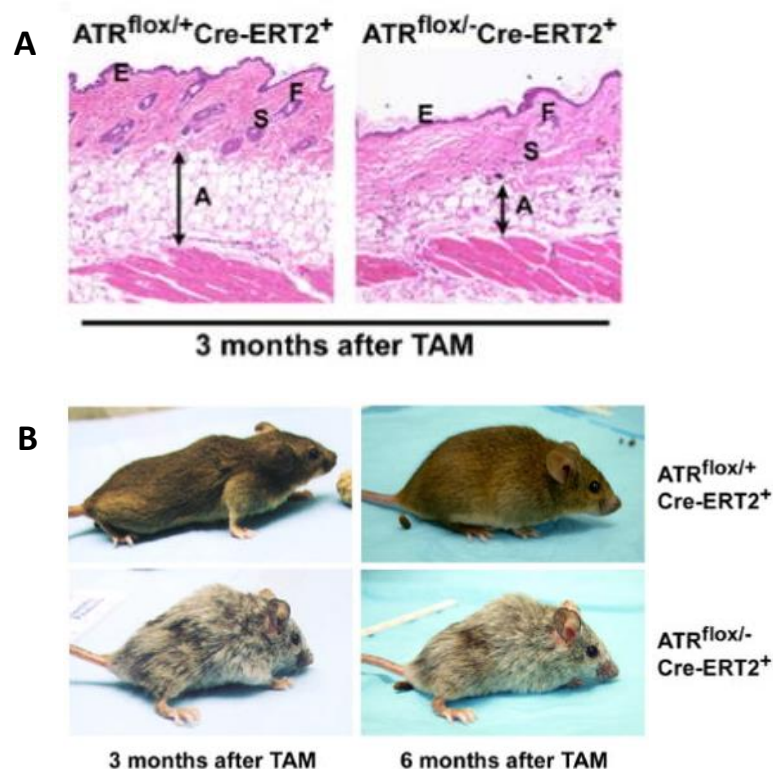


Figure 1.10.2. Abnormalities of subcutaneous fat and accelerated ageing 3 months after induced knockdown of *Atr* in adult mouse. A) Significant reduction in white subcutaneous adipocyte layer of *Atr^{mKO}* mice after 3 months (marked A). **B)** Accelerated ageing observed in *Atr^{mKO}* mice. Modified from ([Ruzankina et al., 2007](#))

Although the group summarised their results with the conclusion that ATR activity appeared to be unessential for the homeostasis of non-dividing cells, this contradicts their observation that the subcutaneous adipose tissue layer was vastly depleted. Very little research into the life-span of rodent adipocytes has been undertaken ([Lee et al., 2010](#)), however it is roughly estimated the life span of rodent and human adipocytes is 3-6 months and 5-10 years respectively ([Neese et al., 2002](#); [Rigamonti et al., 2011](#); [Spalding et al., 2008](#)). Having an established rate of turnover of murine WAT is relevant here to contextualise the disappearance of subcutaneous fat layer in the *Atr*^{mKO} mouse.

1.10.3. Humanised *Atr*^{S/S} mouse

The SS-generating *ATR* A2101G mutation will not generate SS when mutated in mouse *Atr*, due to significant differences in the layout of introns within each orthologue ([Ragland et al., 2009](#)). To address this, and generate a mouse model which faithfully recapitulated the *ATR*^{S/S} mutation and almost all the clinical features characteristic of SS, Murga *et al.* introduced a region of human genomic *ATR* incorporating A2101G and adjacent introns into the mouse *Atr* locus ([Murga et al., 2009](#)). Interestingly, *Atr*^{S/S} mice died within 6 months of birth, exhibiting a ‘cachexic’ appearance and an accelerated aging phenotype. The authors also noted a suppressed IGF-1/growth hormone axis, which could have impacted the growth retardation phenotype. Although a dampened somatotrophic axis is associated with genotoxic stress and progeria ([Bartke, 2005](#)), this is a noteworthy phenotype as components of the insulin signalling pathway have been identified in several screens as putative ATM/ATR substrates (described further in section 1.8) ([Cara et al., 2016](#); [Matsuoka et al., 2007](#); [Stokes et al., 2007](#)). Furthermore,

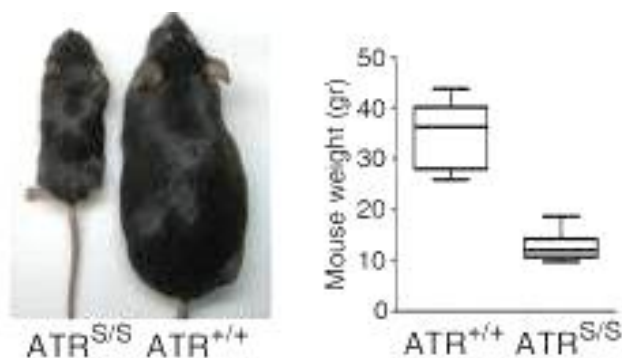


Figure 1.10.3. Humanised *Atr*^{S/S} mouse exhibiting severe microcephaly, low birth weight and dwarfism, characteristic of ATR-SS. Modified from ([Murga et al., 2009](#))

the authors implied a role for ATR in the maintenance of stem cell progenitors due to the development of pancytopenia (loss of all blood cell types) in $ATR^{S/S}$ mice.

1.10.4. $p53^{-/-}/ATR^{S/S}$ mouse

Murga *et al.* observed increased accumulation of p53 and accelerated ageing in $ATR^{S/S}$ mouse embryos; mouse models of increased p53 activity often display accelerated aging phenotypes ([Maier et al., 2004](#); [Tyner et al., 2002](#)). In an attempt to mitigate against the aging phenotypes, the group explored the effect of p53 deficiency on $ATR^{S/S}$ mice. Surprisingly, $ATR^{S/S}/p53^{-/-}$ double mutant animals were born at sub-mendelian ratios, with more dramatic ageing phenotypes than observed in the $ATR^{S/S}$ mice alone. Due to this, $ATR^{S/S}/p53^{-/-}$ mice did not survive further than 2 months. Further to this, the group characterised the enhanced cytotoxicity of $ATR^{S/S}/p53^{-/-}$ as due to increased replicative stress and apoptosis.

In this manner, Murga *et al.* proposed that although ATR haploinsufficiency was tumorigenic; in striking contrast, near-complete inhibition of ATR function appeared to have a cytotoxic effect on $p53^{-/-}$ cells - indicating the therapeutic potential of ATR inhibitors in the selective elimination of p53-deficient tumours ([Murga et al., 2009](#)). Following from this crucial discovery, subsequent investigation has generated understanding of the true potential of small molecule kinase inhibition of ATR (ATRIs) as novel cancer chemotherapeutic agents.

1.10.5. $p53^{-/-}/Atr^{mKO}$ mouse

In the same year, Brown and colleagues also characterised the effects of $p53^{-/-}$ on the adult conditional *Atr* deletion mouse model ([Ruzankina et al., 2009a](#)). Mosaic deletion of *Atr* in adult $p53^{+/+}$ and $p53^{-/-}$ mice was induced with tamoxifen as previously described ([Ruzankina et al., 2007](#)), where adult $p53^{-/-}/Atr^{mKO}$ animals were characterised by cells carrying excessive levels of DNA damage, and synthetic lethality. The enhanced toxicity of $p53^{-/-}/Atr^{mKO}$ in adult mice further reinforced the concept of synthetic lethality between p53-deficient cells and ATR knockdown, evidencing for the first time a specific synthetic interaction between ATR and p53 inhibition in adult mammals ([Ruzankina et al., 2009a](#)).

Mouse models have demonstrated that complete inhibition of ATR function appears to confer selective synthetic lethality in p53-deficient tissues, making it an exciting target for cancer therapy. However, ATR haploinsufficiency also has roles in cancer progression, suggesting a narrow therapeutic window for the use of ATRis. In the next section, I will discuss the roles of ATR as a putative therapeutic target and also as a driver of cancer progression. I will further discuss existing and postulated synthetic lethal approaches in cancer therapy, the development of bioavailable ATRis, and their current standing in clinical trials.

1.11. Cancer and the DDR

DNA damage is inducible from a variety of genotoxic agents. If left unrecognised or inappropriately repaired, lesions can result in the stable incorporation of mutations into the genome. Deleterious mutations carry the potential to induce aberrant cellular behaviour, resulting in malignancies such as cancer ([Hoeijmakers 2009](#)).

The DDR axis inhibits the proliferation of cells lacking genomic integrity, and deviations from typical DDR activity are intimately linked with malignant transformation. The transformation of pre-malignant cells requires increased rates of mutagenesis, and increasing genomic instability generated by compromised DDR function enhances this process ([Halazonetis et al., 2008](#)). Many hereditary cancer predisposition disorders are the result of deleterious germline mutations in DDR proteins or oncogenic effectors, and almost all tumours show functional loss or deregulation of DDR proteins ([Jeggo et al., 2016](#)). Most frequently mutated and notable of these DDR proteins are ATM and tumour suppressor protein p53 ([Cremona and Behrens, 2014](#); [Muller and Vousden, 2013](#)).

1.11.1. Oncogenes

The RAS-MAPK pathway is an essential regulator of cell growth, proliferation, differentiation and senescence pathways ([Aksamitiene et al., 2012](#)). Hence, somatic RAS mutations are highly oncogenic, endowing tumorigenic cells the necessary hallmark for carcinoma development - self-sufficiency in growth signalling ([Pylayeva-Gupta et al., 2011](#)). Oncogenic activation of RAS through numerous mutations is observed in around 20% of all cancers ([Bos, 1989](#)). Oncogenic RAS isoforms (H-RAS, K-RAS and N-RAS) have key roles in malignant transformation, but they also increase the replicative stress

burden within the cell due to increased and aberrant gene transcription ([Kotsantis et al., 2016](#)), increasing the cancer cell dependence on ATR. Schoppy *et al.* and other groups have shown ATR inhibition increases cancer cell sensitivity to oncogene-induced replication stress, resulting in synthetic lethality ([Gilad et al., 2010](#); [Schoppy et al., 2012](#)).

1.11.2. ATR haploinsufficiency

Haploinsufficiency of *ATR/CHK1* is seen in cancer cells exhibiting high microsatellite instability and defective mismatch repair (MMR), most often endometrial, colon and stomach cancers ([Fang et al., 2004](#); [Lewis et al., 2007](#); [Lewis et al., 2005](#)). Gilad *et al.* demonstrated ATR haploinsufficiency in an oncogenic RAS context could act as a driver for oncogenic mutations ([Gilad et al., 2010](#)).

A more recent study has also shown that cancer cell ATR mutations can also modulate the tumour microenvironment through altered expression of inflammatory genes and increased recruitment of pro-tumorigenic macrophages ([Chen et al., 2017](#)). The group noted that 7-13% of melanomas appeared to have loss-of-function mutations in the ATR signalling pathway (ATR or CHK1).

Hypomorphic mutations of ATR have been characterised as the underlying genetic basis of the disorder ATR-SS. Interestingly, a unique pedigree containing 24 individuals with defective ATR function has also recently been characterised. The affected individuals are heterozygous for germline mutations in ATR, resulting in an autosomal-dominant cancer syndrome ([Tanaka et al., 2012](#)). The associated condition comprised of oropharyngeal cancers, skin telangiectases and mild developmental abnormalities of hair, teeth and nails. The authors identified a single mutation (c.6431A>G) that occurred within the p53-activating FAT domain of ATR. Cultured patient fibroblasts showed a compromised ATR-p53 axis following DNA damage, whilst maintaining functional ATR kinase activity. Loss of heterozygosity at the ATR locus was noted in the oropharyngeal tumour tissue, suggesting the underlying ATR mutation is neomorphic, due to its ability to drive tumour formation ([Tanaka et al., 2012](#)).

The cancer predisposition and telangiectasia aspects of this condition bear undeniable similarities to other congenital disorders of the DDR. Mutations resulting in the loss of function of ATR homologue ATM underlie neurodegenerative disorder AT, in

which ocular, skin and pharyngeal telangiectases are common ([Taylor et al., 2015](#)). Further, Fanconi anemia, an autosomal-recessive cancer syndrome caused by defects in several DDR proteins, many of whom are phosphorylated by ATR, is also associated with epithelial cancers ([Wang, 2007](#)).

Further characterisation of this novel mutation in *ATR*, and the pathological consequences of complete homozygosity within an organism is essential. Juxtaposed against the *ATR*-SS mouse, a homozygous mouse model could provide a unique opportunity to uncouple the putative, metabolic impacts of reduced ATR function from its canonical role in DNA repair. Defects in ATR activity increase genomic instability, which can cause either synthetic lethality or enhanced tumorigenesis, dependent on the level of ATR activity. They reinforce the importance of genotyping and assessing tumour heterogeneity for the effective use of synthetic lethality approaches. Utilising a ‘personalised’ genetic approach will prove essential in the targeted treatment of cancer with ATRis.

1.11.3. Synthetic lethality

The DDR carries important implications for the efficacy of cancer therapies. Conventional cancer treatments such as chemo- and radiotherapy act as sensitizers - targeting proliferating tissues in a relatively non-specific manner by increasing the cytotoxic load of DNA damage – cancerous cells are sensitised due to their high proliferative activity and genomic instability ([Bruce and Jay, 2015](#)). However, the relatively non-specific nature of these therapies results in severe side effects, greatly limiting their therapeutic window. Cancers can also resist chemo- and radiotherapies through the acquisition of further mutations to re-activate various DDR pathways ([Holohan et al., 2013](#)). Existing DNA damage-based cancer therapies often fail to be curative.

The increased genomic instability seen in cancers, due to defective branches of the DDR, has also more recently been widely studied as an exploitable target based on synthetic lethal approaches. Synthetic lethality exploits the uniquely exposed vulnerabilities in cancer cells that come hand in hand with favourable carcinogenic mutations. Defective DDR pathways allow cancers elevated rates of mutagenesis and

growth progression, but also drive dependence on the remaining functional DDR components to survive the increased burden of genomic instability. Healthy cells carry the protective redundancy of multiple, functional DDR pathways. Targeted inhibition of the key DDR components that remain in cancer cells results in a highly selective and potent toxicity, due to the resulting acquisition of insurmountable DNA damage in the absence of an appropriate DDR axis ([Beijersbergen et al., 2016](#); [Gilad et al., 2010](#); [Iglehart and Silver 2009](#)).

The synthetic lethality approach was initially demonstrated in *BRCA2*-deficient cancer cells ([Bryant et al., 2005](#); [Farmer et al., 2005](#)). Germline mutations in genes *BRCA1* and *BRCA2* can result in enhanced susceptibility to ovarian, breast and prostate cancers. *BRCA1/2* are essential for homologous recombination (HR) ([Powell and Kachnic, 2003](#)) – with no functional HR pathway, *BRCA2*^{-/-} cancer cells show enhanced dependence on the repair of DNA SSBs to maintain viability, which can be targeted using small molecule inhibitors of PARP1. PARP1 is required for the detection and repair of SSBs via the BER pathway, and PARP1 inhibition results in synthetic lethality in *BRCA2*^{-/-} cancers (Fig 1.11.3). Cancerous cells enter mitosis with largely incomplete DNA replication and experience elevated replicative stress, causing selective cell death ([Nghiem et al., 2001](#)). The first-in-class PARP inhibitor olaparib was approved for use in *BRCA1* or *BRCA2* mutated cancers in 2014, showing milder side effects than conventional therapies ([Frampton, 2015](#)).

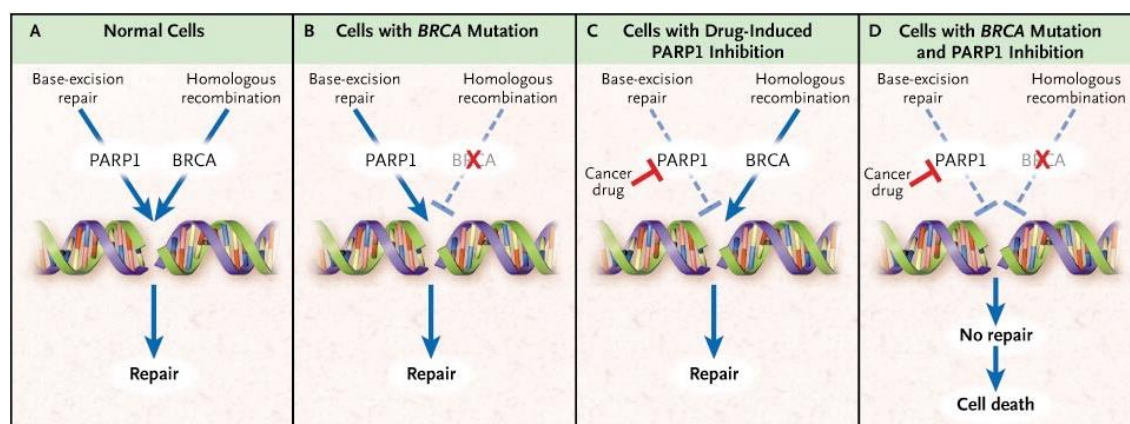


Figure 1.11.3. Synthetic lethality concept of PARPi on BRCA-defective tumours. Taken from ([Iglehart and Silver 2009](#))

ATR inhibition has been widely discussed as a potential, novel anti-cancer agent due to its selective toxicity profile ([Peasland et al., 2011](#); [Reaper et al., 2011](#)). Almost all cancer cells have defective G1 checkpoint activity ([Ho and Dowdy, 2002](#)). This leads to increased dependence on the ATR-dependent intra-S- and G2/M-phase cell cycle checkpoints. Whilst G1-proficient cells remain unaffected, impairing ATR function in G1-defective cells results in premature mitotic entry, mitotic catastrophe and cell death ([Brown and Baltimore, 2000](#)), hence further enhancing the sensitivity of cancerous cells to ATRis.

ATR appears to be essential for maintaining homeostasis in all proliferating tissues ([Ruzankina et al., 2007](#)). However, Schoppy *et al.* found incomplete inhibition of ATR (reducing expression to <10%) was sufficient to induce synthetic lethality in RAS-mutated tumours, without affecting normal proliferative tissues ([Schoppy et al., 2012](#)). Additionally, Vendetti *et al.* reported ATRi synergistic killing with cisplatin in K-RAS mutant tumours ([Vendetti et al., 2015](#)). Jardim *et al.* also demonstrated that ATR/CHK1-defective MMR-deficient cells display enhanced sensitivity to 5-fluorouracil, a commonly used colorectal chemotherapeutic whose clinical use is limited by drug resistance ([Jardim et al., 2009](#)). This suggests therapeutic value of using combination treatment of 5-fluorouracil and ATR inhibition in MMR-deficient cancers. Collectively, this data suggests is a therapeutic window for the use of ATRis in cancer.

1.11.4. Development of ATR inhibitors (ATRis) and ATRi Clinical trials

There appears to be remarkable promise for the use of small molecule ATR kinase inhibitors (ATRis) in ATM- and p53- defective cancers ([Hurley et al., 2006](#); [Ruzankina et al., 2009b](#)), as well as effectively enhancing the selective cytotoxicity of other anticancer drugs including cisplatin and PARP Inhibitors ([Peasland et al., 2011](#); [Reaper et al., 2011](#)).

Small molecule kinase inhibitors of ATR have only recently been developed. Following from their work in the humanised ATR^{S/S} mouse, Fernandez-Capetillo and colleagues developed a cell-based screening approach to identify compounds with ATR inhibitory activity ([Toledo et al., 2011](#)). Using a retroviral system, in which an inducible ATR-stimulating fragment generated enhanced levels of ATR-dependent H2AX phosphorylation (γ H2AX), Toledo *et al.* investigated the impact of over 600 compounds

on ATR activity. Through this technique, the group identified the first compounds with selective ATR inhibitory activity, most notably the dual PI3K/mTOR inhibitor NVP-BEZ235 ([Toledo et al., 2011](#)). Within the same year, Peasland *et al.* characterised ATRi activity of the compound NU6027, originally developed as a CDK2 inhibitor ([Peasland et al., 2011](#)).

1.11.4.1. Vertex Pharmaceuticals

In 2011 Vertex Pharmaceuticals reported the first highly potent and selective ATRi VE-821 ([Charrier et al., 2011](#)). VE-822 (also known as VX-970 – now acquired by Merck) is a VE-821 analogue with improved solubility, potency and selectivity against ATR (Table 1.11.4.1). Pre-clinical studies utilising these inhibitors have validated ATR as a novel therapeutic target *in vitro* – where treatment sensitized cancer cells to cisplatin, ionising

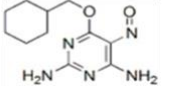
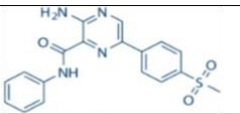
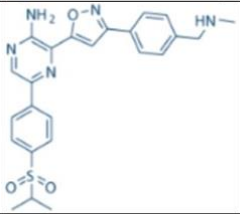
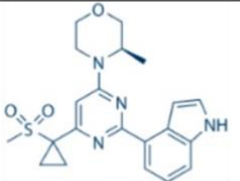
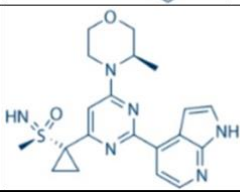
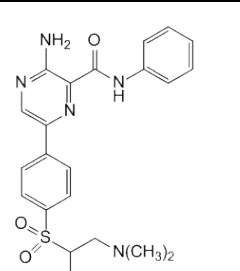
Name	Structure	ATR IC ₅₀	Specificity
NU6027		1 nM	ATR, CDK1 (K _i = 2.5 μM), CDK2 (K _i = 1.3 μM)
VE-821		26 nM	>100-fold ATR vs. ATM/DNA-PK
VE-822/ VX-970		0.2 nM	>100-fold ATR vs. ATM/DNA-PK
AZ20		5 nM	>600-fold ATR vs. ATM/DNA-PK/PI-3K
AZD6738		1 nM	ATR
ATR kinase inhibitor II		12 nM	ATM, DNA-PK (IC ₅₀ > 8 μM)

Table 1.11.4.1. ATR inhibitor molecular structures. Modified from ([Rundle et al., 2017](#))

radiation, PARP inhibitors and other therapies ([Fujisawa et al., 2015](#); [Jossé et al., 2014](#); [Prevo et al., 2012](#); [Vávrová et al., 2013](#)). In xenograft models, VE-822 restored cisplatin sensitivity to resistant tumours, and both VE-821 and VE-822 synergised with radiation and other therapies in pancreatic cancer models ([Hall et al., 2014](#); [Reaper et al., 2011](#)).

1.11.4.2. AstraZeneca

AstraZeneca also generated potent and highly selective ATRis. AZ20 and its orally available analogue AZD6738 (Table 1.11.4.1) were reported in 2013 ([Foote et al., 2013](#)). AZD6738 is reported to have single agent activity in p53- and ATM- deficient tumours, and synergistic anti-tumour activities similar to VE-821 and VE-822 ([2015](#); [Vendetti et al., 2015](#)).

1.11.4.3. Clinical Trials

With proof-of-principle and mechanistic evidence for their therapeutic benefits established, VE-822 and AZD6738 are in early phase clinical trials (Table 1.11.4.3). Taken intravenously, VE-822 is reported as generally well tolerated as a monotherapy, and in combination with carboplatin, with no dose-limiting toxicities. AZD6738 is the first orally

Agent	Phase	Combination	Indication	NCT No.
VE-822	1	irinotecan	Advanced solid tumours	NCT02595931
	1	Veliparib + Cisplatin	Advanced solid tumours	NCT02723864
	1, 2	Topotecan	Advanced small cell lung, cervical, endometrial, ovarian cancers	NCT02487095
	2	Gemcitabine	Advanced ovarian/fallopian tube/primary peritoneal cancer (OC/FT/PP)	NCT02595892
	2	Carboplatin/Gemcitabine	Advanced OC/FT/PP	NCT02627443
	2	Cisplatin/Gemcitabine	Advanced urothelial cancers	NCT02567409
	1	Cisplatin/Radiotherapy	Locally advanced HPV negative SCC head and neck cancers	NCT02567422
	1	Whole brain radiotherapy	Non-small cell lung cancers with brain mets	NCT02589522
	1	Gemcitabine, Cisplatin, Etoposide, Carboplatin	Multiple including p53mut NSCLC, triple neg breast cancers	NCT02157792
AZD6738	1	Single agent and with radiotherapy	Advanced solid tumours	NCT02223923
	1	Paclitaxel	Advanced solid tumours	NCT02630199
	1	Carboplatin, Olaparib, MEDI4736	Advanced solid tumours	NCT02264678

Table 1.11.4.3 Clinical trials ongoing for ATRis VE-822 and AZD6738 (August 2017). Modified from ([Rundle et al., 2017](#))

available ATRi to enter clinical trials - recruitment is ongoing for these trials, and there are no published preliminary results to date ([Rundle et al., 2017](#)).

1.12. Metabolic consequences of ATR deficiency

SS patients and mouse models demonstrate that defective ATR seems to affect adipose tissue homeostasis ([O'Driscoll, 2009](#)), and functions at the mitochondria, in autophagy and insulin signalling have been characterised in the literature ([Hilton et al., 2015](#); [Li et al., 2009](#); [Yi et al., 2017](#)). The presentation of ATR-SS and these novel metabolic functions of ATR deliver a potential hurdle for the use of ATR kinase inhibitors as a cancer therapeutic, as an invariant feature of cancer is metabolic deregulation ([Fearon et al., 2012](#)). Consistently in mouse models with reduced ATR and ATR-SS patients, one aspect of the presentation is a severe lack of subcutaneous fat, suggesting a failure to maintain adipogenic stem cells on an adipogenic program ([O'Driscoll, 2009](#); [O'Driscoll et al., 2004](#)). Currently there is very limited understanding of the underlying mechanisms in which a congenital defect in ATR function affects adiposity or metabolism.

Evidence characterising novel links between the cellular metabolism pathways controlled principally by PIKK member mTOR, and DNA repair mechanics primarily regulated by ATR and ATM, is mounting ([Xu et al., 2012](#)). Although further characterisation is required for a mechanistic understanding of the processes that associate these PIKK-regulated pathways, what can be elucidated is that the ATR-CHK1 signalling axis is fundamentally affected by cellular metabolic status. This begs the question of whether a feedback mechanism could exist here, where ATR activity is also an effector of AKT-mTOR activity and general cell metabolic homeostasis.

The potential unforeseen metabolic consequences of ATRi therapy are of particular concern due to the inherent metabolic deregulation associated with cancer progression, which I will continue to discuss in the next section.

1.12.1. Cancer Cachexia

Cachexia is a chronic disease concomitant with metabolic dysfunction. A considerable comorbidity of cancer, cachexia is defined as the progressive wasting of muscle and adipose tissue regardless of adequate nutritional intake ([von Haehling and Anker, 2014](#)). Widely acknowledged as a marker for poor prognosis and outcome, research into anti-cachexia therapeutics reflect the complexity of the signalling factors and regulatory

pathways involved in nutrient-status recognition, lipolysis and white adipose tissue (WAT) 'browning'. Cachexia is particularly prevalent in advanced cancers – manifesting in 50-80% of all cancer patients and accountable for 20% of mortalities ([von Haehling and Anker, 2014](#)). Cachexia is a multi-faceted disorder, associated with resistance to traditional cancer therapies and in itself appears to be refractory to clinical intervention ([Fearon et al., 2012](#)). The 'browning' of WAT has been implicated as one of the underlying molecular mechanisms of cancer cachexia (Fig 1.12.1) ([Argiles et al., 2014](#); [Fearon et al., 2012](#); [Kir et al., 2014](#); [Tsoli et al., 2012](#)). Increased brown adipose tissue (BAT) leads to greater resting energy expenditure in cachexic patients, due to the inherent thermogenic activity of this tissue type, resulting in muscle and adipose tissue wasting ([Bing et al., 2000](#)). The underlying mechanism(s) that cancers utilise to induce adipose browning is a current topic in cachexia research, and to date remains incompletely characterised at the molecular level.

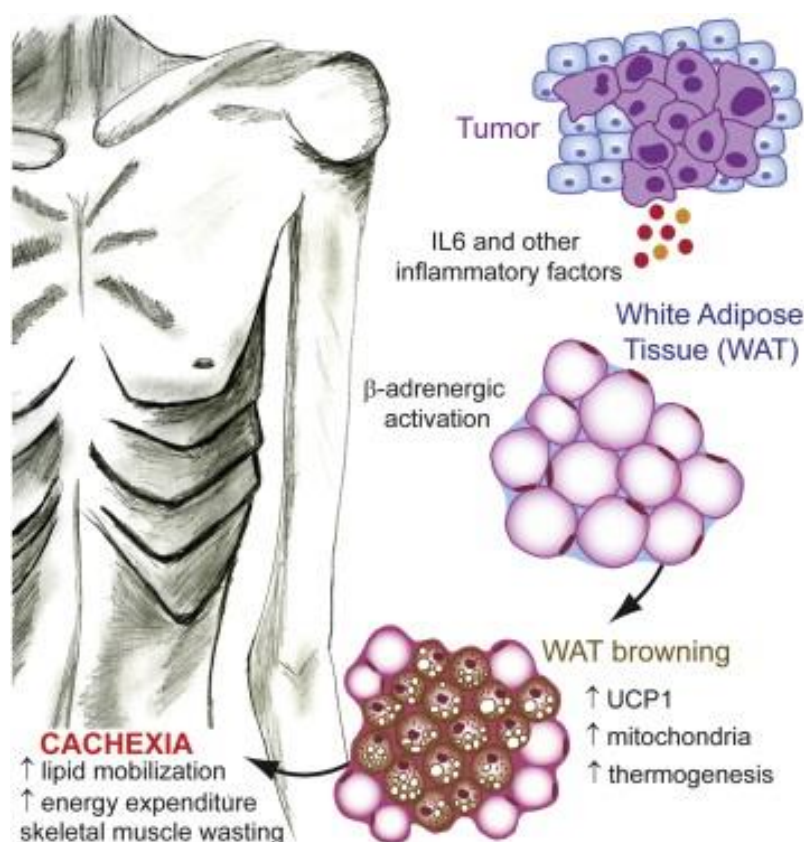


Figure 1.12.1. Cancer Cachexia. Through multiple mechanisms, cancer cells promote WAT browning, resulting in enhance lipid mobilisation and energy expenditure, generating the cachexic presentation of severe weight loss. Taken from ([Petruzzelli et al.](#))

Successful tumours are capable of inducing mass hydrolysis of triglycerides (TGs) stored in WAT for utilisation of free fatty acids (FFAs) and glycerol. This results in the release of fatty acids (FAs) into the plasma, that can be utilised by cancerous cells for the increasing rates of FA β -oxidation required to sustain proliferation. The dependency of non-glycolytic cancer cells on FA oxidation is enhanced in hypoxic and low-nutrient tumour microenvironments ([Kamphorst et al., 2013](#)).

Further to this, alterations increasing the avidity of lipid synthesis, metabolism and LD formation are also gaining recognition as hallmarks of highly proliferative cancers, appearing to increase resistance to chemotherapy ([de Gonzalo-Calvo et al., 2015](#); [Qiu et al., 2015](#); [Yue et al., 2014](#)). Changes in cancer cell lipid membrane composition, from unsaturated to saturated phospholipids, can fundamentally alter membrane fluidity and signal transduction, potentially blocking the uptake of chemotherapeutic drugs ([Rysman et al., 2010](#)). Bioactive lipids influence many tumorigenic cellular processes, including cell growth, migration and metastasis. For example, sphingosine-1-phosphate (S1P) induces angiogenesis via S1P receptor binding, facilitating growth and metastasis ([Kunkel et al., 2013](#)). Hence, changes in the lipidomic status of cancer cells are affiliated with tumour progression (Fig 1.12.2).

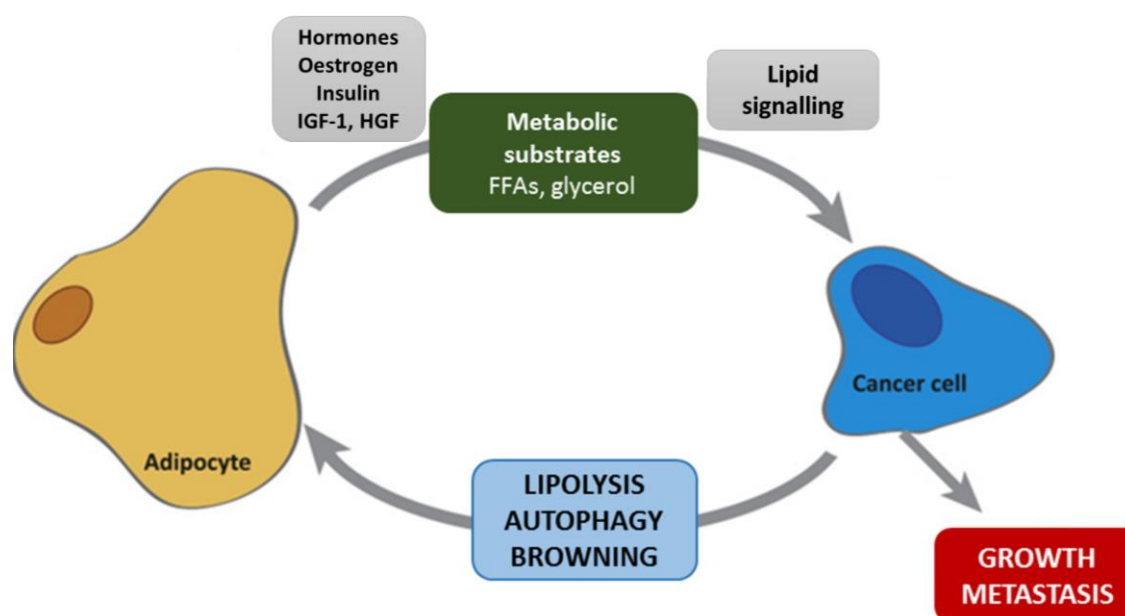


Figure 1.12.2. Simplified schematic of lipid-metabolic reprogramming in cancer. Cancer cells signal to adipocytes to undergo lipolysis, autophagy and browning to increase the volume of metabolites available for growth. Modified from ([Hoy et al., 2013](#))

Therapeutic strategies must be considered to carefully target and exploit the metabolic reprogramming and dependency on altered lipid utilisation and FA oxidation observed in many types of cancer. Furthermore, the metabolic consequences of novel therapies such as ATRis must be carefully considered, to avoid deleterious changes that could induce metabolic dysfunction. Changes in host metabolism (to increased catabolic events) could behave as a driver for tumour progression and cachexia, through the enhanced provision of bioactive lipids and metabolites from the dissolving WAT.

In this thesis, I aimed to investigate the consequence of reduced ATR activity on the functionality of post-mitotic white adipocytes, and cycling preadipocytes. I also investigated the effects of ATRi treatment as preadipocytes undergo adipogenic differentiation.

In **Chapter Three**, I investigate the effects of ATRi treatment on differentiating preadipocytes, assessing their capacity to successfully undertake adipogenesis.

In **Chapter Four**, I assess the consequences of chronic ATRi treatment on the lipid-metabolic status of mature adipocytes.

In **Chapter Five**, I characterise novel defects following reduced ATR function in cycling preadipocytes.

In **Chapter Six**, I further characterise the phenotypes I have discovered by assessing the impact of ATRi on endoplasmic reticulum (ER) function.

Chapter Two

Materials and Methods

2.1. Cell culture

Cell lines were thawed from liquid nitrogen in a 37°C waterbath and re-suspended in appropriate medium. All cells were maintained in a humidified atmosphere at 37°C in 5% CO₂. To split cultures, adherent cells were washed 1X in PBS and incubated in 0.25% trypsin-PBS at 37°C until completely detached. Fresh media was added to the cell suspension to neutralise trypsin before centrifugation at 1800g for 2 min. Cell pellets were re-suspended in an appropriate volume of fresh culture medium and plated. For storage in liquid nitrogen, $\sim 1 \times 10^7$ cells were pelleted, re-suspended in 1ml of medium supplemented with 10% DMSO (except from 3T3-L1s – 5% DMSO), and transferred to cryotubes. Cryotubes were then cooled slowly to -80°C before being transferred into liquid nitrogen storage.

3T3-L1 preadipocytes were cultured in DMEM supplemented with 10% new born calf serum (NBCS), L-Glutamine (2mM), penicillin (500 U/ml) and streptomycin (50mg/ml). To reduce adipogenic induction arising from growth arrest, flasks were split before cells reached 80% confluence, and passage number would be increased. At passage >20, cells were no longer used for adipogenic differentiation.

HEK-293 cells were cultured in DMEM supplemented with 10% foetal calf serum (FCS), L-Glutamine (2mM), penicillin (500 U/ml) and streptomycin (50mg/ml)

MG63 cells were cultured in MEM supplemented with 10% FCS, L-Glutamine (2mM), penicillin (500 U/ml) and streptomycin (50mg/ml)

C2C-12 cells were cultured in DMEM supplemented with 10% FCS, L-Glutamine (2mM), penicillin (500 U/ml) and streptomycin (50mg/ml)

Cell Line	Source/Reference
3T3-L1 (murine preadipocytes)	GDSC cell bank
C2C12 (murine myoblasts)	Prof. Simon Morley, School of Life Sciences, University of Sussex, UK
HEK-293	GDSC cell bank
MG63 (human osteosarcoma)	American Type Culture Collection (ATCC)
RPE (retinal pigment epithelium)	GDSC cell bank

Table 2.1. Cell lines utilised in this thesis.

RPE cells were cultured in DMEM:F12 supplemented with 10% FCS, L-Glutamine (2mM), penicillin (500 U/ml) and streptomycin (50mg/ml)

2.2. Adipogenic differentiation of 3T3-L1 preadipocytes

3T3-L1 preadipocytes were cultured as previously described. To induce adipogenic differentiation, 3T3-L1 preadipocytes were plated at 90% confluency and allowed up to 7 days to reach a post-confluent state before addition of adipogenic cocktail. Adipogenic cocktail (1 µg/ml insulin (I2643), 0.5 mM isobutylmethylxanthine (IBMX – I5879), 1 mM dexamethasone (D4902), 2 µg/ml Rosiglitazone (R2408) all purchased from Sigma-Aldrich) was added to a basal medium (DMEM with 10% FCS, penicillin/streptomycin) on day 1. Adipogenic cocktail was refreshed after 24 hrs (day 2). On day 3, media was supplemented with 5 µg/ml insulin. On day 4, media was replaced for fresh basal medium supplemented with 1 µg/ml insulin. On day 5, media was replaced for basal medium only. Mature adipocytes were left for 4-7 days to acquire lipid droplets before experiments were initiated.

2.3. Extract preparation

2.3.1. Urea-based whole cell extract

Cells were washed 1X in PBS, pelleted and stored immediately at -20°C. Cell pellets were then re-suspended in urea-based lysis buffer (9M urea, 50mM Tris-HCl pH7.5, 10mM β-mercaptoethanol), and sonicated for 10-15 seconds at 30% amplitude.

2.3.2. IP extracts

Freshly pelleted cells were resuspended in 100-300µL IP buffer (50mM Tris.HCl pH7.5, 150mM NaCl, 2mM EDTA

50mM NaF, 25mM β-glycerolphosphate, 0.1mM sodium orthovanadate, 0.2% Triton-X100, 0.3% Igepal, protease inhibitor cocktail (11836170001 Roche)) and incubated on ice for 1hr.

Cell lysates were then centrifuged (3 min, 13,000 rpm, 4°C) and supernatant transferred to a pre-cooled eppendorf. Protein concentration of lysates was determined using the Bradford Protein Assay reagent (Bio-Rad Laboratories) at a UV absorbance of 595nm. Lysates were stored at -20°C or boiled in 5X SDS-loading buffer (5% SDS, 10% Glycerol,

10% β -mercaptoethanol, 125mM Tris-HCL pH6.8 and 0.2% bromophenol blue) and loaded onto SDS-PAGE gels.

2.4. Cell fractionations

All cell fractionations were prepared on ice using a 4°C centrifuge.

2.4.1. Endoplasmic Reticulum (ER) fractionation

ER were fractionated from HEK 293 cells using Endoplasmic Reticulum Isolation Kit (ER0100 Sigma). 2×10^8 PBS-washed cells were re-suspended in hypotonic buffer provided (3x volume of cell pellet) and incubated for 20 min at 4°C before being spun at 600g for 5 mins. Pellets were then re-suspended in isotonic buffer provided (2x volume of cell pellet) and homogenised using 10 strokes in a Dounce tissue homogenizer (D9063 Sigma). 5% of each lysate was collected at this point as the whole cell extract. Samples were spun at 1000g for 10 min and supernatant transferred to a clean, cold tube. Pellets were collected and stored at -20°C as the crude nuclear fraction. Samples were spun at 12,000g for 15 mins and 10% of the post-mitochondrial supernatant fraction (PMF) was stored at -20°C for further analysis. The remaining PMF was transferred to a suitable tube with enough space for the addition of 7.5X sample volume. ER were further enriched from this fraction using the CaCl_2 precipitation method - with vigorous agitation, 8mM CaCl_2 (7.5X sample volume) was added to the PMF and incubated for 15 mins to precipitate ER. Samples were spun at 8,000g for 10 mins with the rough-ER microsomes enriched in the final pellet.

2.4.2. Nuclear/Cytoplasmic fractionation

8×10^6 PBS-washed cells were re-suspended in 900mL ice-cold buffer (0.1% NP40-IGEPAL/PBS, Roche complete EDTA-free protease inhibitor tablet). 300mL of cell lysate was transferred to a cold tube, sonicated (15 seconds at 30% amplitude), centrifuged (13,000 rpm, 3min) and stored at -20°C as WCE. The remaining 600ml of cell lysate was pulse spun for 10 secs and the top 300ml of supernatant removed and transferred to a fresh tube (cytoplasmic fraction). The remaining supernatant was discarded and the nuclear pellet washed 5X in ice-cold PBS before resuspension in urea buffer and sonication as previously described.

2.5. siRNA knockdowns

All siRNA oligonucleotides used were SMARTpool siGENOME siRNA (Dharmacon). 3T3-L1 cells were transfected using METAFECTENE® PRO (Cambio) and Lipofectamine RNAiMAX (13778075 ThermoFisher Scientific) according to manufacturer's instructions. With the exception of siRNA mediated knockdown of *Atr* in confluent 3T3-L1 preadipocytes, all siRNA was transfected into a suspension of logarithmically growing cells. Following trypsinisation, 3.5×10^5 cells were re-suspended in 3mL of fresh, warm media to which the siRNA:lipid complex mixture was added. Media would be refreshed after 6h and cells would be analysed at 24h or 48h post transfection.

Target	Transfection reagent	Oligo Ref/NCBI accession number
<i>Atr</i>	Lipofectamine RNAiMAX	M-062167-01-0005; NM_019864.1
<i>p62/Sqstm1</i>	METAFECTINE® PRO	M-047628-01-0005; NM_001290769.1
<i>Atg12</i>	METAFECTINE® PRO	M-050953-01-0005; NM_026217.3
<i>Atg16L1</i>	METAFECTINE® PRO	M-051699-01-0005; NM_001205391.1

Table 2.5. siRNA oligonucleotides utilised in this thesis

2.6. cDNA overexpression

2.6.1. METAFECTINE PRO

T25 flasks were seeded with 3.5×10^5 3T3-L1 cells and left overnight for cells to adhere. DNA was mixed with serum free media (SF) (3.75mg of DNA in 100mL SF) and added to the reagent mixture (7.5mL METAFECTINE PRO in 100 SF) and incubated 20 mins at RT. The DNA:lipid complex mixture was added to each flask and media refreshed 4 hrs post transfection. Samples were harvested for analysis 24h or 48hrs post transfection.

2.6.2. Calcium Phosphate

HEK-293 cells were seeded at 40% confluency in 10cm plates and allowed to become fully adherent overnight. A DNA mixture (5mg DNA, 61ml 2M CaCl_2 and 435uL ddH₂O) was prepared and added dropwise into 500ml bubbled 2XHBS (50mM HEPES, 280mM NaCl, 2.8mM Na_2HPO_4) for each plate. The final mixture was added dropwise onto each 10cm plate. After 24hrs, plates were gently washed 1X in PBS and media refreshed. The following day, plates were harvested for ER fractionation- or immunoprecipitation-based analysis.

2.6.3. Lipofectamine® 3000 Transfection

6-well plates were seeded with 2×10^5 3T3-L1 cells/well and allowed to become adherent. A DNA mixture (2 µg DNA, 4 µL P3000 Reagent, 100 µL SF) was prepared and added to the reagent mixture (2 µL Lipofectamine 3000, 100 µL SF) and incubated for 15 mins at RT. The DNA:lipid complex was added directly to each well and media was refreshed 4 hrs post transfection. Samples were harvested for analysis 24 or 48 hrs post transfection.

Plasmid	Source/Reference
ATR	A generous gift from Tony Carr, GDSC
ATR-CT ATR-D6 ATR-KD	A generous gift from Atsushi Higashitani, Institute of Genetic Ecology, Tohoku University
Calnexin	RC200229 Origene
RHEB	RC200307 Origene
VPS4b	RC208019 Origene

Table 2.6.3. cDNA constructs utilised in this thesis

2.7. FLAG-Immunoprecipitation

Using the Calcium Phosphate method previously described, HEK 293 cells were transfected with various cDNA constructs encoding a FLAG-tagged protein of interest. Samples were lysed in IP extraction buffer as previously described. To equilibrate before immunoprecipitation, ANTI-FLAG® M2 Affinity Gel (Sigma A2220) beads were washed 3X in ice-cold IP buffer with centrifugation of 1000 g for 1 min at 4°C. 350-500 µg of cell lysate was then immunoprecipitated with 25-40 µL washed ANTI-FLAG® M2 Affinity Gel beads in a final volume of 500 µL. The mixture was agitated for 1-2 hrs at 4°C. After centrifugation at 1000 g for 1 min at 4°C, unbound/flowthrough supernatant was collected and stored at -20°C for further analysis. ANTI-FLAG® M2 Affinity Gel beads and bound proteins were washed 2X in ice-cold IP buffer and 1x in ice-cold TBS before bound proteins were eluted with 3X FLAG peptide (Sigma F4799) described below.

2.8. 3X FLAG peptide elution

FLAG-tagged proteins were eluted from ANTI-FLAG® M2 Affinity Gel beads via 2X serial elution steps with 40-80 µL of 100 µg/ml 3X FLAG peptide in TBS (50 mM Tris-HCl, pH 7.4, 150 mM NaCl). Each elution lasted 15 mins at 4°C with agitation throughout.

Samples were then spun (1000 g, 1 min, 4°C), and supernatant removed. Elution steps were 'pooled' together and boiled for 10 mins at 96°C in an appropriate volume of 5X SDS loading buffer. Remaining ANTI-FLAG® M2 Affinity Gel beads were then washed 2X in IP buffer, resuspended in ~60 µL IP buffer and 15 µL 5X SDS loading buffer and boiled. All samples were stored at -20°C for further analysis or loaded directly onto SDS-PAGE gels.

2.9. SDS-PAGE/Western blotting

Protein gels and western blotting were carried out using the Bio-Rad Mini-PROTEAN III gel system. Protein extracts (5-50 µg) were boiled and denatured in SDS loading buffer as previously described, and resolved by SDS-PAGE (Sodium Dodecyl Sulphate-Polyacrylamide Gel Electrophoresis) on acrylamide gels (6-15% with 4% stacking gel). Gels were resolved at 120-220V in TGS running buffer (25 mM Tris-HCl, 250 mM Glycine, 0.1% (w/v) SDS), with Precision Plus Protein Prestained Dual Colour Standards (1610374 Bio-Rad) used as a molecular weight marker. Following adequate resolution, gels were transferred onto a PVDF membrane (1620177 Bio-Rad) using Trans-blot SD Semi-Dry Transfer Cell (1703940 Bio-Rad) in semi-dry transfer buffer (20% methanol, 30 mM Tris-HCl, 200 mM Glycine 0.03% SDS) for 1-2 hrs at 100A. Membranes were blocked in 5% BSA (unless stated otherwise) in TBS with 0.2% Tween-20 (TBS-T) for 45 minutes. Membranes were then probed with primary antibody in 5% BSA/TBS-T overnight at 4°C on an orbital shaker. Membranes were washed 3X in TBS-T for 7 min and probed with HRP-conjugated secondary antibodies (DAKO) for 45 mins before a further 3X TBS-T washes. Proteins were detected on Amersham Hyperfilm (28906836 GE Healthcare Life Sciences) using enhanced chemiluminescence (Amersham ECL Prime Reagent RPN2232, SLS, or SuperSignal™ West Femto Maximum Sensitivity Substrate 34096, ThermoFisher Scientific).

2.10. Site directed mutagenesis

Site directed mutagenesis were completed using the QuikChange II Site-Directed Mutagenesis Kit (#200524 Agilent). Oligonucleotides were purchased from Eurofins Genomics.

Following the mutagenic PCR reaction, Dpn1 was added to samples to digest parental DNA at 37°C overnight. Following restriction enzyme digest, samples were purified using QIAquick PCR Purification Kit (28104 Qiagen) before transformation into E.Coli using the heat shock method. Transformed E.Coli were streaked onto agar plates supplemented with the appropriate resistance marker and left overnight at 37°C for colonies to develop. Single colonies were selected and amplified overnight for sequencing. Plasmid DNA was extracted from amplified colonies using QIAprep Spin MiniPrep Kit (27104 Qiagen) and sent for Sanger sequencing at GATC Biotech. E.Coli samples successfully containing the appropriate mutation were then re-amplified overnight and plasmid DNA extracted using QIAGEN Plasmid Maxi Kit (12163 Qiagen) ready for transfection into mammalian cells.

Volume	Reagent
5µl	10x Reaction Buffer
10-50ng	dsDNA template
120ng	Fwd and Rev primers
1µl	dNTP mix
	ddH ₂ O to final vol. 50µl

Table 2.10.1. Mutagenic PCR reaction mix per sample

Segment	Cycles	Temperature	Time
1	1	95	30 seconds
2	15-18	95	30 seconds
		58	1 minute
		68	10-15 minutes

Table 2.10.2. Mutagenic PCR reaction conditions

Mutation	Primers
VPS4b T317A	Forward: 5' GACCgCTCAGAACAGTCTCACGG 3' Reverse: 5' TGAGcGGTCCCTAGGTGCAGT 3'
T317D	Forward: 5' GGACCGATCAGAACAGTCTCAC 3' Reverse: 5' CTGATCGGTCCCTAGGTGCAG 3'
E235Q	Forward 5' TGATcAAATTGATTCTCTGTGGTTCAAGAAGTGAAAATGA 3' Reverse 5' ATTTgATCAATGAAGATAATGGAGGGCTTGTCTCTC 3'

Table 2.10.3. Mutagenic PCR primers

2.10.1. Agarose gel electrophoresis

0.8-1.2% agarose gels were made by dissolving Ultrapure Electrophoresis Grade Agarose (Invitrogen) in 1XTAE buffer (0.4 M Tris acetate, 1 mM EDTA, 0.3 µg/ml ethidium

bromide). Ethidium bromide was added to the cooled mixture after it had been heated to dissolve agarose. Samples were prepared in loading buffer (Orange G, O3756 Sigma) and resolved in TAE buffer (40 mM Tris, 20 mM Acetate, 1 mM EDTA) alongside a 1kb DNA ladder (Invitrogen). DNA was visualised using a UV transilluminator.

2.11. Triglyceride and Free Fatty Acid Quantification

2.11.1. Oil Red O

Lipid content of mature 3T3-L1 adipocytes was quantified using histochemical lipid stain Oil Red O (O0625 Sigma). 3T3-L1 adipocytes were differentiated as previously described in 6 well plates, fixed in 10% formalin for 1 hr and washed 2X in ddH₂O. Samples were incubated in 60% isopropanol for 5 minutes and left to dry fully at RT. Working solution of Oil Red O was prepared according to manufacturer's instructions and 1 mL added per well for 10 mins. Oil Red O solution was aspirated and plates were gently dipped in ddH₂O 3-5X to wash excess Oil Red O without disturbing the fragile cell monolayers. At this stage microscopy images were acquired for analysis. To elute Oil Red O, plates were dried fully at RT before addition of 1 ml 100% isopropanol for 5 mins with gentle agitation. The Oil Red O/isopropanol solution was then transferred to a cuvette and quantified at a UV absorbance of 500nm.

2.11.2. Media Triglyceride Quantification

Media triglyceride was quantified using PicoProbe Triglyceride Quantification Assay Kit (Fluorometric) (ab178780 Abcam). T25 flasks of 3T3-L1 preadipocytes were differentiated in 6 mL adipogenic media as previously described. Daily throughout cell culture treatments, 100 μ L media (1.7% total volume) was removed from each flask and stored at -20°C for further analysis, and 100 μ L fresh media added back containing the appropriate drug concentration. Upon completion of timecourse, media samples were thawed and spun at 13,000 g for 2 mins to remove cell debris. Media samples were prepared for analysis on a 96 well plate according to manufacturer's instructions and quantified using a fluorescence microplate reader at Ex/Em = 535/587 nm.

2.11.3. Free Fatty Acid (FFA) Quantification

Media FFA was quantified using Free Fatty Acid Quantification Kit (ab65341 Abcam). Samples were collected as described previously for quantification of media triglycerides.

Samples were prepared on a 96 well plate according to manufacturer's instructions and quantified using a fluorescence microplate reader at (Ex/Em = 535/587 nm).

2.12. Cell Viability Assays

CellTiter-Blue® Cell Viability Assay (G8080 Promega) and Cell Counting Kit – 8 (96992 Sigma) were applied directly to samples in a 96 well plate according to manufacturer's instructions and done in duplicate to increase reliability. CellTiter-Blue fluorescence was quantified using a fluorescence microplate reader at Ex/Em = 579/584 nm. Cell Counting Kit – 8 absorbance was measured at 450 nm using a microplate reader. Samples were incubated until readings reached a linear range (1-4 hrs), which was cell-type dependent. The linear range of fluorescence/absorbance was established via generation of a standard curve from samples of known cell numbers.

2.13. Immunofluorescence

Cells mounted on coverslips were washed 2X with PBS and fixed using 3.7% paraformaldehyde for 10 mins at RT followed by 2X PBS washes. Samples were permeabilised by the addition of 100 µL of lysis solution (0.2% Triton X-100/PBS) for strictly 2 mins following by 2X PBS washes. Cells were blocked by addition of 100 µL 5% BSA/PBS for 10 mins followed by 1X PBS wash. Cells were treated with 100 µL primary antibody (dilutions determined in Table 2.15.2) in 5% BSA/PBS for 0.5-2 hrs at RT followed by 3X PBS washes. Cells are exposed to a second blocking step (5% BSA/PBS, 10 mins RT) and washed 1X in PBS before addition of the appropriate fluorescently-labelled secondary (1:200 in 5%BSA/PBS) for 30 mins. At this stage (if required) DAPI and fluorescently-conjugated Phalloidin (dilutions determined in Table 2.15.2) would be directly added to the slides without a wash step and incubated for 15 mins at RT. Samples would be subjected to 4X PBS washes before mounting with VectaShield (H-1000 VECTOR LABORATORIES LTD.), with slides sealed with nail polish.

Image acquisition was carried out under two microscopes:

- Zeiss AxioObserver Z1 epifluorescence microscope equipped with ApoTome2 structured illumination system, 40x/1.3 oil Plan-Apochromat, 63x/1.4 oil Plan-

Aprochromat and 100x/1.4 oil Plan-Aprochromat objectives and a Hamamatsu ORCA-Flash4.0 LT camera.

- Zeiss AxioPlan 2 epifluorescence microscope equipped with 10x/0.3 NA PLAN-NEOFLUAR, 40x/0.75 NA PLAN-NEOFLUAR and 100x/1.4 NA oil PLAN-APOCHROMAT objectives and a Hamamatsu photonics KK CCD camera.

2.14. Fluorescent Probes

BODIPY 493/503, MitoTracker Red CMXRos, MitoTracker Green FM, Calcium Green-1 AM and MitoSox Red were used according to manufacturer's instructions at stated dilutions to selectively stain live cells for analysis by flow cytometry. Cells were stained whilst in suspension and filtered through a BD FACs falcon tube to ensure single cell suspension. All FACs data was collected on a BD Accuri C6 flow cytometer using BD Accuri C6 software. Fluorescent probes stated in table x were used according to manufacturer's instructions at stated the dilutions to selectively probe cells for analysis by fluorescence microscopy.

Probe	Cat No.	Supplier	Dilution (IF/FC)	Function
BODIPY 493/503	D3922	ThermoFisher Scientific	2 μ M IF/FC	Neutral lipid stain
Lysosensor Green DND-153	L7534	ThermoFisher Scientific	1 μ M IF	Fluorescence at neutral pH
Mitotracker Red CMXRos	M7512	ThermoFisher Scientific	250nM FC/IF	Mitochondrial visualisation
Alexa Fluor® 488 Phalloidin	#8878	Cell Signalling	1:200 IF	Cytoskeleton stain
DyLight™ 554 Phalloidin	#13054	Cell Signalling	1:200 IF	Cytoskeleton stain
Acridine Orange	A9231	Sigma-Aldrich	1mM IF	Bright fluorescence in acidic compartments
DAPI	D9542	Sigma-Aldrich	20ng/ml IF	DNA probe
MitoTracker Green FM	M7514	ThermoFisher Scientific	250nM FC	Mitochondrial Mass
Calcium Green™-1, AM, cell permeant	C-3012	Life Technologies Ltd	2.5mM FC	Calcium indicator

Table 2.14. Fluorescent probes utilised in this thesis

2.15. Reagents

Reagent	Cat. No.	Supplier
3-Methyladenine	M9281	Sigma
AlbuMax	11021-029	Life Technologies
ATMi (KU55933)	KU-55933	Strattech
ATR kinase inhibitor II	118510	Merck Chemicals

Bafilomycin A1	B1793	Sigma
BAPTA	A4926	Sigma
BAPTA-AM	A1076	Sigma
CSA	30024	Sigma
Cyclodextrin	H107	Sigma
Dexamethasone	D4902	Sigma
HydroxyUrea	H8627	Sigma
IBMX	I5879	Sigma
Insulin	91077C	Sigma
Lovastatin	1530	Tocris
Obatoclox	S1057	Selleckchem
Rosiglitazone	R2408	Sigma
Thapsigargin	T9033	Sigma
UCN-01	U6508	Sigma
VE-821	S8007-SEL	Selleckchem
VE-822	S7102-SEL	Selleckchem

Table 2.15.1. Reagents utilised in this thesis.

Antibody	Cat No.	Supplier	Dilution WB/IF
53BP1	A300-272A	Bethyl	1:200 IF
AKT	#4691	Cell Signaling	1:1000 WB
AMPK	#2532	Cell Signaling	1:1000 WB
ATF2	sc-6233	Santa Cruz	1:1000 WB
ATF4	#11815	Cell Signaling	1:1000 WB
ATF6	#65880	Cell Signaling	1:1000 WB
ATG12	#2011	Cell Signaling	1:1000 WB
ATG16L1	#8089	Cell Signaling	1:1000 WB
ATM	#2873	Cell Signaling	1:1000 WB
ATR	sc-1887	Santa Cruz	1:1000 WB
ATR (IF)	GTX116010	GeneTex	1:500 IF
ATRIP	sc-33790	Santa Cruz	1:1000 WB
α -tubulin	ab4074	Abcam	1:10,000 WB
acetylated tubulin	T7451	Sigma	1:1500 IF
β -actin	#4967	Cell Signaling	1:1000 WB
BiP	ab21685	Abcam	1:2000 WB
β -tubulin	sc-9104	Santa Cruz	1:2000 WB
C/EBP β	#3087	Cell Signaling	1:1000 WB
CHK1	#2360	Cell Signaling	1:1000 WB
CREB	#4820	Cell Signaling	1:1000 WB
DRP1	#8570	Cell Signaling	1:1000 WB
eIF2 α	#9722	Cell Signaling	1:1000 WB
FLAG	F3165	SIGMA	1:5000 WB
γ H2AX	#9718	Cell Signaling	1:1000 WB
GFP	#2555	Cell Signaling	1:500 WB

H2A	#2578	Cell Signaling	1:1000 WB
IRS1	#2382	Cell Signaling	1:1000 WB
KAP1	A300-274A	BETHYL	1:1000 WB
Lamin B	sc-6216	Santa Cruz	1:1000 WB
LAMP1	ab24170	Abcam	1:1000 WB/ 1:1000 IF
LC3	#4599	Cell Signaling	1:1000 WB/1:100 IF
p44/42 MAPK	#9101	Cell Signaling	1:1000 WB
p62	#5114	Cell Signaling	1:1000 WB
p-AKT S473	#4060	Cell Signaling	1:1000 WB
p-AKT T308	#4056	Cell Signaling	1:1000 WB
p-AMPK T172	#2535	Cell Signaling	1:1000 WB
p-ATF2 T71	#9221	Cell Signaling	1:1000 WB
p-ATR T1989	GTX128145	GeneTex	1:1000 WB
p-CAMKII T286	#12716	Cell Signaling	1:1000 WB
p-Chk1 S345	#2341	Cell Signaling	1:500 WB
p-CREB S121	16589	Pierce	1:1000 WB
p-CREB S133	#9191	Cell Signaling	1:1000 WB
PDI	ab2792	Abcam	1:1000 WB/1:500 IF
p-eIF2a S51	#3398	Cell Signaling	1:1000 WB
PERILIPIN A	#9349	Cell Signaling	1:1000 WB/1:100 IF
PGC1 α	ab54481	Abcam	1:1000 WB
p-H3 S10	Sc-8656	Santa Cruz	1:1000 WB
p-HSL S563	#4139	Cell Signaling	1:1000 WB
p-IRS1 Y989	sc-17200	Santa Cruz	1:500 WB/1:50 IF
p-KAP1 S824	A300-767A	Bethyl	1:1000 WB
p-MAPKAP2 T334	#3007	Cell Signaling	1:1000 WB
p-p38 MAPK TT180/Y182	#4511	Cell Signaling	1:1000 WB
PPAR γ	#2443	Cell Signaling	1:1000 WB
Pre-Lamin A/Lamin A	sc-6214	Santa Cruz	1:1000 WB/1:100 IF
p-S6 S240/S244	#5364	Cell Signaling	1:1000 WB
p-SQ/TQ	#2851	Cell Signaling	1:500 WB
p-SQ/TQ *QG	#6966	Cell Signaling	1:500 WB
RAB7	#9367s	Cell Signaling	1:1000 WB/1:100 IF
RCAS1	#12290	Cell Signaling	1:200 IF
S6	#2217	Cell Signaling	1:1000 WB
Syntaxin 6	#2869	Cell Signaling	1:50 IF
TFEB	A303-673A	Bethyl	1:1000 WB
UCP2	sc-6526	Santa Cruz	1:1000 WB
UCP1	ab23841	Abcam	1:1000 WB
WIPI1	ab128901	Abcam	1:1000 WB
XBP-1s	#12782	Cell Signaling	1:1000 WB

Table 2.15.2. Antibodies utilised in this thesis.

Chapter Three

Results I: The Impact of Pharmacological
Inhibition of ATR on Adipogenesis

3.1. Introduction

A hypomorphic splicing mutation in *ATR* was the first identified mutation associated with Seckel Syndrome (SS) ([O'Driscoll et al., 2003](#)). Growth retardation and lipodystrophy are, amongst others, key striking clinical features of this microcephalic primordial dwarfism (MPD) disorder (Fig 3.1.A). Further to this, mice generated from humanised model of ATR-SS die within 6 months displaying cachexia (Fig 3.1.B) ([Murga et al., 2009](#)).

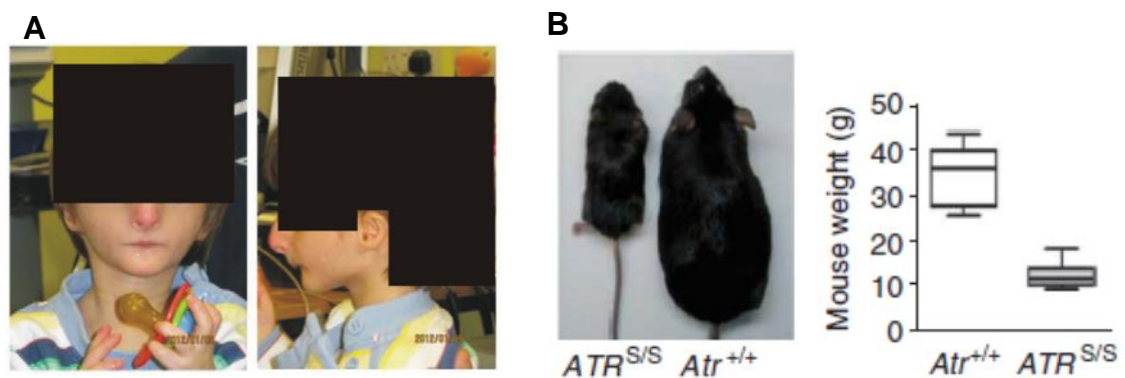


Figure 3.1. ATR-SS has the clinical feature of lipodystrophy. A) ATRIP-SS patient at 2 years, displaying lipodystrophy visible in the face and neck. **B)** Humanised ATR-SS mouse recapitulated the MPD presentation of SS and died at 6 months displaying a cachexic presentation. Images taken from ([Ogi et al., 2012](#)) and ([Murga et al., 2009](#))

A 'cell autonomous' role for ATR in maintaining adiposity has been previously described. Ruzankina *et al.* investigated the effects of *Atr* deletion on adult mice; generating a tamoxifen-inducible *Atr* knockdown system that could efficiently delete ATR both spatially and temporally within the mouse ([Ruzankina et al., 2007](#)). Through this system, Ruzankina *et al.* were able to identify new characteristics of ATR deficiency not associated with reduced ATR during development. *Atr* deletion in adult mice ablated canonical ATR-CHK1 signalling at the intra-S-phase checkpoint, required for the effective maintenance and replication of proliferating stem cell populations. Reduced ATR functionality caused the depletion of proliferative stem cell precursors, necessary for tissues that require constitutive regeneration e.g. skin, white adipose tissue (WAT), and intestinal epithelia, resulting in atrophy of these tissues ([Ruzankina et al., 2007](#)). However, within the same study, the group further described a striking and disproportionate atrophy of non-proliferative, terminally differentiated WAT following

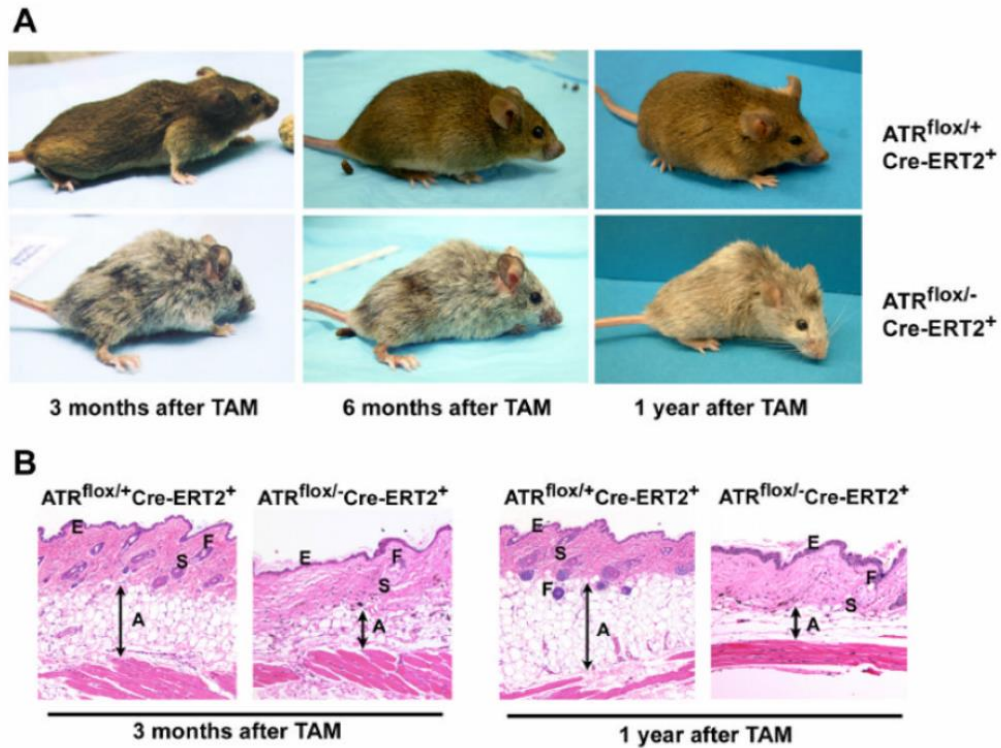


Figure 3.2. *Atr* deletion in adult mice results in disproportionate wasting of adipose tissue. A) Tamoxifen-inducible *Atr* deletion in adult mouse. Top row demonstrates *Atr*-proficient mice, bottom row is *Atr* deletion mouse following 3 months to 1 year of tamoxifen where accelerated ageing and weight loss are apparent. **B)** Skin sections from *Atr*-proficient and *Atr*-deletion mice following tamoxifen. *Atr* deletion results in striking atrophy of subcutaneous adipose tissue (labelled A) Taken from ([Ruzankina et al., 2007](#))

Atr deletion (Fig 3.2.A and B). This is an unusual result, as mature adipocytes are G₀ and do not require the cell cycle checkpoint functions of ATR.

The cachexic-like appearance observed in SS, and mouse models of ATR deficiency, imply reduced ATR function has consequences on the homeostatic regulation of metabolism. The aetiology behind these metabolic consequences of ATR deficiency, further observed in SS and other models, has not been adequately explored.

To reinforce the importance of investigating the consequences of impaired ATR function on metabolism, one must consider the use of small molecule inhibitors of ATR as novel cancer chemotherapeutic agents. An inherent aspect of almost all late-stage cancers is metabolic dysregulation and reprogramming ([Hsu and Sabatini, 2008](#)). Through poorly characterised mechanisms, catabolic processes become uncoupled from their regulatory networks, resulting in the net benefit of increased nutrients available to the tumour to facilitate further growth. Such drastic metabolic reprogramming results

in a co-morbidity characterised by severe weight loss – cancer cachexia ([Argiles et al., 2014](#)).

Investigating the aetiology of ATR deficiency-induced lipodystrophy could provide novel insight for the outcomes of individuals utilising prolonged and high doses of small molecule kinase inhibitors of ATR (ATRi) as a cancer therapeutic. ATRi usage in cancer could have unforeseen negative impacts, through the disruption of WAT homeostasis, driving a cachexic presentation which is commonly associated with poor outcomes and the development of therapeutic resistance. Further to this, a surprising number of putative substrates have been identified for ATR and ATM through proteomics screens in the last decade, where many have roles in insulin signalling and cell metabolism, suggesting uncharacterised roles of ATR in the regulation of metabolic pathways ([Matsuoka et al., 2007](#); [Stokes et al., 2007](#)).

In this chapter, I investigate a novel impact of ATR inhibition on the metabolic function and homeostasis of differentiating preadipocytes. I briefly summarised the physiological role of WAT in chapter one. Here, I first will discuss how mesenchymal stem cells commit to the adipogenic lineage, the induction and execution of adipogenic differentiation, and the regulatory mechanisms that control the decision to undergo adipogenesis, before detailing my experimental findings.

3.1.1. Overview of Adipogenesis

Adipocytes are derived from mesenchymal stem cells (MSCs) residing in the vascular stroma of adipose tissue. Throughout the entire mammalian lifespan, signalling factors trigger the conversion of these pluripotent MSCs into partially committed preadipocytes, restricting them to the adipocyte lineage. In healthy adults, 15-20% of adipose tissue is comprised of cycling preadipocytes ([Tchkonia et al., 2010](#)), poised to undergo maturation into terminally differentiated adipocytes in periods of calorific excess. Hence, when investigating the metabolic consequences of small molecule ATRi treatment in a cancer therapeutic context, it is relevant to study the outcomes of ATRi on adipogenic differentiation, as well as on terminally differentiated adipocytes.

Upon adipogenic induction, preadipocytes undergo multiple rounds of mitosis (mitotic clonal expansion) before the transcriptional and metabolic reprogramming

required to induce the adipocyte phenotype. Following MCE, essential master adipogenic transcription factor Peroxisome Proliferator-Activated Receptor gamma 2 (PPAR γ 2) is subject to epigenomic activation, inducing the transcription of adipose-specific genes necessary for the full adipogenic gene profile and hypoplasia of the adipose tissue. PPAR γ 2 is required for adipogenic differentiation, and is used widely as a marker for successful adipogenic induction ([Farmer, 2005](#)).

3.1.2. Mesenchymal Stem Cell (MSC) Commitment

Briefly, MSCs are the common progenitor of adipocytes and osteoblasts. A variety of external cues dictate the decision of MSCs to commit to adipo- or osteogenic differentiation. Reciprocal signalling processes inhibit and promote these opposing fates via the expression of differing lineage-specific transcription factors, to ultimately maintain the appropriate balance of each cell population ([Chen et al., 2016](#)). Among others, members of the bone morphogenic protein (BMP) ([Tang et al., 2016](#)) and wingless-type MMTV integration site (WNT) ([Bowers and Lane, 2008](#)) families are key mediators of commitment to the adipocyte lineage and play dual roles (Fig 3.1.2) ([Chen et al., 2016](#)). The composition and concentration of these cytokines in the microenvironment surrounding the MSCs dictates on to which lineage they will impinge ([Chen et al., 2016](#)). Commitment to the adipocyte lineage is also induced by elevated

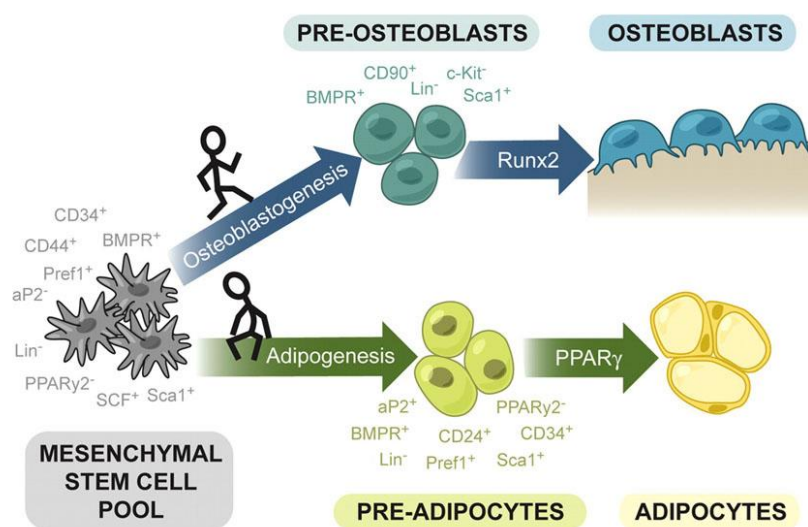


Figure 3.1.2. Schematic of mesenchymal stem cell commitment. Multiple external factors dictate when and to which lineage MSCs will differentiate. Taken from ([Luu et al., 2009](#))

glucose uptake and excessive energy intake ([Shepherd et al., 1993](#)), however it remains unclear how this metabolic state is signalled to MSCs.

3.1.3. Terminal Differentiation of Preadipocytes

A recent surge of interest into adipocyte function has occurred, as obesity and its concomitant morbidities and mortalities are steadily reaching epidemic levels ([Ogden et al., 2006](#)). This has led to increased understanding into the complex, temporally regulated transcription cascade that regulates the maturation of preadipocytes into terminally differentiated adipocytes. Until recently, attention has vastly been focused on nuclear ligand Peroxisome proliferator-activated receptor gamma (PPAR γ) and the CCAAT-enhancer-binding protein (C/EBP) family of transcription factors. It is only now becoming clear that almost every essential signalling pathway can influence the decision to induce terminal adipogenic differentiation.

Adipogenesis is initiated following a shift between pro- and anti-adipogenic extracellular factors including Ca²⁺ ([Jensen et al., 2004](#)), insulin, static strain and many other micro-environmental factors ([Pope et al.](#)). *In vitro*, cell confluence induces growth

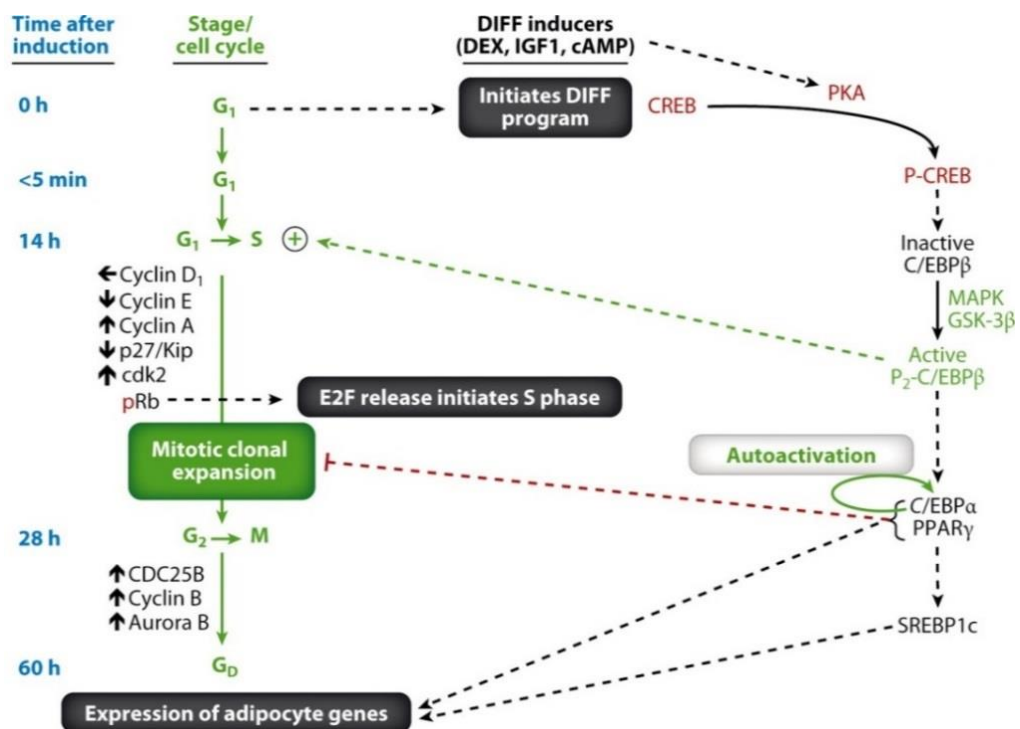


Figure 3.1.3. Temporal schematic of adipogenic differentiation *in vitro*. Multiple cues and checkpoints must be successfully passed in a coordinated manner to successfully complete adipogenesis. Taken from ([Tang and Lane, 2012](#))

arrest and the transient formation of primary cilia. Primary cilia are solitary mechano- and chemosensory organelles that emanate from the cell surface, sensitizing preadipocytes to incoming adipogenic signals via the recruitment of insulin growth factor-1 receptor (IGF1R) and downstream signalling molecules to the cilia basal body ([Dalbay et al., 2015](#); [Satir et al., 2010](#)). Primary cilia appear essential for adipogenesis *in vitro* – the model adipogenic cell line 3T3-L1, and human mesenchymal stem cells (hMSCs), will not differentiate without primary cilia function ([Dalbay et al., 2015](#); [Zhu et al., 2009](#)).

Insulin acts at the IGF1R, inducing phosphorylation of insulin receptor substrate 1 (IRS-1) and initiation of the phosphatidylinositol-4,5-bisphosphate 3-kinase (PI3K) signalling cascade. The result of which, is pro-adipogenic phosphorylation of cAMP-response element binding protein (CREB) (p-S133) within 5 minutes, which induces expression of C/EBP β (Fig 3.1.3) ([Zhang et al., 2004a](#)). C/EBP β must further be phosphorylated by mitogen-activated protein kinase (MAPK) and Glycogen synthase kinase 3 beta (GSK-3 β), before it can demonstrate the correct conformation required for DNA binding ([Tang et al., 2005](#)). C/EBP family member C/EBP homologous protein-10 (CHOP10) also acts as a dominant negative isoform to repress C/EBP family activity, dimerising with C/EBP β to prevent it from interacting with DNA ([Ron and Habener, 1992](#)). CHOP10 expression decreases several hours after adipogenic induction - this acts as a 'fail safe' mechanism to ensure cells enter mitotic clonal expansion (MCE) before C/EBP β can initiate the next stages of the adipogenic cascade.

When C/EBP β is released, it activates DNA transcription via directly binding to the promoter of *KLF5*, encoding zinc-finger transcription factor kruppel-like factor 5 (KLF5), and C/EBP α . KLF5 and the C/EBP factors function in concert at the *PPARG2* promoter (encoding PPAR γ 2) to induce expression ([Oishi et al., 2005](#)). Induction of C/EBP δ requires glucocorticoids and C/EBP β . In contrast to its vital role in the differentiation of WAT, it appears C/EBP α is not required for brown adipose tissue (BAT) development in mice ([Linhart et al., 2001](#)). The increased transcription and ligand binding of PPAR γ 2 terminates MCE, central to the further coordinated transcription of genes required for the adipocyte phenotype (Fig 3.1.3) ([Tang et al., 2003](#)). PPAR γ and C/EBP α continue to

cooperatively activate genes, whose final expression produces the mature adipocyte phenotype.

3.1.4. Regulators of PPAR γ

PPAR γ 2 is highly expressed in WAT and BAT, and is the only factor identified to date that is both essential and sufficient for successful adipogenesis ([Farmer, 2006](#)). Importantly, mutations of the *PPARG* gene have been associated with infantile onset lipodystrophy and insulin resistance in humans ([Dyment et al., 2014](#)). Consequently, the transcription and expression of PPAR γ 2 is subject to stringent regulation from a variety of factors, ensuring stable expression is obtained only when distinct parameters are met.

PPARG is expressed as two isoforms, PPAR γ 1 and PPAR γ 2. PPAR γ 2 expression is restricted almost entirely to adipogenic tissue, whereas PPAR γ 1 is far more ubiquitous ([Farmer, 2006](#)). Alternate promoter usage results in the generation of *PPARG1* and *PPARG2* mRNA from the same locus, which are identical other than an additional sequence encoding for 30 amino acids at the N-terminus of PPAR γ 2 ([Tontonoz et al., 1994](#)). Several studies have demonstrated that within a PPAR γ 2-deficient context, PPAR γ 1 is capable of inducing adipogenesis to an equivalent extent, suggesting PPAR γ 1 can compensate for some of the adipogenic roles of PPAR γ 2 ([Mueller et al., 2002](#); [Zhang et al., 2004b](#)). However, PPAR γ 2 appears to be essential in the regulation of insulin sensitivity.

Here, I will review the principal contributors involved in inducing and/or regulating PPAR γ 2 expression.

3.1.4.1. Chromatin remodelling

Eukaryotic genomes are packaged into chromatin through the architectural wrapping of each 146 base pairs of DNA onto a single nucleosome ([Kornberg and Lorch, 1999](#)). Nucleosomes consist of histone octamers of four core histone units (H2A, H2B, H3 and H4), and nucleosome occupancy at a gene site correlates inversely with gene transcription ([Lee et al., 2004](#)). The combination of covalent histone modifications on their N-terminal tails affects chromatin structure and subsequent gene expression.

A number of epigenetic factors regulate PPAR γ 2 expression. During adipogenesis, nucleosomes occupying the *PPARG* site are subject to both histone modification and alteration by chromatin remodelling complexes, to achieve *PPARG* transcription initiation ([Lee and Ge, 2014](#)). Di- and tri-methylated H3K9 is widely considered a hallmark of condensed chromatin (heterochromatin) – areas of transcriptionally silent genes ([Sims Iii et al., 2003](#)). Throughout adipogenesis, histones at the *PPARG2* promoter are subject to hyperacetylation at H3K9 and H3K27 (positive inducers of gene transcription) via enhanced recruitment of histone acetyl transferases (HATs), and H3K9 demethylation via the downregulation of histone lysine methyltransferases (HKMTs) SETDB1 and G9A (*EHMT2*) ([Okamura et al., 2010](#)). Together, these processes enable chromatin relaxation at the *PPARG2* promoter, allowing transcriptional machinery access to the site. Following chromatin relaxation, C/EBP factors bind directly to the *PPARG2* promoter and initiate the recruitment of RNA polymerase Pol II and the SWI/SNF chromatin remodelling complex ([Salma et al., 2004](#)). SWI/SNF disrupts the core conformation of nucleosomes by altering DNA-histone binding at the *PPARG2* locus, stabilising the interaction of Pol II, facilitating preinitiation complex formation and transcription ([Côté et al., 1998](#)).

Interestingly, HKMT G9A has recently been identified as a putative ATM/ATR substrate, with a second paper identifying a novel role for G9A at the replication fork ([Dungrawala et al., 2015](#); [Matsuoka et al., 2007](#)). However, the latter study concluded G9A activity in the context of replication stress was in fact ATR-independent. Although this is evidence to argue against a role for ATR in the regulation of G9A HKMT activity, it remains an attractive target for further substrate validation due to the dense clusters of conserved S/TQ motifs observed in both G9A and its homologue EHMT1 ([Stokes et al., 2007](#)).

3.1.4.2. Pre-Lamin A

Laminopathies are a group of rare genetic disorders caused by mutations in genes encoding for proteins of the nuclear lamina ([Nagano and Arahata, 2000](#)). For example, mutations in *LMNA* (encoding Lamin A) can cause Dunnigan-type familial partial lipodystrophy, characterised by insulin resistance, lipodystrophy of the extremities and torso and dyslipidaemia ([Hegele, 2000](#)). In fact, a common (if not invariant) clinical

feature of laminopathies is lipodystrophy and accelerated ageing ([Worman and Bonne, 2007](#)).

This presentation is generated by amino acid substitutions in Lamin A and Lamin C, which have been postulated to alter adipocyte-specific functions of Lamin A ([Capanni et al., 2005](#)). An underlying mechanism in which defective Lamin A/C processing results in metabolic impairments has been characterised – abnormally accumulating pre-Lamin A sequesters SREBP1 at the nuclear rim, inhibiting its transcriptional activity at the *PPARG* locus ([Capanni et al., 2005](#)). Through this mechanism, Lamin A/C processing has input into the control of PPAR γ 2 expression and subsequent adipogenesis.

Accumulation of pre-Lamin A also appears to increase genomic instability, resulting in increased activation of checkpoint kinases ATR and ATM, inducing early replicative senescence and the accelerated aging seen in several laminopathies ([Liu et al., 2006](#)). Fractions of ATR have been reported to localise at perinuclear regions with Lamin A in prophase and in response to mechanical stress. ATR inhibition and ATR-Seckel cells also display delayed nuclear envelope breakdown and Lamin A disintegration prior to metaphase ([Kumar et al., 2014](#)). In some laminopathies, ATR fails to appropriately localise at DNA repair foci ([Manju et al., 2006](#)), suggesting an element of feedback between these two proteins. Interestingly, Lamin A and pre-Lamin A also contain several S/TQ motifs, including a TQ motif proximal to pre-Lamin A's C-terminal farnesylation site, where farnesylation is an essential precursory step in the Lamin A maturation process. Several groups have recognised these S/TQ motifs in putative ATR/ATM substrate screens ([Matsuoka et al., 2007](#); [Stokes et al., 2007](#)).

3.1.4.3. *NAD⁺/SIRT1 (Sirtuin 1)*

SIRT1 is a NAD-dependent deacetylase that acts as an intermediary in a wide array of cellular processes. SIRT1 appears to play fundamental roles in metabolism, ageing and senescence ([Brooks and Gu, 2009](#); [Cao et al., 2016](#); [Fang et al., 2014](#)). SIRT1 is uniquely dependent on NAD⁺ for its catalytic activity rendering it sensitive to cellular nutrient status, and through the deacetylation of a wide variety of targets it behaves as a crucial resistance factor to stress-induced apoptosis. For example, in response to caloric restriction, SIRT1 deacetylates KU70 inducing the sequestration and inhibition of pro-

apoptotic factor BCL-2 associated X protein (BAX) ([Cohen et al., 2004](#)). PPAR γ is also a SIRT1 target ([Han et al., 2010](#)), where deacetylation and binding to inhibitory factors appears to inhibit adipogenesis ([Picard et al., 2004](#)), and induce brown remodelling in mature adipocytes ([Qiang et al., 2012](#)).

Importantly, SIRT1 is inhibited following induction of the base excision repair branch of the DNA damage response (DDR) ([Fang et al., 2014](#)). PARP1 (poly (ADP-ribose) polymerase) assists the repair of single stranded nicks by transferring chains of poly-ADP-ribosyl moieties (PAR groups) derived from NAD $^{+}$ onto itself and other acceptor proteins ([D'Amours et al., 1999](#)). In this manner, PARP1 activation is concomitant with depletion of NAD $^{+}$ and inactivation of SIRT1. For example, Fang *et al.* recently characterised mitochondrial abnormalities in the nuclear excision repair disorder Xeroderma Pigmentosum A (XPA), where defective mitophagy was due to decreased activation of the NAD $^{+}$ -SIRT1-PGC1 α axis, which in turn was driven by hyperactivation of PARP1 ([Fang et al., 2014](#)).

3.1.4.4. Calcineurin/NFAT (nuclear factor of activated T cells)

Ca $^{2+}$ -dependent serine/threonine phosphatase Calcineurin transduces intracellular Ca $^{2+}$ status to a variety of signalling pathways, including the dephosphorylation and nuclear translocation of members of the NFAT transcription factor family ([Li et al.](#)). Overexpression of mutant, constitutively active NFATc1 transforms 3T3-L1 cells and inhibits adipogenesis at the level of PPAR γ 2 induction ([Neal and Clipstone, 2003](#)), an effect that appears to be mediated by Calcineurin ([Neal and Clipstone, 2002](#)), suggesting a Ca $^{2+}$ -dependent negative regulatory role for Calcineurin in adipogenesis.

3.1.4.5. p38 MAPK signalling

Stress-response kinase p38 MAPK (p38 mitogen-activated protein kinase) appears to have opposing roles in adipogenesis, dependent on the temporality and duration of its activation. Most studies characterising a role for p38 in adipogenesis were conducted in the partially committed 3T3-L1 cell line, with the use of small molecule inhibitors. Early reports validated the requirement of p38 MAPK activation in 3T3-L1 adipogenesis, observing a decrease in C/EBP β phosphorylation when differentiating cells were treated with p38 inhibitors ([Engelman et al., 1999](#); [Engelman et al., 1998](#); [Takenouchi et al.,](#)

[2004](#)). A role in mesenchymal commitment has also been observed, where BMP2 steers C3H10T1/2 MSCs into the adipocyte lineage through p38 activation ([Hata et al., 2003](#)).

However, further reports show p38 activity has an inhibitory role in adipogenesis. p38 substrate growth arrest and DNA damage 153 (CHOP/GADD153) inhibits adipogenesis due to its dominant-negative regulation of C/EBPs – a function that is abolished with the ablation of p38-dependent phospho sites ([Wang and Ron, 1996](#)). p38 MAPK also appears to negatively regulate adipogenesis, through the phosphorylation and cytoplasmic sequestration of PPAR γ -inducing transcription factor NFATc4 ([Ho et al., 1998](#); [Yang et al., 2002](#)).

Activating transcription factor 2 (ATF2) belongs to the ATF/CREB family of transcription factors and is primarily activated by stress-response kinases such as p38 MAPK. ATF2 binds to cAMP-responsive elements (CRE) within a promoter region, transducing stress-kinase signalling into the transcription of target genes. ATF2 is induced early in the adipogenesis program and is suggested to play a collaborative role with C/EBP β , in the promotion of adipogenesis-inducing transcription factors including PPAR γ ([Lee et al., 2001](#)).

ATF2 has also been identified as an essential DNA damage response (DDR) protein ([Bhoumik et al., 2007](#)). Following IR, ATF2 is phosphorylated on its C-terminal domain by ATM, inducing its co-localisation with DNA repair machinery components γ -H2AX and the MRN complex ([Bhoumik et al., 2005](#)).

3.1.4.6. Free Fatty Acids

Several fatty acids act as endogenous PPAR γ ligands. As PPAR γ 2 is a key modulator of lipid-metabolism related genes, this allows adipose and non-adipose tissues alike the ability to protect against excessive lipid overload by enhancing lipid storage, transport and release pathways ([Medina-Gomez et al., 2007](#)). The detrimental effects associated with excessive cellular fatty acid uptake are termed ‘lipotoxicity’. PPAR γ 2 expression can be induced in WAT in response to changes in the ‘lipidomic’ status of the cell – resulting in increased lipid storage, which in turn reduces peripheral lipotoxicity of the muscles and liver. Hence, when fatty acid uptake exceeds the oxidative capacity of the cell, PPAR γ 2 induction enhances protective lipid droplet formation.

3.1.4.7. mTOR (*mechanistic target of rapamycin*)

The involvement of mTOR signalling in adipogenesis has been well documented. Through pharmacological and genetic manipulation of its regulators and targets, mTOR is believed to have critical and complex inputs into adipogenesis ([Kim and Chen, 2004](#); [Yoon et al., 2013](#)). mTORC1 appears to both positively and negatively influence PPAR γ activity, through the phosphorylation status of ribosomal protein S6 kinase beta-1 (S6K1), and inhibition of the insulin receptor substrate 1 and protein kinase B (IRS1-AKT)-PPAR γ pathway. mTORC1 and mTORC2 have multiple regulatory effects on PI3K-AKT signalling, which is indispensable for PPAR γ activation ([Yoon et al., 2013](#)). Adipose tissue-specific knockout of essential mTORC1 component *Raptor* (encoding Regulatory-associated protein of mTOR) results in lean mice with enhanced levels of BAT ([Polak et al., 2008](#)), and constitutive mTORC1 activity via deletion of *Tsc2* (encoding Tuberous Sclerosis Complex 2) in MEFs results in enhanced adipogenesis ([Zhang et al., 2009](#)). Overexpression of DEP domain-containing mTOR-interacting protein (DEPTOR), an endogenous inhibitor of mTOR results in obese mice ([Laplante et al., 2012](#)), yet mTORC1 inhibitor rapamycin has an inhibitory effect on adipogenesis ([Yeh et al., 1995](#)).

ADD1/SREBP1 (sterol responsive element binding protein) is a transcription factor induced early in the adipogenic program, whose expression specifically increases activity of PPAR γ through the SREBP1-dependent generation of a secreted PPAR γ ligand ([Kim et al., 1998](#); [Spiegelman et al., 1997](#)). SREBP1 maturation, activity and nuclear accumulation is positively regulated by mTORC1, adding an additional mechanism into mTORC1's regulation of PPAR γ function ([Laplante and Sabatini, 2013](#)). It is believed that the positive and negative effects mTORC1 exerts on adipogenesis are delicately dependent on differing thresholds of mTORC1 activity, and that this signalling threshold dictates the final effect of mTOR on PPAR γ activity ([Yoon et al., 2013](#)).

3.1.5. 3T3-L1 Adipogenesis

The 3T3-L1 cell line is the gold standard for modelling adipogenic differentiation in vitro. As murine preadipocytes, 3T3-L1 cells can be induced with an adipogenic cocktail to undergo adipogenic differentiation into functional adipocytes (Fig 3.1.4.A and B) ([Poulos et al., 2010](#)). For some *in vitro* adipogenic models (including the 3T3-L1 cell line),

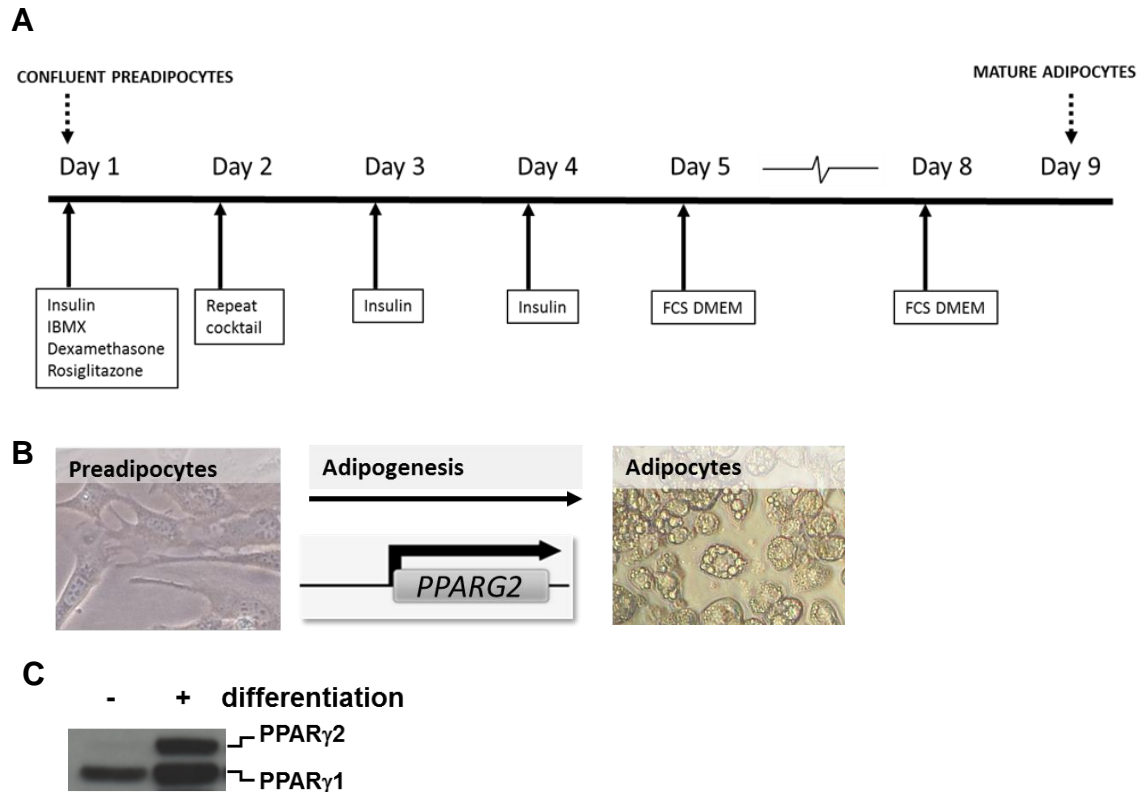


Figure 3.1.5. 3T3-L1 adipogenesis overview. **A)** To induce adipogenesis, post-confluent preadipocytes were cultured in adipogenic supplemented media (described in chapter 2) for 48 hrs. Adipogenic cocktail was further supplemented with insulin after 48 hrs (day 3) and refreshed on day 4. On day 5, maintenance media was applied. **B)** After 7 days of adipogenic differentiation, mature adipocytes are obtained. Mature adipocytes were allowed up to 4 days to acquire lipid droplets, which can be stained and quantified with neutral lipid stain Oil Red O. **C)** PPAR γ 2 expression is induced throughout adipogenesis. PPAR γ 2 is identifiable on western blot as the higher migrating form of PPAR γ .

exposure of arrested preadipocytes to adipogenic inducers triggers synchronous, post-confluence cell cycle re-entry (mitotic clonal expansion - MCE) prior to differentiation. Whether MCE is an artefact of *in vitro* adipogenesis modelling, or a bone fide prerequisite to *in vivo* adipogenesis remains controversial ([Qiu et al., 2001](#); [Tang et al., 2003](#)).

The highly specific ATR kinase inhibitor II (Calbiochem – referred to hereon as ATRi II) was released for commercial use early in this project (2014). Because of this, ATRi II has been the inhibitor of choice for many of the following experiments. Following from 2014, other ATRis became commercially available, including VE-821 and the clinically relevant analogue VE-822. Subsequently, to add clinical significance to results acquired with ATRi II, I have validated key experiments with VE-822 or VE-821. Utilising

a structurally dissimilar ATRi to gain an equivalent result also suggests that this data is not due to an off-target effect of the ATRi compound in question.

I aimed to investigate the impacts of small molecule ATR inhibitors on preadipocytes as they undergo adipogenic differentiation, to characterise a relationship between ATR functionality and the adipogenic capability of 3T3-L1 preadipocytes. It is relevant to investigate the effects of ATR inhibition on cells as they undergo adipogenic differentiation, as from development and throughout adulthood, our adipose tissue is undergoing constant regeneration, requiring successful adipogenesis.

3.2. Results

3.2.1. Small molecule inhibition of ATR decreases adipogenic differentiation of 3T3-L1 preadipocytes

I assessed successful adipogenic differentiation through histochemical staining with triglyceride (TG) stain Oil Red O (ORO) and western blotting of adipogenic proteins. The ability to acquire large cytoplasmic lipid droplets (LDs) is a definitive characteristic of mature adipocytes, making ORO a reliable marker of successful adipogenesis ([Kraus et al., 2016](#)). Further, ORO staining can be quantified following extraction, allowing the significance of changes in ORO staining to be fully investigated.

Small molecule kinase inhibitors of ATR (ATRi) induced a drastic reduction in the adipogenic capacity of 3T3-L1 preadipocytes. Fig 3.2.1.A shows undifferentiated and differentiated 3T3-L1 cultures stained with ORO, where cultures were co-treated with or without ATRi and ATMi (KU-55933) throughout differentiation. ORO staining is quantified in Fig 3.2.1.B, where treatment with ATRi II throughout differentiation induces a ~9 fold decrease in adiposity ($p < 0.001$) and VE-822 reduces TG content 2.5 fold ($p < 0.01$). The decreased TG content induced by ATRi treatment throughout adipogenesis is not phenocopied with ATMi treatment, where instead decreased viability accounted for the small decrease in ORO staining (data not shown). This result indicates that ATRi treatment throughout adipogenic differentiation appears to induce a significant reduction in adipogenic capability of 3T3-L1 preadipocytes.

To investigate the cause of decreased adipogenesis following ATRi treatment, expression of adipogenic regulator PPAR γ 2 in differentiating 3T3-L1 preadipocytes treated with or without ATRi was assessed (Fig 3.2.1.C & D). PPAR γ 2 expression is induced early in unperturbed 3T3-L1 adipogenesis (lanes 2, 4 and 6). Strikingly, co-treatment with ATRi throughout adipogenesis results in specific and almost complete failure to induce PPAR γ 2 protein expression (lanes 3, 5 & 7). This indicates that the failure to accumulate LDs characteristic of successful adipogenic differentiation

following ATRi treatment (Fig 3.2.1.A and B) is due to a failure to induce PPAR γ 2 expression, requisite for adipogenesis.

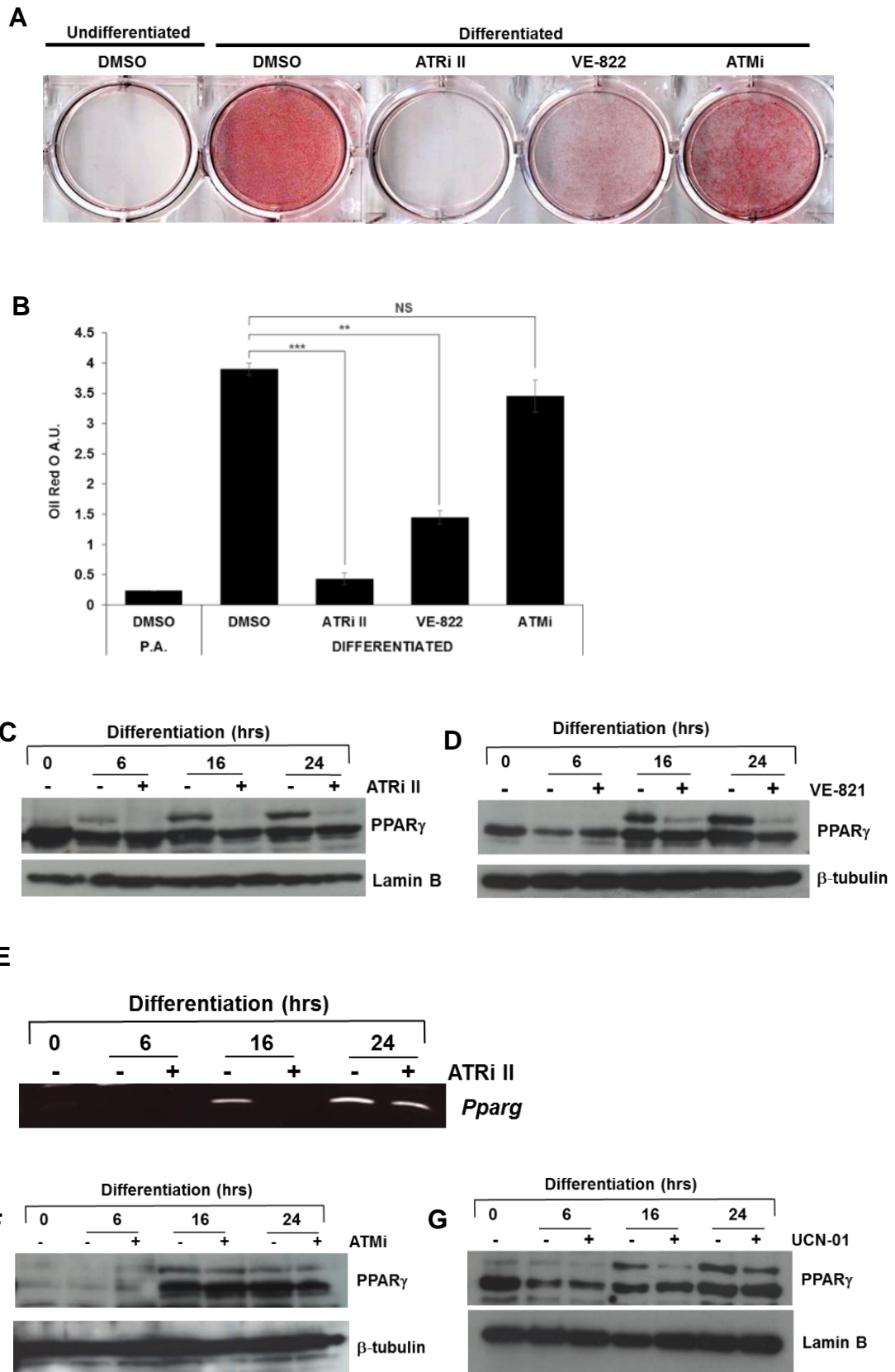


Figure 3.2.1 Adipogenesis of 3T3-L1 cells co-treated with or without small molecule kinase inhibitors of ATR. Successful adipogenesis and accumulation of triglycerides can be observed in 3T3-L1 cell cultures following 10 days in adipogenic medium as determined by Oil Red O (ORO) staining and western blotting of adipogenesis marker PPAR γ 2. **A)** ORO staining of confluent 3T3-L1 preadipocytes (well 1) and terminally differentiated 3T3-L1 adipocytes treated with ATRi and ATMi throughout adipogenesis. ATRi II, VE-822 and KU-55933 (ATMi) (all 10 μ M) were added daily with adipogenic cocktail. **B)** Quantification of ORO staining. ORO was eluted from dried, stained samples in 100% isopropanol and quantified at UV absorbance of 500 nm. Treatment with ATRi II (***) and VE-822 (**) but not ATMi throughout adipogenesis significantly decreases ORO staining indicating reduced triglyceride accumulation and reduced adipogenesis. Statistically significant differences compared to DMSO-treated samples; *** $p < 0.001$ and ** $p < 0.01$ two tailed t-test. Error bars represent standard deviation. **C)** PPAR γ 2 protein expression is induced in early adipogenesis. PPAR γ 2 expression is not induced in samples co-treated with ATRi II or in **D)**, samples co-treated with VE-821. Lamin B and β -tubulin utilised as loading controls. **E)** Semi-quantitative rtPCR was utilised to assess *Pparg* gene product levels. PCR primers targeted a region of *Pparg* specific to both γ 1 and γ 2 isoforms. *Pparg* mRNA levels are increased ~16hrs and 24hrs post-adipogenic induction but not in ATRi II-treated samples. **F)** ATMi does not affect adipogenic PPAR γ 2 induction. β -tubulin utilised as loading control **G)** CHK1i UCN-01 (50 nM) reduces PPAR γ 2 expression at 16 hrs post adipogenic induction. Lamin B utilised as loading control. All images representative of results obtained in at least three independent experiments.

Semi-quantitative RT-PCR was utilised to assess if the ATRi-induced reduction in PPAR γ 2 expression was due to defects at a transcriptional level. Fig 3.2.1.E shows reduced *Pparg* expression following treatment with ATRi II throughout adipogenesis, suggesting reduced production or enhanced degradation of *Pparg* mRNA. This suggests ATR inhibition may affect adipogenesis at stages of the adipogenic cascade that prelude induction of PPAR γ 2 transcription.

PPAR γ 2 expression was induced and maintained appropriately following co-treatment with ATMi (Fig 3.2.1.F). Checkpoint kinase 1 inhibitor (CHK1i, UCN-01) co-treatment appeared to modestly affect PPAR γ 2 induction, a defect that was recovered at later time points (Fig 3.2.1.G).

3.2.2. ATRi has limited effects on viability and S-phase kinetics of Mitotic clonal expansion (MCE)

Before induction of PPAR γ 2 protein expression, differentiating preadipocytes must successfully advance several junctures (discussed in section 3.1.2) ensuring adipogenesis is instigated successfully only where distinct parameters are met. One essential prerequisite to the induction of *Pparg*2 gene transcription is the induction of MCE ([Tang and Lane, 2012](#)).

ATRi is toxic to cycling cells, resulting in mitotic catastrophe and cell death, or cell cycle arrest ([Hitomi et al., 2008](#)). I assessed the effects of ATRi on the viability of differentiating cultures to ensure the decreased adipogenic profile was not a result of decreased viability, induced by ATRi-enhanced replicative stress. Utilising the WST-8 viability assay, Fig 3.2.2.A represents viability of ATRi-treated 3T3-L1 cultures throughout adipogenesis. At later time points, there appears to be decreased but not significant change in the viability of cultures treated with ATRi, and at 24 hrs there is no significant change in viability ($p = >0.05$). Reduced PPAR γ 2 expression is observed as early as six hours (Fig 3.2.1.C), suggesting decreased viability at early time points is not the cause of the failure to express this adipogenic master regulator.

Inhibition of ATR throughout S-phase results in replication fork collapse and the increased generation of double strand breaks (DSBs), where replication machinery arrives at unrepaired single strand breaks (SSBs). DNA-DSBs induce ATM and DNA-PK activity as part of the DDR, an early event of which is the phosphorylation of histone variant H2AX at S139 (γ H2AX). Western blotting in Fig 3.2.2.B and C demonstrate increased γ H2AX and ATM-dependent KAP1-associated protein-1 (KAP1) phosphorylation following ATRi treatment throughout adipogenesis. Fig 3.2.2.C also shows ATR-dependent CHK1 phosphorylation (S345) and activation throughout early adipogenesis. This is likely due to canonical ATR-CHK1 signalling at the intra-S-phase checkpoint, where the p-CHK1 signal is enhanced by the high synchronicity of these cells cultures as they enter S-phase at these time points. Taken together, this data is indicative of increased DNA-DSBs and ATM and/or DNA-PK activation throughout adipogenesis, in the absence of ATR-CHK1 signalling.

Due to the inherent role of ATR in modulating the intra-S-phase checkpoint, I hypothesised the ATRi-induced failure to express PPAR γ 2 may be due to replication fork stalling and cell cycle arrest, resulting in failure to complete MCE. To assess the S-phase kinetics of MCE following ATRi I utilised thymidine analogue EdU (5-Ethynyl-2'-deoxyuridine), which can be incorporated into cells undergoing DNA synthesis and labelled to identify S-phase cells. Fig 3.2.2.D shows fluorescence microscopy of EdU-treated cultures at 24 hrs differentiation, the early stage of MCE. Quantification of EdU-positive cells in Fig 3.2.2.E shows ~80% cells undergoing adipogenesis without ATRi are

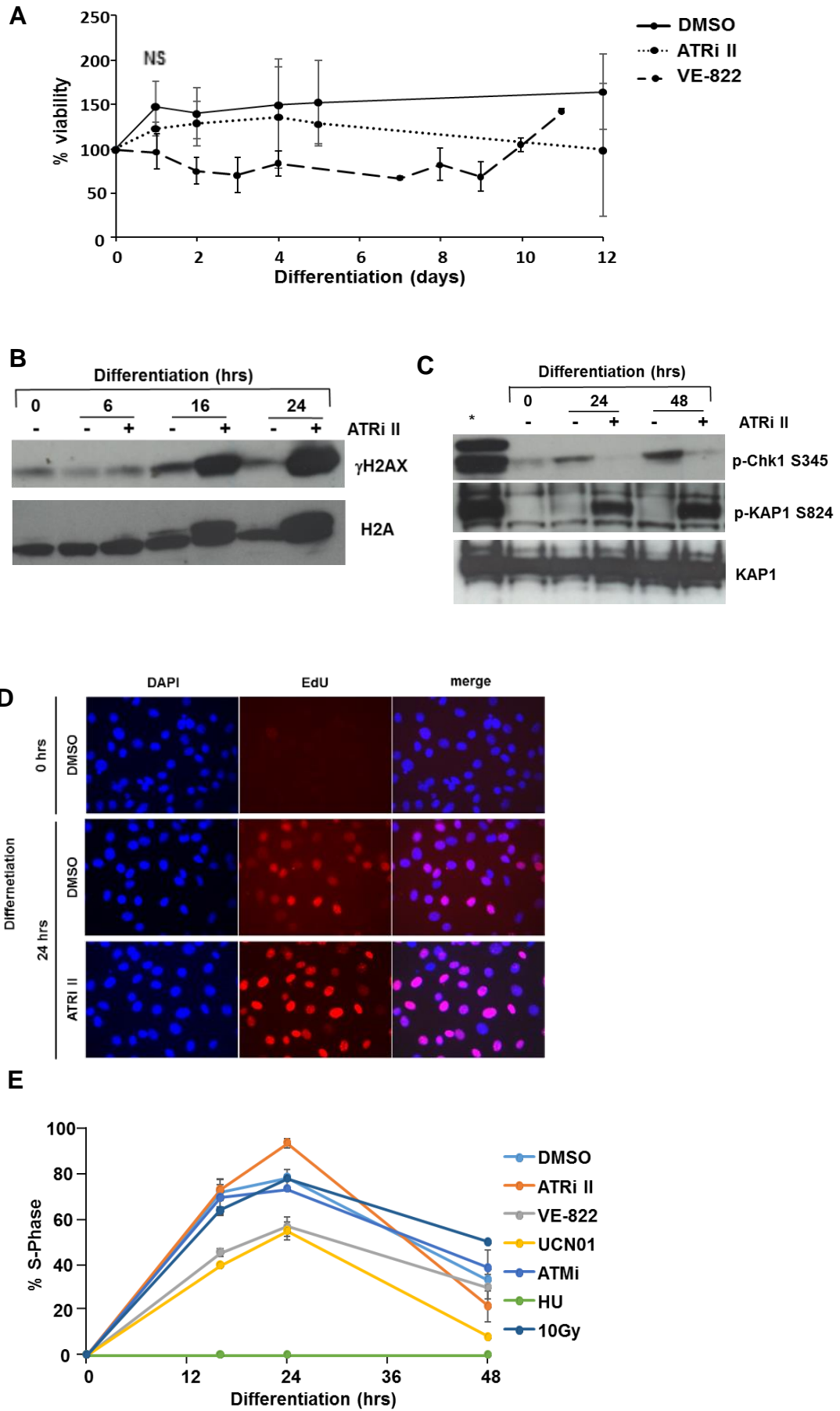


Figure 3.2.2. Effects of ATRi on viability and S-phase kinetics of mitotic clonal expansion. **A)** WST-8 viability assay was utilised to assess toxicity of ATRis throughout adipogenesis with no significant decrease at 24 hrs post induction ($p > 0.05$). **B)** Western blotting shows increased γ H2AX expression throughout adipogenesis with ATRi II, suggesting presence of ATRis induces DDR activation. Native H2A utilised as loading control (lower band). **C)** p-CHK1 S345 indicates ATR-CHK1 signalling axis is activated throughout MCE stage of adipogenesis. ATRi II treatment ablates ATR-dependent p-CHK1 S345 throughout adipogenesis. KAP1 is phosphorylated at S824 in ATRi-treated samples suggesting ATRi-induced ATM activation. * indicates positive controls – 3 hrs 500 μ M hydroxyurea (HU) treatment for p-CHK1 S345 and 10 Gy for p-KAP1 S824. KAP1 used as a loading control. **D)** Fluorescence microscopy of EdU-labelled (S-phase) 3T3-L1 cells undergoing adipogenesis +/- ATRi II at 40x magnification. **E)** Quantification of EdU-positive cells treated with DNA-damage inducing agents and DDR inhibitors throughout adipogenesis (ATRi II, VE-822, ATMi all 10 μ M, 300 nM UCN-01, 500 μ M HU, 10 Gy). Error bars signify SD. All images representative of results obtained in at least three independent experiments.

undergoing DNA synthesis at 24 hrs post adipogenic induction. ATRi II treatment appears to increase synchronicity (90% at 24 hrs) whereas VE-822 treatment reduces S-phase synchronicity to <60%. It appears higher volumes of cells are still undergoing DNA synthesis at 48 hrs when treated with VE-822. CHK1i (UCN01) and VE-822 treatment have similar S-phase induction at 24 hrs, although <10% of cells in CHK1i treated cultures are undergoing DNA synthesis at 48 hrs (Fig 3.2.2.E).

Interestingly, cultures treated with 10 Gy radiation (inducing high levels of DNA SSBs and DSBs) at the initiation of adipogenesis appear to traverse MCE comparably to untreated cultures, suggesting high burdens of DNA damage are compatible with MCE progression. Samples treated with HU fail to undergo any DNA synthesis at all, due to the inhibitory activity of HU on ribonucleotide reductase inducing a severe reduction in the dNTP pools essential for DNA replication.

Taken together, the data in Fig 3.2.2.E suggests that although the two ATRis tested have differing effects on the S-phase kinetics of MCE, the ATRi-induced block in adipogenesis is not due to a failure to traverse MCE, or due to high levels of DNA damage or replication stress, induced by loss of canonical ATR signalling in S-phase.

3.2.3. ATRi does not induce consistent defects in the early adipogenic cascade

As I was observing defects in adipogenesis within the first 24 hrs of induction with ATRis, I next assessed the activity of proteins associated with the early adipogenic signalling cascade. CREB is phosphorylated at S133 within five minutes of adipogenic induction,

rendering it transcriptionally active and able to induce expression of C/EBP β . Interestingly, ATM also phosphorylates CREB at S121 after DNA damage, which decreases the DNA binding affinity of CREB, hence inhibiting its adipogenic activity ([Trinh et al., 2013](#)). I hypothesised that the ATRi-dependent ATM activation (Fig 3.2.2.B, C) observed throughout adipogenesis might enhance ATM-dependent CREB S121 phosphorylation, inducing an adipogenic block.

Fig 3.2.3.A shows western blotting of p-CREB S121 with no change observable between samples treated with/without ATRi throughout adipogenesis. Fig 3.2.3.B shows no significant difference in CREB S133 phosphorylation and C/EBP β expression of samples treated +/- VE-821, 6-24 hrs post adipogenic induction, where appropriate regulation of these proteins is most essential for successful adipogenesis. Considering the high levels of DDR activity observed throughout adipogenic differentiation in cultures co-treated with ATRis (Fig 3.2.2.B, C), it is surprising not to see a change in the

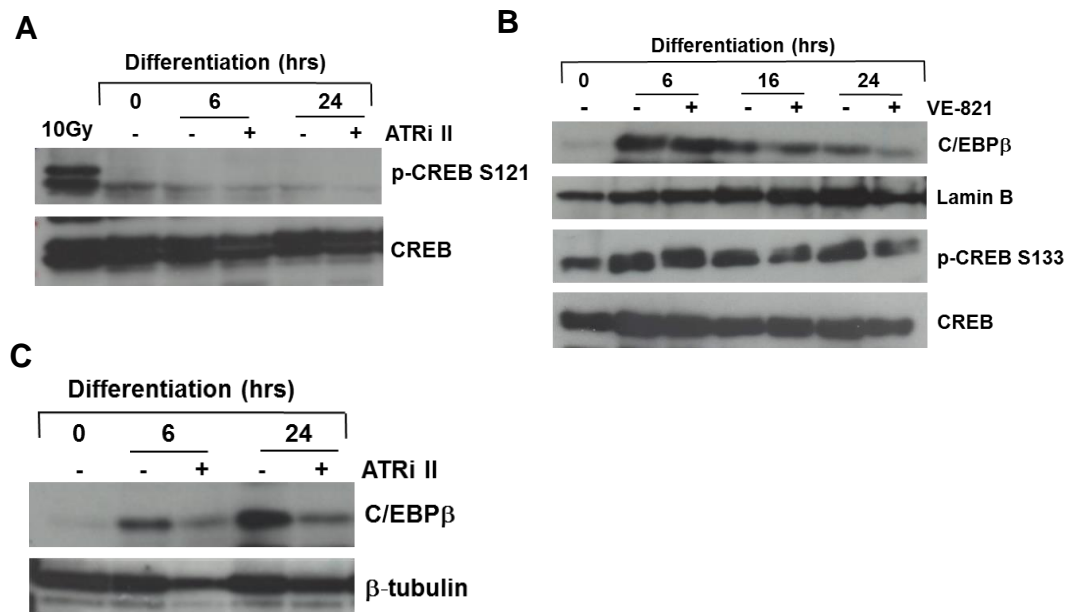


Figure 3.2.3 Assessment of early adipogenic cascade. **A)** ATM-dependent, inhibitory CREB phosphorylation at s121 shows no increase following ATRi treatment suggesting the ATRi-induced ATM activation observed in Fig 3.2.2.C is not causing the adipogenic block at the level of CREB activity. CREB used as a loading control. **B)** C/EBP β and p-CREB S133 are induced early in the adipogenic cascade. Both appear normal following VE-821 treatment. Samples here were treated with VE-821 up to 2 hrs before induction of adipogenesis to ensure complete inhibition of ATR prior to adipogenic induction. Lamin B and CREB utilised as loading controls for C/EBP β , and p-CREB S133 respectively. **C)** C/EBP β expression is decreased following ATRi II treatment, suggesting an adipogenic block at the level of C/EBP β here. This phenotype was unreproducible with other ATRis, suggesting this may not be the cause of ATRi-induced reduction of PPAR γ 2 expression. β -tubulin utilised as a loading control. All images representative of results obtained in at least three independent experiments.

phospho-status of this ATM substrate – perhaps this phospho-site may be ATR-dependent. It is noteworthy that CREB activity is most important within the first minutes of adipogenic induction, hence phosphorylation by ATM, induced by DSBs >16 hrs into adipogenesis is unlikely to affect the role of CREB in early adipogenesis.

Fig 3.2.3.C shows decreased protein expression of C/EBP β following co-treatment with ATRi II. However, this phenotype of reduced C/EBP β expression was not recapitulated with other ATRis. To ensure differences were not due to differing rates of cellular ATRi uptake and incomplete inhibition of ATR kinase activity at adipogenic induction, cultures were pre-treated with VE-821 up to 2 hrs before addition of adipogenic cocktail (Fig 3.2.3.B), with no effect on C/EBP β expression.

3.2.4. p38 MAPK pathway is activated following ATR inhibition throughout adipogenesis

MAPKs transduce stress signals to downstream effectors, working in concert to generate tailored responses to varying types of cell stress ([Roux and Blenis, 2004](#)). Small molecule kinase inhibition of p38 MAPK has been documented to increase the replicative capacity of ATR-Seckel cells, by limiting the p38 MAPK-mediated cellular stress response ([Tivey et al., 2013](#)). Considering this relationship of increased p38 activity concomitant with reduced ATR function and replicative stress, and the complex roles of p38 MAPK in adipogenesis, I assessed p38 MAPK activity following ATRi treatment.

Western blotting in Fig 3.2.4.A shows phospho-p38 MAPK T180/T182 throughout 6-24 hrs of adipogenesis +/- VE-821. At six hrs post-adipogenic induction, p-p38 MAPK appears to decrease, suggesting a reduction in p38 MAPK activity at this time point in unperturbed adipogenesis (lane 2). However, p38 MAPK phosphorylation levels remain unchanged following induction of adipogenesis in the presence of ATRis (Fig 3.2.4.A, lane 3). To assess the functional significance of this sustained p38 MAPK activity in ATRi-treated cultures undergoing adipogenesis, I investigated the phospho-status of several p38 MAPK substrates. MAPKAP2 (Mitogen-Activated Protein Kinase-Activated Protein Kinase 2) is directly phosphorylated by p38 MAPK at T334. Fig 3.2.4.A shows increased p-MAPKAP2 T334 following ATRi-treatment of differentiating 3T3-L1 cultures.

This phosphorylation is not observed in differentiating cells with ATR function, or in unperturbed, undifferentiated cells (Fig 3.2.4.A, lane 1) where p38 MAPK phospho-status is more similar to samples treated with ATRi.

Cross-talk exists between the endoplasmic reticulum (ER) unfolded protein response (UPR) and MAPK pathways, where p38 MAPK is phosphorylated following ER stress. Activated p38 MAPK is also capable of phosphorylating ER-stress transcription factors activating transcription factor 6 (ATF6) and CHOP ([Darling and Cook, 2014](#)). Although the physiological relevance of this phosphorylation on CHOP is unclear, CHOP

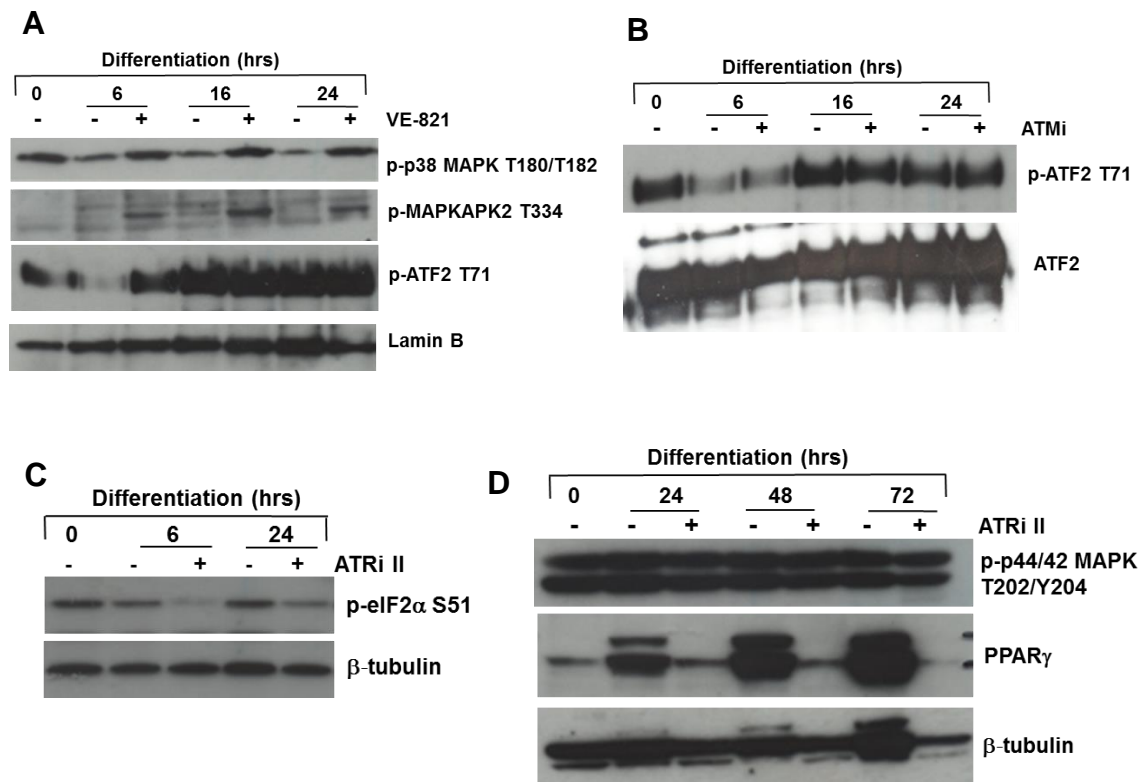


Figure 3.2.4 p38 MAPK is activated throughout adipogenesis following ATR inhibition. **A)** Western blotting demonstrates p38 MAPK is dephosphorylated at T180/182 upon induction of adipogenesis at 6 hrs through to 24 hrs. p38 MAPK remains phosphorylated following co-treatment with VE-821 throughout adipogenesis. Increased p38 MAPK T180/182 has functional significance where p38 MAPK phospho-substrates MAPKAP2 (T334) and ATF2 (T71) have increased activation throughout adipogenesis following ATRi treatment. ATF2 is dephosphorylated at T71 6 hrs post adipogenic induction; however p-ATF2 is increased at this time following ATRi treatment. Lamin B used as loading control. **B)** ATMi treatment throughout adipogenesis does not increase p38 MAPK-dependent ATF2 phosphorylation at 6 hrs post-adipogenic induction, suggesting this phenomenon is ATM-independent. ATF2 used as loading control. **C)** ER stress marker p-eIF2α S51 is decreased following ATRi treatment throughout adipogenesis. β-tubulin used as loading control. **D)** p-p44/42 MAPK is unchanged following ATRi in adipogenic context. PPARγ expression is not recovered at later time points throughout adipogenesis following ATRi treatment. β-tubulin used as a loading control. All images representative of results obtained in at least three independent experiments.

activity is intimately linked to ER Ca^{2+} release, which has an inhibitory effect on adipogenesis ([Graham et al., 2009](#); [Li et al., 2009](#)). Increased ER stress signalling through the eIF2 α (Eukaryotic Initiation Factor 2)–ATF4-CHOP signalling axis results in attenuated adipogenic differentiation in mice ([Han et al., 2013](#)), leading me to hypothesise that increased p38 MAPK activity following ATRi treatment throughout adipogenesis could be indicative of ER stress or dysfunction.

To investigate the functional significance of increased p38 MAPK activity and potential ER stress induction throughout adipogenesis, I assessed phosphorylation of ER stress marker eIF2 α . eIF2 α is phosphorylated by protein kinase RNA-like ER kinase (PERK) at S51 in one branch of the UPR. Interestingly, Fig 3.2.4.C shows decreased p-eIF2 α S51 following ATRi treatment at early time points throughout adipogenesis, indicative of reduced ER stress or reduced PERK activity.

p44/42 MAPK (also known as extracellular regulated signal-kinase ERK 1/2) is phosphorylated transiently and rapidly at T202/Y204 following induction into adipogenesis ([Prusty et al., 2002](#)). p44/42 MAPK is also activated following DNA damage, downstream of ATM and ATR ([Wei et al., 2011](#)). Considering the cross-talk between these pathways, and the ATRi-induced ATM activation I observed throughout 3T3-L1 adipogenesis (Fig 3.2.2.B and C), I wanted to investigate p44/42 MAPK activity. Fig 3.2.4.D shows western blotting of p-p44/42 MAPK throughout adipogenesis – with no change apparent following ATRi treatment, suggesting the reduced PPAR γ 2 protein expression is not a result of DNA-damage induced impingement on p44/42 MAPK adipogenic signalling. Fig 3.2.4.D also shows a longer timecourse of PPAR γ expression, where PPAR γ 2 is ablated as far as 72 hrs into adipogenesis following ATRi treatment, suggesting this defect in expression is not recovered at later timepoints.

3.2.5. ATRi treatment does not block adipogenesis through increased Calcineurin activity

Increased $[\text{Ca}^{2+}]_{\text{cyt}}$ (cytoplasmic Ca^{2+} concentration) enhances p38 MAPK activity and is an effector and result of ER stress ([Kania et al., 2015](#); [Wright et al., 2007](#)). Considering the observed increase in p-p38 MAPK T180/T182 following ATRi treatment throughout adipogenesis, and decreased eIF2 α activity following ATRi (Fig 3.2.4.), I hypothesised

that ATRi treatment could be inducing anti-adipogenic increases in $[Ca^{2+}]_{cyt}$. Increased $[Ca^{2+}]_{cyt}$ will activate Ca^{2+} -dependent phosphatase Calcineurin, increasing the anti-adipogenic effect of NFATc1, summarised in Fig 3.2.5.A.

Cyclosporin A (CsA) is an immunosuppressant drug that inhibits Calcineurin activity through non-competitive inhibition when it is bound to its target Cyclophilin A ([Sieber and Baumgrass, 2009](#)). To test the hypothesis that the ATRi-induced block in PPAR γ 2 expression is caused by increased Ca^{2+} -Calcineurin-NFATc1 signalling, I co-treated

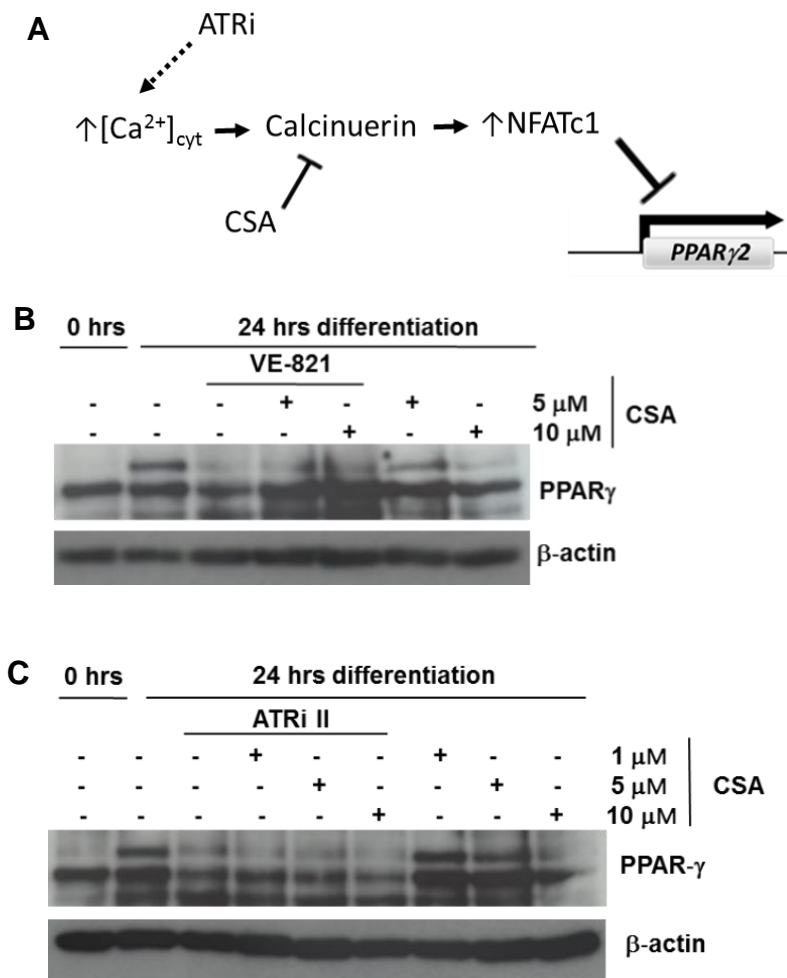


Figure 3.2.5. ATRi does not block adipogenesis in a Calcineurin-dependent manner. **A)** Hypothesised mechanism in which ATRi blocks adipogenesis through increased Ca^{2+} -dependent Calcineurin activity, resulting in increased activity of NFATc1, which has an inhibitory effect on adipogenesis. CsA is an inhibitor of Calcineurin, resulting in alleviation of the adipogenic block imposed by increased Calcineurin activity. **B) & C)** Western blotting of co-treatment with CsA and VE-821 (B) or ATRi II (C) throughout 24 hrs adipogenic differentiation. CsA co-treatment with either ATRi does not rescue PPAR γ 2 expression, suggesting ATRi does not block adipogenesis through increased Calcineurin activity. CsA appears in fact to inhibit PPAR γ 2 expression in a dose dependent manner in this model system. β -actin utilised as loading control. All images representative of results obtained in at least three independent experiments.

differentiating 3T3-L1 cultures with CsA and ATRis throughout adipogenesis (Fig 3.2.5.B & C). If this mechanism were relevant in this context, CsA treatment would recover PPAR γ 2 expression following ATRi.

Fig 3.2.5.B and C show western blots of PPAR γ following treatment with CsA and ATRis throughout adipogenesis. Interestingly, CsA treatment alone negatively affected adipogenesis in a dose-dependent manner, by reducing PPAR γ 2 expression (last 2 and 3 lanes, Fig 3.2.5.B and C). Treatment with CsA did not rescue PPAR γ 2 expression when co-treated with ATRi II or VE-821 throughout adipogenesis, suggesting that increased Calcineurin-dependent NFATC1 activity is not the cause of the ATRi-induced adipogenic defects I have observed.

3.2.6. ATRi does not block adipogenesis through defective pre-Lamin A processing

Considering the existing relationship between ATR and Lamin A processing (summarised in section 3.1.4.2), there is precedence for a potential, novel role for ATR in Lamin A maturation. I hypothesised ATRi throughout adipogenesis might induce defects in the Lamin A processing pathway, resulting in sequestration of SREBP1 and the observed failure to induce PPAR γ 2 (summarised in Fig 3.2.6.A).

Lovastatin is a farnesyl transferase inhibitor – application to cell cultures blocks pre-Lamin A farnesylation and hence successful maturation into Lamin A, resulting in accumulation of pre-Lamin A localised to the nuclear periphery. Utilising lovastatin as a positive control, I assessed the effects of ATRis on pre-Lamin A accumulation via indirect immunofluorescence (IF). An antibody specific to both pre-Lamin A and Lamin A was utilised to detect perinuclear accumulation of pre-Lamin A by IF, associated with reduced pre-Lamin A maturation. Fig 3.2.6.B shows distinct perinuclear accumulation of pre-Lamin A following treatment with lovastatin. Fig 3.2.6.B also shows that this perinuclear accumulation of pre-Lamin A is not observed in samples treated with ATRi II. I also assessed protein expression levels of pre-Lamin A and Lamin A by western blot (Fig 3.2.6.C).

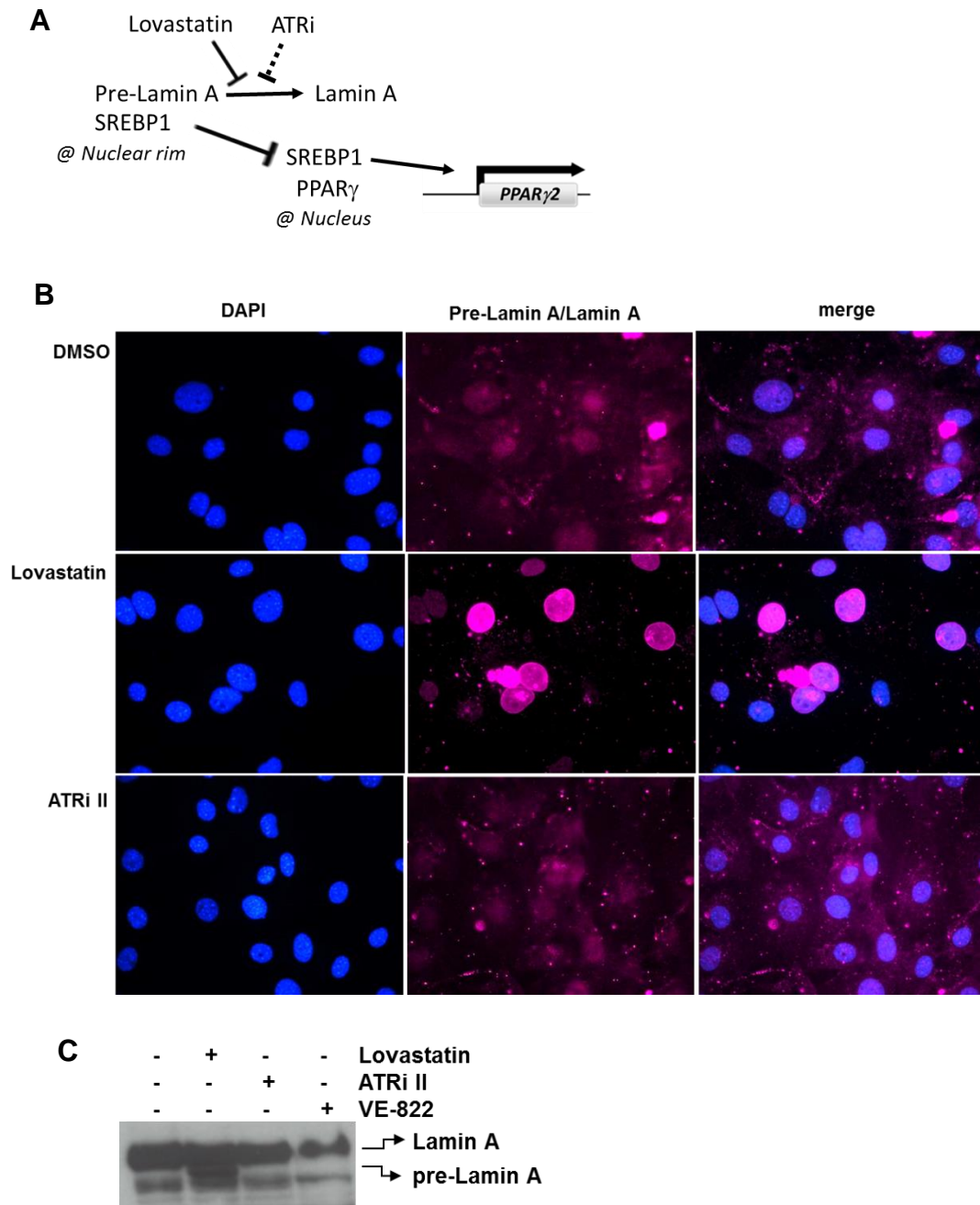


Figure 3.2.6. ATRi does not block adipogenesis through defective Pre-Lamin A processing. **A)** Proposed mechanism of ATRi-induced adipogenic block through. ATRi results in defective processing of pre-Lamin A, resulting in accumulation. Increased pre-Lamin A sequesters SREBP1 at the nuclear periphery, inhibiting its nuclear adipogenic activity. Farnesyl transferase inhibitor lovastatin is used as a positive control due to its activity inhibiting farnesylation-dependent processing of pre-Lamin A. $[Ca^{2+}]_{cyt}$ – cytoplasmic Ca^{2+} concentration **B)** Immunofluorescence microscopy utilising an antibody specific to both Lamin A and pre-Lamin A. Lamin A/pre-Lamin A is enriched at the nuclear periphery following lovastatin treatment but not ATRi treatment. 40x. **C)** Western blotting of 3T3-L1 cells treated with ATRis and lovastatin utilising Lamin A/pre-Lamin A antibody. Lovastatin treatment increases expression of a lower-migrating band, presumed to be pre-Lamin A. Neither VE-822 nor ATRI II induced increases in pre-Lamin A here, further reinforcing that ATRi is not inducing defects in pre-Lamin A processing. Upper band (Lamin A) used as loading control. All images representative of results obtained in at least three independent experiments.

Lovastatin treatment induced a lower migrating form of Lamin A that can be identified as pre-Lamin A (Fig 3.2.6.C, lane 2). ATRi treatments did not appear to induce an increase in the lower migrating band equivalent to lovastatin, leading me to deduce that altered pre-Lamin A processing is not the cause of the ATRi-induced defects in adipogenic differentiation.

3.2.7. ATRi reduces insulin sensitivity in a primary cilia-independent manner, resulting in reduced mTORC1 activity

A role for ATR in primary cilia function has recently been established, where impairing ATR functionality resulted in impaired cilia-dependent signalling ([Stiff et al., 2016](#)). Post-confluent preadipocytes acquire primary cilia enriched in IGF-1 receptors, which behave as adipogenic sensitizers, amplifying incoming differentiative signals ([Zhu et al., 2009](#)).

I assessed the insulin sensitivity of post-confluent and cycling 3T3-L1 preadipocytes treated with ATRi, and further investigated if such alterations in insulin sensitivity were dependent on the presence of primary cilia. The phospho-status of AKT and IRS1 can act as markers of insulin sensitivity. Asynchronous, cycling 3T3-L1 preadipocytes do not express primary cilia, whereas post-confluent 3T3-L1 cultures will produce primary cilia as a requisite to adipogenesis (Fig 3.2.7.A) ([Zhu et al., 2009](#)). Hence, to delineate a role for primary cilia in the ATRi-induced adipogenic defects I have observed, I investigated the insulin sensitivity of confluent preadipocytes as well as asynchronous samples after treatment with ATRis. If ATR-inhibited cultures could not appropriately propagate adipogenic signals due to dysfunctional formation or signalling at the primary cilia, insulin sensitivity should remain unaffected in ATRi-treated, non-ciliated cells.

I confirmed that confluent 3T3-L1 preadipocytes formed primary cilia using immunofluorescence against primary cilia marker acetylated tubulin (Fig 3.2.7.A). Fig 3.2.7.B shows western blotting of proteins containing insulin-sensitive phospho-sites in confluent and asynchronous cells, before and after acute insulin treatments, where samples were pre-treated with or without VE-822 for 30 minutes. Five minutes post insulin addition, phosphorylation of IRS1 at Y989 and AKT at S473 and T308 is markedly increased, suggesting induction of the insulin-PI3K-AKT signalling axis (lane 3).

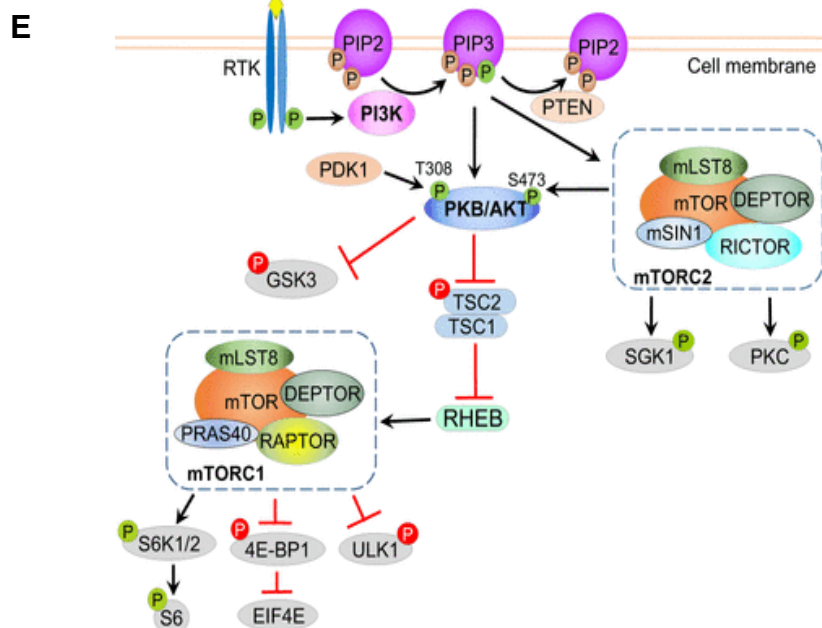
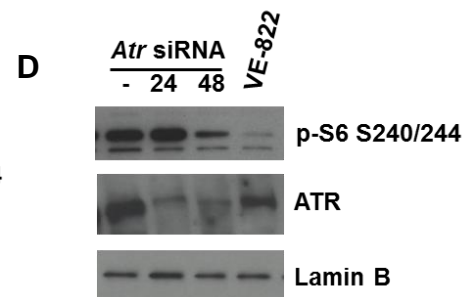
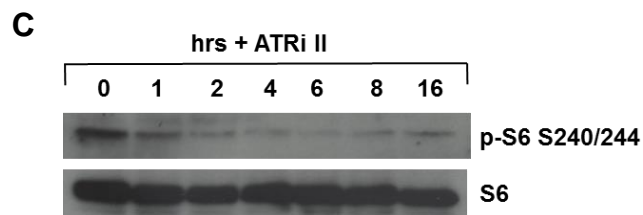
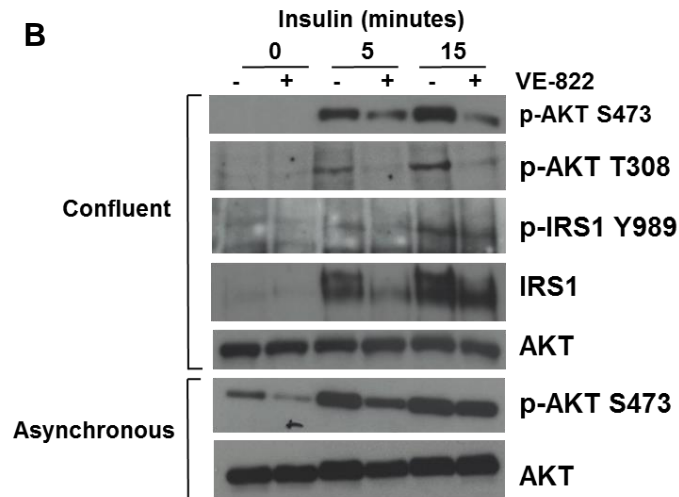
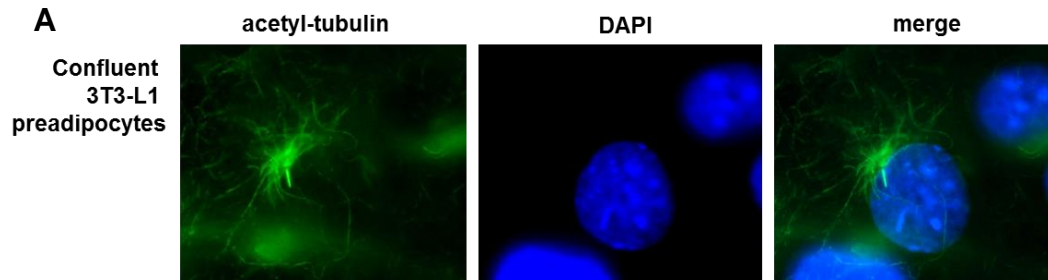


Figure 3.2.7 Acute ATRi treatment and *Atr* siRNA reduces insulin sensitivity and mTORC1 activity in 3T3-L1 preadipocytes. **A)** Immunofluorescence of confluent 3T3-L1 preadipocytes with DAPI (blue) and primary cilia marker acetylated tubulin (green) shows transient formation of primary cilia. Images taken at 100x. **B)** Western blotting of insulin-sensitive phospho-proteins AKT and IRS1 following insulin and ATRi treatment, in confluent and asynchronous cells. Cell cultures were treated with ATRi for 30 minutes before addition of insulin. Insulin induces phosphorylation of AKT and IRS1 within minutes, regardless of confluence. When co-treated with ATRi and insulin, samples display impaired AKT and IRS1 phosphorylation kinetics. In asynchronous samples, decreased p-AKT S473 following ATRi is recovered at 15 minutes. Increased degradation of native IRS1 in ATRi-treated confluent samples suggests rates of IRS1 phosphorylation could be equivalent +/- ATRi, but degradation is causing reduced signal as assessed by western blotting here. AKT utilised as loading control. **C)** p-S6 S240/244 is decreased following ATRi treatment in cycling cells, indicative of reduced mTORC1 activity. S6 utilised as loading control. **D)** *Atr* siRNA induces decreased S6 phosphorylation at 48 hrs. 4 hrs of ATRi VE-822 treatment also decreased p-S6 S240/244. All images representative of results obtained in at least three independent experiments. **E)** Simplified schematic of PI3K-AKT-mTORC1/2 pathway. AKT is phosphorylated on S473 and T308 by mTORC2 and PDK1, respectively, in response to insulin. mTORC1 complex activates S6K, resulting in S6 phosphorylation. Taken from ([Yu and Cui, 2016](#)).

Strikingly, in samples pre-treated with VE-822, both AKT and IRS1 phosphorylations are dramatically reduced, suggesting cells without functional ATR are less sensitive to insulin (Fig 3.2.7.B, lanes 4 & 6). Reduced p-AKT S473 was also observed following ATRi treatment in asynchronous cells, where cells treated with ATRi alone exhibited decreased p-AKT S473 compared to their unstimulated counterpart. This suggests ATRi induces defects in the PI3K-AKT signalling pathway in the absence of stimulation by insulin. The decreased AKT activity in both ATRi-treated confluent and asynchronous cells suggests that the ATRi-induced defects in the PI3K-AKT signalling axis I have observed are independent of primary cilia presence, and furthermore that ATRi treatment is reducing mTORC2 activity. As both PDK- and mTORC2-dependent AKT sites are ablated following ATRi treatment, it is possible ATRi may prevent recruitment of AKT to the plasma membrane, where these phosphorylation events occur.

AKT has downstream activator effects on mTORC1 via inhibitory phosphorylations of the TSC1/2 complex (Fig 3.2.7.E). The TSC complex has GTPase activity, and functions to maintain mTORC1 activator RHEB-GTP in an inactive RHEB-GDP state. Inactivation of the TSC complex by AKT results in active RHEB-GTP, which can activate mTORC1. Reduced AKT activity results in decreased mTORC1 activity. To assess the downstream effects of compromised insulin signalling following ATRi, I assessed p-S6 S240/244 as an indirect marker of mTORC1 activity. S6 is a substrate of S6 kinase, itself a direct target of mTORC1. Fig 3.2.7.C shows asynchronous 3T3-L1 preadipocytes

treated with ATRi II for 1-16 hours. Following addition of ATRi, as early as one hour there is decreased phosphorylation of S6, suggesting reduced mTORC1 activity when ATR lacks kinase activity. To validate that this was not due to an off-target effect of ATRi II, I utilised *Atr* siRNA to ablate ATR expression in cycling 3T3-L1 preadipocytes. Fig 3.2.7.D shows p-S6 S240/244 following *Atr* siRNA and VE-822 treatment. After four hours VE-822 treatment, and 48 hrs *Atr* siRNA treatment, S6 phosphorylation is drastically decreased, suggesting this is not an off target effect of ATRi treatment. Interestingly, ATR is depleted after 24 hrs of *Atr* siRNA treatment, yet at this time point, S6 phosphorylation remains unaffected, hinting at a threshold-based mechanism in which reduced ATR functionality may affect mTORC1.

3.2.8. *Atr* siRNA induces PPAR γ 2 expression

To investigate if differentiating 3T3-L1 preadipocytes with reduced (as opposed to inhibited) ATR would display the same adipogenic defects as those treated with ATRis throughout adipogenesis, I transiently transfected confluent preadipocytes with *Atr* siRNA prior to adipogenic differentiation.

siRNA knockdown depletes mRNA in a targeted manner to reduce protein product, requiring active gene transcription of the protein of interest to deplete expression. Hence, transient transfection of siRNA is commonly undertaken in cycling cells that have high levels of transcriptional activity. As confluence is a prerequisite to adipogenesis, transient genetic ablation of ATR before initiation of adipogenesis required transfection of *Atr* siRNA into confluent cell cultures. However, a benefit of utilising growth-arrested cells in this experiment was the circumvention of toxicity associated with depleting ATR in a cycling cell population.

Transient transfection of *Atr* siRNA required optimisation to ensure ATR protein expression was ablated at the initiation of adipogenesis and throughout. It was also necessary to assess the consequence of transfection reagents on adipogenic induction. Induction of the adipogenic program was evaluated by western blotting of PPAR γ 2. Treatment of differentiating cultures with transfection reagent alone did not affect PPAR γ 2 expression (Fig 3.2.8, lane 5). Very surprisingly, genetic ablation of *Atr* induced PPAR γ 2 expression in the absence of adipogenic cocktail (lane 3), and appeared to

enhance PPAR γ 2 expression following adipogenic induction (lane 6). Considering the impaired PPAR γ 2 induction following ATRi treatment throughout adipogenesis (Fig 3.2.8, lane 7), this interesting result of enhanced PPAR γ 2 expression following *Atr* siRNA alone could provide insight into the multifaceted, threshold-based regulatory mechanisms that govern the decision to proceed into terminal adipogenic differentiation. This result suggests inhibition of ATR may have a different outcome to ATR absence in this context, or perhaps ATRi treatments have off-target impacts. Over expression of a dominant-negative, KD-ATR construct could provide insight here and address this difference.

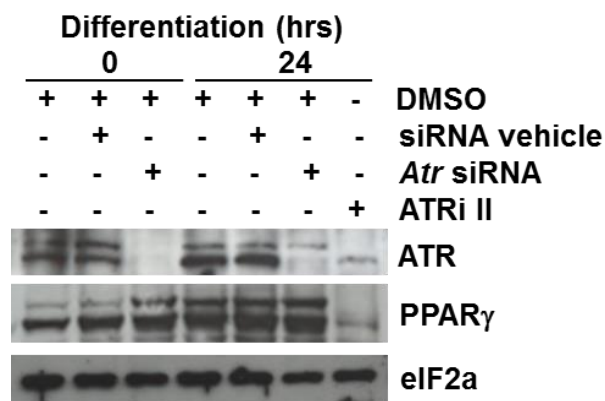


Figure 3.2.8. *Atr* siRNA induces PPAR γ 2 expression in the absence of adipogenic inducers. Confluent preadipocytes were transfected with multiple hits of *Atr* siRNA, resulting in almost complete ablation of ATR protein expression at the initiation of adipogenesis (Fig 8a, lane 3). Both higher and lower migrating bands of ATR have been depleted, suggesting two forms of ATR. *Atr* siRNA treatment did not reduce viability and cells remained confluent throughout transfection. Following successful ATR knockdown, samples were induced to differentiate with adipogenic cocktail as previously described. After 24 hrs adipogenesis, cultures treated with *Atr* siRNA consistently appeared to recover small levels ATR expression, specifically the higher migrating band (lane 6). Treatment with ATRi II throughout adipogenesis appeared to deplete the higher migrating ATR band, whilst some lower migrating ATR remained. Depletion of ATR expression through small molecule kinase inhibition is induced by a failure of ATR to auto-trans-phosphorylate at T1989, reducing overall protein stability. Representative of results obtained in four independent experiments.

3.3. Summary

In summary, I have found that:

- ATRis decrease adipogenic differentiation in 3T3-L1 cells (section 3.2.1)

The decreased adipogenic capability of cells treated with ATRis is not due to:

- Decreased viability or altered S-phase kinetics of MCE (section 3.2.2)
- Defects in the early adipogenic signalling cascade (section 3.2.3)
- Increased Calcineurin activity (section 3.2.5)
- Defective pre-Lamin A processing (section 3.2.6)

However, I have observed, in response to ATRi treatment:

- A functionally relevant reduction in insulin sensitivity, in a primary cilia-independent manner, resulting in reduced mTORC1 activity (section 3.2.7)
- Increased p38 MAPK activity and increased phosphorylation p38 MAPK substrates (section 3.2.4)

Furthermore:

- *Atr* siRNA unexpectedly induces PPAR γ 2 expression in post-confluent 3T3-L1 preadipocytes, independently of other adipogenic inducers, in marked contrast to my findings with ATRi (section 3.2.8)

3.4. Discussion

A significant clinical feature commonly observed in SS is lipodystrophy, suggesting a failure to maintain adipogenic stem cells on a differentiative program ([O'Driscoll, 2009](#); [O'Driscoll et al., 2004](#)). Mice generated from a humanized model of SS recapitulate this presentation of diminished WAT, and a common feature of both SS patient cell lines and mouse models is suppression of the insulin-somatotrophic axis ([Murga et al., 2009](#)). Patients and mouse models of SS demonstrate that defective ATR seems to disproportionately affect adipose tissue ([O'Driscoll, 2009](#)). Currently, there is limited understanding of the underlying mechanisms in which this congenital defect in ATR function affects adiposity or metabolism.

In this chapter, I investigated whether the cachexic presentation of ATR-SS is due to 'cell autonomous' effects of loss of ATR, due to the essential role of ATR in cell replication, or whether ATR signalling has an uncharacterised role in the differentiation of WAT. I have characterised a novel impact of ATR deficiency on the dynamic process of adipogenic differentiation. The negative effect of clinically relevant ATRis on adipocyte biology requires further investigation, to ensure the impacts that I have observed *in vitro* will not drive a cachexic presentation in a cancer setting *in vivo*, associated with poor patient outcome and prognosis.

ATR inhibition with clinically relevant small molecule kinase inhibitors blocks adipogenic differentiation in 3T3-L1 preadipocytes, as indicated by failure to increase adipogenic marker PPAR γ 2 following induction with an adipogenic cocktail. In this novel consequence of ATRi treatment, ATRi-treated differentiating preadipocytes underwent MCE successfully, which suggests that although high levels of DSBs and DDR signalling were present, differentiation was not blocked due to defects in the ATR-dependent intra-S-phase checkpoint. Using western blotting of PPAR γ 2 alone, it was unclear whether the novel adipogenic defects observed with ATRis were independent of canonical ATR signalling through CHK1, as CHK1i also caused reduced PPAR γ 2 protein induction. By assessing MCE kinetics, I demonstrated that CHK1i induces a defect in MCE suggesting that, although both CHK1i and ATRi induce defects in adipogenesis, they are through differing MCE-dependent and -independent mechanisms respectively.

Furthermore, I assessed adipogenesis following ATMi treatment and DNA damaging agents – neither ATMi nor ionising radiation-induced DNA damage had an effect on adipogenic differentiation, suggesting that the adipogenic defects observed with ATRi treatment were not due to cell autonomous effects of loss of ATR, elevated replicative stress or DNA damage signalling, and more specifically reduced ATR-CHK1 signalling. This result is highly indicative that the impacts of ATRi treatment on adipogenic differentiation are occurring through a novel mechanism.

I examined several potential mechanisms that could have contributed to an ATRi-dependent failure to induce PPAR γ 2. I demonstrated ATR inhibition did not generate defects in pre-Lamin A processing, and further did not block adipogenesis through Calcineurin-dependent increases in nuclear NFATC1 activity.

Probably the most striking consequences of ATR inhibition I observed were defects in the Insulin-PI3K-AKT-mTORC1 pathway. I observed decreased insulin-dependent phosphorylation of IRS1 and AKT, and reduced mTORC1 activity with ATRi and *Atr* siRNA, as assessed by S6 phosphorylation. These results appeared cell cycle and primary cilia independent, as they were observed in cycling (non-ciliated) and post-confluent (ciliated) 3T3-L1 preadipocytes. In striking contrast, I saw a remarkable *induction* of PPAR γ 2 when I ablated ATR expression in post-confluent preadipocytes with *Atr* siRNA, in the absence of any adipogenesis-inducing drugs. At face value, these results appear contradictory. Many models could be postulated to explain how *Atr* siRNA could induce adipogenesis – for example, perhaps ATR is required to maintain post-mitotic cell cycle arrest, where ablation of ATR allows preadipocytes to enter MCE without other adipogenic stimulation.

However, I propose a mechanism that unifies my observations on the regulation of adipogenesis following reduced ATR function. mTORC1 has essential inputs into adipogenesis at the level of PPAR γ 2 induction, through downstream target S6K and the 4EBP1-eIF4e axis ([Zhang et al., 2009](#)). mTORC1 also has inhibitory effects on adipogenesis through the inhibition of the IRS1-AKT-PPAR γ axis (Fig 3.4.1.A). Complete inhibition of mTORC1 through Rapamycin treatment or deletion of essential mTORC1 subunit RAPTOR causes complete inhibition of S6K activation, resulting in blocked

adipogenic differentiation at the level of PPAR γ 2 (Fig 3.4.1.B). Phosphorylation of S6K substrate S6 rapidly decreases following ATRi treatment, indicative of mTORC1 inhibition, and it is through this pathway that I propose ATRi treatment generates an adipogenic block at the level of PPAR γ 2 expression. Furthermore, following ATRi treatment I observe reduced IRS1 expression, concomitant with reduced IRS1 and AKT activation, indicating that this arm of mTOR signalling, required for adipogenesis, is also compromised following ATRi treatment.

To explain the increased adipogenesis following *Atr* siRNA, I suggest that incomplete depletion of ATR results in incomplete depletion of mTORC1 activity, alleviating mTORC1-dependent inhibition of IRS1, whilst minimal mTORC1-dependent S6K activity remains. Increased IRS1 activity could potentially lead to hyperactivation of AKT and enhanced adipogenic differentiation (Fig 3.4.1.C). In Fig 3.4.1.D (also shown in

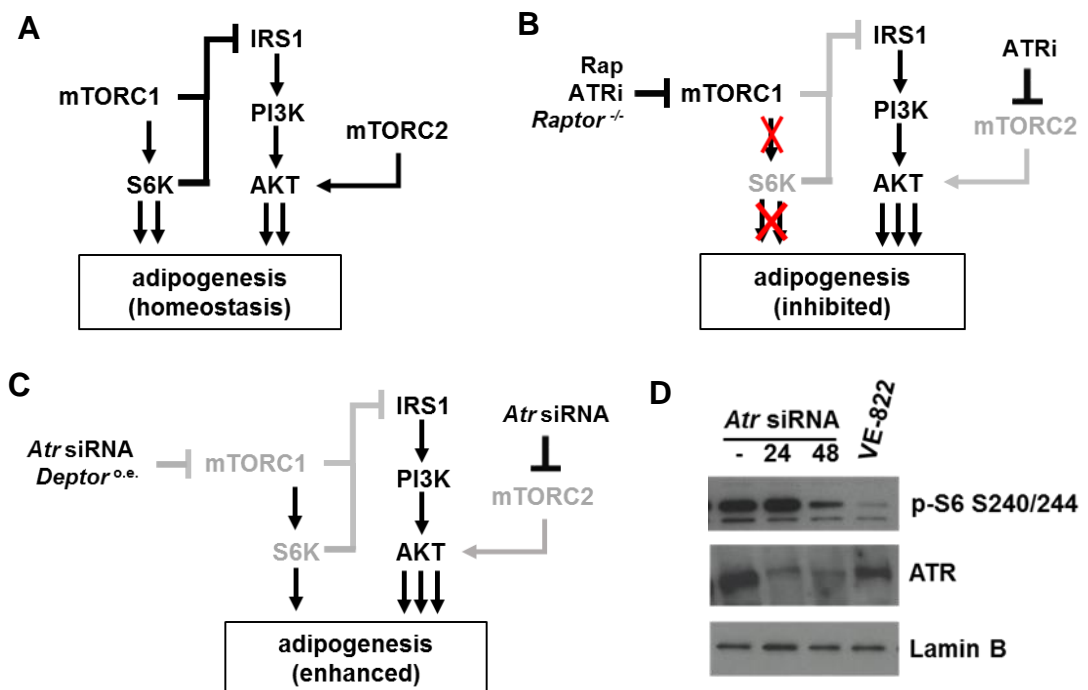


Figure 3.4.1. Schematisation of postulated mechanisms of reduced adipogenesis following ATRi, and enhanced adipogenesis following *Atr* siRNA. Grey shading denotes reduced activity. **A)** mTORC1 activity maintains adipogenic homeostasis through pro-adipogenic activation of S6K, and anti-adipogenic downregulation of the IRS1-PI3K-AKT axis. **B)** Following ATRi, mTORC1 function is fully inhibited resulting in attenuation of S6K activation, inhibiting adipogenesis. Also observed following mTORC1 inhibitor Rapamycin (Rap) and *Raptor* knockout. **C)** Following *Atr* siRNA, mTORC1 is partially inhibited, resulting in minimal S6K activity and reduced inhibition of the IRS1-PI3K-AKT axis, enhancing adipogenesis – also observed following *Deptor* overexpression. Edited from (Yoon et al., 2013). **D)** *Atr* siRNA reduces S6K activity as assessed by S6 phosphorylation (S240/S244), whereas VE-822 (10 μ M, 2 hrs) completely ablates S6 phosphorylation, supporting this hypothesis.

Fig 3.2.7.D), I do observe different impacts on p-S6 S240/244 between ATRi and *Atr* siRNA; the latter treatment has a more modest impact suggesting incomplete mTORC1 inhibition. Yoon et al. have previously postulated this model, where partial depletion of mTOR in 3T3-L1 cells resulted in enhanced adipogenesis ([Yoon et al., 2013](#)). Furthermore, another group discovered that overexpression of DEPTOR, an endogenous mTOR inhibitor, resulted in enhanced adipogenesis against their predictions ([Laplanche et al., 2012](#)). Laplanche *et al.* characterised this phenomenon similarly, as via the dampening of mTORC1-mediated feedback inhibition of insulin signalling via IRS1, resulting in enhanced activity of the IRS1-AKT-PPAR γ axis (Fig 3.4.1.C). In the case of ATRi and *Atr* siRNA treatments, this hypothesis would be easily testable through by assessing AKT phosphorylation at mTORC2-dependent site S473. Alternatively, assessing the effects of overexpression of mTORC1 activators (such as constitutively inactive TSC2) following ATRi treatment on PPAR γ 2 expression.

A failure to maintain preadipocytes within an adipogenic program following treatment with ATRis could constitute evidence for a novel role for ATR in metabolism. The consequences of ATRi treatment on the adipogenic capability of preadipocytes, that I have characterised in this chapter, have potential for the therapeutic use of ATRis in cancer as they reveal potentially undesirable metabolic consequences. Further, this data may provide a pathomechanistic link between the cachexic presentation of SS and ATR deficiency. It is essential to next investigate the effects of chronic ATRi treatment on the metabolic homeostasis of mature, terminally differentiated adipocytes.

Chapter Four

Results II: Impact of Chemical ATR
Inhibition on Mature Adipocytes

4.1. Introduction

In Chapter three I found that treating differentiating 3T3-L1 preadipocytes with small molecule kinase inhibitors of ATR (ATRi) resulted in failure to successfully complete the adipogenic program, a result that carries significance for those who may be treated with ATRi as a cancer chemotherapeutic. Cancer patients are at high risk of metabolic dysfunction as the tumour tissue encourages the body to increase catabolic processes and generate metabolites to facilitate cancer progression {Argiles, 2014 #858}. The earliest adaptive event tumours undertake is an extensive shift towards glycolysis and glucose dependency, known as the Warburg effect ([Warburg, 1956](#)). Cancer cells undergo distinct metabolic reprogramming to sustain their growth at the detriment of the host, generating the cachexic presentation that is so frequently observed in late-stage cancers.

In this chapter, I investigate the effects of chronic ATRi treatment on adipocyte metabolism. I will first discuss several aspects of adipocyte biology in further detail, before detailing my findings.

4.1.1. *Adipocyte and adipose tissue overview*

Almost all animal species are equipped with a mechanism to promote energy storage during periods of calorific excess, and mobilization of this supply when nutrition is scarce ([Gesta et al., 2007](#)). Adipose tissue is specialized connective tissue, which functions as a major energy reserve in the form of stored triglycerides (TGs). In humans, lipid-storing white adipocytes (WAT) are the most abundant constituent of adipose tissue, encompassed within a stromal-vascular fraction composed of a variety of structure-forming cells including preadipocytes, fibroblasts and macrophages ([Berg and Scherer, 2005](#)). Cycling preadipocytes provide a constant supply of adipocyte precursors, which upon appropriate induction, undergo adipogenic differentiation, allowing this metabolic tissue the essential plasticity required to adapt to variable energy output and nutrient statuses. Following excess calorific intake, a small reserve of carbohydrates are stored within the liver as glycogen. When liver glycogen levels are maximal, hepatocytes and adipocytes utilise excess glucose in the *de novo* fatty acid synthesis pathway for assembly of very-low-density lipoproteins (VLDL) and triglycerides ([Coleman R. A.,](#)

[2000](#)). VLDLs export triglycerides from the liver to the adipose tissue, where they are incorporated into the lipid droplet ([Tang and Lane, 2012](#)).

Adipose tissue is a vastly dynamic organ, with key roles in many pathways reaching further than its established role in metabolic homeostasis ([Sethi and Vidal-Puig, 2007](#)). Two functionally distinct types of adipocyte tissue are found in mammals – WAT and brown adipose tissue (BAT). BAT is a thermogenic tissue, with high mitochondrial content and enhanced fatty acid oxidation, designed to dissipate chemical energy as heat via the elevated expression of mitochondrial uncoupling protein UCP1 ([Wang et al., 2015](#)). BAT protects new-born and hibernating mammals from hypothermia, and the trans-differentiation of WAT to BAT (known as ‘adipocyte browning’) is inducible through several mechanisms, including cold exposure ([Wang et al., 2015](#)).

As well as providing insulation and mechanical support, adipose tissue also has endocrine functions – secreting numerous bioactive peptides, known as adipokines, that can promote inflammatory responses ([Berg and Scherer, 2005](#)), influence food intake via the hypothalamus ([Halaas et al., 1995](#)) and regulate haemostasis ([Blüher and Mantzoros, 2015](#)) among other central and peripheral immune-regulatory functions ([Greenberg and Obin, 2006](#)). Adipose tissue is also innervated by the sympathetic nervous system. This renders neurological stimuli an additional regulator of fat mobilisation, via neuronal secretion of adrenergic hormones acting directly at the adipose tissue ([Rodbell, 1966](#)).

The diversity of adipose tissue function and regulation is reiterated in the variety of pathological conditions associated with its dysfunction. Characterising the complex mechanisms behind these pathologies may allow us to identify novel therapeutic targets against the metabolic diseases and co-morbidities that are rapidly becoming a global epidemic.

4.1.2. The lipid droplet

Lipid droplets (LDs) are found in almost all cells, and are the intracellular site of neutral lipid storage. LDs not only act as a reservoir of energetic substrates, utilised in times of inadequate nutrition, but also provide essential membrane components and bioactive lipid mediators [Welte \(2015\)](#). One of the defining characteristics of WAT and BAT

differentiation is the accumulation of LDs, which occupy the vast majority of the cytoplasm. White adipocytes generally contain one gigantic, nascent LD, whereas brown adipocytes contain many multilocular LDs, to increase access of lipolytic machinery to the lipid content via the increased surface-to-volume ratio (Fig 4.1.2) ([Strzyz, 2016](#)).

Many proteins function at the LD surface to facilitate the controlled release and uptake of TGs. In contrast to almost all other organelles, which contain aqueous content within a lipid bilayer, LDs consist of a single phospholipid monolayer ([Tauchi-Sato et al., 2002](#)). LD synthesis and maturation is poorly understood. Widely postulated is the model of membrane budding of the cytoplasmic leaflet of the endoplasmic reticulum

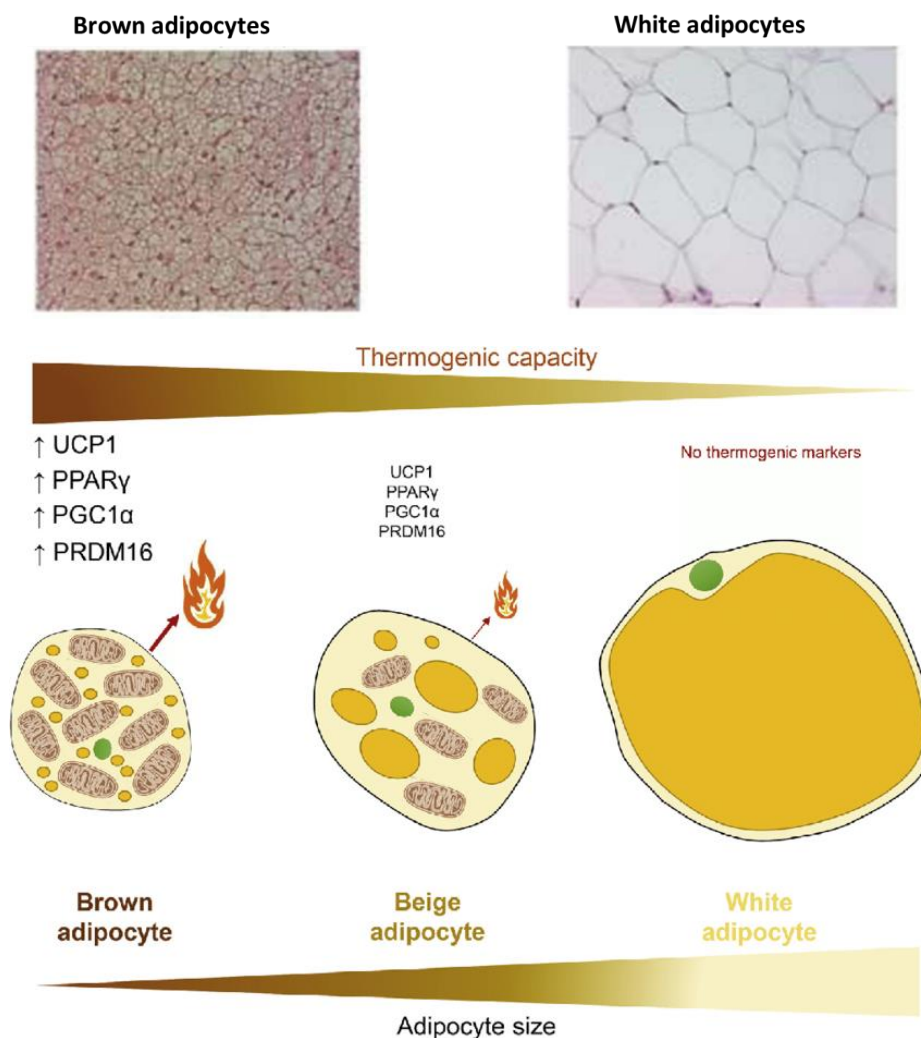


Figure 4.1.2. Sub-types of adipocyte. White adipocytes contain one vast lipid droplet, brown adipocytes have high mitochondrial content and many, small lipid droplets. White adipocytes have no thermogenic capacity, but can be induced to express thermogenic markers and increased mitochondria (beige adipocytes). Brown adipocytes have high thermogenic capacity. Modified from ([Sepa-Kishi and Ceddia, 2016](#)) and ([Contreras et al., 2016](#))

(ER) membrane ([Murphy and Vance, 1999](#); [Ploegh, 2007](#); [Zweytick et al., 2000](#)). Lipid droplets are known to physically interact with other organelles, including the ER, mitochondria and peroxisomes ([Walther and Farese, 2012](#)). Association with the mitochondria may be important for the direct transfer of FAs (liberated from lipolysis) to sites of oxidative phosphorylation ([Tarnopolsky et al., 2007](#)).

4.1.2.1. Lipid Synthesis

The lipid synthesis pathway involves the conversion of acetyl-CoA into FAs, cholesterol, phosphoglycerides and lipids (sphingolipids, DAGs and TGs) – summarised in Fig 4.1.2.1. Most acetyl-CoA used for *de novo* FA/cholesterol synthesis is derived from glucose, via the glycolytic tricarboxylic acid (TCA) cycle. Acetyl-CoA is converted to malonyl-CoA by acetyl-CoA carboxylase (ACC). These acetyl groups behave as the common precursor of almost all lipids, and are repeatedly condensed by fatty acid synthase (FASN) generating the saturated FA palmitic acid, which acts as the primary building block for the further generation of a diverse spectrum of lipid components ([Baenke et al., 2013](#)).

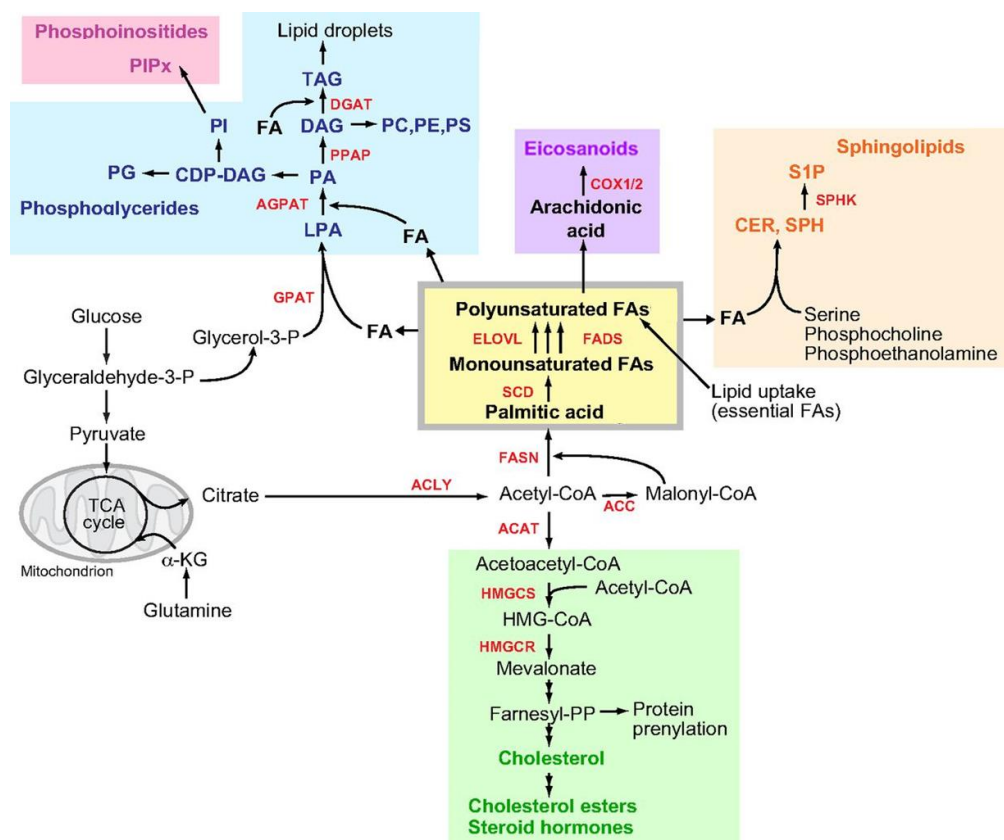


Figure 4.1.2.1. Schematic of lipid synthesis pathways. Acetyl-CoA is the common intermediate in all lipid synthesis. FA – fatty acids; ACC – acetyl-CoA carboxylase; FASN – FA synthase; Glycerol-3-P – glycerol-3-phosphate. Modified from ([Baenke et al., 2013](#))

Cholesterol is generated from acetyl-CoA via the mevalonate pathway. FAs are converted to DAGs/TGs, phosphoinositides and phosphoglycerides via the glycerol phosphate pathway – glycerol-3-phosphate is utilised as glycerol backbone to generate lipid groups. Phosphoglycerides are required as essential membrane components.

4.1.2.2. Lipolysis

Lipolysis is the catabolism of TGs ([Zechner et al., 2012](#)). Within adipocytes, lipolysis is under hormonal regulation and can be executed in a nutrient-dependent manner ([Zimmermann et al., 2004](#)). Lipases are recruited to the LD membrane, facilitating the controlled release of lipids into the cytoplasm for immediate hydrolysis. At the LD membrane, PERILIPIN A (*PLIN1*) is the main regulatory factor of lipolysis. Upon stimulation by β -adrenergic receptor agonists or other Protein Kinase A (PKA) activators, PERILIPIN A is phosphorylated by PKA, enabling it to facilitate the translocation of Hormone-sensitive lipase (HSL) to the LD, and activation of adipocyte TG lipase (ATGL) ([Subramanian et al., 2004](#); [Sztalryd et al., 2003](#)). Sequentially, ATGL hydrolyses TGs to DAGs, HSL hydrolyses DAG to monoacylglycerol, and monoacylglycerol lipase catalyses the final hydrolysis into FAs and glycerol (Fig 4.1.2.2) ([Lass et al., 2011](#)).

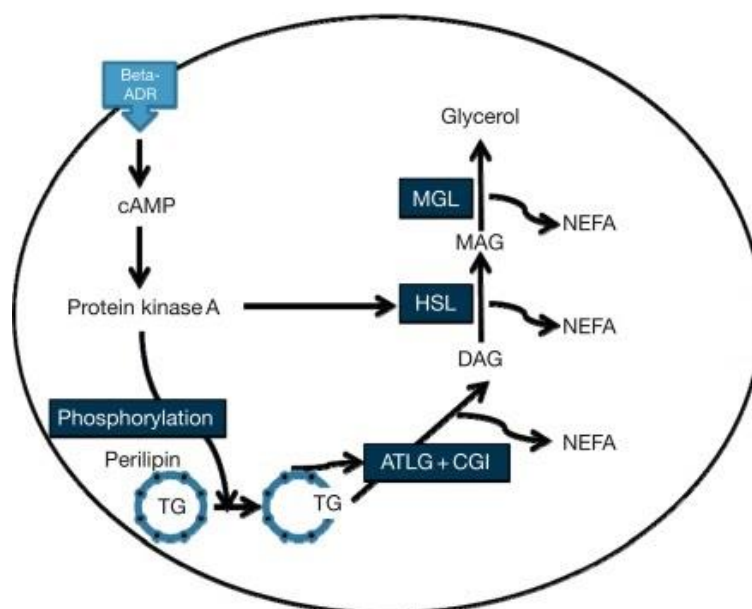


Figure 4.1.2.2. Schematic of lipolysis. TG – triglyceride; ATGL – adipose triglyceride lipase; CGI – comparative gene identification-58; NEFA – non-essential fatty acids (FAs); DAG – diacylglycerol; MAG – monoacylglycerol; HSL – hormone-sensitive lipase; MGL – monoacylglycerol lipase. Modified from ([Baenke et al., 2013](#); [Ojha et al., 2014](#))

Another mechanism has been described for the utilisation of TGs stored within the LD – lipophagy. Lipophagy (autophagic degradation of lipid droplets) appears to play a critical role in energy metabolism during fasting in non-adipose tissues. Double membraned autophagosomes have been observed forming in and around the LD surface, pinching off small portions of the LD. Lipids are degraded by lipases contained within the lysosome following fusion. Surprisingly, Microtubule-associated protein 1A/1B-light chain 3 (LC3-II) is constitutive member of the LD membrane proteome, suggesting autophagy plays an important role in the regulation of lipid metabolism ([Singh et al., 2009a](#)).

4.1.3. Adipocyte browning

Within WAT, a sub-population of inducible ‘brown-like’ or ‘beige’ adipocytes exists, capable of developing thermogenic activity in response to a variety of factors (Fig 4.1.2). The activity of BAT and inducible ‘beige’ adipocytes has been demonstrated to suppress weight gain and reduce metabolic disease ([Kopecky et al., 1995](#)), making the pathways involved exciting and novel targets for the treatment of obesity. Initially perceived as transdifferentiated white adipocytes, a recent study has suggested beige adipocytes are derived from their own distinct progenitor ([Wu et al., 2012](#)). However, the induction of ‘beige’-like adipocytes in 3T3-L1 white adipocyte cultures has been demonstrated in multiple studies ([Asano et al., 2014](#); [Parray and Yun, 2016](#)), suggesting an element of fluidity remains uncharacterised within these functionally distinct varieties of adipocyte.

Brown adipocytes contain uniquely high levels of uncoupling protein-1 (UCP1)-expressing mitochondria. UCP1 activity generates thermogenesis through the controlled uncoupling of oxidative phosphorylation and ATP synthesis. As a transmembrane protein, UCP1 increases the permeability of the inner mitochondrial membrane (IMM), allowing protons pumped into the intermembrane space to return to the mitochondrial matrix. This results in a net decrease in the proton gradient required for efficient ATP production, where protons returning to the mitochondrial matrix dissipate their energy as heat ([Wang and Seale, 2016](#)).

UCP1 is generally induced in beige adipocytes via elevated intracellular cAMP-induced PKA activation and induction of lipolysis (Fig 4.1.3). TGs stored in the LD are

hydrolysed to FFAs and released, where they activate existing mitochondrial UCP1 and their oxidation generates heat. Increased cytoplasmic FFAs can induce white adipocyte browning, and furthermore induce PPAR γ 2 activation, to increase expression of adipocyte-specific genes (discussed further in section 3.1.3.6). Increased PKA activation also leads to increased expression of thermogenic genes, via the activation of p38 MAPK and downstream transcription factors activating transcription factor 2 (ATF2) and PPAR γ coactivator 1-alpha (PGC1 α) (Lo and Sun, 2013; Peirce et al., 2014). ATF2 and PGC1 α can be induced through the activation of other signalling pathways that result in increased

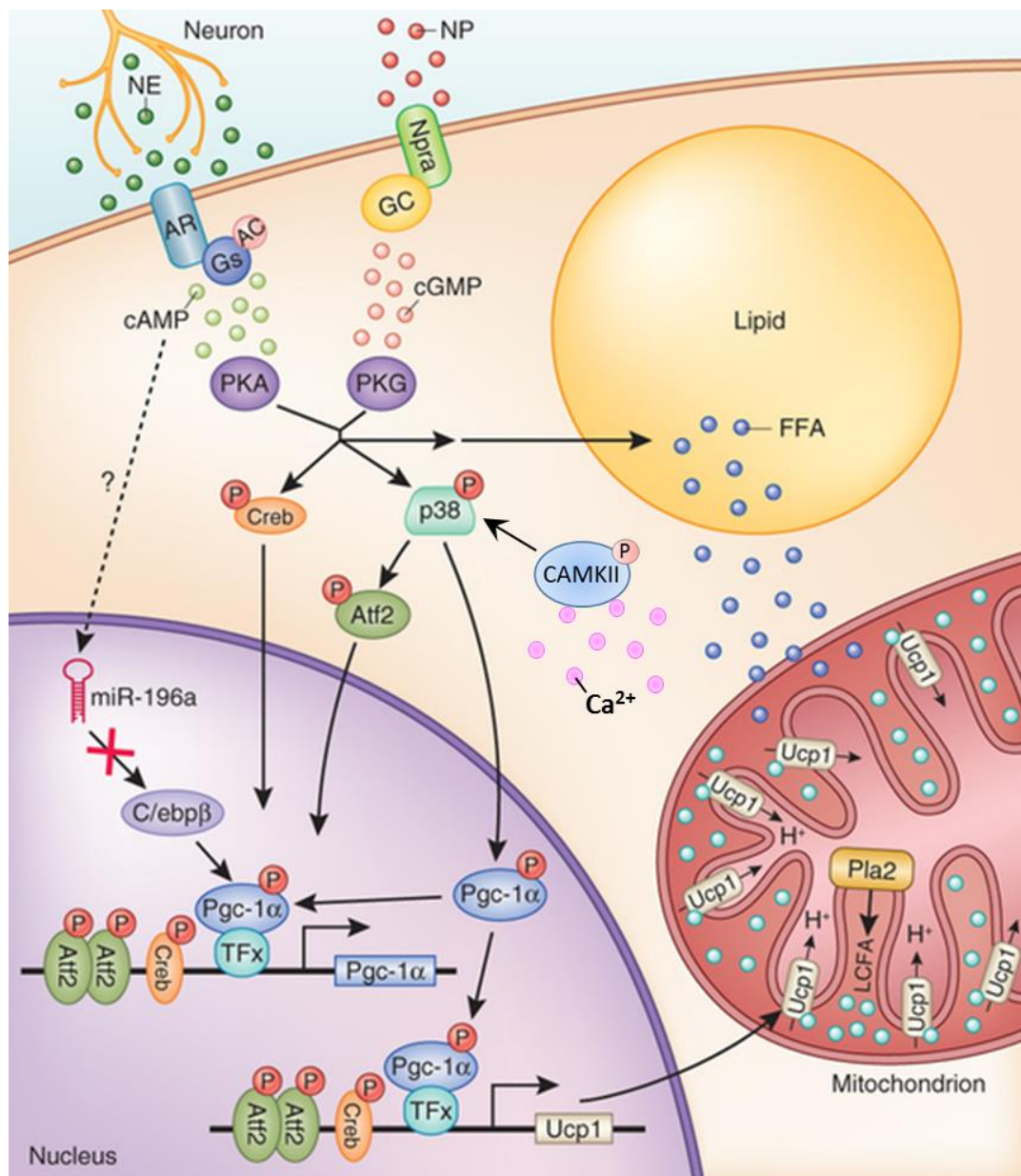


Figure 4.1.3. Schematic of adipocyte browning. Nervous innervation of WAT allows β -adrenergic stimulation, one mechanism of inducing adipocyte browning. Increased p38 MAPK activity is also a common mediatory event in browning induction. Edited from (Harms and Seale, 2013)

p38 MAPK activation, including increased $_{\text{cyt}}[\text{Ca}^{2+}]$ (cytoplasmic Ca^{2+} concentration) via Ca^{2+} /calmodulin-dependent protein kinase II (CAMKII)-dependent activation of p38 MAPK (Fig 4.1.3) ([Wright et al., 2007](#)).

Impaired autophagy in WAT has also been implicated in WAT browning. Recently, the return of UCP1-inducible ‘beige’ adipocytes to their nascent, fat-storing WAT status has been characterised as dependent on increased mitophagy and TFEB (Transcription factor EB)-mediated lysosomal biogenesis ([Altshuler-Keylin et al., 2016](#)), where genetic and pharmacological inhibition of autophagy retained the subpopulation of beige adipocytes. Knockdown of autophagy proteins ATG5, ATG7, or pharmacological inhibition of autophagic or lysosomal function inhibits lipid accumulation in differentiating 3T3-L1 preadipocytes. Adipocyte-specific knockdown of *Atg7* in mice results in a lean phenotype, due to an increased beige adipocyte population and BAT, suggesting autophagy is one of several determinants in adipocyte differentiation and the balance between BAT and WAT ([Singh et al., 2009b](#)).

4.1.3.1. 4E-BP1

4E-BP1 (or eIF4E-BP1 - eukaryotic translation initiation factor 4E (eIF4E) binding protein 1) reversibly binds to eukaryotic initiation factor eIF4E, repressing its ability to initiate translation in the eIF4F complex. Knockout of 4E-BP1 gene *Eif4ebp1* in mice results in

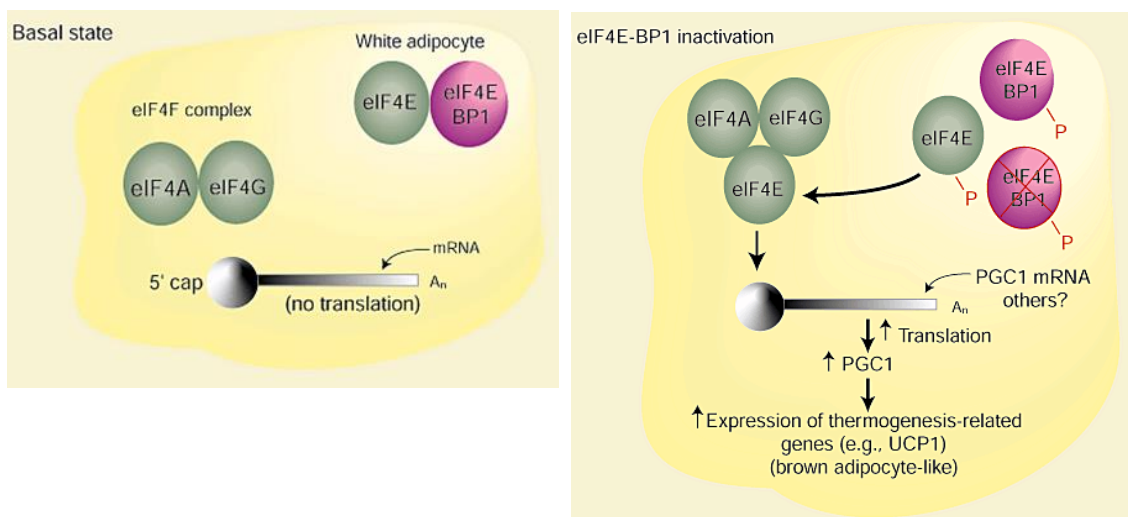


Figure 4.1.3.1. Mechanism of eIF4E-BP1 (4E-BP1) inactivation-induced browning. In the basal state, eIF4E-BP1 binding to eIF4E sequesters eIF4E, inhibiting initiation of cap-dependent translation. Inactivation of eIF4E-BP1, through mTORC1-dependent phosphorylation results in dissociation of eIF4E from eIF4E-BP1 resulting in increased translation of PGC1 α and expression of thermogenic genes. Modified from ([Chen and Farese, 2001](#))

increased metabolic rate, decreased WAT and the increased appearance of BAT ([Tsukiyama-Kohara et al., 2001](#)). It was suggested this effect was due to increased PGC1 α translation. 4E-BP1 association with eIF4E is regulated by mechanistic target of rapamycin (mTOR)-dependent phosphorylation – when mTORC1 is active, phosphorylated 4E-BP1 releases eIF4E, allowing the initiation of cap-dependent translation. This mechanism appears to allow mTOR activity a role in adipocyte browning ([Showkat et al., 2014](#)).

In this chapter, I investigate the effects of ATRi treatment on mature, non-cycling, post-mitotic adipocytes, to ascertain the potential impacts of ATRis on WAT homeostasis. My results in chapter three indicate that ATRi treatment of differentiating preadipocytes has dramatic effects on their capacity to successfully differentiate. Investigating the effects of ATRis on WAT could also be relevant in the proposed use of ATRi in cancer. Furthermore, to characterise the pathomechanism behind the cachexic-like presentation of Seckel Syndrome (SS) and ATR deficiency, and the apparent attrition of WAT in the conditional adult *Atr* deletion mouse model ([Ruzankina et al., 2007](#)).

4.2. Results

4.2.1. Chronic ATRi treatment does not affect adipocyte viability or induce the DDR

Before investigating a role for ATR in adipocyte metabolism, it was important to assess the effects of ATR inhibition on the canonical ATR signalling axis in mature adipocytes. As adipocytes are not cycling cells, I hypothesised I would not observe decreased viability following ATR inhibition, as these cells have no requirement of the role of ATR in cell replication. Utilising the WST-8 viability assay, I assessed viability of 3T3-L1 adipocytes throughout chronic treatment with ATRis. Fig 4.2.1.A demonstrates no significant changes in viability were observed following treatment with ATRis (ATRi II,

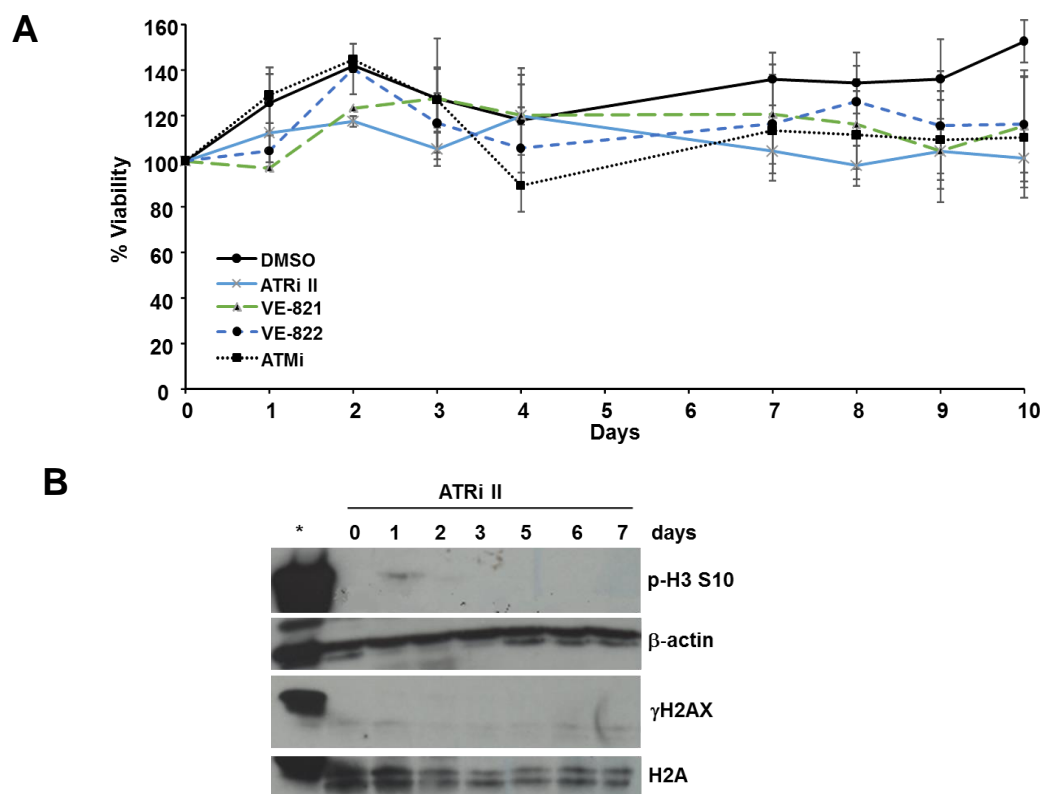


Figure 4.2.1. Chronic ATRi treatment of mature 3T3-L1 adipocytes does not affect viability or induce the DNA damage response. **A)** Viability of 3T3-L1 adipocytes throughout chronic treatment with ATRis and ATMi (all 10 μ M) where no significant change is observed until day 10. **B)** Western blotting of DSB marker γ H2AX and mitosis initiation marker p-H3 S51 – both showing no change following ATRi treatment, suggesting the canonical activity of ATR is non-essential in this system. * indicates positive controls, 10 Gy for γ H2AX and asynchronous preadipocytes of p-H3 S51. β -actin utilised as loading control for p-H3 S10, native H2a as loading control for γ H2AX. All images representative of results obtained in at least three independent experiments.

VE-822, and VE-821) or ATMi (KU-55933). The observed increases in viability are likely due to replication of a small pool of preadipocyte-like cells that remain following the completion of adipogenesis.

To further confirm the G₀ nature of these cells, I assessed phosphorylation of histone H3 at S10 – an established marker of chromatin condensation and mitosis. Using asynchronous, cycling preadipocytes as a positive control, Fig 4.2.1.B shows H3 appears unphosphorylated at S10 in untreated mature adipocytes, and in those chronically treated with ATRi, indicative of an absence of mitotic cells. This indicates that the essential function of ATR in cell replication may not be required in mature adipocytes.

In Chapter 3, I demonstrated that ATRi treatment of differentiating 3T3-L1 preadipocytes induces ATM activation, due to the increased replication stress-induced DNA damage acquired in the absence of ATR function, as assessed by increased γ H2AX. I did not observe this in mature adipocytes treated with ATRis, as shown in Fig 4.2.1.B, indicating that there is no replication-stress mediated DDR activation following ATRi treatment. This further reinforces the reduced requirement of the ATR-DDR signalling axis in terminally differentiated 3T3-L1 adipocytes.

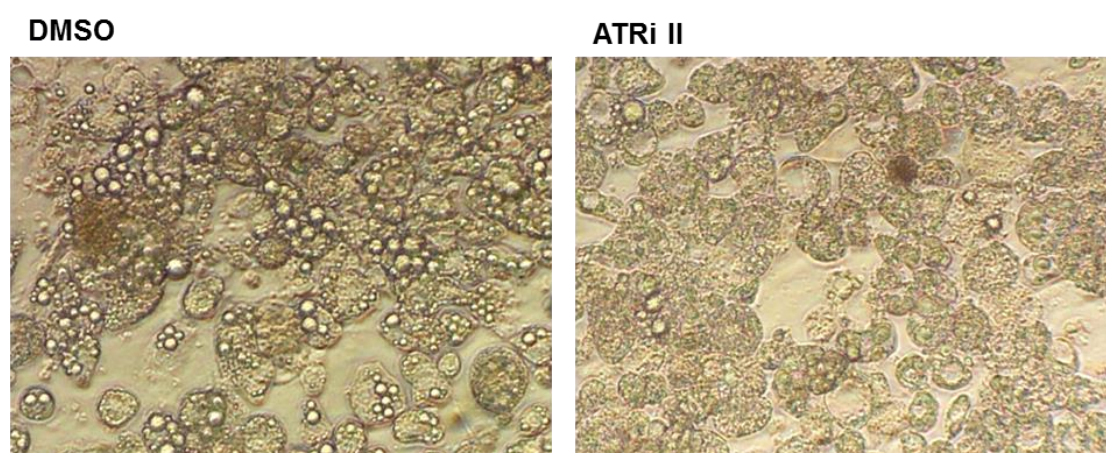
4.2.2. Acute ATRi treatment results in decreased lipid droplet (LD) integrity

Whilst treating mature adipocytes with ATRis to assess the consequences of reduced ATR functionality on their viability, I observed interesting morphological changes. Cytoplasmic LDs, clearly visible in untreated adipocytes, were far less apparent following chronic ATRi II treatment. Fig 4.2.2.1.A shows brightfield microscopy images of untreated mature 3T3-L1 adipocytes, and also samples treated with ATRi II for 6 days, where large LDs were no longer visible. Having confirmed that chronic ATRi treatment was not inducing DNA damage and had no effect on the viability of mature 3T3-L1 adipocytes, I set out to investigate the effects of chronic ATRi treatment on the adiposity (ability to store TGs) of these cells.

I utilised Oil Red O (ORO – described in chapter 3) to assess the TG content of mature 3T3-L1 adipocytes treated with ATRis following successful adipogenic

differentiation – hypothesising that ATRi-treated adipocytes would have decreased adiposity. Fig 4.2.2.1.B shows TG content (as assessed by ORO quantification) of mature adipocytes treated with ATRis and ATMi for 7 days. I observed significant decreases in TG content following treatment with ATRis VE-822 ($p < 0.01$) and ATRi II ($p < 0.05$), but not with ATMi ($p > 0.05$). The viability of adipocytes treated with ATRis remained unaffected at 7 days treatment (Fig 4.2.1.A), hence the observed 30% decrease in adiposity observed following ATRi is not due to decreased viability. This striking result is indicative of metabolic reprogramming events following chronic ATRi treatment.

A



B

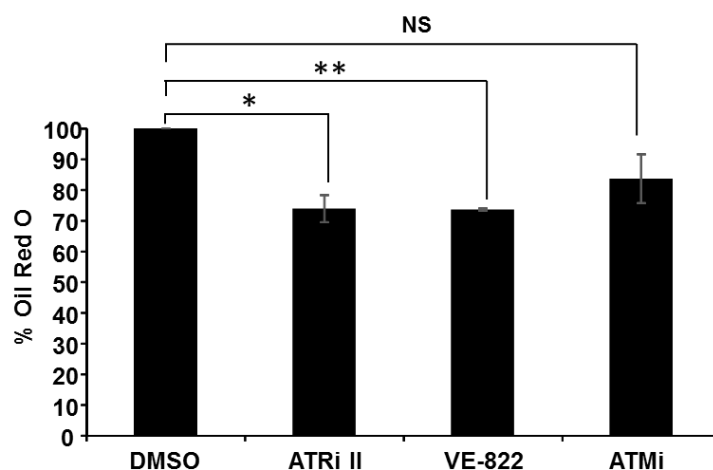


Figure 4.2.2.1 Chronic ATRi treatment reduces TG content of mature 3T3-L1 adipocytes. A) Brightfield microscopy images of mature 3T3-L1 adipocytes treated with or without ATRi II for 6 days. Untreated adipocytes have characteristic LDs within cytoplasmic compartment. Following chronic ATRi II treatment LDs appear less frequent and largely fragmented. **B)** Quantification of TG content of mature adipocytes treated with ATRis (10 μ M) daily for 7 days, as assessed by Oil Red O staining. ATRi- and ATMi-treated samples were normalised to the DMSO-treated control for quantification. ATRi II (*) and VE-822 (**) induce significant decreases in TG content where * $p < 0.05$ and ** $p < 0.01$ – statistically significant changes compared to DMSO treatment (two-tailed T test). No significant decrease observed in TG content following ATMi treatment.

To further investigate the cause of the decreased TG content of adipocytes treated with ATRi, I assessed changes in LD membrane protein PERILIPIN A by western blotting and immunofluorescence (IF), utilising fluorescent triglyceride stain BODIPY 493/503 to visualise LDs.

Fig 4.2.2.2.A and B shows western blotting of adipocytes chronically treated with ATRis to investigate PERILIPIN A expression. Fig 4.2.2.2.A and B demonstrate a drastic decrease in PERILIPIN A expression following treatment with ATRis - ATRi II (Fig 4.2.2.2.A) and VE-822 (Fig 4.2.2.2.B). This phenotype was not observed with ATMi (Fig 4.2.2.2.C). Interestingly, treatment with ATRi II consistently induced a large but transient increase in PERILIPIN A expression at days 1 and 2 (Fig 4.2.2.A lanes 2 and 3).

To further investigate the functional relevance of the decreased PERILIPIN A protein expression following ATRi treatment, I assessed LD integrity and PERILIPIN A localisation to the LD membrane using IF. Fig 4.2.2.2.D shows IF of mature 3T3-L1 adipocytes treated with DMSO or ATRi II for 4 days, stained with antibody to PERILIPIN A and nuclear stain DAPI. I chose to assess PERILIPIN A by IF after 4 days of ATRi treatment, as this was the earliest time PERILIPIN A expression levels were consistently depleted. In DMSO-treated samples, PERILIPIN A evenly coats the LD membrane (Fig 4.2.2.2.D). Drastically and unexpectedly, following 4 days of ATRi II treatment, the even LD-coating of PERILIPIN A appears fragmented, where small gaps without PERILIPIN A at the LD membrane can be observed. The inconsistent placement of this remaining protein implies the fundamental role of PERILIPIN A in the regulation of lipolysis could be compromised following ATRi treatment.

To further investigate this phenomenon, I co-stained mature adipocytes with PERILIPIN A and BODIPY 493/503 to investigate how PERILIPIN A depletion and fragmentation could be effecting intracellular TG content. Fig 4.2.2.2.E shows BODIPY 493/503 (green, neutral lipids) contained within PERILIPIN A-coated LDs in untreated adipocytes. Following 4 days ATRi treatment, the cytoplasmic compartment is stained with BODIPY 493/503, indicating increased cytoplasmic lipid content, concomitant with fragmented PERILIPIN A staining at the LD membrane. This is concerning considering TGs do not often remain unprocessed within the cytoplasm, and highly suggestive of a 'leaky'

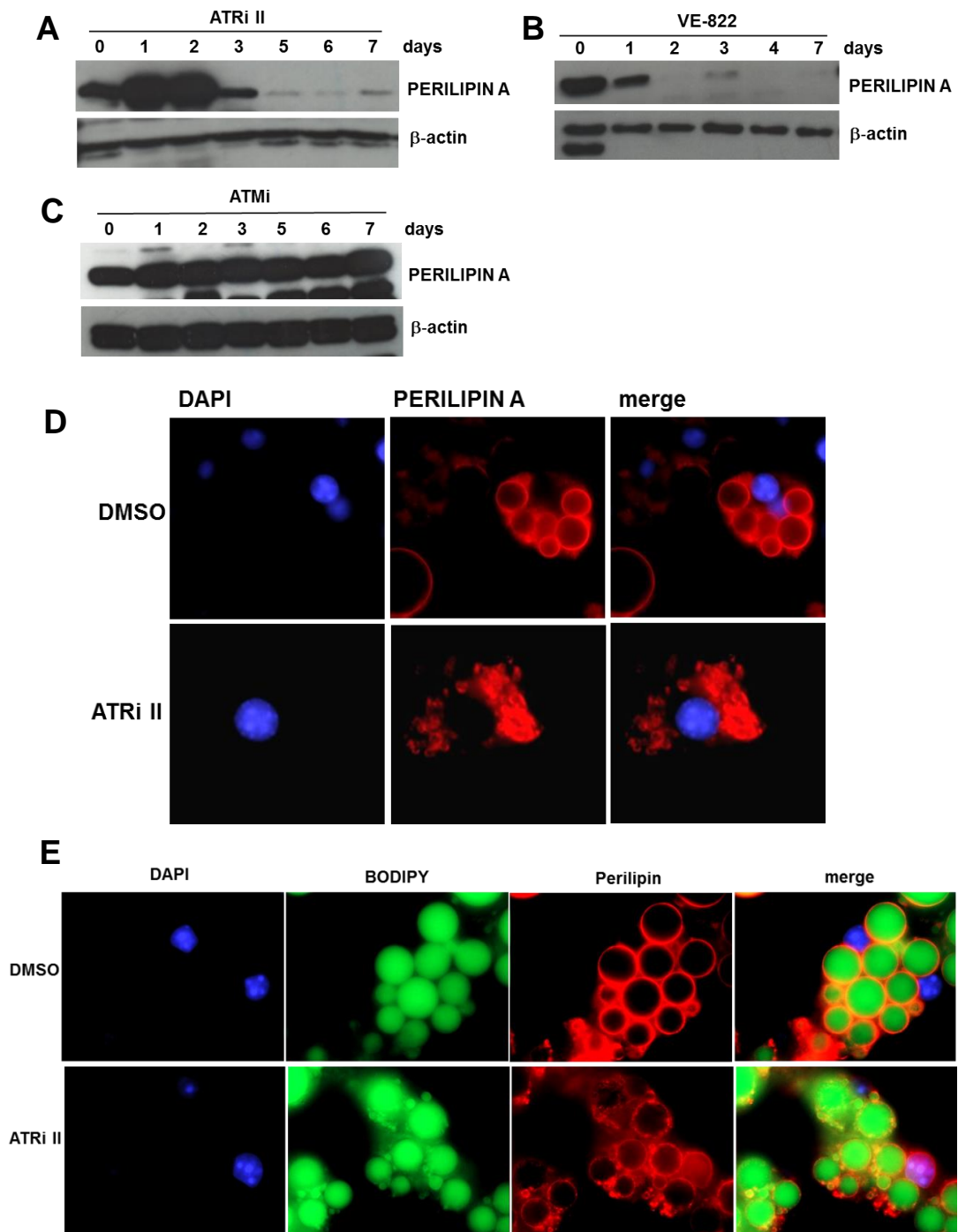


Figure 4.2.2.2. Chronic ATRi treatment decreases lipid droplet integrity of 3T3-L1 adipocytes. **A)** and **B)** Western blotting of mature adipocytes treated with ATRi II (**A**) and VE-822 (**B**) (both 10 μ M, refreshed every 48 hrs) for lipid droplet protein PERILIPIN A show dramatic decreases following chronic ATRi treatment. PERILIPIN A levels were consistently and transiently increased following ATRi II treatment. **C)** ATMi did not affect adipocyte PERILIPIN A expression in this system. β -actin utilised as loading control in all WBs here. **D)** PERILIPIN A immunofluorescence staining of 3T3-L1 adipocytes (PERILIPIN A red; DAPI blue) following 4 days treatment with ATRi II or DMSO. Following ATRi II treatment, PERILIPIN A has lost consistency around the LD membrane and LDs appear fragmented. **E)** Immunofluorescence staining of mature adipocytes with PERILIPIN A (red) and neutral lipid stain BODIPY 493/503 (green). In DMSO treated samples, TGs are contained within the LD, with limited cytoplasmic staining. PERILIPIN A evenly coats the LD membrane. Following 4 days ATRi II treatment, TGs have leaked into the cytoplasmic compartment and PERILIPIN A appears compromised at the LD membrane. Images captured at 100x. All images representative of results obtained in at least three independent experiments.

LD membrane and TG release that is uncoupled from adequate lipolysis.

Mature 3T3-L1 adipocytes treated with ATRi have reduced TG content (Fig 4.2.2.1.B). TG release from the LD is inherently coupled to lipolytic pathways to ensure unhydrolysed TGs do not accumulate in the cytoplasmic compartment. However, TG stain BODIPY 493/503 is increased within the cytoplasm following ATRi treatment in Fig 4.2.2.2.E. I wanted to investigate if the reduced ‘adiposity’ of mature adipocytes following ATRi treatment was due to increased lipolysis, or an aberrant release of intracellular TGs. To investigate this, I treated mature 3T3-L1 adipocytes chronically with ATRi II (10 days) and assessed the FFA and TG content of cell culture media throughout treatment. In this experiment, I utilised FACS analysis of BODIPY 493/503 to confirm I was observing a decrease in cellular adiposity following ATRi, shown in Fig 4.2.2.3.A, where 10 days ATRi II treatment reduces TG content of mature adipocytes by 50%. I utilised a plate-reader based enzymatic assay to quantify media TG content of adipocytes treated with or without ATRi II for 10 days. Fig 4.2.2.3.B shows that in untreated 3T3-L1 adipocytes, media TG content increases slowly over 10 days. In

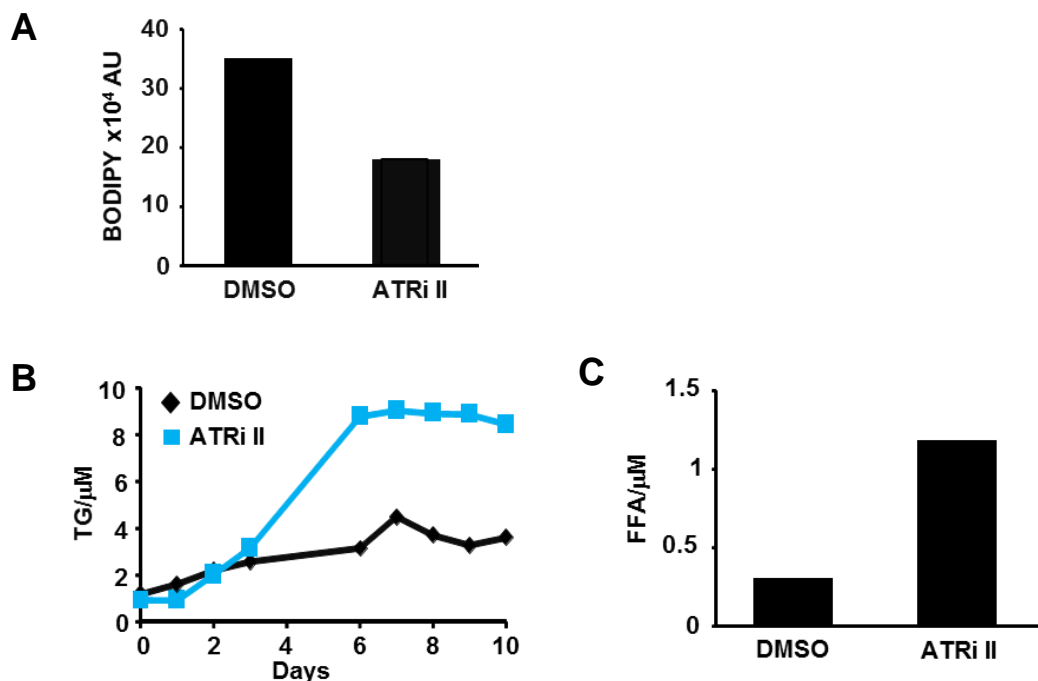


Figure 4.2.2.3. Chronic ATRi treatment induces FFA and TG release. **A)** FACS quantification of cellular TG content of mature 3T3-L1 preadipocytes following 10 days ATRi II treatment (10 μ M) using BODIPY 493/503. TG content is decreased by 50% following ATRi. **B)** Media TG content throughout 10 days ATRi II treatment shows a striking increase in TG release when adipocytes are treated with ATRi. **C)** Quantification of media FFA content following 10 days ATRi II treatment shows increased media FFA, suggesting enhanced lipolysis.

cultures treated with ATRi II, there is a striking increase in media TG content, indicating uncontrolled TG release concomitant with the loss of PERILIPIN A expression (Fig 4.2.2.2A). In Fig 4.2.1.A I demonstrated ATRi treatment of mature adipocytes did not induce a significant loss of viability, suggesting this striking increased in media TG content is not due to cell death. I also assessed media FFA concentration after 10 days ATRi treatment of mature adipocytes, where media FFAs are 3-fold higher in ATRi II-treated samples, indicative of enhanced lipolysis (Fig 4.2.2.2.C).

My data thus far is indicative of profound changes in TG release upon chronic treatment with ATRis, potentially due to compromised LD integrity, with reduced PERILIPIN A expression and enhanced lipolysis.

4.2.3. ATRi induces adipocyte ‘browning’

Upon appropriate stimulation, white adipocytes can undergo the transcriptional reprogramming required for thermogenesis, usually a defining characteristic of brown adipocytes. This likely reversible transdifferentiation process is termed adipocyte ‘browning’; where the induced white adipocytes are coined ‘beige’ or ‘brite’ adipocytes. Brown and beige adipocytes contain lower protein expression levels of PERILIPIN A than white adipocytes, and lower TG content; hence I hypothesised the decreased PERILIPIN A following ATRi treatment could perhaps be indicative of adipocyte browning.

PGC1 α is the master regulator of mitochondrial biogenesis – essential for mitochondrial gene transcription to express the thermogenic, brown adipocyte phenotype. To increase mitochondrial content PGC1 α must be expressed, rendering it a marker of adipocyte browning. UCP1 expression is also required to achieve the mitochondrial uncoupling required for thermogenesis, and is not expressed in WAT, making UCP1 another reliable marker of beige/brown adipocytes. Fig 4.2.3.A shows western blotting of mature 3T3-L1 adipocytes treated chronically with ATRi II - where transient induction of PGC1 α and UCP1 following treatment with ATRi II is observed. This indicates a mass metabolic reprogramming of white adipocytes treated with ATRi, into the programmed catabolism of stored TGs. Fig 4.2.3.A also shows increased PKA-dependent activating phosphorylation of HSL at S563 – further indicative of increased lipolysis, required to generate FFAs which could then be channelled towards uncoupled

β -oxidation and thermogenesis. These striking metabolic phenotypes following ATRi treatment indicate that chronic ATR deficiency has profound impacts on adipocyte metabolism – where no reduction of viability or increased replication stress is apparent.

The dedifferentiation of mature 3T3-L1 adipocytes has been documented ([Zoico et al., 2016](#)). I questioned, considering the absence of common adipocyte markers such as PERILIPIN A in ATRi-treated mature adipocytes, whether these cells were undergoing ‘dedifferentiation’ following the transient browning phenomenon. PPAR γ is a reliable marker of white adipocytes, hence I used western blotting to investigate PPAR γ expression following chronic ATRi treatments in mature, post-mitotic adipocytes. Interestingly, Fig 4.2.3.A shows PPAR γ 1 and 2 are upregulated following the transient increase in PGC1 α . *PPARG* is a target of transcription factor PGC1 α , hence the increased expression of both PPAR γ isoforms could be as a result of PGC1 α activity. The increased generation of FFAs (or their reduced metabolism following return of UCP1 and PGC1 α to basal levels) could also be inducing PPAR γ expression. Regardless, PPAR γ induction here suggests I am not observing a dedifferentiation of ATRi-treated adipocytes to a preadipocyte-like state.

Increased PGC1 α expression induces mitochondrial biogenesis. I utilised flow cytometry analysis of mitochondrial probe MitoTracker Green FM to quantify the mitochondrial content of 3T3-L1 adipocytes following 10 days of ATRi II treatment. Fig 4.2.3.B demonstrates that following ATRi treatment, mitochondrial content is significantly increased by ~80%. Such an extreme increase in mitochondrial content is further evidence to suggest mass metabolic reprogramming and adipocyte browning following ATRi treatment. Interestingly, at 6 days ATRi treatment, PGC1 α and UCP1 expression consistently returns to basal levels, although the mitochondrial mass of ATRi-treated adipocytes remains high.

I investigated the long-term effects (>7 days) of ATRi treatment on mature adipocytes, with the aim of further assessing the metabolic significance of the transient browning phenomenon I have observed (Fig 4.2.3.C). After treating mature adipocytes with ATRi II for 10 days, I utilised western blotting to probe for deviations in phospho-status and expression of the following proteins:

- **LC3-I/II**

LC3-I/II status is a widely recognised marker of autophagic flux. Following ATRi treatment, the lower migrating LC3-II band has decreased, suggesting a reduced accumulation of autophagosomes/increased autophagic clearance.

- **DRP1 (Dynamin-1-like protein)**

Translocation of DRP1 to the mitochondria is a precursor to mitochondrial fission. The modest decrease in expression here following ATRi could be indicative of long-term downregulation of this mito-fission protein.

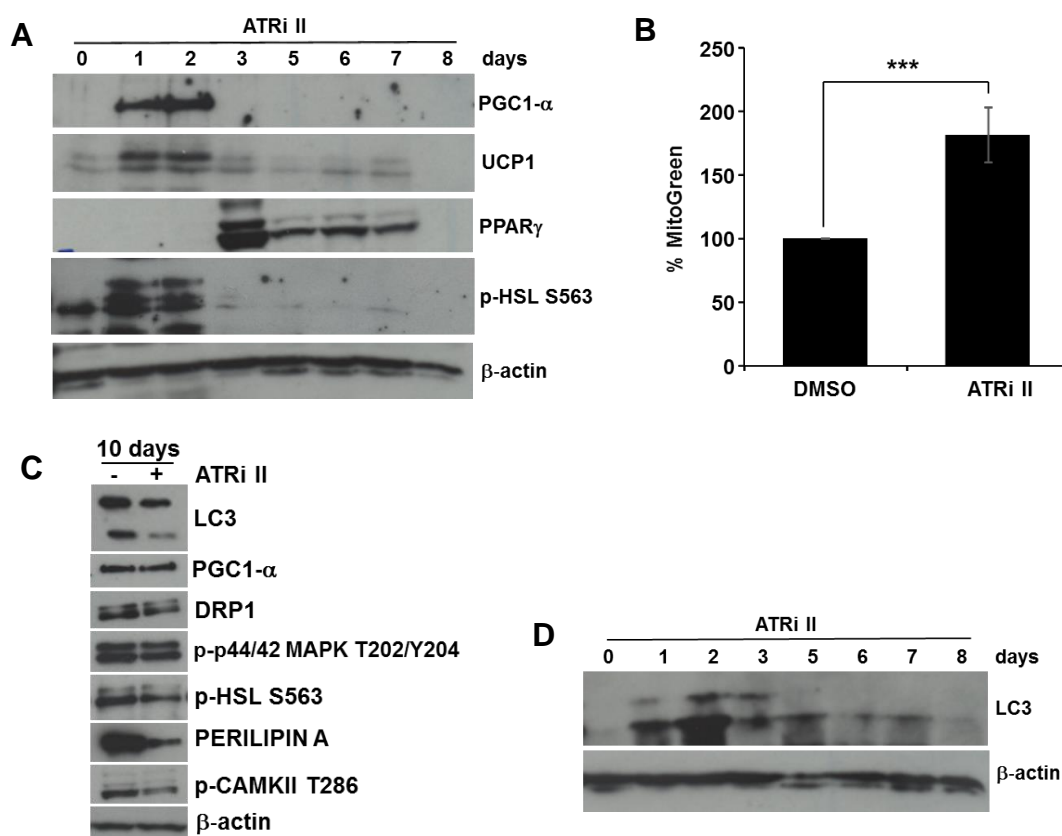


Figure 4.2.3. ATRi treatment induces markers of adipocyte 'browning'. **A)** Western blotting of browning markers PGC1a and UCP1, PPAR γ and p-HSL S563, and β -actin as loading control. Transient adipocyte browning is observed with increased p-HSL S563, indicative of increased lipolysis. **B)** Quantification of mitochondrial mass of mature 3T3-L1 adipocytes treated with ATRi II for 7 days, assessed by flow cytometry using mitochondrial probe MitoTracker Green FM. ATRi was refreshed every 48 hours. **C)** Western blotting of proteins involved in several key pathways that influence adipocyte browning following 10 days treatment with or without ATRi. LC3 - Microtubule-associated protein 1A/1B-light chain 3; DRP1 - Dynamin-1-like protein; p44/42 MAPK - p44/42 Mitogen-activated protein kinase; CAMKII - Ca²⁺/calmodulin-dependent protein kinase II. β -actin as loading control. **D)** Western blotting of autophagic flux marker LC3 following ATRi treatment of mature adipocytes. Expression of LC3-I and LC3-II is increased at 24 hrs ATRi treatment (lane 2), and further at day 2 (lane 3) indicating increased autophagic processing. Day 3 of ATRi treatment onwards LC3 status slowly decreases back to basal levels. β -actin utilised as loading control. All images representative of results obtained in at least three independent experiments.

- **PGC1 α**

PGC1 α remains stable here, consistent with my previous findings that increased PGC1 α expression is a transient event. Interestingly, these adipocyte cultures appear to have much higher basal levels of PGC1 α than those in Fig 4.2.3.B, however this may be due to variation between batches of polyclonal PGC1 α antibody.

- **p-p44/42 MAPK T202/Y204 (p44/42 Mitogen-activated protein kinase)**

This activating phosphorylation has implications in browning and BAT differentiation, however I observe no change in p44/42 MAPK levels.

- **p-HSL S563 and PERILIPIN A**

p-HSL S563 appears unchanged following ATRi treatment, which is interesting considering PERILIPIN A expression remains decreased after 10 days.

- **p-CAMKII T286 (Ca²⁺/calmodulin-dependent protein kinase II)**

The activating T286 phosphorylation on this Ca²⁺-sensitive kinase is an early event in Ca²⁺-induced adipocyte browning, via the p38 MAPK-ATF2 signalling cascade. After 10 days ATRi treatment, CAMKII activity appears modestly decreased.

I chose to further investigate autophagy protein LC3 following my observations in Fig 4.2.3.C – subtle changes in autophagic status of white adipocytes can be sufficient to induce browning, and furthermore increased autophagic activity is observed during the ‘beige’-to-white transition ([Altshuler-Keylin et al., 2016](#)). Autophagy is a highly regulated process, sensitive to cellular nutrient-status. I hypothesised that, considering the altered and aberrant metabolic status of mature adipocytes treated with ATRis, perhaps altered autophagic processing could be a driver or consequence of browning.

Fig 4.2.3.D shows western blotting of LC3-I/II throughout chronic treatment with ATRi II – where large increases in LC3-II following ATRi treatment in mature adipocytes are observed, indicative of enhanced or blocked autophagy, at the same time points I observe the transient browning phenotype. This change in LC3 processing, observed in Fig 4.2.3.D following the ATRi treatment of mature adipocytes, indicates that autophagy may have a role in the transient browning I have observed. Perhaps, autophagy is

upregulated following the aberrant induction into adipocyte browning, in a measure to restore these 'beige' adipocytes back to their original white adipocyte status.

4.2.4. ATRi induces Ca^{2+} -p38 MAPK-ATF2 signalling in adipocytes

In Fig 4.2.3.C I also observed decreased activating phosphorylation of CAMKII (T286), indicative of changes in the cytoplasmic Ca^{2+} status within adipocytes treated with ATRi. Increases in intracellular Ca^{2+} comprise one established inducer of browning in WAT ([Wright et al., 2007](#)). Increased Ca^{2+} activates CAMKII, which in turn activates p38 MAPK, resulting in increased activation of browning transcription factors ATF2 and PGC1 α . In chapter 3 I observed increased p38 MAPK activity and early ATF2 induction following ATRi treatment throughout 3T3-L1 adipogenesis (section 3.2.4). Investigating changes in CAMKII and p38 MAPK activity in ATRi-treated adipocytes could provide mechanistic insight into how ATR inhibition could be inducing transient adipocyte browning.

I further investigated CAMKII activity throughout chronic ATRi treatment of mature adipocytes via western blotting of p-CAMKII T286. Fig 4.2.4 shows p-CAMKII T286 transiently increased at the same time points we observe UCP1 and PGC1 α induction. Activation of CAMKII at these time points appears to have functional relevance, as downstream of CAMKII, adipocyte browning mediator p38 MAPK also

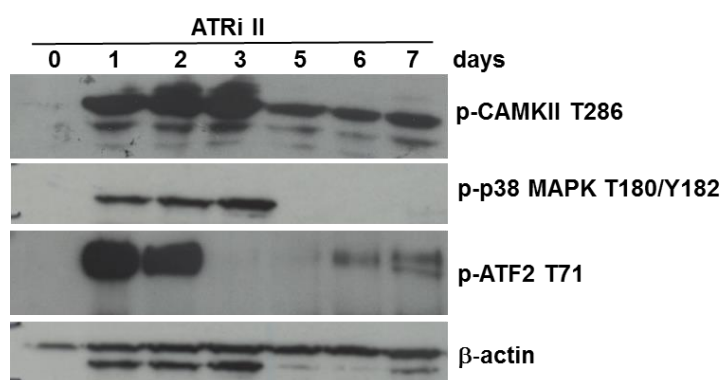


Figure 4.2.4. ATRi treatment activates the Ca^{2+} -p38 MAPK-ATF2 signalling axis in mature adipocytes. CAMKII is activated following chronic ATRi II treatment in mature adipocytes as assessed by p-CAMKII T286 activity. CAMKII appears highly phosphorylated in the first 3 days of ATRi II treatment, however it still remains phosphorylated at later time points. p38 MAPK is also activated transiently for three days following ATRi treatment. Browning transcription factor and p38 MAPK substrate ATF2 is concomitantly phosphorylated at T71, although this activity returns to basal levels after just 2 days of ATRi II treatment. β -actin used as loading control.

appears activated at these time points, as assessed by activating phosphorylations at T180/Y182. ATF2, a p38 MAPK substrate and transcription factor responsible for adipocyte browning in response to increased CAMKII activity, appears transiently activated following ATRi treatment, as assessed by activating p38-dependent phosphorylation at T71. The increased and transient activation of this adipocyte browning axis, from Ca^{2+} -sensitive signal transducer to transcriptional activator, strongly suggests this pathway contributes to the transient browning and metabolic reprogramming following ATRi treatment.

This indicates ATRi treatment may induce adipocyte browning via marked shifts in the Ca^{2+} -status of mature adipocytes. Ca^{2+} is also a fundamental regulator of autophagy, hence ATRi-induced deregulation of intracellular Ca^{2+} status may have also induced the increased autophagic processing I observed in Fig 4.2.3.E following ATRi treatment.

4.3. Summary

In this chapter I have shown you:

- Chronic treatment of 3T3-L1 adipocytes with ATRis does not affect viability or induce the DNA damage response (section 4.2.1)

Chronic ATRi treatment in mature 3T3-L1 adipocytes results in:

- Profoundly reduced PERILIPIN A expression, 'leaky' LDs with decreased TG content and enhanced lipolysis (section 4.2.2)
- Transient expression of markers of adipocyte browning - UCP1, p38 MAPK and PGC1 α (section 4.2.3)
- Increased mitochondrial mass (section 4.2.3)
- Activation of Ca²⁺-dependent signalling axis related to expression of beige adipocyte markers (section 4.2.4)

4.4. Discussion

In this chapter, I have characterised and investigated several novel consequences of chronic treatment of mature, white 3T3-L1 adipocytes with small molecule ATRis. The net effect of chronic ATRi treatment in this model system I have observed is a programmed metabolic shift towards catabolism. This phenomena was not a secondary effect of ATRi-induced DNA damage. Instead, a variety of cytoplasmic signalling pathways not previously associated with DNA repair and cell cycle checkpoint signalling appear to have been affected by kinase inhibition of ATR.

The metabolic reprogramming that these cells have undertaken is reminiscent of the browning of WAT observed in cancer cachexia. I have demonstrated that the increased activity of factors that are more commonly associated with beige and brown adipocytes, has significant effects on the metabolic status of white adipocytes - following chronic ATRi treatment, mitochondrial mass is drastically increased and TG content markedly reduced. Although the ATRi-induced expression of browning-associated proteins was transient, after 7 days of ATRi treatment TG content remained significantly decreased. After 10 days of ATRi treatment, mitochondrial content was increased by ~80%, suggesting the impact of the browning phenotypes are not transient and have long-lasting effects on cellular metabolism. Further characterisation and eventual mechanistic evidence is required to fully understand the implications of ATR deficiency on adipose biology.

Following ATRi treatment of at least 24 hrs, increased activation of CAMKII and p38 MAPK results in the transient upregulation of transcriptional activators required for browning. At the same time points, I also observe increased UCP1 and p-HSL S563, indicative of increased lipolysis and uncoupled β -oxidation at the mitochondria. Notably, HSL has recently been implied in the transdifferentiation of white adipocytes to beige/brown, where its activity of inducing lipolysis and suppressing lipogenesis supports the browning transition ([Kim et al., 2016](#)).

Furthermore, following ATRi treatment, a striking loss of LD membrane protein PERILIPIN A is observed, where what little PERILIPIN A remains appears

fragmented across the LD membrane. Concomitantly, I observed cytoplasmic staining with TG marker BODIPY 493/503, indicative of uncontrolled TG release into the cytoplasm. It is clear that inhibiting the kinase activity of ATR has fundamental implications in WAT biology, where ATRis are driving white adipocytes into a beige-like metabolic state. It is difficult to discern whether the decreased PERILIPIN A is a cause or consequence of the ATRi-induced phenotypes I observe in adipocytes. For example, decreased PERILIPIN A could facilitate uncontrolled TG release as I observed, and perhaps increased HSL activity is a compensatory mechanism to process released TGs, which generates high levels of FAs and induces browning; however, decreased PERILIPIN A expression is also one aspect of the beige adipocyte phenotype.

Although I did not assess mTORC1 activity in mature adipocytes, in chapter 3 I demonstrated reduced mTORC1 activation following acute ATRi-treatments in

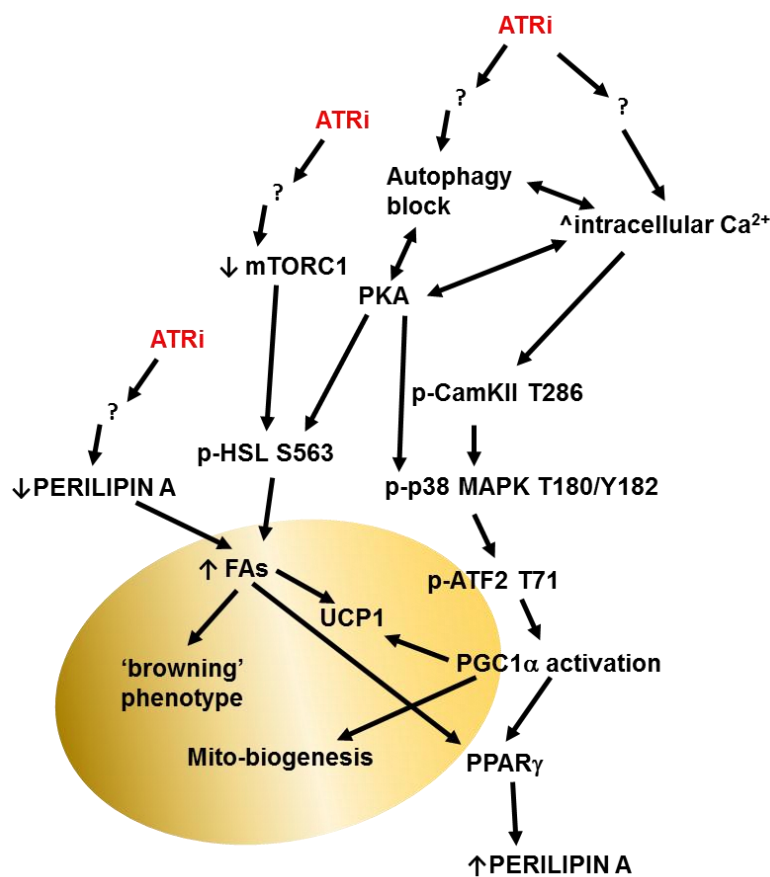


Figure 4.3. Schematic of pathways associated with ATRi-induced adipocyte browning. Gold shading denotes markers of beige/brown adipocytes. ATRi could induce 3T3-L1 adipocyte ‘browning’ via: 1) Decreasing expression of PERILIPIN A, inducing increased FA release; 2) Reduced mTORC1 activation, increasing HSL-dependent lipolysis of TGs into FAs; 3) Blocked autophagy, generating increased $[Ca^{2+}]_{cyt}$ or enhanced PKA activity; 4) Through increasing $[Ca^{2+}]_{cyt}$ through an unknown mechanism.

preadipocytes. Rapamycin is an established immunosuppressant. Inhibition of mTORC1 with rapamycin has been shown to activate HSL, increasing lipolysis with the clinical outcome of hypertriglyceridemia and elevated circulating FFAs ([Soliman et al., 2010](#)). Considering the reduced activity of mTORC1 following ATRi in preadipocytes and increased HSL activity following ATRi in mature adipocytes, perhaps ATRi-induced reduction in mTORC1 activity has a central role to play in these adipocyte phenotypes following ATRi.

The putative mechanisms I have discussed here, that may explain the adipocyte phenotypes following ATRi, are summarised in Fig 4.3.

Interestingly, consistent with the end of the transient 'browning' event, (day 1-2 of ATRi treatment) I observed increases in LC3-II, indicative of increased autophagy. As autophagy has recently been directly implicated in the beige-to-white transition ([Altshuler-Keylin et al., 2016](#)), I postulate that perhaps this increased LC3-II signal is the precursory event to the loss of browning markers UCP1 and PGC1 α . At this point, UCP1-dependent uncoupling of the respiratory chain will become diminished. Perhaps, with mitochondrial β -oxidation beginning to return to basal levels of efficiency, the cytoplasmic FAs that would have previously been metabolised will increase in concentration and activate PPAR γ . I postulate that this is why we see PPAR γ expression increasing only following the loss of UCP1 and PGC1 α . Further to this, the increased FA release induced by ATRi treatment may have concerning physiological implications. Not only are increased circulating FAs associated with insulin resistance and cardiovascular disease, but more importantly FA mobilisation from WAT is associated with cancer progression ([Edmonson, 1966](#); [Liu, 2006](#)).

I have shown in this chapter that chronic ATRi treatment has a fundamental effect on adipocyte homeostasis. Here, I have characterised a relationship between ATR deficiency and defective white adipocyte metabolism and homeostasis. This work provides the first pathomechanistic insight between the cachexic presentation of SS and ATR deficiency. Furthermore, for the first time, concerning metabolic consequences of ATRi treatment have been uncovered, where ATRi treatment of white adipocytes appears to increase lipolysis and FA mobilisation; both of which are considered factors

aspects of cancer cachexia and tumour growth and progression. Further work must be undertaken to fully understand the pathways responsible for the metabolic consequences following ATRi treatment. In addition, a complete understanding of the pathways associated with ATRi-induced metabolic dysfunction could allow the generation of novel synthetic-lethality co-treatments – where ATRi may be utilised with drugs targeting metabolic pathways, for example, mTORC1 inhibitor rapamycin.

Chapter Five

Results II: Compromised ATR function
results in defective autophagy

5.1. Introduction

In Chapter 4, I demonstrated a change in microtubule-associated protein 1A/1B-light chain 3 (LC3) processing in mature 3T3-L1 adipocytes following treatment with ATR inhibitors (ATRIs), indicative of altered autophagic processing. I also showed in Chapter 3 that mechanistic target of rapamycin complex 1 (mTORC1) activity was attenuated in 3T3-L1 preadipocytes, following acute ablation of ATR function with ATRIs and also following transient knockdown of ATR with *Atr* siRNA. mTORC1 is a fundamental regulator of autophagy, and appropriate autophagy is required for effective adipogenic differentiation. Hence, I wanted to further characterise the effects of acute ATRi treatments on autophagic processing.

Autophagy is intrinsically a survival-promoting pathway. There are dual roles for autophagy in cancer progression, although in most contexts the upregulation of autophagic pathways facilitates tumorigenesis. Enhanced autophagy ensures maintenance of functional mitochondria, suppression of p53 induction, and allows cancerous cells increased ability to survive micro-environmental stresses ([White, 2015](#)). The relationship between autophagy and cancer is complex however; 40-75% of breast, prostate, and ovarian cancers lack essential autophagy gene *Beclin 1*, indicating that autophagy may play a role in the suppression of these tumour types ([Qu et al., 2003](#)). Pre-clinical data has demonstrated that autophagy inhibitors can restore tumour chemo-sensitivity and potentiate existing therapies, establishing autophagy inhibitors as a novel therapeutic target ([Yang et al., 2011](#)). Early clinical trials report autophagy inhibitor hydroxychloroquine is not well tolerated however, and the development of lower-toxicity compounds is required to make the autophagy axis a valid target for cancer therapy ([Rosenfeld et al., 2014](#)).

Here I will review the key pathways associated with autophagic processing. I will give particular focus to the factors I have manipulated and investigated, to reveal novel consequences of ATR deficiency on cellular autophagic function.

The term autophagy was first coined in 1963 by Nobel Prize-winning Belgian scientist Christian de Duve ([Ohsumi, 2014](#)). Autophagy is now the umbrella term for the catabolic processes cells utilise for the recycling and degradation of cytoplasmic

constituents. 18 autophagy-essential proteins were initially identified in *S.cerevisiae*, aptly named the autophagy (ATG)-related proteins ([Thumm et al., 1994](#); [Tsukada and Ohsumi, 1993](#)). Following this initial characterisation in yeast, the molecular basis of mammalian autophagy has been subject to extensive research. Almost all constituents of the mammalian autophagy machinery are homologues of those observed in yeast. The high conservation of this process from yeast to man is evidence to the essential nature of the autophagy process.

Appropriate induction of macroautophagy (hereafter referred to as autophagy) ensures salvage of metabolites during periods of nutrient stress, removal of misfolded or aggregated proteins, elimination of intracellular pathogens and clearance of damaged organelles ([Glick et al., 2010](#)). Collectively, autophagy maintains cellular homeostasis, facilitating core anabolic processes by enforcing stringent proteomal/organelle quality controls, and the recovery of nutrients from deleterious cellular components.

With many common constituents, the endocytic pathway acts as a companion to autophagy, through the systematic uptake of nutrients and macromolecules from the extracellular microenvironment ([Hytinen et al., 2013](#)). Where autophagy coordinates the degradation intracellular cargoes, endocytosis allows effective reclamation of extracellular material, with the two pathways converging at the common end-point of lysosomal degradation.

Mechanistically, autophagy requires the combined activity of several cytoplasmic complexes, which can be categorised into sequential steps (Fig 5.1). Autophagy is induced from an array of intra- and extra-cellular cues, cargos targeted for autophagic degradation are packaged as the phagophore membrane is expanded and closed to form mature autophagosomes. Cargo-bound autophagosomes are then transported into the proximity of lysosomes via the dynein-microtubule trafficking machinery ([Fu et al., 2014](#)), and degraded by lysosomal proteases following lysosomal fusion.

Autophagy and the endoplasmic reticulum (ER) stress response are also intimately linked. Accumulation of excessive misfolded proteins in the ER leads to the activation of a homeostatic signalling network committed to recuperating ER function.

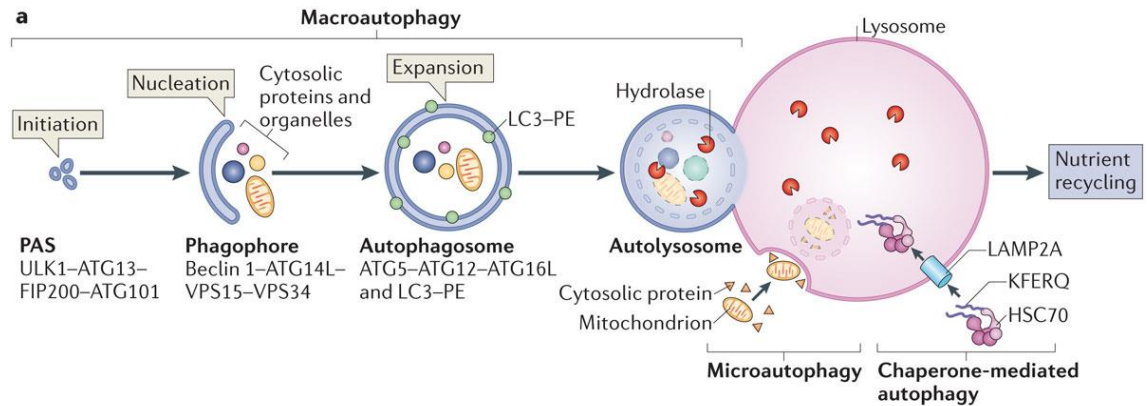


Figure 5.1. Autophagy complexes - initiation to lysosomal fusion. The ULK1 complex mediates PAS formation, and the PI3K complex induces nucleation. Then, the ATG5-ATG12-ATG16L1 complex conjugates LC3-I into LC3-II (LC3-PE) allowing association of cargos targeted for degradation. Taken from ([Kaur and Debnath, 2015](#))

Collectively, this is termed the unfolded protein response (UPR), and one aspect of this highly orchestrated response is the induction of autophagy. ER stress is a potent inducer of autophagy, due to the enhanced requirement of this degradation pathway to clear misfolded/aggregated proteins ([Rashid et al., 2015](#)). Several transcription factors initiated by the UPR directly promote transcription of autophagy-protein containing genes ([B'chir et al., 2013](#)), a key function of AMP-activated protein kinase (AMPK) is to induce autophagy in response to ER-stress mediated toxicity ([Lee et al., 2012](#)), and further to this, the loss of ER-luminal Ca^{2+} that often accompanies ER stress is adequate to induce autophagy via AMPK-dependent mTORC1 inhibition ([Høyer-Hansen et al., 2007](#)).

Defective autophagic processing has recently been associated with a variety of pathologies, including cancer and neurodegenerative disorders such as Parkinson's disease, Alzheimer's and amyotrophic lateral sclerosis ([Jiang and Mizushima, 2014](#)). The underlying mechanisms in which faulty autophagy induces these neurological deficits are currently subject to extensive research ([Nixon, 2013](#)). What can be ascertained is the undoubtable housekeeping role of autophagy in terminally differentiated neurons, and that defects at any point in proteasomal management can result in neurological disorder ([Mizushima and Komatsu, 2011](#)).

5.1.1. Phagophore formation and nucleation

Following incoming signals to induce autophagy, initiation begins with the formation of a phagophore assembly site (PAS) within proximity of the endoplasmic reticulum (ER) (Fig 5.1.1.1) ([Sanchez-Wandelmer et al., 2015](#)). Different protein complexes interact at the PAS to orchestrate the formation of autophagosomes. The ULK1/2 complex consists of UNC51-like kinase (ULK), autophagy protein 13 (ATG13), FAK family kinase interaction protein of 200 kDa (FIP200) and ATG1. During initiation, the ULK1/2 complex is directed to the ER, along with the autophagy-specific class III PI3K complex, which consists of vacuolar protein sorting 34 (VPS34) PI3K and regulatory subunits ATG14L, VPS15 and Beclin 1 (Fig 5.1.1.1) ([Xie and Klionsky, 2007](#)).

Membrane-bound ATG9 cycles between the PAS and peripheral sites in vesicles, delivering membrane for phagophore expansion/elongation ([Yamamoto et al., 2012](#)). Efficient anterograde delivery of ATG9 vesicles to the PAS requires transport factors ATG23 and ATG27 – proteins also believed to have an essential role in ATG9 vesicle biogenesis ([Yamamoto et al., 2012](#); [Yen et al., 2007](#)). Although ATG9 vesicles provide *some* membrane for the formation of autophagosomes, they do not provide the amount of lipid required for a complete autophagosome. The origins of the majority of the lipid membrane required for phagophore biogenesis remain controversial, but it is most likely

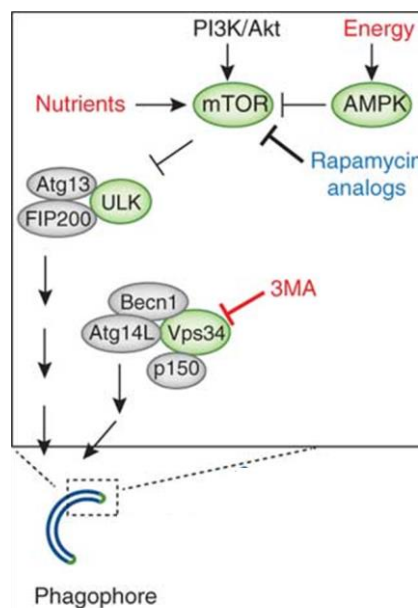


Figure 5.1.1.1. Phagophore formation and nucleation complexes. The ULK1/2 and PI3K complexes associate with the PAS to instigate phagophore formation. VPS15 is also known as p150. Taken from ([Cheong et al., 2012](#))

derived from a Golgi-related secretory pathway, as well as multiple other sources ([Bernard and Klionsky, 2014](#)).

Nucleation requires the PI3K complex; double-membraned phagophores are compelled into curvature by the deposition of multiple phosphatidylinositol groups (PIs) on the 'cytoplasmic' membrane face. In close proximity, these lipid groups favour positive membrane curvature and allow recruitment of the PI(3)P-binding WD repeat domain phosphoinositide-interacting protein (WIPI) family, to facilitate the final steps autophagosome formation ([Dooley et al., 2014](#)). The exact function of the ATG2-WIPI complex in autophagosome formation is not clear, although it appears necessary for and dependent on the appropriate distribution of ATG9 vesicles ([Reggiori et al., 2004](#)).

Recruitment of two ubiquitin-like conjugation complexes mediates phagophore membrane elongation, on distinct ER domains known as 'omegasomes' ([Axe et al., 2008](#)). The localisation of these conjugation complexes to the PAS/omegasome is dependent on ATG9 and the PI3K complex. The C-terminus of ATG12 is covalently conjugated to a lysine residue at the centre of ATG5 – a process catalysed by the ubiquitin-E1-like and ubiquitin-E2-like proteins ATG7 and ATG10, respectively (Fig 5.1.1.2) ([Mizushima et al., 1998](#)). Following conjugation, ATG5 interacts directly with ATG16L1 to form the trimeric ATG12-ATG5-ATG16L1 complex. ATG16L1 contains a homo-dimerization domain, hence binding of ATG16L1 to ATG12-ATG5 prompts the dimerization of ATG12-ATG5-ATG16L1 trimers (Fig 5.1.1.2) ([Fujioka et al., 2010](#)).

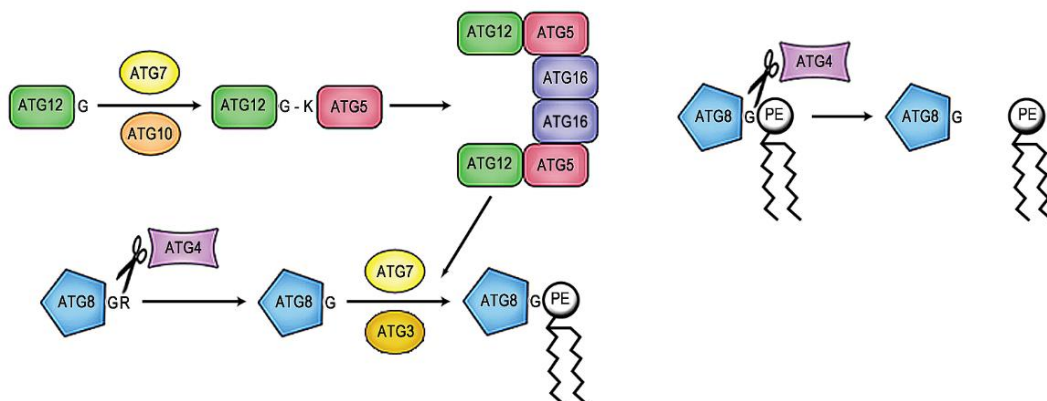


Figure 5.1.1.2. ATG12-ATG5-ATG16 complex formation and LC3-I conjugation. ATG7 and ATG10 conjugate ATG12 to ATG5. ATG12-ATG5 then interacts with ATG16L1, inducing dimerization of ATG12-ATG5-ATG16L1 trimers. ATG4 primes LC3 (ATG8) for conjugation to PE (LC3-II), a reaction catalysed by ATG7, ATG3, and ATG12-ATG5. ATG4 cleaves LC3-II following completion of autophagosomal formation. Modified from ([Williams et al., 2012](#))

ATG16L1 directly binds to the ULK1 complex subunit FIP200, an interaction required for amino-acid starvation-induced autophagy response (ULK1-dependent), although this interaction is not required for autophagy induced by glucose deprivation (ULK1-independent) ([Gammoh et al., 2013](#)). ATG16L1 has also been implicated in the utilisation of the plasma membrane as a membrane source due to its interaction with clathrin-coated structures ([Ravikumar et al., 2010](#)).

The ATG12-ATG5 conjugate also functions as the E3-like enzyme required for the conjugation of phosphatidylethanolamine (PE) to LC3-I (microtubule-associated protein 1 light chain 3, mammalian homologue of Atg8) to generate LC3-II ([Hanada et al., 2007](#)). ATG7 and ATG3 act as the E1- and E2-like enzymes for this conjugation (Fig 5.1.1.2). LC3-II can stably associate with numerous autophagic components and is used widely as a marker within analysis of autophagic processing ([Mizushima and Yoshimori, 2007](#)). LC3-II is required for the expansion of autophagic membranes, as well as cargo recognition, closure of the isolation membrane and lysosomal fusion ([Kabeya et al., 2000](#)).

Closure and detachment of mature autophagosomes from the ER is poorly understood. When formation is completed, conjugated LC3-II on the outer autophagosomal membrane is cleaved from PE by ATG4, releasing LC3 back into the cytoplasm (Fig 5.1.1.2) ([Kirisako et al., 2000](#)). Detachment and disassembly of the ATG complexes appears to be regulated by inactivation of the ULK1 complex and clearance of PI(3)P at the autophagosome membrane ([Karanasios et al., 2013](#); [Lamb et al., 2013](#)). ULK1 is one of the earliest proteins to dissociate from the completed autophagosome, and disassembly of the ATG machinery appears to be dependent on ULK1 kinase inactivity ([Karanasios et al., 2013](#)). The mechanism in which PI(3)P turnover clears ATG complexes from mature autophagosomes is likely that the hydrolysis of PI(3)P to PI leads to the dissociation of the PI(3)P-binding WIPI family, or that high local concentrations of PI(3)P inhibit ATG machinery disassembly ([Sanchez-Wandelmer et al., 2015](#)).

5.1.2. Transport and lysosomal fusion

To complete autophagy and degrade the contents of the mature autophagosome, autophagosomal-lysosomal fusion must occur. LC3-II appears to be required for transporting autophagosomes into the vicinity of lysosomes ([Nair et al., 2012](#)). Once

autophagosomes are formed, they are transported across the microtubule network in a dynein-dependent manner, towards the nuclear periphery and residence of late endosomes and lysosomes ([Fass et al., 2006](#); [Kimura et al., 2008](#)). The role of microtubule machinery in autophagosome-lysosome fusion has been secured by evidence that autophagosome migration to the perinuclear region is microtubule- and dynein-dependent in primary neurons ([Cheng et al., 2015](#)), and loss of function of dynein leads to accumulation of autophagosomes and failure to clear aggregated proteins in cultured cells, *Drosophila* and mice ([Ravikumar et al., 2005](#)).

Three distinct families, identified from general intracellular membrane trafficking pathways, work in concert to orchestrate lysosomal fusion – RAS-related proteins in brain (RAB) GTPases, membrane-tethering complexes, and Soluble N-ethylmaleimide-sensitive factor activating protein receptor (SNARE) proteins ([Bento et al., 2016](#)). With roles not restricted to autophagy, the RAB GTPase family act as master regulators of vesicle sorting and coordinators of membrane-bound traffic throughout the cell ([Stenmark, 2009](#)). Specifically referring to autophagy, RAB7 appears to play fundamental, multifunctional roles in coordinating the journey of the mature phagosome towards the lysosomal fusion process, and is a widely established marker of late endosomes/autophagosomes ([Bucci et al., 2000](#)).

Following recruitment to the autophagosomal membrane, dependent on the interacting effector, RAB7 can mediate both plus- and minus-end transport across the microtubule. Large effector protein FYCO1 (FYVE and coiled-coil domain containing 1) interacts via C-terminal domains with RAB7, LC3 and PI(3)P whilst concomitantly interacting with the kinesin motor protein via its N-terminal coiled-coil domain to mediate movement in the plus direction. Minus-end transport to the perinuclear region is mediated via interaction between the dynein-dynactin motor, oxysterol-binding-protein-related protein 1 (ORP1L), RAB7 and effector protein RAB-interacting lysosomal protein (RILP) (Fig 5.1.2) ([Wang et al., 2011](#)).

The homotypic fusion and vacuole protein sorting (HOPS) complex acts as the primary membrane-tethering factor to facilitate autophagosome-lysosomal fusion, via the capture and bridging of RAB-labelled vesicles, and initiation of fusion in conjunction with the SNARE proteins ([Bröcker et al., 2010](#)). Amongst the six subunits of HOPS, VPS39

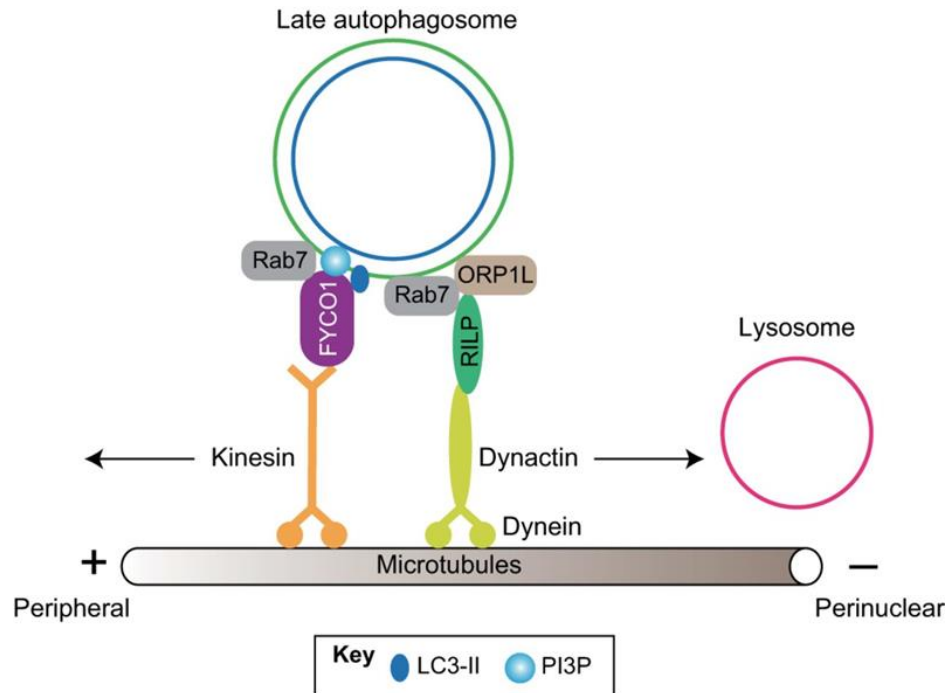


Figure 5.1.2. RAB7 and FYCO1- or RILP-ORP1L-mediated transport of late autophagosomes across the microtubule. Kinesin drives autophagosomes towards the cell periphery, dynein-dynactin mediates transport to the perinuclear region, towards lysosomal fusion. Image modified from ([Nakamura and Yoshimori, 2017](#))

activates RAB7 and VPS16 interacts with the UV Radiation Resistance Associated (UVRAG) complex ([Bröcker et al., 2010](#)). Active RAB7 appears to displace the fusion-inhibiting interaction between Rubicon and UVRAG, increasing the availability of the UVRAG complex to associate with the VPS16 subunit of HOPS. This further activates RAB7 ([Sun et al., 2010](#)), propagating a strong feed-forward mechanism to instigate membrane fusion.

SNARE proteins anchored on opposing membranes at the fusion site interact to form a *trans*-SNARE complex inducing membrane fusion. Three Q-SNAREs on the acceptor membrane associate with one R-SNARE on the donor membrane ([Jahn and Scheller, 2006](#)). Autophagosome-bound Q-SNARE Syntaxin 17 has a direct role in fusion through its interaction with lysosomal R-SNARE vesicle-associated membrane protein 8 (VAMP8), although this appears to be dependent on a priming step by essential autophagy protein ATG14L1 ([Diao et al., 2015](#)).

SNARE protein function appears to be disrupted in several lysosomal storage disorders (LSDs) – rare, inherited metabolic disorders caused by defects in lysosomal function ([Fraldi et al., 2010](#)). LSDs can arise from a variety of mechanistic defects,

resulting in compromised degradation of deleterious cytoplasmic components. Currently over 50 disorders have been characterised, with widely varying pathological presentations including abnormal skeletal and neurological development, blindness, deafness and early death ([Parenti et al., 2015](#)) ([Boustany, 2013](#)). LSDs can be caused by elevated cholesterol accumulation in the lysosomal membrane – causing sequestration and inactivity of SNAREs within these compartments. Reduced activity of SNARE proteins results in gross impairments of membrane sorting and fusion, and lysosomal dysfunction ([Fraldi et al., 2010](#)).

Lysosomal biogenesis is also regulated by mTORC1. TFEB (transcription factor EB) is the key regulator of lysosomal biogenesis, the transcriptional activator of the Coordinated Lysosomal Expression and Regulation (CLEAR) network of >470 lysosome-associated genes ([Palmieri et al., 2011](#); [Settembre et al., 2012](#)). mTORC1-dependent phosphorylation of TFEB sequesters it within the cytoplasm in times when lysosomal activity is adequate. Following starvation (when enhanced autophagy is paramount) mTORC1 activity is decreased, relieving TFEB of inhibitory phosphorylations, resulting in TFEB translocation to the nucleus where it stimulates genes required for lysosomal biogenesis proteins ([Roczniak-Ferguson et al., 2012](#)).

5.1.3. Starvation-induced autophagy

The autophagy response to starvation is bulk degradation of cytoplasmic components, to recover non-essential macromolecules and substrates for survival. Central to the induction of autophagy following nutrient deprivation and other stress conditions is the ULK1 complex ([Wong et al., 2013](#)). The ULK1 complex is a substrate of mTOR, 60 kDa Tat-interactive protein (TIP60) and AMPK, and its phospho- and acetyl- status is inherently dependent on the activity of these kinases (Fig 5.1.1.1) ([Glick et al., 2010](#)). Upon starvation, mTORC1 activity is decreased, resulting in the elimination of inhibitory mTOR-dependent phosphorylations on ULK1 and increased acetylation by TIP60. ULK1 appears to act as a scaffold for the recruitment of downstream ATG proteins, and is essential for autophagy in mammals ([Hara et al., 2008](#)). However, how the ULK1 complex transduces incoming signals from these nutrient status-sensing kinases to the downstream autophagic machinery is unknown.

Starvation-induced autophagy also requires PI3K complex activity. Beclin 1 is required for the interaction between core PI3K complex subunits VPS34 and ATG14L1, without which the complex cannot localise to the PAS ([Matsunaga et al., 2010](#)). The PI3K complex cannot be effectively activated without the liberation of subunit Beclin 1 from an inhibitory association with anti-apoptotic BH3 family members B-cell lymphoma 2 (BCL-2), B-cell lymphoma-extra-large (BCL-XL) or Induced myeloid leukaemia cell differentiation protein (MCL-1) ([Kang et al., 2011](#)). The Beclin 1-BCL-2 interaction can be disrupted through competitive displacement of Beclin 1 by other BCL-2 family members, including truncated BH3 interacting-domain death agonist (tBID), BCL-2-associated death promoter (BAD) and BCL2/adenovirus E1B 19 kDa protein-interacting protein 3 (BNIP3) ([Sinha and Levine, 2008](#)). BCL-2/BCL-XL can also be competitively displaced by Beclin 1-binding proteins including ATG14L1 and UVRAG ([Bento et al., 2016](#)). Further to this, posttranslational modification of Beclin 1 and its inhibitory interactants, that induce disassociation or enhance association, is a key mechanism of regulating autophagic activity of Beclin 1. These include (but are not limited to) Beclin 1 phosphorylation by death associated protein kinase (DAPK) ([Zalckvar et al., 2009](#)), and phosphorylation of BCL-2 by c-Jun N-terminal kinase 1 (JNK1) and extracellular signal-regulated kinase (ERK) ([Wei et al., 2008](#)). Following association with the PI3K complex, ULK1 additionally phosphorylates ATG14L1-Beclin 1 to induce autophagy ([Bento et al., 2016](#)).

5.1.4. Receptor-mediated autophagy

Receptor-mediated autophagy is the selective targeting of cellular components for autophagic degradation. This directed approach requires additional levels of regulation above the autophagic machinery utilised for bulk degradation. A variety of target cargoes have been characterised including misfolded proteins, organelles and pathogens ([Stolz et al., 2014](#)). Receptors recognise labelled cargoes, binding them to the growing autophagosomal membrane via LC3-interacting regions (LIRs) ([Slobodkin and Elazar, 2013](#)).

In mammals, the most common modification targeting a component for degradation is ubiquitylation – almost all characterised autophagy receptors harbour Ub-binding domains (UBDs) and LIRs ([Kirkin et al., 2009](#)). The ubiquitin-proteasome system (UPS) of rapid targeted degradation was initially thought to function

independently of selective autophagy, but the discovery of such high frequency of UBDs in autophagy receptors indicates levels of cross-talk between these degradation pathways ([Kraft et al., 2010](#)).

P62/Sequestosome 1 (p62/SQSTM1 – hereon referred to as p62) is one such cargo receptor that interacts with ubiquitylated targets, and is an autophagic substrate ([Seibenhener et al., 2004](#)). Cargo-bound p62 is conveyed to the PAS where it is tethered to the developing inner-autophagosomal membrane, via the interaction between p62 and LC3-II. Degradation of p62 occurs as the p62-cargo-containing autophagosomes fuse with lysosomes (Fig 5.1.4) – a block in autophagic processing will induce the accumulation of intracellular p62 ([Bjørkøy et al., 2005](#)). This renders p62 a useful marker of blocked autophagy when analysed with autophagic flux indicator LC3-I/II ([Bjørkøy et al., 2009](#)). However, p62 protein expression levels can be ambiguous, as it is also subject to transcriptional regulation by an array of factors, including oxidative damage-sensor nuclear factor erythroid 2–related factor 2 (NRF2) ([Jiang et al., 2015](#)), TFEB, and ER stress/UPR transcription factor activating transcription factor 4 (ATF4) ([Kouyama et al., 2006](#)). P62 also has the unique activity of upregulating nutrient-status sensor mTORC1 activity via its Raptor subunit, at the lysosomal membrane – allowing autophagic activity further input into the regulation of this master kinase ([Duran et al., 2011](#)).

Interestingly, adipocyte-specific *p62*-deficient mice are obese and exhibit decreased metabolic rates. *p62* deficiency in this model resulted in impaired mitochondrial function and brown adipose tissue (BAT) thermogenesis, indicating a role for p62 in the regulation of adipogenesis or adipocyte homeostasis ([Müller et al., 2013](#)).

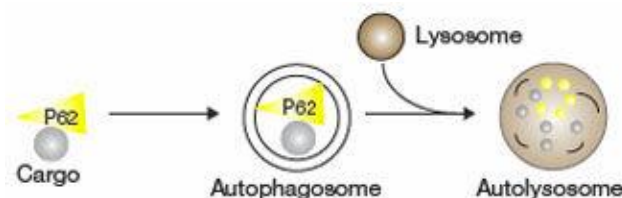


Figure 5.1.4. Role of p62 in receptor-mediated autophagy. P62 recognises and binds to ubiquitylated targets. Cargo-bound p62 interacts with LC3-II on the inner autophagosomal membrane. Following lysosomal fusion, p62 and cargo are degraded. Taken from ([Rusten and Stenmark, 2010](#))

5.1.5. Interpreting LC3-I/LC3-II western blotting

Changes in autophagic flux can be assessed through western blotting of LC3-I/II. Yet, both increased autophagic induction and a block in autophagic degradation can alter levels of LC3-II (Fig 5.1.5.A). Co-treatment with autophagy inhibitors here will produce an additive or epistatic effect on LC3-I/LC3-II status, dependent on which is the cause of altered autophagic flux (Fig 5.1.5.C). Assessing LC3 status following co-treatment with autophagy inhibitors allows the delineation of changes in autophagic induction or degradation.

Bafilomycin A is an inhibitor of vacuolar H⁺ ATPase (V-ATPase) which functions to inhibit autophagy at the late stage of autophagosome-lysosomal fusion. Treatment with Bafilomycin A blocks autophagic degradation, resulting in increased LC3-II as autophagosomes accumulate (Fig 5.1.5.B). To test if an observed change in LC3-I/II status is due to a block in autophagic degradation, samples can be co-treated with Bafilomycin A and the treatment in question (for example, ATRi). One of two outcomes can occur following this co-treatment, as shown in Fig 5.1.5.C (lane 3). If you observe an additive increase in LC3-II following Bafilomycin A co-treatment, you are observing enhanced autophagy induction; however, if you observe a block in autophagic degradation, the LC3 status will remain unchanged. Bafilomycin A co-treatment with autophagy inducers results in increased LC3-II, due to the additive effect of enhanced levels of autophagic induction concomitant with inhibition of autophagic degradation generating LC3-II positive autophagosomes. Furthermore, 3-methyladenine (3-MA),

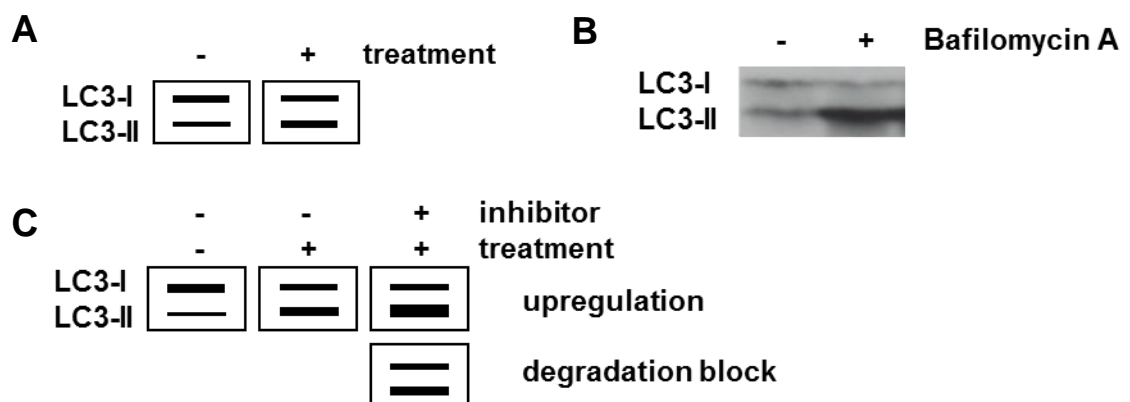


Figure 5.1.5. Assessing autophagy with western blotting of LC3. A) and C) See text for narrative. B) Western blot of cycling 3T3-L1 preadipocytes treated with or without Bafilomycin A (50 nM, 2 hrs) show increased expression of LC3-II, indicative of a block in autophagosomal maturation/fusion.

an inhibitor of PI3K and early autophagosome formation, can be utilised to assess at which point an observed block in autophagy is occurring.

Considering the role of autophagy in cancer progression, therapy and adipogenic differentiation, and my data in chapter 4 showing LC3-I/II status is affected by ATRi, it is important to investigate the effects of ATRi treatment on the autophagy axis. If ATRi treatments were to affect cellular autophagic status, novel combination strategies could be explored to capitalise on cancer cell dependency of enhanced autophagy. Conversely, there may be unforeseen consequences of chronic ATRi treatment in the treatment of cancer.

5.2. Results

5.2.1. *ATRi results in defective autophagy and p62 accumulation*

I utilised western blotting of LC3 to assess autophagic flux in cycling 3T3-L1 preadipocytes following acute treatments with ATRi, and *Atr* siRNA. I chose to study the effects of acute treatments with ATRi in 3T3-L1 preadipocytes as these cells require canonical ATR function throughout cell replication, rendering longer ATRi treatments highly cytotoxic.

Fig 5.2.1.1.A shows western blotting of LC3 in cycling 3T3-L1 preadipocytes treated with ATRi II for 0-16 hrs. Altered LC3 processing is observed following 2 hrs treatment with ATRi II, where LC3-II levels (Fig 5.2.1.1.A, lower migrating band) are drastically increased from 6-16 hrs of ATRi treatment. To ensure this was not a cell-type specific response, I repeated this time course in the murine C2C12 myoblast cell line (Fig 5.2.1.1.B), where increased LC3-II following ATRi treatment is observed with similar kinetics to the 3T3-L1 preadipocytes. Fig 5.2.1.1.C further shows ATRi-induced increases in LC3-II are also dose-dependent, where just 10 nM VE-822 is sufficient to induce small changes in LC3-I/II ratio. To further investigate the shift in LC3 status following ATRi, I visualised cells treated with or without VE-822 using IF microscopy with an anti-LC3 antibody. Fig 5.2.1.1.D shows cycling 3T3-L1 preadipocytes stained for LC3, AlexaFluor-conjugated phalloidin (to visualise the actin cytoskeleton) and DAPI. In untreated cells, LC3-I/II staining is mainly nuclear. Following ATRi treatment, there appears to be increased LC3-I/II within the cytoplasmic compartment, suggesting changes in cellular autophagy activity.

I utilised ATMi to confirm the autophagic phenomenon I was observing was ATRi-specific, and not due to inhibition of an apical DNA damage response (DDR) PIKK (phosphoinositide 3-kinase (PI3K)-related protein kinase) (Fig 5.2.1.1.E). Here, ATMi appears to induce increased LC3-II levels after 4 hrs of treatment, although when compared to LC3-II induction following 8 hrs ATRi treatment (last lane, Fig 5.2.1.1.E), it appears relatively small. Following these experiments, roles for ATM in the regulation of pexophagy and autophagy following DNA damage-inducing agents have been

characterised, suggesting inhibition of ATM activity would likely affect the autophagic processing of LC3-I/II ([Chen et al., 2015](#); [Zhang et al., 2015](#)). In one respect, this renders ATMi a less effective control in the investigation into the effects of ATR inhibition on autophagy; however, established roles for ATM in the autophagy pathway also

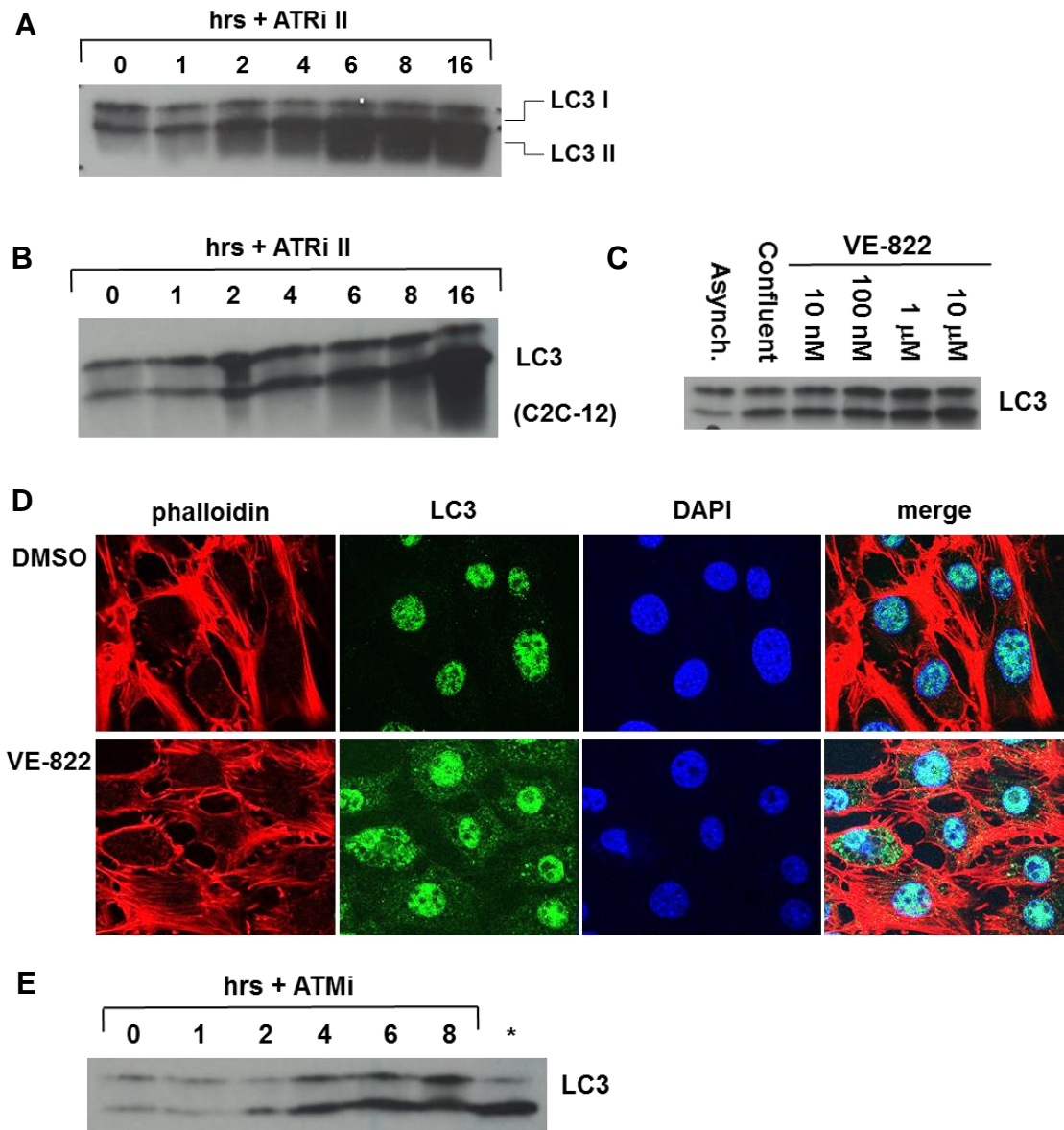


Figure 5.2.1.1. ATRi induces aberrant autophagic processing. **A)** and **B)** Western blotting analysis of LC3-I/II following 0-16 hrs ATRi II treatment (10 μ M) in cycling 3T3-L1 preadipocytes (**A**) and cycling C2C-12s (**B**). With limited effects on LC3-I, ATRi treatment induces drastic increases LC3-II after 2 hrs, indicative of enhanced or blocked autophagy. **C)** ATRi induced changes in LC3-II status are dose-dependent. In asynchronous 3T3-L1 preadipocytes, 4 hrs treatment with VE-822 at every dose tested induces altered LC3 processing. **D)** IF microscopy of LC3 following ATRi treatment shows increased cytoplasmic LC3 expression. Actin stain AlexaFluor-phalloidin (red), LC3-I/II (green), DAPI (blue). Images taken at 100x magnification. **E)** Western blotting of LC3 following ATMi treatment of cycling 3T3-L1 preadipocytes, where * is 8 hrs ATRi II treatment. ATMi induces modest changes in LC3-I/II. All images representative of results obtained in at least three independent experiments.

demonstrate there is existing crosstalk between a DDR PIKK and the systems controlling intracellular degradation.

LC3 has also been associated with endosomal maturation, endocytosis and the processing of other membrane-bound cellular components ([Hytinen et al., 2013](#)). To confirm the changes I observed in LC3 were autophagy-dependent and autophagy-specific, I ablated ATG12 expression using *Atg12* siRNA, and assessed LC3 processing following ATRi treatment. ATG12 is essential for autophagy, autophagy cannot occur without ATG12 expression ([Mizushima et al., 2001](#)). Fig 5.2.1.2.A shows successful knockdown of ATG12 following *Atg12* siRNA transfection (lanes 3&4). Treatment with VE-822 when ATG12 expression is unperturbed induces increased LC3-II expression, however following ATG12 ablation, the ATRi-dependent increase in LC3-II is lost (lanes 2&4). This strongly suggests the ATRi-induced increases in LC3-II I have observed are dependent on a functional autophagy axis. This indicates that the altered LC3-I/II status I observe after ATRi is due to a defect in autophagy-dependent processing of LC3.

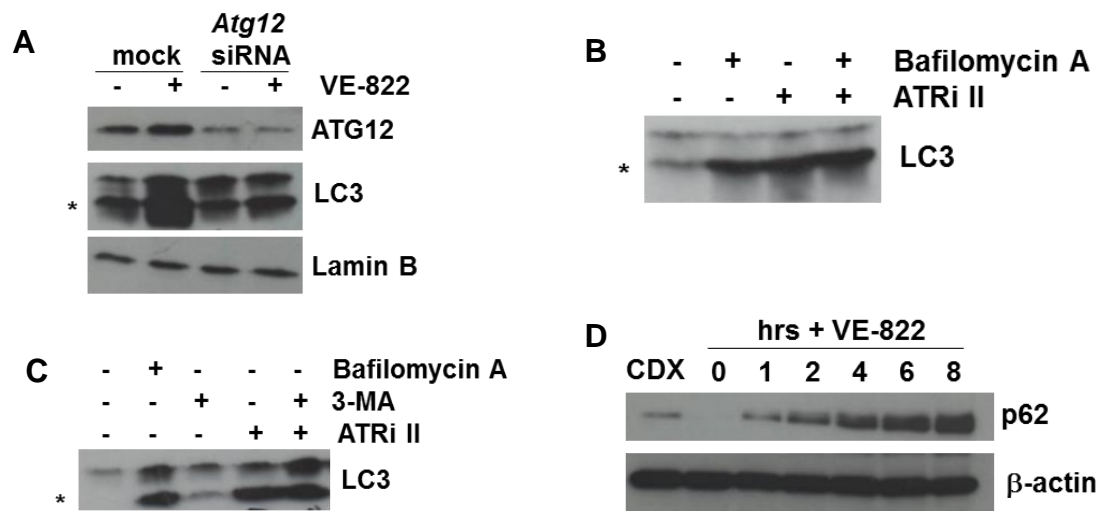


Figure 5.2.1.2. ATRi induces aberrant autophagic-dependent LC3 processing. **A)** *Atg12* siRNA ablates ATRi-induced LC3-II increase. Cycling 3T3-L1 preadipocytes were transfected with *Atg12* siRNA. 48 hrs post transfection ATG12 is successfully knocked down and samples were treated with ATRi II for 6 hrs. Following siRNA treatment, VE-822 no longer induces LC3-II increase indicating shifted LC3 status is autophagy-dependent. Lamin B used as loading control. **B)** 50 nM Bafilomycin A treatment has an epistatic effect on LC3 status when co-treated with ATRi, indicating ATRi treatment induces an autophagic block at the stages of lysosomal fusion. **C)** 3-MA (10 mM, 4 hrs) has an additive effect on LC3-I and -II following ATRi treatment, indicating ATRi treatment is not blocking early autophagy (lanes 3-5). **D)** VE-822 treatment induces drastic increases in p62 expression after 1 hr treatment. CDX denotes cyclodextrin (16hrs, 10 mM) – an inducer of p62 and positive control. * denotes LC3-II band. β-actin used as loading control for p62 western blotting. All images representative of results obtained in at least three independent experiments.

To further characterise at which stage ATRi was affecting autophagic LC3 processing, I co-treated ATRi-treated 3T3-L1 preadipocytes with Bafilomycin A and assessed LC3 status by western blotting. Bafilomycin A treatment increased LC3-II levels equivalent to ATRi treatment (Fig 5.2.1.2.B, lanes 2 and 3). Co-treatment with both compounds did not have an additive effect on LC3-II status, suggesting that ATRi is inducing an autophagic block at the level of autophagosomal maturation and lysosomal fusion. To further confirm that the observed ATRi-induced block in autophagy was not occurring at earlier stages of the autophagy process, I assessed the effects of co-treatment with ATRi II and 3-MA. 3-MA induces increases in LC3-I (Fig 5.2.1.2.C, lane 3), due to the inhibition of early autophagosome formation and LC3-I conjugation to LC3-II. Co-treatment of ATRi and 3-MA had an additive effect, where both LC3-I and -II were increased, indicating the two compounds affect autophagy at differing nodes.

p62 is degraded throughout autophagic processing. Hence, a block in autophagic degradation will induce increased p62 expression, as p62-containing autophagosomes accumulate within the cytoplasm. Fig 5.2.1.2.D shows striking increases in p62 protein levels following treatment with VE-822. The significance of the increased p62 levels observed with ATRi treatment is reinforced when considering lane 1 of Fig 5.2.1.2.D - treatment with cyclodextrin, an inducer of p62 expression that I utilised as a positive control. These results suggest that acute treatments with ATRis have a fundamental impact on autophagic processing.

5.2.2. Genetic approaches to compromise ATR phenocopy ATRi-induced defects in autophagy and p62 accumulation

I wanted to confirm the autophagy defects I was observing following ATRi treatments were not due to a non-specific effect of small molecule kinase inhibitors of ATR. To investigate this, I utilised genetic approaches to ablate ATR protein function and assess LC3-I/II status.

ATR-ATRIP exists in a stable homodimer, requiring *trans*-autophosphorylation to become activated and remain stable ([Nam et al., 2011](#)). Hence, overexpression of a kinase-dead (KD) ATR construct can induce a dominant-negative effect on ATR kinase activity, through the dilution of available kinase-active ATR. Wild-type (WT) ATR

dimerises with KD-ATR and fails to *trans*-autophosphorylate and activate. Through the overexpression of KD-ATR, it is possible to investigate the effects of reduced ATR kinase function without reducing total ATR protein expression. Due to this, KD-ATR overexpression is considered more similar to the effects of small molecule kinase inhibition than siRNA approaches, which ablate protein expression rather than kinase activity specifically.

I overexpressed a KD-ATR construct in cycling 3T3-L1 preadipocytes to assess the effects of ablating ATR kinase activity on LC3-I/II and p62 kinetics. As a control, I also overexpressed WT-ATR, which has been previously shown to induce autophagic cell death ([Mori et al., 2013](#)). Fig 5.2.2.A shows both WT- and KD-ATR transient overexpression induces p62 and LC3 phenotypes similar to treatment with ATRi, where KD-ATR appears to induce the strongest increase in p62 and LC3-II between the two constructs. This suggests that altering either ATR expression *or* activity has a considerable effect on autophagic status.

I utilised *Atr* siRNA to deplete total ATR, where 24 and 48 hrs following transient siRNA transfection ATR expression is ablated (Fig 5.2.2.B, lanes 2 and 3). After 48 hrs of ATR knockdown with *Atr* siRNA, an increase in LC3-II is observed equivalent to 4 hrs ATRi treatment, further suggesting the autophagic block I observed following ATRi is a genuine effect of depleting ATR function. Furthermore, I observed increased p62

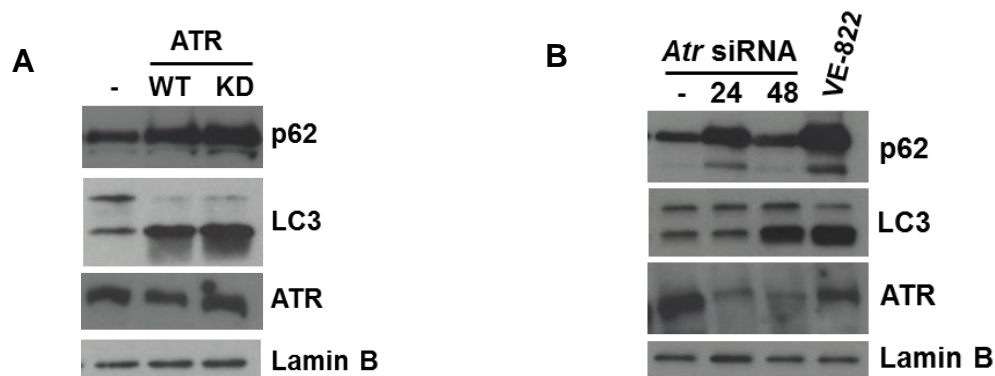


Figure 5.2.2. Over expression of WT and KD-ATR constructs and *Atr* siRNA results in enhanced p62 and autophagic block. A) Western blotting of cycling 3T3-L1 preadipocytes transfected with untagged WT-ATR and KD-ATR show altered LC3 processing and increased p62 expression compared to transfection reagent alone. Lamin B used as loading control **B)** *Atr* siRNA induces LC3 and p62 phenotypes equivalent to ATRi treatment. Interestingly, siRNA treatment induced increased LC3-II and p62 expression at separate time points following transfection, indicating that the two phenomenon may occur independently of one another. Lamin B used as loading control. All images representative of results obtained in at least three independent experiments.

expression following 24 hrs *Atr* siRNA treatment, although this effect was not sustained 48 hrs post siRNA transfection (Fig 5.2.2.B). Interestingly, increased p62 and LC3-II are not observed here at the same time, indicative that ATRi-induced p62 accumulation may not be directly linked to the ATRi-induced block in autophagy.

5.2.3. ATRi-induced p62 accumulation is autophagy- and DDR-independent

In section 5.2.2, I discovered that the kinetics of increased p62 and LC3-II following ATR ablation appear to deviate from one another. Because of this, I wanted to investigate and confirm if the ATRi-induced p62 accumulation I observe is independent of the ATRi-induced block in autophagy. To do this, I ablated autophagy-essential protein ATG16L1 in cycling 3T3-L1 preadipocytes using *Atg16L1* siRNA. Following ATRi treatment of samples with normal ATG16L1 expression, p62 and LC3-II are increased (Fig 5.2.3.A, lane 2). Following ATRi treatment and genetic ablation of ATG16L1, LC3-II has not increased (lane 4), reinforcing that the ATRi-induced increases in LC3-II are autophagy-dependent. However, following ATRi treatment and ATG16L1 knockdown, p62 expression is increased equivalent to samples with an intact autophagy axis (lanes 2&4). As cells

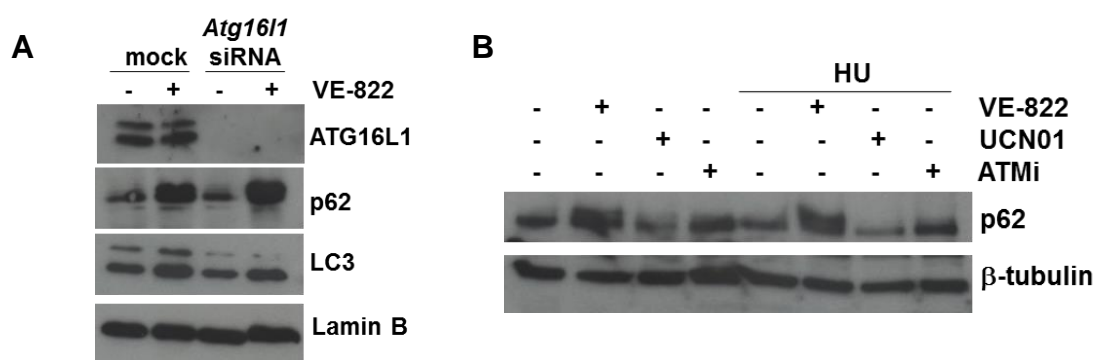


Figure 5.2.3. Increased p62 expression following ATRi is independent of autophagy and DNA damage induction and signalling. **A)** *Atg16L1* siRNA transfection of cycling 3T3-L1 preadipocytes results in effective knockdown of ATG16L1. Following ATRi treatment (VE-822, 10 μ M) LC3-II and p62 expression is increased. ATRi treatment following *Atg16L1* siRNA does not increase LC3-II levels, but p62 expression remains enhanced indicating that ATRi-induced increase in p62 protein expression is autophagy-independent. Lamin B used as loading control. **B)** Western blotting of p62 expression following 4 hrs CHK1i (UCN01, 300 nM) ATMi (KU55933, 10 μ M) and ATRi (VE-822, 10 μ M) and HU treatment (500 μ M). CHK1i appears to modestly reduce p62 expression, indicating that the ATRi-induced increase in p62 expression is independent of deficits in ATR-CHK1 signalling. HU treatment does not affect p62 expression alone or in concert with ATRi, CHK1i or ATMi, indicating that enhanced replicative stress is not responsible for the ATRi-induced increase in p62 expression. β -tubulin used as a loading control. All images representative of results obtained in at least three independent experiments.

cannot undertake autophagy without ATG16L1, this indicates ATRi-induced p62 accumulation is autophagy-independent. This suggests that two separate phenomena may be occurring within the cell to generate an accumulation of p62 and an autophagic block in response to acute ATR kinase inhibition. This result also indicates that the increased p62 protein expression observed following ATRi treatment may be due to increased transcription of *p62*, rather than reduced autophagic degradation.

Following the discovery that the majority of ATRi-induced p62 accumulation was autophagy-independent, I wanted to further characterise this phenomenon. I wanted to assess if p62 accumulation was independent of ATRi-induced DNA damage, and also of the canonical ATR-CHK1 signalling axis. I treated cycling 3T3-L1 preadipocytes with CHK1i, ATMi, and hydroxyurea (HU) to assess the effects of these treatments on p62 expression (Fig 5.2.3.B). HU induces replication stress through the depletion of dNTP pools required for DNA synthesis, rendering it an effective inducer of replication stress - an established effect of ATRi treatment. Strikingly, CHK1i UCN01 did not have any impact on p62 expression (Fig 5.2.3.B, lane 3). This indicates that the p62 accumulation I have observed using two structurally distinct ATRis, *Atr* siRNA and over expression of KD-ATR cannot be recapitulated by inhibiting an established ATR-dependent DDR kinase. ATMi treatment appeared to induce a modest increase in p62 expression (Fig 5.2.3.B, lane 4), however roles for ATM in pexophagy have been characterised ([Zhang et al., 2015](#)) suggesting p62 accumulation is to be expected following ATMi treatment. Further to this, treatment with HU did not augment p62 accumulation alone or following CHK1, ATM or ATR kinase inhibition treatment (lanes 5-8), suggesting ATRi-induced p62 accumulation is independent of DNA damage or replication stress induced by inhibition of ATR kinase activity.

5.2.4. ATRi induces TFEB translocation and lysosomal biogenesis

P62 is transcriptionally regulated by several factors, including master lysosomal biogenesis regulator TFEB ([Settembre et al., 2012](#)). TFEB activity is regulated by mTORC1-dependent inhibitory phosphorylations at the lysosome. I hypothesised that, considering the reduced mTORC1 activity following acute ATRi treatment and *Atr* siRNA I observed in chapter 3, nuclear TFEB activity could be increased following ATRi treatments, resulting in enhanced p62 transcription. TFEB activity can be assessed by

cellular localisation; sequestration in the cytoplasm by mTORC1 renders it inactive, and following activation, it translocates to the nucleus to activate gene targets.

2-Hydroxypropyl- β -cyclodextrin (hereon cyclodextrin) can be utilised in cell culture as an inducer of TFEB activation. Using cyclodextrin as a positive control, I treated cycling 3T3-L1 preadipocytes with ATRi and fractionated the nuclear compartment to assess TFEB translocation via western blotting. Untreated samples contain relatively low nuclear TFEB levels (Fig 5.2.4.A, lane 1). Following addition of cyclodextrin, nuclear TFEB content is visibly increased (lane 3). As hypothesised, nuclear TFEB levels are also increased following ATRi treatment (lane 2), suggesting that ATRi-induced reduction in mTORC1 activity has functional significance - increasing TFEB-mediated lysosomal biogenesis and p62 expression.

WIPI1 and Lysosomal-associated membrane protein 1 (LAMP1) are also targets of TFEB-mediated gene transcription. To further assess the significance of ATRi-induced increased TFEB activity, I assessed WIPI1 and LAMP1 expression in 3T3-L1 preadipocytes following ATRi treatment by western blotting. Cyclodextrin was used as a positive control in this experiment. Treatment with cyclodextrin induces increased LAMP1

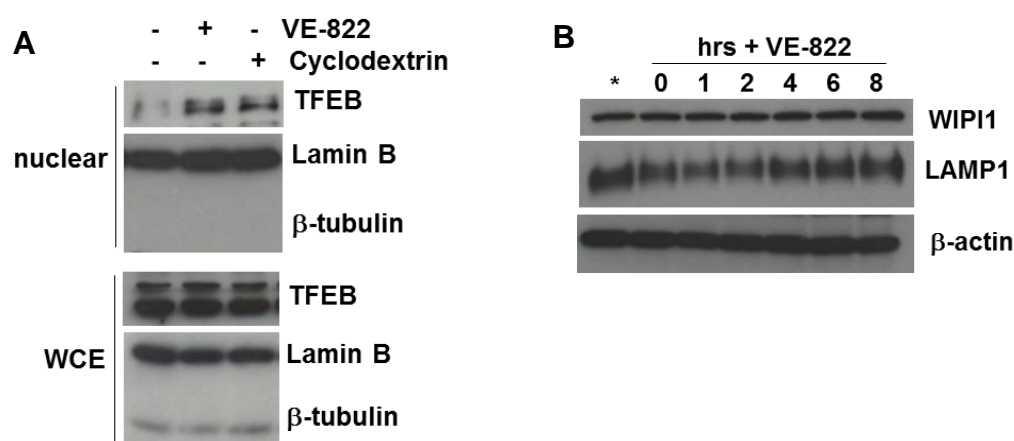


Figure 5.2.4. ATRi induces TFEB translocation and expression of lysosomal markers. A) Western blotting of nuclear and whole-cell extracts (WCE) for TFEB following ATRi treatment. Cyclodextrin used as positive control (lane 3). Lamin B used as loading control for nuclear extract; β -tubulin used as a loading control in WCE, and as a marker of cytoplasmic compartment in nuclear extracts. 4 hrs VE-822 treatment increased nuclear TFEB equivalent to cyclodextrin, indicative of enhanced TFEB-mediated lysosomal biogenesis. **B)** Western blotting of WIPI1 and lysosomal marker LAMP1 (TFEB transcriptional targets) following ATRi treatment. * indicates cyclodextrin treatment as positive control (16 hrs, 10 mM). LAMP1 expression increases following ATRi equivalent to cyclodextrin after 6 hrs, indicative of increased TFEB-mediated transcription and expression of LAMP1. β -actin used as loading control. All images representative of results obtained in at least three independent experiments.

expression when compared to untreated samples (Fig 5.2.4.B, lanes 1 & 2), but WIPI1 expression remains unaffected. After 6 hrs ATRi treatment, LAMP1 expression is increased equivalent to cyclodextrin. At 8 hrs ATRi treatment a small increase can be observed in WIPI1 expression (lane 7). This potentially indicates ATRi-induced TFEB nuclear translocation is inducing lysosomal biogenesis, as assessed by LAMP1 protein expression levels.

5.2.5. Altering cellular Ca^{2+} status affects ATRi-induced p62 accumulation

In chapter 4, I demonstrated that mature 3T3-L1 adipocytes treated with ATRi II for 24 hrs had increased Ca^{2+} /calmodulin-dependent protein kinase II (CAMKII) activation as assessed by western blotting of p-CAMKII T286, indicative of altered intracellular Ca^{2+} . Since fluctuations in cytoplasmic Ca^{2+} concentration have a fundamental effect on autophagy, I wanted to investigate if alterations in Ca^{2+} flux were inducing the autophagic phenotypes following ATRi treatment.

I examined the relationship of Ca^{2+} with ATRi-induced increased p62 expression and ATRi-induced autophagic block by co-treating cells with ATRi and Krebs-Henseleit (KH) medium. KH medium is Ca^{2+} -free, hence I was able to investigate whether extracellular Ca^{2+} was required to induce ATRi-dependent increases in p62 and/or LC3-II. Cycling 3T3-L1 preadipocytes were treated with ATRi II or VE-822 for 2 hrs in standard or Ca^{2+} -free KH medium. In unperturbed samples, VE-822 and ATRi II treatment increased p62 expression and enhanced LC3-II (Fig 5.2.5.A, lanes 1, 3 & 5). Samples incubated in KH medium (lanes 2, 4 & 6) have decreased p62 expression and enhanced LC3-II expression. Interestingly, following ATRi treatments in KH medium, p62 expression is no longer increased, suggesting a Ca^{2+} -dependent mechanism is responsible for the ATRi-induced increases in p62. Culturing 3T3-L1 preadipocytes in KH medium appears to induce strong induction of LC3-II (lane 2), where co-treatment with ATRis gives no additive effect, indicating a role for Ca^{2+} in the observed autophagic block.

Taken together, these results could also suggest Ca^{2+} -free medium is enhancing autophagic processing which overrides the effects induced by ATRi treatment. The reduced p62 expression following KH medium treatment suggests the concomitant

enhanced LC3-II is not the result of a block in autophagy, rather an upregulation. Enhanced autophagy will increase the rate of p62 degradation, and furthermore reduce the expression of LC3-I as it is conjugated into LC3-II, both phenotypes observed after KH medium treatment.

From Fig 5.2.5.A it is clear that Ca^{2+} status affects ATRi-induced p62 expression. To further investigate a role for Ca^{2+} homeostasis in the phenotypes I have observed following ATR deficiency, I studied the effects of Ca^{2+} chelators on ATRi-induced changes in autophagic flux. Chelating intracellular or extracellular Ca^{2+} enables the delineation of potential pathways that could alter Ca^{2+} flux. BAPTA (1,2-bis(o-aminophenoxy)ethane-N,N,N',N'-tetra-acetic acid) is a cell-**impermeable** Ca^{2+} chelator, that should function similarly to KH medium incubation. BAPTA is a metabolic product of BAPTA-AM, a cell-**permeable** Ca^{2+} chelator that can control intracellular Ca^{2+} levels. BAPTA-AM sequesters intracellular Ca^{2+} , rendering the cell insensitive to changes in Ca^{2+} release.

I utilised BAPTA and BAPTA-AM to investigate the effects of depleting intra- and extra-cellular Ca^{2+} following ATRi treatment in 3T3-L1 preadipocytes (Fig 5.2.5.B). Neither BAPTA nor BAPTA-AM affected ATRi-induced increased LC3-II (Fig 5.2.5.B, lanes 2, 4 and 6), however BAPTA appeared to modestly reduce p62 induction following ATRi (lane 4). This supports the observation in Fig 5.2.5.A that KH medium ablates ATRi-induced p62 induction, suggesting that altering the availability of extracellular Ca^{2+} may have a role in p62 induction.

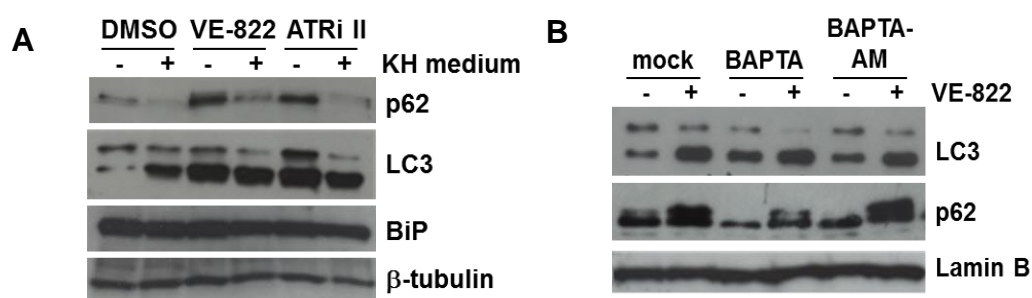


Figure 5.2.5. Depleting extracellular Ca^{2+} inhibits ATRi-induced p62 accumulation. **A)** Western blotting of p62 and LC3. Cycling 3T3-L1 preadipocytes were incubated in Ca^{2+} -free KH medium and ATRis for 2 hrs. KH medium prevented ATRi-induced p62 expression. KH medium increased LC3-II in untreated cells, which was additive following ATRi treatment indicating ATRi-induced autophagic block was not dependent on extracellular Ca^{2+} . β -tubulin used as loading control. **B)** p62 and LC3 following BAPTA-AM, BAPTA and ATRi treatment. Neither chelator affects ATRi-induced LC3-II, however BAPTA reduced p62 similar to KH medium following ATRi. Lamin B used as loading control. All images representative of results obtained in at least three independent experiments.

5.3. Summary

In this chapter, I have demonstrated that acute ATR inhibition treatment results in:

- Enhanced autophagy-dependent expression of LC3-II, indicative of a block in autophagy at the stages of autophagosomal maturation (section 5.2.1)
- Autophagic phenotypes of increased LC3-II and p62 accumulation, that are mimicked with *Atr* siRNA and overexpression of KD-ATR construct (section 5.2.2)
- p62 accumulation, that appears independent of autophagy blockage, CHK1 activity and replication stress (section 5.2.3)
- Increased TFEB nuclear translocation and increased expression of TFEB transcriptional targets LAMP1 and p62 (section 5.2.4)

The ATRi-induced increase in p62 expression appeared dependent on extracellular Ca^{2+} availability. ATRi induced autophagic block as assessed by LC3 status was not affected by cell permeable or cell-impermeable calcium chelators (section 5.2.5)

5.4. Discussion

In this chapter, I have demonstrated that small molecule kinase inhibitors of ATR, *Atr* siRNA and overexpression of a KD-ATR construct result in profound defects in autophagic processing, as well as autophagy-independent increases in p62.

In Chapter 4, I demonstrated chronically ATRi-treated mature white adipocytes undertook a transdifferentiation process into beige adipocytes. p62 deficiency in mice has been shown to reduce metabolic rate, reduce BAT thermogenesis and enhance white adipocyte differentiation in an p44/42 MAPK-dependent manner ([Müller et al., 2013](#); [Rodriguez et al., 2006](#)). Perhaps the increased p62 expression levels I observe following ATRi treatment of 3T3-L1 preadipocytes has a role in the adipocyte browning I observed following ATRi in Chapter 4. The ATRi-induced increase in p62 expression appeared independent of CHK1 activity and replication stress, strongly indicating that this phenotype was not dependent on reduced ATR-CHK1 DDR signalling.

Strikingly, normal p62 expression was recovered by extracellular Ca^{2+} chelation and Ca^{2+} -free media, indicating a role of Ca^{2+} here. Throughout this work, a common theme of dysregulated modulation and availability of Ca^{2+} is becoming apparent in my ATRi-dependent phenotypes. ATRi-induced increased p62 expression was independent of the ATRi-induced defects in autophagy processing, which in turn appeared insensitive to changes in cellular Ca^{2+} status. This indicates that ATR deficiency may be impinging on more than one pathway to generate these autophagic phenotypes. Following from these results I considered it important to next investigate the effects of ATR deficiency on the two Ca^{2+} -modulating organelles – the mitochondria and the ER.

In Chapter 3, I showed mTORC1 activity was suppressed following acute ATRi treatments in 3T3-L1 preadipocytes. The reduced mTORC1-dependent cytoplasmic sequestration of TFEB, resulting in enhanced lysosomal biogenesis, adds further functional significance to the reduction in mTORC1 activity following acute ATRi treatments. Interestingly, ATRi treatments, a KD-ATR construct and *Atr* siRNA all induced a block in autophagy at the stage of autophagosomal maturation and lysosomal fusion, indicating that increased TFEB-mediated lysosomal biogenesis, a pathway commonly

associated with enhanced autophagic clearance, was not adequate to recover the ATR-deficiency induced autophagic block.

For full activation of mTORC1, p62 must interact with mTORC1 at the lysosome ([Duran et al., 2011](#)). The reduced mTORC1 activity following ATRi indicates that increased p62 expression is not inducing mTORC1 activation, suggesting the defects I have observed in mTORC1 signalling following ATRi may exist upstream of the mTORC1 complex.

Essential autophagy protein ATG16L1 mediates the conjugation of LC3-I to LC3-II. Interestingly, ATG16L1 S269 appeared in a putative ATR/ATM substrate screen ([Stokes et al., 2007](#)). If ATG16L1 were to be an ATR substrate in my system, where ATRi induces defects in autophagy, the only considerable effect of ATR on ATG16L1 activity in this model would be to repress LC3-I conjugation. ATRi treatment would relieve this potential repressive, ATR-dependent phosphorylation at S269, allowing the ATG5-ATG12-ATG16L1 complex to aberrantly conjugate LC3 increasing levels of membrane bound LC3-II, generating the observed ATRi-induced increases in LC3-II. However, the epistatic effect of Bafilomycin A and ATRi treatment on LC3-II status disproves this model – if ATRi was inducing ATG16L1-dependent increases in LC3-II conjugation, Bafilomycin A co-treatment would have produced an additive increase in LC3-II, due to increased autophagic induction by the loss of ATR-dependent repressive phosphorylation of ATG16L1, and inhibition of degradation by Bafilomycin A.

This data has positive implications for the proposed use of ATRis in the treatment of cancer. Roles for autophagy in almost every stage of tumour metastasis have been described ([Mowers et al., 2017](#)). Tumour cells capable of increased stress-induced autophagy can become chemoresistant, where eventual tumour regrowth and progression is frequent ([Lu et al., 2008](#)). Furthermore, preclinical models have described the recovery of chemosensitivity and enhanced therapy-induced tumour cell death with autophagy inhibitor treatments ([Amaravadi et al., 2007](#); [Ding et al., 2009](#)).

I have characterised a novel block in autophagic processing following depletion of ATR functionality, with clinically relevant ATRis as well as genetic approaches. If the autophagic phenotypes induced by ATRi treatment I have characterised *in vitro* are

recapitulated *in vivo*, there are additional, as yet unconsidered potential therapeutic benefits for the usage of ATRi in cancer therapy. If ATRi treatments *in vivo* were capable of interrupting the enhanced autophagic processing observed frequently in cancers, novel synthetic lethality strategies could be developed, for example, co treatment with the first-in-class proteasome inhibitor Bortezomib, currently used as a therapeutic in cancers such as multiple myeloma ([Scott et al., 2016](#)).

Chapter Six

Results IV: Characterisation of a
Novel ATRi-induced Vacuolation Phenotype

6.1. Introduction

In chapter 5, I characterised novel impacts of ablating ATR function on autophagic processing and lysosomal biogenesis in cycling 3T3-L1 preadipocytes, where some ATRi-induced phenotypes were rescued by Ca^{2+} chelation. In chapter 4, I dissected what appeared to be Ca^{2+} -dependent metabolic reprogramming of mature 3T3-L1 adipocytes following chronic ATRi treatments. The role of Ca^{2+} dynamics in autophagic induction, adipogenesis, and the ‘browning’ of white adipose tissue (WAT) is established in literature ([Høyer-Hansen et al., 2007](#); [Jensen et al., 2004](#); [Kania et al., 2015](#); [Wright et al., 2007](#)). The recovery of some of the observed ATRi-induced phenotypes by modulating Ca^{2+} availability led me to consider a putative role for ATR at the key Ca^{2+} -sequestering organelles, the mitochondria and the endoplasmic reticulum (ER). Perhaps reducing ATR function has an effect on the regulation of these highly dynamic organelles, which could be indirectly causing altered Ca^{2+} sequestration or release, resulting in the variety of ATRi-induced phenotypes I have observed throughout my studies.

In this chapter, I discover a profound impact of ATR deficiency on ER function, and striking effects of acute ATRi treatment on mitochondrial dynamics. I conclude that acute ATRi treatments have a fundamental effect on the ER in my experimental system, with potentially secondary effects on mitochondrial function. Because of this, this chapter is focused mostly around the impact of ATRi on ER functionality, hence the introduction to these results will be centred on the roles of the ER in maintaining cellular homeostasis.

The endoplasmic reticulum (ER) is a vast, cytoplasmic organelle, consisting of a network of planar cisternae and tubular membrane structures. ER tubules stretch throughout the cytoplasm and are termed the ‘smooth’ ER due to their diminished association with ribosomes. The smooth ER primarily modulates Ca^{2+} homeostasis, fatty acid and phospholipid synthesis and lipid bilayer assembly ([Chaudhari et al., 2014](#)). The smooth ER also forms abundant membrane contact sites (MSCs) with other organelles. The smooth ER forms MSCs with the mitochondria, which is notable as the biogenesis of this organelle does not originate from the ER membrane.

Perinuclear, ribosome-covered ER sheets make up the rough ER, required for the synthesis and processing of secreted, luminal and membrane proteins. Many classes of protein require extensive modification, chaperone-mediated folding, membrane incorporation and translocation to their appropriate regions in ER-derived vesicles. Although the nuclear envelope comprises a diverse proteome typically not enriched in the ER, their membranes are continuous ([Hetzer, 2010](#)). The ER performs a plethora of homeostatic, housekeeping cellular functions, which I will briefly review here.

6.1.1. *The endomembrane system*

The endomembrane system is the term for the extensive network of lipid membranes retained within the cell, consisting collectively of the ER, lysosomes, and Golgi Apparatus (GA) (Fig 6.1.1). Coordinated budding and fusion events, mediated by the microtubule network and specialised protein complexes at these organelles, generates membrane that can be utilised in organelle biosynthesis, vesicular trafficking and autophagy. Central to these processes is the ER – providing membrane for autophagosome and endosome formation, and receiving retrograde vesicles from the GA ([Araki and Nagata, 2011](#); [Murphy and Vance, 1999](#); [Nakamura and Yoshimori, 2017](#); [Nebenführ, 2002](#); [Sanchez-Wandelmer et al., 2015](#); [Scott et al., 2014](#)).

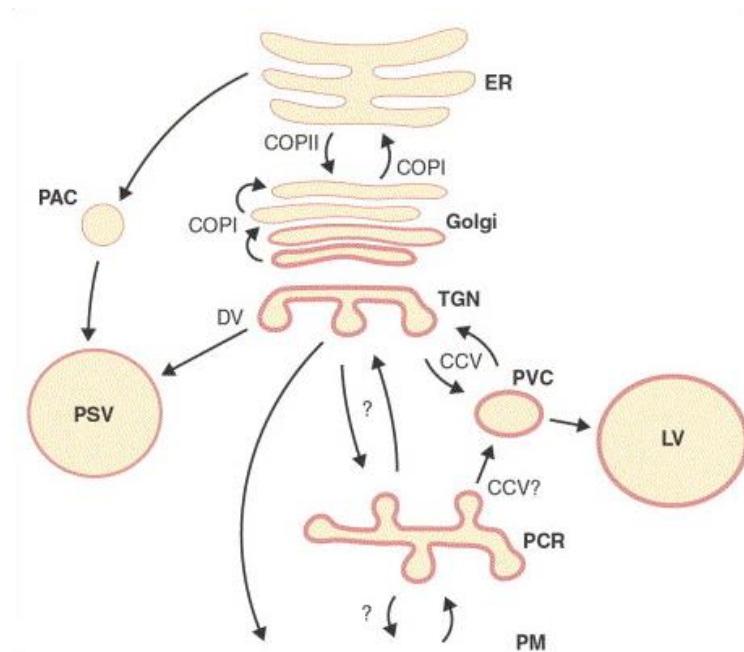


Figure 6.1.1. The endomembrane system. Lipid membranes are constantly transported throughout the cytoplasm to maintain organelle homeostasis. ER – Endoplasmic reticulum; COPI/II – coat protein complex I/II; TGN – trans Golgi network; CCV – clathrin-coated vesicles; DV – dense vesicles; PAC – precursor accumulating vesicles; LV – lytic vesicle. Taken from ([Nebenführ, 2002](#))

Interestingly, ATR has been proposed to potentially have novel roles in the endomembrane transport network – proteins enriched with evolutionarily conserved ATR/ATM substrate motifs are over-represented in vesicle trafficking and cytoskeletal pathways ([Cara et al., 2016](#)), and vesicle-associated membrane protein 2 (VAMP2) has recently been validated as a novel ATR substrate involved in neurotransmitter release ([Li et al., 2009](#)). Notable putative ATR substrates with roles in membrane transport include:

- **Dynein subunits (cytoplasmic dynein 1 intermediate chain 2 - DYNC1I2 p-S95; DYNC1 heavy chain 1 - DYNC1H1 multiple sites)** – required for minus-end transport of all membrane-bound cargos across the microtubule network towards the nuclear periphery ([Cara et al., 2016](#); [Kimura et al., 2008](#); [Matsuoka et al., 2007](#)).
- **Syntaxin 6 (p-S129)** – Soluble NSF Attachment Protein Receptor (SNARE) protein, associated with the trans-Golgi network (TGN) and early endosomes. Required with VAMP2 for insulin-dependent glucose transporter 4 (GLUT4) translocation to the plasma membrane in endocrine cells ([Jung et al., 2012](#); [Matsuoka et al., 2007](#)).
- **Vacuolar protein sorting-associated protein 4b (VPS4b p-T317)** - An AAA⁺-ATPase (ATPases Associated with diverse cellular Activities) implicated in multi-vesicular body (MVB) transport, required for endosomal sorting and trafficking through its function in the disassembly and dissociation of the endosomal sorting complexes required for transport-III (ESCRT-III) complex from membranes ([Obita et al., 2007](#)) ([Matsuoka et al., 2007](#)).

6.1.2. *Intracellular Ca²⁺ Homeostasis*

As well as providing membrane for a variety of other organelles within the endomembrane system, the ER also functions in concert with the mitochondria to tightly govern intracellular Ca²⁺. Specific temporal and spatial thresholds of [Ca²⁺]_{cyt} (cytoplasmic Ca²⁺ concentration) activate a variety of Ca²⁺-dependent kinases, allowing signal transduction through multiple cascades resulting in fundamental shifts in metabolic and transcriptional programming. Maintenance of low [Ca²⁺]_{cyt} (100-300 nM)

by the ER and mitochondria, where the luminal concentration of Ca^{2+} is significantly higher (10-100 μM), and the availability of Ca^{2+} -dependent kinases of varying sensitivity, allows each cell the toolkit to create and respond to diverse temporal and spatial shifts in Ca^{2+} ([Berridge et al., 2000](#)). Cells have exploited the versatile nature of this intracellular messenger, with Ca^{2+} efflux controlling diverse intracellular processes including proliferation, differentiation, secretion, metabolism, membrane trafficking, gene transcription and apoptosis ([Berridge et al., 2000](#)).

6.1.2.1. Ca^{2+} sequestration

In skeletal and cardiac muscle, calsequestrin acts as the primary Ca^{2+} -binding protein. In almost all other tissues, Ca^{2+} is sequestered in the ER lumen by Ca^{2+} -dependent chaperones binding immunoglobulin protein (BiP), calnexin (CANX) and protein disulphide isomerase (PDI), as well as calreticulin ([Papp et al., 2003](#)). Ca^{2+} -binding proteins such as these also carry other essential functions, including chaperone function and influence over ER Ca^{2+} release and uptake, underscoring the intimate relationship between $[\text{Ca}^{2+}]_{\text{ER}}$ and general ER functionality ([Berridge, 2002](#)).

6.1.2.2. Ca^{2+} channels/pumps

Many luminal and transmembrane proteins housed at the ER control Ca^{2+} movement across its membrane. Ca^{2+} flux through the ER requires extensive regulation under basal conditions, as well as in response to external stimuli ([Raffaello et al., 2016](#)). ATP-dependent smooth ER Ca^{2+} ATPase (SERCA) pumps Ca^{2+} into the ER lumen, and is responsible for maintaining the significant Ca^{2+} gradient between the ER and cytoplasm. SERCA pump activity is increased upon ER Ca^{2+} release ([Periasamy and Kalyanasundaram, 2007](#)). Following Ca^{2+} release and subsequent depletion of $[\text{Ca}^{2+}]_{\text{ER}}$, store-operated Ca^{2+} entry (SOCE) works to sustain the enhanced $[\text{Ca}^{2+}]_{\text{cyt}}$ through facilitating refilling of the ER with Ca^{2+} from the extracellular environment ([Smyth et al., 2010](#)). Protein families coordinate SOCE; ER-membrane bound stromal interaction molecule 1 family (STIM) and plasma membrane-bound Ca^{2+} -release-activated Ca^{2+} channel protein 1 (ORAI1). ER Ca^{2+} depletion induces oligomerisation and translocation of STIM1 across the ER membrane to ER-plasma membrane junctions, where it interacts with ORAI, inducing Ca^{2+} influx into the ER ([Raffaello et al., 2016](#)).

Two subtypes of Ca^{2+} channel also exist on the ER membrane – the inositol 1, 4, 5-triphosphate receptor (IP_3R) and Ryanodine receptor family (RyRs). Following stimulation, these channels act alone or in concert to rapidly release ER Ca^{2+} into the cytoplasm. RyRs form vast homotetramers, whose primary opening trigger is Ca^{2+} binding at multiple sites of differing affinities ([Van Petegem, 2012](#)).

Depletion of ER Ca^{2+} underlies the pathophysiology of several diseases including diabetes mellitus, vascular disease and sensory neuropathy ([Mekahli et al., 2011](#)). Further to this, compounds that alter ER Ca^{2+} -channel function are clinically distinguished in the treatment of hypertension and heart disease, such as IP_3R channel blocker Verapamil ([Zanchetti et al., 1998](#)). Increases in cytoplasmic IP_3 stimulate the release of Ca^{2+} from the ER via the IP_3R . Increased IP_3 pools are generated through the activation of phospholipase C (PLC) following ligand-GPCR (G protein-coupled receptor) binding, where PLC functions to cleave $\text{PI}(4, 5)\text{P}_2$ into DAG and $\text{I}(1, 4, 5)\text{P}_3$ ([Raffaello et al., 2016](#)). IP_3Rs are also opened as part of Ca^{2+} -induced Ca^{2+} release - a positive feedback mechanism also associated with RyRs. Until a specific threshold that is inhibitory, increasing $[\text{Ca}^{2+}]_{\text{cyt}}$ increases IP_3R open probability. IP_3R activity is modified by a variety of factors, including Ca^{2+} -binding protein calmodulin ([Hirota et al., 1999](#)) and pro-survival BH3 family members B-cell lymphoma 2 (BCL-2) and B-cell lymphoma-extra large (BCL-XL) ([Distelhorst and Bootman, 2011](#)). Several Ca^{2+} -dependent kinases function in the induction of autophagy, such as Ca^{2+} /calmodulin-dependent kinase kinase-beta (CAMKK β) ([Glick et al., 2010](#); [Høyer-Hansen et al., 2007](#); [Kania et al., 2015](#)).

6.1.3. *The BCL-2 family*

As well as roles in modulating ER and mitochondrial Ca^{2+} homeostasis, a fundamental role of BCL-2 family members is in the control of cell fate. This family of pro- and anti-apoptotic proteins have dynamic relationships with one another, where their activities culminate in a sensitive ‘molecular switch’ between the survival and death pathways within the cell – autophagy and apoptosis ([Youle and Strasser, 2008](#)). The decision to undertake either programmed cell death or enhance autophagic, survival-associated pathways is generated by BCL-2 family members through the competitive binding and sequestration of one another, inhibitory and activatory phosphorylations from upstream regulators and multiple other mechanisms. Three functional groups, with

opposing roles, exist within the BCL-2 family, working in concert to decide cell fate (Fig 6.1.3.1):

- 1) Pro-survival ‘multi-region’ members** – BCL-2, BCL-XL, Induced myeloid leukaemia cell differentiation protein (MCL-1)
- 2) Pro-apoptosis ‘BH3-only’ effectors** – sub-classified into ‘sensitizers’ (BCL-2-associated death promoter - BAD) and ‘activators’ (BH3 interacting-domain death agonist - BID, BCL-2-like protein 11 - BIM, p53 upregulated modulator of apoptosis - PUMA, Phorbol-12-myristate-13-acetate-induced protein 1 - NOXA)
- 3) ‘Executioner’ members** - BCL-2 homologous antagonist/killer (BAK) and BCL-2-associated X protein (BAX)

Activation of the ‘executioner’ proteins BAK/BAX is central to the induction of apoptosis. Activation of BAK/BAX induces a conformational change, resulting in their oligomerisation, allowing them to form pores in the mitochondrial outer membrane (MOM) ([Wei et al., 2001](#)). The permeabilised MOM releases cytochrome C into the cytoplasm, activating apoptotic effector caspases to initiate programmed cell death pathways and degradation of cellular components. BAK is constitutively membrane

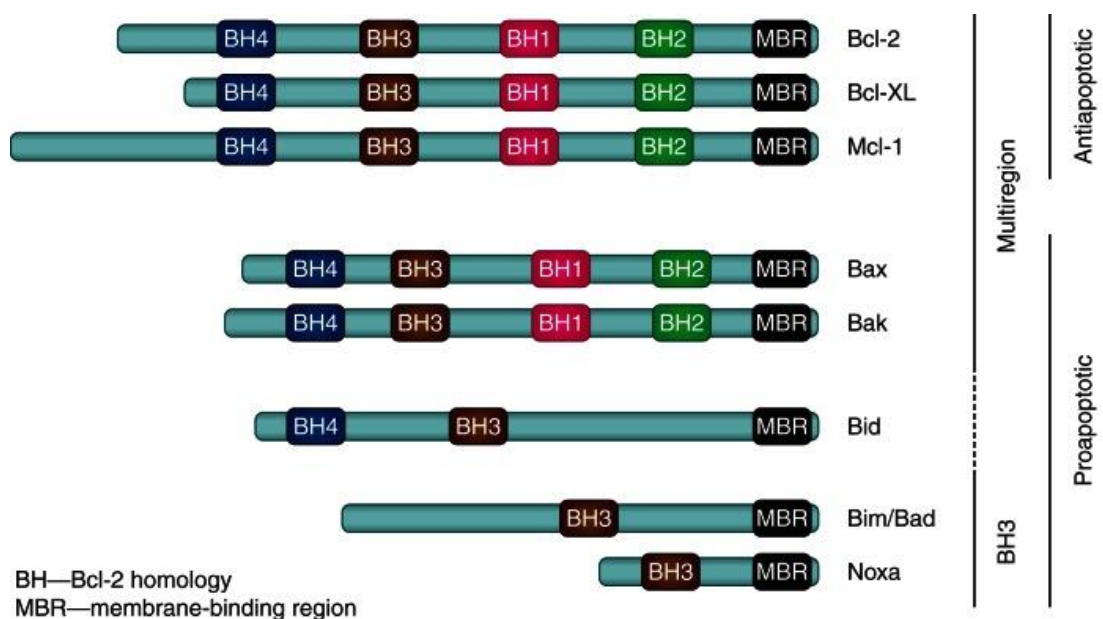


Figure 6.1.3.1. Structure of BCL-2 family members. Pro-survival members are multi-region, executioners BAK/BAX are also multi-region, pro-apoptosis members are generally BH3-only, with the exception of BID. Taken from ([Shamas-Din et al., 2013](#))

bound, whereas BAX remains cytoplasmic until activated, and elements of redundancy exist between these two BCL-2 members ([Westphal et al., 2011](#)).

In unperturbed cells, the opposing actions of the pro-survival (multi-region) and pro-apoptosis (BH3-only) BCL-2 family members on BAX/BAK remains in a stable, pro-survival state of equilibrium. This is achieved through the mutual sequestration of opposing members, posttranslational modifications (PTMs) from upstream effectors, and targeted degradation ([Shamas-Din et al., 2013](#)). Pro-survival, multi-region members (such as BCL-2, BCL-XL, and MCL-1) sequester BH3-only proteins, and bind to and inhibit BAK/BAX oligomerisation to prevent apoptosis ([Emily et al., 2001](#); [Willis et al., 2005](#)). These pro-survival family members prevent the mitochondrial association of BAX and sequester BAK, effectively inhibiting apoptosis (Fig 6.1.3.2). Pro-survival BCL-2 also binds to and inhibits Beclin 1 from inducing autophagy, where this interaction can be interrupted (and autophagy induced) by activated BH3-only proteins that sequester BCL-2, as well as PTMs of BCL-2 ([Kang et al., 2011](#)). Hence, in unperturbed conditions pro-

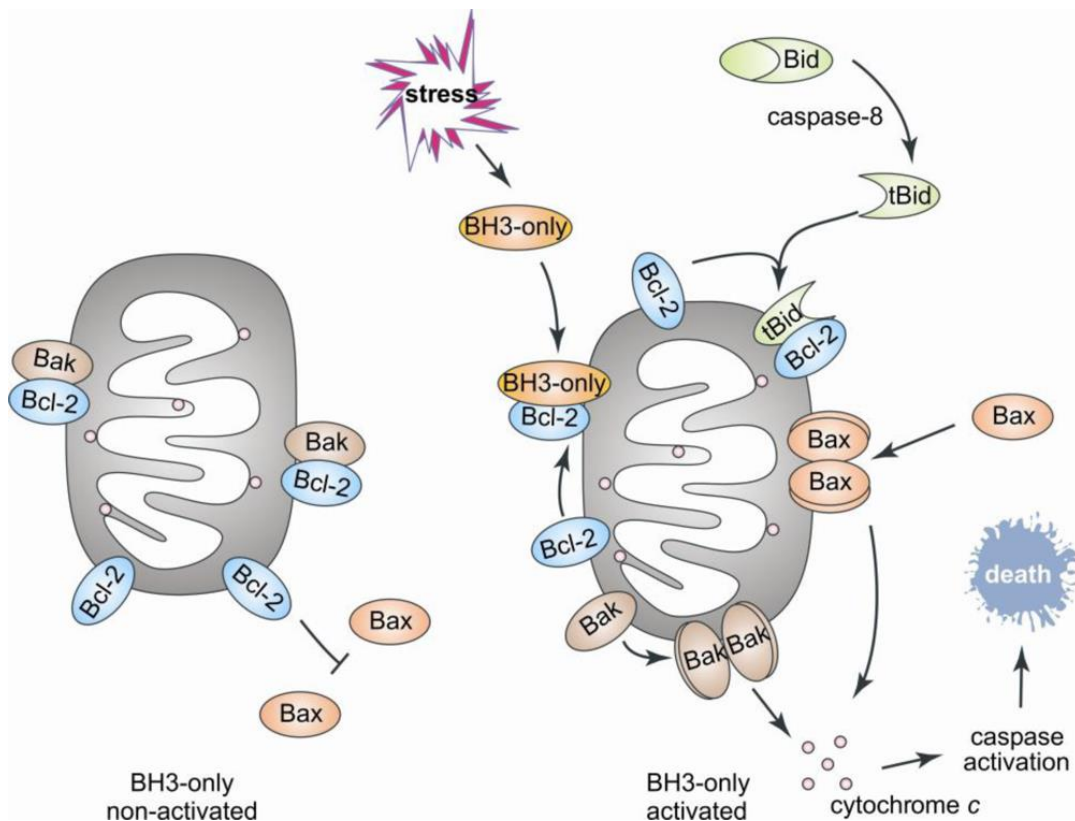


Figure 6.1.3.2. Simplified schematic of BCL-2 family mechanisms of action. In unperturbed cells, BAK and BAX are sequestered by pro-survival members (such as BCL-2). Following activation of pro-apoptotic members, mutual sequestration of multi-region and BH3-only members occurs, increasing likelihood of BAK/BAX oligomerisation. Taken from ([Rautureau et al., 2010](#))

survival BCL-2 family members inhibit autophagy, but their sequestration by BH3-only proteins in times of stress effectively induces pro-survival, autophagic activation.

BAK/BAX oligomerisation is induced by the binding of activated, BH3-only effectors coined 'activators', such as truncated BID (tBID), BIM and PUMA ([Kuwana et al., 2005](#)). BH3-only 'activator' proteins can bind to BAK/BAX as well as mutually sequester other pro-survival multi-region members with varying specificities; 'sensitizers' such as BAD can only sequester pro-survival members, and do not have the binding affinity for direct activation of BAX/BAK. 'Sensitizer' BH3-only members can also displace 'activator' BH3-only proteins from their mutual sequestration with pro-survival members, allowing them to go forward in activating BAK/BAX ([Giam et al., 2008](#)).

BID/tBID will preferentially bind to pro-survival, multi-region BCL-2 proteins ([Cheng et al., 2001](#)), however if it is displaced by another BH3-only protein, it will bind to and activate BAK. Using sequence alignments, Hilton *et al.* (2015) interestingly noted that the BH3-like domains of ATR resembled those within the pro-survival, multi-region BCL-2 family (such as BCL-2). ATR co-precipitated with tBID at the mitochondria, appearing to sequester and inhibit the pro-apoptotic function of tBID, suggesting a genuine functional significance of the BH3-like domains of ATR ([Hilton et al., 2015](#)). Furthermore, BID/tBID is an established ATR substrate following DNA damage ([Liu et al., 2011](#); [Zinkel et al., 2005](#)).

As well as influencing IP₃R activity, ER-associated BCL-2 also increases ER membrane Ca²⁺ permeability, causing Ca²⁺ to 'leak' back into the cytoplasm ([Oakes et al., 2003](#)). This has the net effect of reducing the impact of agonist-induced ER Ca²⁺ release, reducing the activity of kinases dependent on sharp increases in [Ca²⁺]_{cyt} for activation such as autophagy inducer CAMKKβ, and reducing Ca²⁺ transfer from the ER to the mitochondria to initiate apoptosis ([Høyer-Hansen et al., 2007](#); [Mattson and Chan, 2003](#)).

6.1.4. Protein folding and quality control

Perhaps the most vital role of the ER is as the quality control centre of newly synthesised proteins. Stringent quality control parameters on the production of secreted, large or membrane-bound proteins at the ER ensure misfolded proteins or aggregates do not

enter the cytoplasm and compromise proteomic homeostasis. Resident ER chaperones and enzymes aid protein folding, signal peptide cleavage, and PTMs such as N-linked glycosylation and the formation of disulphide bridges ([Araki and Nagata, 2011](#)).

One example of such surveillance of newly synthesised proteins is the management of PTMs required to generate glycoproteins. Ca^{2+} -responsive chaperones CANX and Calreticulin will recognise proteins carrying untrimmed N-glycan groups – binding to them to prevent aggregation or premature export from the ER whilst they are optimally folded ([Williams, 2006](#)). Following cleavage of a single glucose residue by glucosidase II, these glycosylated polypeptides are released from CANX/Calreticulin for the next quality control check by UDP-glucose/glycoprotein glucosyl-transferase (UGGT) ([Gelebart et al., 2005](#)). UGGT assesses the folded conformation of released glycoproteins; if they are not appropriately folded they are reglucosylated, sending them back to CANX/calreticulin for another chance to reach their correct conformation ([Hebert et al., 2005](#)).

Another major chaperone system resident to the ER is mediated by BiP. BiP is a key member of the heat shock protein 70 (HSP70) family of chaperones ([Kaufman et al., 2002](#)), and like CANX and Calreticulin, BiP also acts as a Ca^{2+} buffer, binding the ion with 1:1 stoichiometry in the ER lumen ([Lamb et al., 2006](#)). Further from this, in unperturbed conditions BiP binds to and regulates the activities of the three unfolded protein response (UPR) inducers - activating transcription factor 6 (ATF6), inositol requiring kinase 1 ($\text{IRE1}\alpha$) and protein kinase RNA-like ER kinase (PERK) – making it a key modulator of the UPR ([Bertolotti et al., 2000](#)). Multiple cochaperones mediate the activity and stimulation of BiP as well as nucleotide exchange factors (NEFs). ADP-bound BiP will bind to substrates with closed hydrophobic regions, preventing aggregation of unfolded polypeptides, ensuring they remain soluble ([Kampinga and Craig, 2010](#)).

The ER also facilitates the formation of disulphide bonds – important covalent bonds required to ensure the folding, stability and correct quaternary structure of many proteins. Oxidoreductases (within the PDI family) facilitate disulphide bridge formation at cysteine residues, through their catalytic oxidation and isomerisation activities ([Ellgaard and Ruddock, 2005](#)).

Following successful folding, proteins that require further PTMs exit the ER via ER exit sites (ERES), and are shuttled to the GA via specialised vesicles. The GA functions as a molecular assembly line, completing complex PTMs before membrane-bound proteins can reach full maturation. When the ER is not able to successfully facilitate protein folding, terminally aggregated or misfolded proteins are targeted for degradation. The ERAD and autophagy pathways work to remove and degrade these polypeptides.

6.1.5. *The ER stress response*

6.1.5.1. *ER-Associated Degradation (ERAD)*

ERAD is the series of pathways that removes inoperably misfolded proteins from the ER for targeted proteasomal degradation ([Grootjans et al., 2016](#)). A substantial fraction of proteins entering the ER for processing will never reach their native states. Hence, the folding protein population within the ER lumen is under constant surveillance to ensure terminally misfolded polypeptides are recognised, dislocated and degraded. Central to the ERAD system are ER transmembrane complexes containing E3 ubiquitin ligases ([Denic et al., 2006](#)). The ERAD E3s work in concert with adaptor proteins (including BiP) to survey overlapping but distinct substrates with diverse topologies, which require removal ([Smith et al., 2011](#)).

Terminally misfolded proteins are polyubiquitinated and subsequently extracted from the ER membrane by AAA⁺ ATPase valosin-containing protein (VCP/p97 – referred to hereon as p97), allowing them to be escorted to the proteasome ([Ye et al., 2005](#)). Interestingly, p97 is also phosphorylated by ATR (S784) in response to UV-induced DNA damage ([Livingstone et al., 2005](#)), within a consensus sequence required for localisation to specific cellular compartments and nuclear-cytoplasmic shuttling ([Song et al., 2015](#)). Phospho-p97 S784 is localised to sites of DNA DSBs, and is proposed to be required for the removal of ubiquitinated proteins from chromatin ([Vaz et al., 2013](#)). Further to this, over-expression of dominant negative p97 construct, or p97 siRNA results in ER swelling, due to the accumulation of misfolded proteins within the ER with no effective ER secretory pathway to remove them for degradation ([Mimnaugh et al., 2006](#)).

6.1.5.2. The UPR

Times of increased translation that exceed the ER's capacity to appropriately fold and modify newly synthesised polypeptides, can result in the accumulation of mis- or unfolded proteins, referred to as ER stress. When the ERAD pathways are no longer sufficient to manage degradation of these terminally misfolded proteins, pathways collectively termed the UPR are initiated to re-establish normal function of the ER ([Chakrabarti et al., 2011](#)). If adequate restoration of ER function does not occur, the UPR will result in apoptosis via the down-regulation of pro-survival members of the BCL-2 family (BCL-2, BCL-XL). Here I will briefly review the three branches of the UPR.

The UPR is regulated by three transmembrane receptors: ATF6, IRE1 α , and PERK (Fig 6.1.5.2).

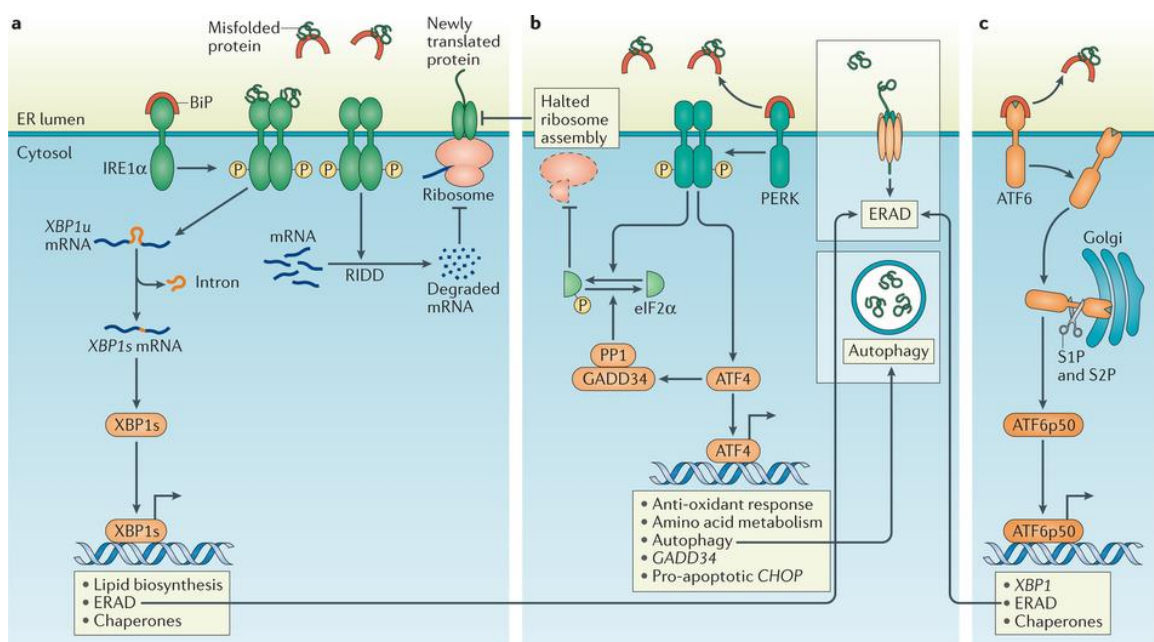


Figure 6.1.5.2. The three arms of the UPR. BiP activates IRE1 α , PERK and ATF6, inducing transcriptional cascades that result in the upregulation of ER chaperones and ERAD proteins. Taken from ([Grootjans et al., 2016](#)).

6.1.5.3. PERK

The main function of the PERK cascade is to modulate translation. Dissociation of BiP from the ER-luminal N-terminus initiates PERK dimerization and C-terminal autophosphorylation ([Kebache et al., 2004](#)). PERK activation attenuates protein

translation via phosphorylation of eukaryotic initiation factor 2 α (eIF2 α) at S51, preventing eIF2 α dissociation from partner initiation factor eIF2B, inhibiting its critical translation initiation activity ([Gebauer and Hentze, 2004](#)). Inhibition of translation initiation ensures the folding demand on the ER can begin to diminish. Not all translation is blocked however – mRNA containing the sequence for an internal ribosome entry site (IRES) in the upstream open reading frame (UORF) can bypass the eIF2 α block, allowing targeted translation ([Schröder and Kaufman, 2005](#)). *ATF4* is one such gene that evades the eIF2 α transcriptional block, encoding CCAAT-enhancer-binding protein (C/EBP)-factor activating transcription factor 4 (ATF4). ATF4 drives many pro-survival functions, including ER chaperone expression, oxidative stress resistance and regulation of glucose and amino acid metabolism ([Chakrabarti et al., 2011](#); [Seo et al., 2009](#)).

Interestingly, ATF4 has also been implicated in the regulation of adipogenesis through the targeted activation of C/EBP β and PPAR γ ([Yu et al., 2014](#)). This is further bolstered by the generation of *Atf4*^{-/-} mice that present with hypoglycaemia and lean fat mass ([Seo et al., 2009](#)), suggesting further uncharacterised roles for ATF4 in metabolism.

6.1.5.4. ATF6

The key role of the ATF6 pathway is to induce a gene expression program that increases chaperone activity and enhances degradation of unfolded proteins ([Chakrabarti et al., 2011](#)). ATF6 upregulates BiP, PDI and X box-binding protein 1 (XBP1), a transcription factor that requires further mRNA processing by activated IRE1 α before translation. Like PERK and IRE1, ATF6 activation is induced by BiP dissociation from the luminal N-terminus of ATF6. Activation is followed by translocation to the GA - the factors controlling ATF6 translocation remain relatively unclear, but there appears to be requirement for (and redundancy between) two N-terminal Golgi localisation sequences (GLS), one of which is the binding site of BiP ([Shen et al., 2002](#)).

ATF6 acquires its transcription activity in a unique manner. Following Golgi localisation, ATF6 undergoes regulated intramembrane proteolysis (RIP) by S1P (serine protease site-1 protease) and S2P (metalloprotease site-2 protease) – the coordinated cleavage of luminal peptides ([Wang et al., 2000](#)). This results in a transcriptionally active 50 kDa fragment of ATF6, which translocates to the nucleus and regulate expression of

CRE- and ER-stress response element (ERSE)- promoter genes ([Kokame et al., 2001](#)). ATF6 activation also induces expression of HSP70-binding DNAJ protein P58^{IPK}, which binds to the cytosolic, C-terminal kinase domain of PERK and inhibits its activity ([Yan et al., 2002](#)).

6.1.5.5. *IRE1 α*

The IRE1 α pathway is the most evolutionarily conserved limb of the UPR and has opposing roles. Following BiP dissociation, IRE1 α is activated following homo-oligomerisation and autophosphorylation of its cytosolic C-terminus ([Shamu and Walter, 1996](#); [Welihinda and Kaufman, 1996](#)). IRE1 α contains both an endoribonuclease and Ser/Thr kinase domain, which can transduce signals simultaneously upon activation, triggering two distinct signalling axes. IRE1 endoribonuclease activity cleaves a short intron from XBP1 mRNA, generating the transcriptionally active frameshift variant XBP-1s ([Lee et al., 2002](#)). XBP-1s dimerises and potently regulates the expression of multiple ER chaperones, as well as PERK-inhibiting P58^{IPK} and ER-associated degradation (ERAD) pathway proteins ([Yan et al., 2002](#)).

The cytosolic kinase activity of IRE1 α activates adaptor proteins such as tumour necrosis factor receptor-associated factor 2 (TRAF2), resulting in signal transduction and subsequent activation of the mitogen-activated kinases p38 mitogen activated protein kinase (p38 MAPK) and c-Jun N-terminal kinase (JNK) ([Urano et al., 2000](#)). IRE1 α also phosphorylates several other kinases, however their role in the UPR is poorly understood ([Hu et al., 2006](#); [Nguyễn et al., 2004](#)). JNK functions to phosphorylate and activate pro-apoptotic BCL-2 family member BIM whilst simultaneously suppressing pro-survival member BCL-2, via inhibitory phosphorylations at several sites ([Lei and Davis, 2003](#); [Wei et al., 2008](#)) which ultimately results in BAX/BAK-dependent apoptosis. Activated p38 also phosphorylates BCL-2, further inducing inhibition ([De Chiara et al., 2006](#)). Inhibition of BCL-2 by the IRE1 α branch of the UPR results in the liberation of autophagy inducer Beclin1 ([Wei et al., 2008](#)), resulting in pro-survival upregulation of autophagy. Signals initiated from IRE1's kinase domain are largely pro-apoptotic, and it is likely this branch of the UPR is activated after PERK and ATF6. Through these three

pathways, the ER works to recover appropriate protein folding and synthesis and initiate apoptosis where this is no longer possible.

In the previous chapters, I have characterised novel impacts of acute ATRi treatment on cycling and post-mitotic cells, where it appears reduced ATR functionality has profound effects on metabolism. Clinically relevant ATRis appear to induce defects in autophagy and adipogenic differentiation, as well as inducing the ‘browning’ of mature white adipocytes, phenotypes which could have concerning implications if recapitulated *in vivo*. In this chapter, I investigate the impacts of ATR deficiency on ER functionality – with the aim of uncovering putative mechanistic links between the defects I have observed previously following ATRi treatments.

6.2. Results

6.2.1. *ATR inhibition and Atr siRNA induce conspicuous cytoplasmic vacuolisation*

In chapter 5, I treated cycling 3T3-L1 preadipocytes with *Atr* siRNA and ATRis to investigate the effects of depleting ATR activity on autophagy. Whilst undertaking these experiments, I noticed the unusual and striking phenomenon of conspicuous cytoplasmic vacuolisation within minutes of treating samples with ATRis. Fig 6.2.1.1 shows brightfield microscopy of conspicuous cytoplasmic vacuolisation in cycling 3T3-L1

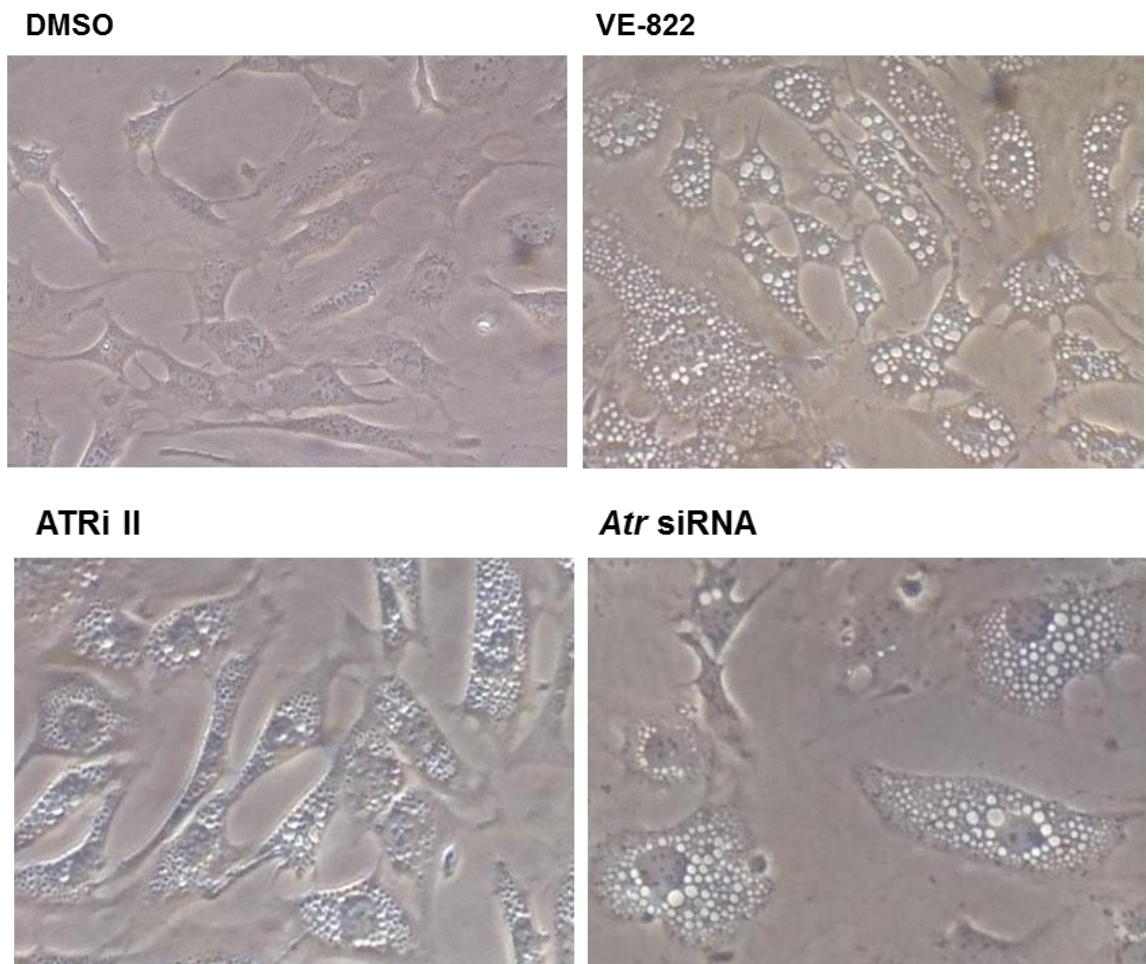


Figure 6.2.1.1. ATRis and *Atr* siRNA induce mass cytoplasmic vacuolisation. Brightfield microscopy of cycling 3T3-L1 preadipocytes treated with ATRis for 1 hr, and ~18 hrs post *Atr* siRNA transfection. Treatment with ATRis induced vacuoles after >10 minutes treatment in 3T3-L1 preadipocytes, which increased in size and number in a time- and dose-dependent manner. *Atr* siRNA transiently and inconsistently induced vacuolisation, suggesting almost complete ablation of ATR function may be necessary to induce vacuolisation. All images representative of results obtained in at least three independent experiments.

preadipocytes, treated with ATRis and *Atr* siRNA. That I also observed cellular vacuolisation following genetic ablation of ATR suggests this phenotype was not due to off-target effects of small molecule ATRis. Interestingly, vacuolisation following *Atr* siRNA was a transient event, and cytoplasmic vacuolisation was not observed consistently following *Atr* siRNA treatments. This suggests that the vacuolisation event observed following depletion of ATR function might be dependent on a temporal threshold of ATR activity, expressed only when kinase function of ATR is ablated acutely and entirely. *Atr* siRNA consistently induced increased p62 expression and blocked autophagy (as assessed by LC3-I/II), suggesting that the cytoplasmic vacuolisation may be independent of the autophagy block following depletion of ATR function. Additionally, *Atg12* and *Atg16L1* siRNA treatments to ablate the autophagy axis did not affect ATRi-induced vacuolisation (data not shown). This striking phenotype was observed in every cell type treated with all ATRis tested – summarised in Table 6.2.1. ATRi-induced cytoplasmic vacuolisation did not appear cell-cycle dependent, and appeared almost within minutes following ATRi treatment, suggesting it is independent of replication stress-induced DNA damage. Vacuolisation did not appear to carry inherent toxicity, as confluent cells treated with ATRis did not lose viability.

Cell line	Origin
MG63	human osteosarcoma
3T3-L1	mouse preadipocytes
C2C12	mouse myoblasts
1BR3	human fibroblast
HEK293	human embryonic kidney cells
RPE	human retinal pigment epithelium

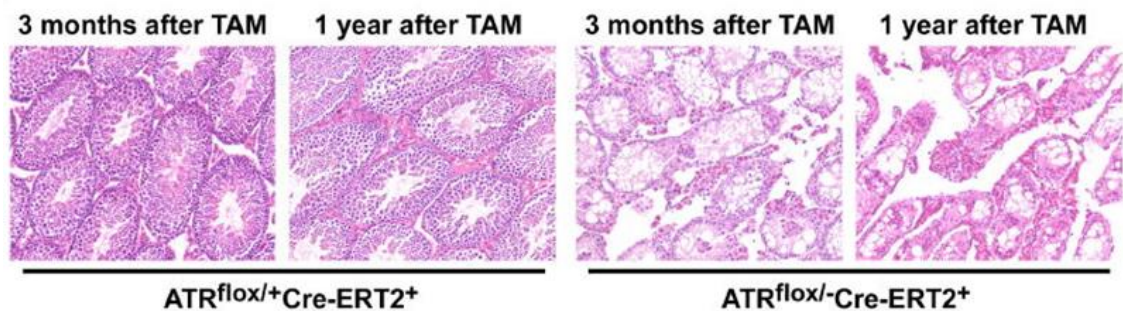
Table 6.2.1. Cell types where ATRi treatment induced conspicuous cytoplasmic vacuolisation.

Incidentally, on closer inspection of existing mouse models of ATR deficiency, vacuolar phenotypes are strikingly apparent. Ruzankina *et al.* (2007) described dramatic testicular atrophy after conditional deletion of *Atr* in adult mice - in the supporting images, vacuolisation can be observed ([Ruzankina et al., 2007](#)) (Fig 6.2.1.2.A). The authors failed to comment on this phenotype. Additionally, in the supplementary material of a paper characterising a mouse model of ATR-Seckel Syndrome, Murga *et al.*

(2009) also comment briefly on the presence of vacuoles within the primary follicles of newborn *Atr^{s/s}* ovaries, shown in Fig 6.2.1.2.B ([Murga et al., 2009](#)).

I have shown here that an array of approaches inducing reduced ATR function result in a cytoplasmic vacuolisation phenotype. Existing literature, and my data utilising ATRi and *Atr* siRNA, suggest that this is a veritable and previously uncharacterised effect of ATR deficiency. It is plausible that such a profound cytoplasmic remodelling event could be the cause or consequence of dramatic alterations in cellular homeostasis.

A



B

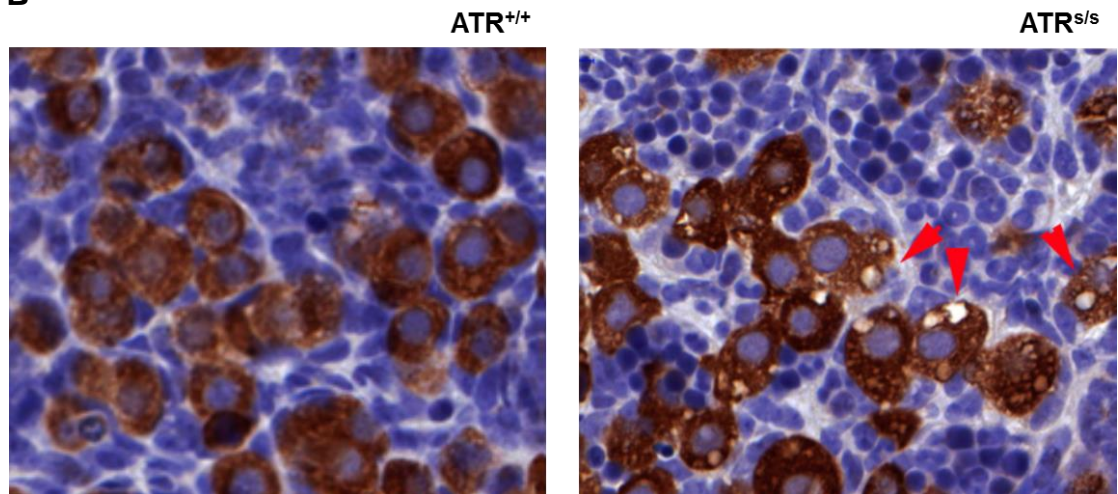


Figure 6.2.1.2. ATR deficiency-induced vacuolisation phenotypes exist in literature. A) Inducible knockdown of *Atr* in adult mouse testicular tissue induces mass cytoplasmic vacuolisation at 3 months and 1 year post-knockdown. Image taken from ([Ruzankina et al., 2007](#)). **B)** Cytoplasmic vacuoles are observed in the ovarian follicles of a humanised mouse model of ATR-SS, 1 day after birth (red arrows).

6.2.2. Contents of ATRi-induced vacuoles are pH neutral

Considering the cytoplasmic vacuolisation I observed following ATRi treatment was so prominent, I wanted to investigate the origins of this phenotype. Such a vast

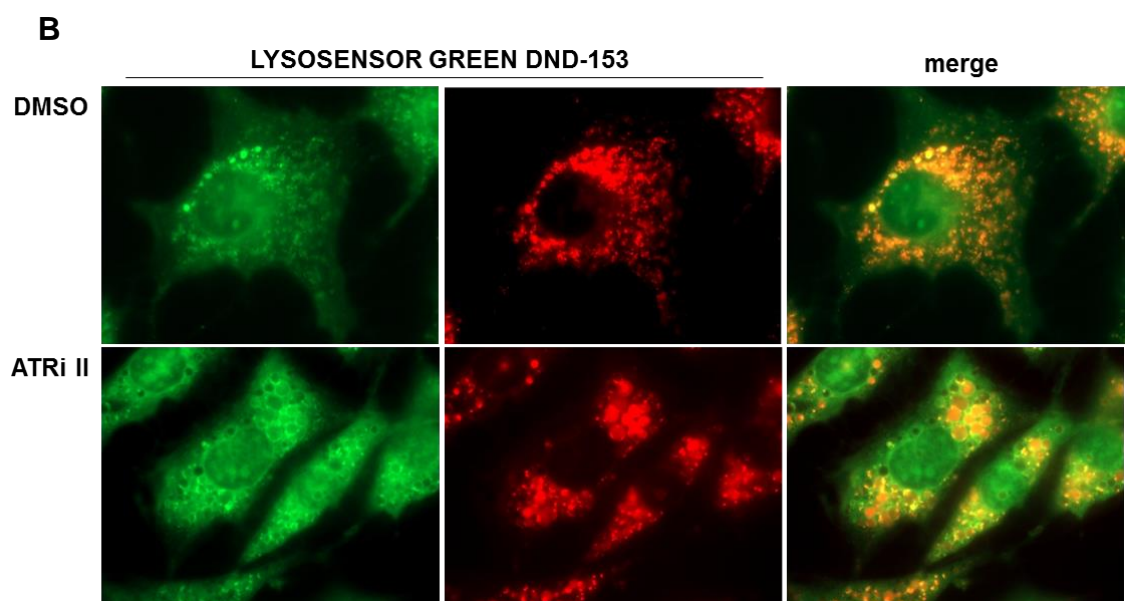
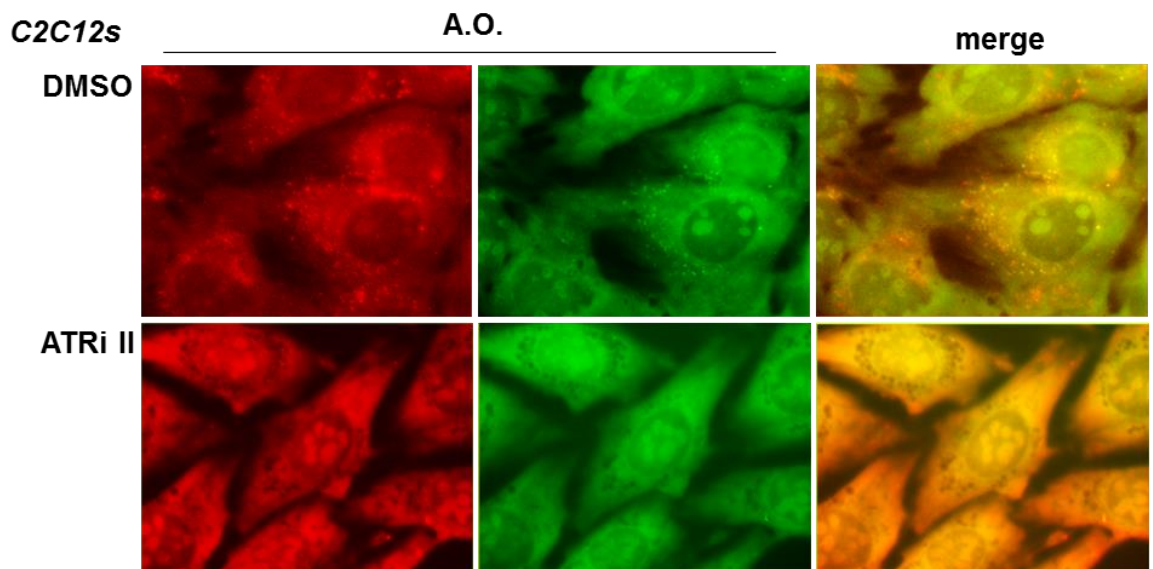
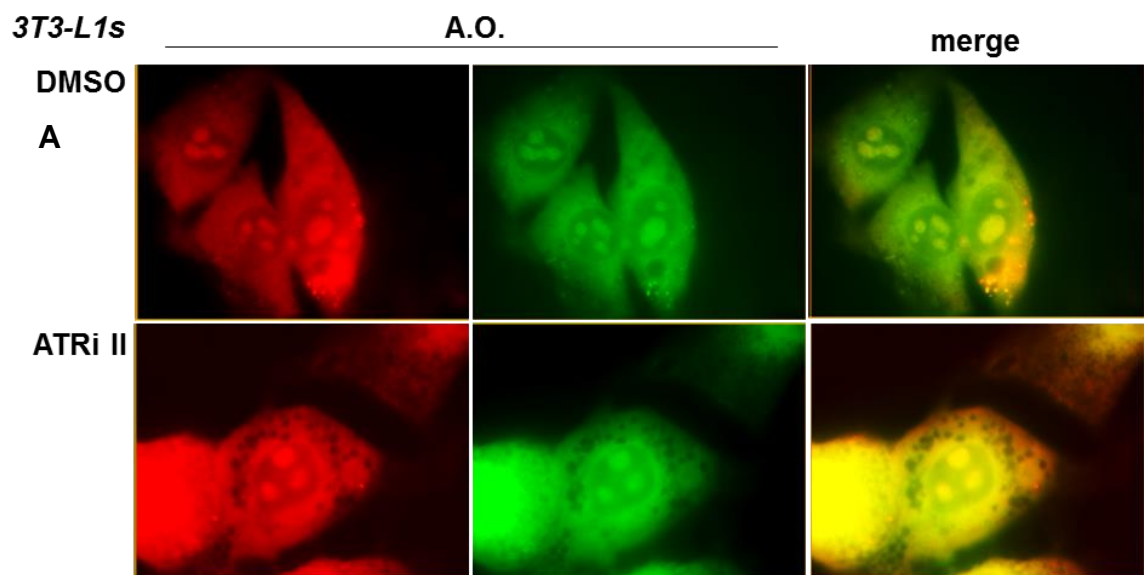
reorganisation of the cytoplasm likely influenced the defective adipogenesis (chapter 3) and autophagy (chapter 5) I observed previously following ATRi treatments.

Considering the block in autophagy I observed in chapter 4, I hypothesised that the ATRi-induced vacuoles could have arisen from blocked autophagic processing. Perhaps the accumulation of autophagosomes (as assessed by LC3-I/II status after Bafilomycin A and ATRi treatment) was generating aberrant, swollen autophagosomes or lysosomes. Swollen autophagosomes generated by a block in autophagic degradation have been described in literature ([Mleczak et al., 2013](#)). Lysosomes are acidic in content whereas autophagosomes are pH neutral. Assessing the pH of vacuoles induced by ATRis would provide insight into their origin.

To investigate the pH of ATRi-induced vacuoles, I utilised Acridine Orange (A.O.), a pH-sensitive fluorescent probe commonly used to label acidic compartments within the cell. Fig 6.2.2.A shows A.O.-stained cycling 3T3-L1 preadipocytes treated with ATRi II. A.O. exhibits bright orange fluorescence in acidic compartments, which can be observed in untreated samples. Following ATRi treatment, vacuoles did not stain orange, suggesting that they are not acidic in nature.

To confirm that the vacuoles observed following ATRi treatments were pH neutral, I utilised pH-neutral fluorescent probe LysoSensor Green DND-153. LysoSensor Green DND-153 can be used for microscopic analysis of cellular vacuolisation events, selectively staining neutral cellular compartments red. Following 3 hrs of ATRi treatment, vacuoles have up taken LysoSensor Green DND-153, indicative of pH neutral content (Fig 6.2.2.B). This indicates that the vacuoles cannot be functional, acidic lysosomes.

Figure 6.2.2. (Overleaf) ATRi-induced vacuoles are pH neutral. A) Acridine Orange (A.O.) staining of cycling 3T3-L1 preadipocytes and C2C12 myoblasts treated with ATRi II for 2 hrs. ATRi-induced vacuoles are clearly visible as dark holes in the cytoplasm. A.O. was not uptaken by ATRi-induced vacuoles, indicating they are not acidic. Images taken at 100x. **B)** Cycling 3T3-L1 preadipocytes were stained with 2 μ M LysoSensor Green DND-153 throughout 3 hrs of ATRi II treatment. Uptake of LysoSensor Green DND-153 into ATRi-induced vacuoles indicates they are pH neutral. Images captured at 100x. All images representative of results obtained in at least three independent experiments.



6.2.3. *ATRi induces mitochondrial fission*

I hypothesised that the cytoplasmic vacuoles observed following ATRi treatments could derive from swollen mitochondria. Considering the metabolic and autophagy defects I have characterised in the previous chapters, I wanted to investigate the effect of ATRi treatment on mitochondrial dynamics. The mitochondrial network is highly dynamic, where fusion and fission events, biogenesis and mitophagy (mitochondrial autophagy) can occur within minutes of appropriate stimulation ([Westermann, 2012](#)). Generally, mitochondria exist in extensive branched structures that undergo constant remodelling, undertaking fission following changes in nutritional status or to prepare for cell division.

MitoTracker Red is a fluorescent probe that labels live mitochondria dependent on membrane potential, allowing visualisation of mitochondrial events via fluorescence microscopy. Cycling 3T3-L1 preadipocytes were treated with ATRi for 2 hours and stained with MitoTracker Red (Fig 6.2.3.A). ATRi II and VE-822 treatments appear to have induced mitochondrial fission apparent by the fractured appearance of mitochondria following treatment. It is also clear that MitoTracker Red staining is not localised to the vacuolar structures induced by ATRi treatment, suggesting vacuoles are not swollen mitochondria. To further assess the consequences of ATRi treatment on mitochondrial dynamics, I utilised MitoTracker Green (described in section 4.2.3.) to assess mitochondrial mass by flow cytometry (FACS).

Fig 6.2.3.B. shows FACS analysis of 3T3-L1 preadipocytes treated with or without ATRi II for 2 hrs. Strikingly, mitochondrial mass is increased over 5-fold following ATRi treatment. This is reminiscent of the 80% increase in mitochondrial mass observed in mature adipocytes following chronic treatment with ATRi II (Fig 4.2.3.B). In Chapter 4, I observed that 24 hr treatment of mature 3T3-L1 adipocytes with ATRi induced increased PGC-1 α expression and mitochondrial mass. To investigate if the increased mitochondrial mass in preadipocytes after acute ATRi treatment was a result of increased mito-biogenesis, I assessed PGC-1 α expression via western blotting. Fig 6.2.3.C shows no change in PGC-1 α expression following ATRi treatments, suggesting that increased mito-biogenesis is not responsible for the increased mitochondrial content observed after ATRi treatment. The massive increase in mitochondrial content

following ATRi treatments could be explained by considering the highly dynamic nature of the mitochondrial network – perhaps the autophagic block induced by ATRi treatment (characterised in chapter 5) could be preventing effective mitophagy, resulting in an accumulation of defective mitochondria.

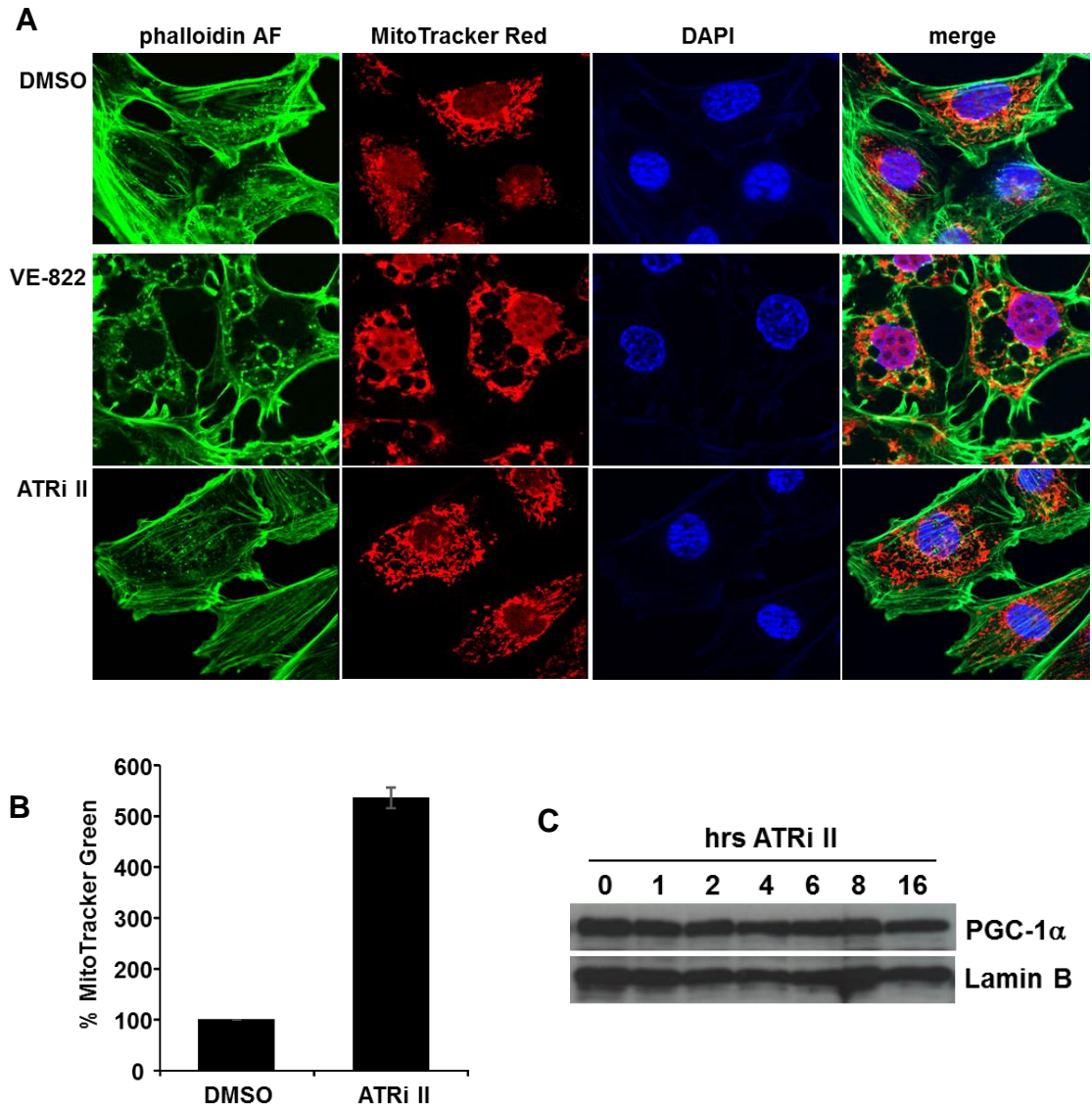


Figure 6.2.3. ATRi treatment induces profound changes in mitochondrial dynamics. A) MitoTracker Red staining of cycling 3T3-L1 preadipocytes treated with ATRis for 2 hrs. AlexaFluor-conjugated Phalloidin (green), MitoTracker Red and DAPI (blue). Following treatment with VE-822 or ATRi II (10 μ M), mitochondria appear to have lost perinuclear localisation and are fragmented throughout the cytoplasm, indicative of mitochondrial fission. **B)** Flow cytometry analysis of mitochondrial mass utilising MitoTracker Green AM-1. Following 2 hrs treatment with ATRi II, mitochondrial mass has increased 5-fold. Results normalised to the corresponding untreated sample. **C)** Western blotting of mito-biogenesis marker PGC-1 α in cycling 3T3-L1 preadipocytes shows no change following acute ATRi II treatments, suggesting increased mitochondrial content following ATRi is not due to increased biogenesis. Lamin B used as loading control. All images representative of results obtained in at least three independent experiments.

6.2.4. *ATRi-induced vacuoles are swollen ER*

Continuing my investigation into the origins of the ATRi-induced cytoplasmic vacuoles, I utilised immunofluorescence microscopy (IF) of ER and Golgi apparatus (GA) markers following ATRi treatments of 3T3-L1 preadipocytes. RCAS1 (receptor binding cancer antigen expressed on SiSo cells) is a GA-associated protein, commonly utilised as a marker of the GA. Fig 6.2.4.1.A shows IF of RCAS1, where in untreated 3T3-L1

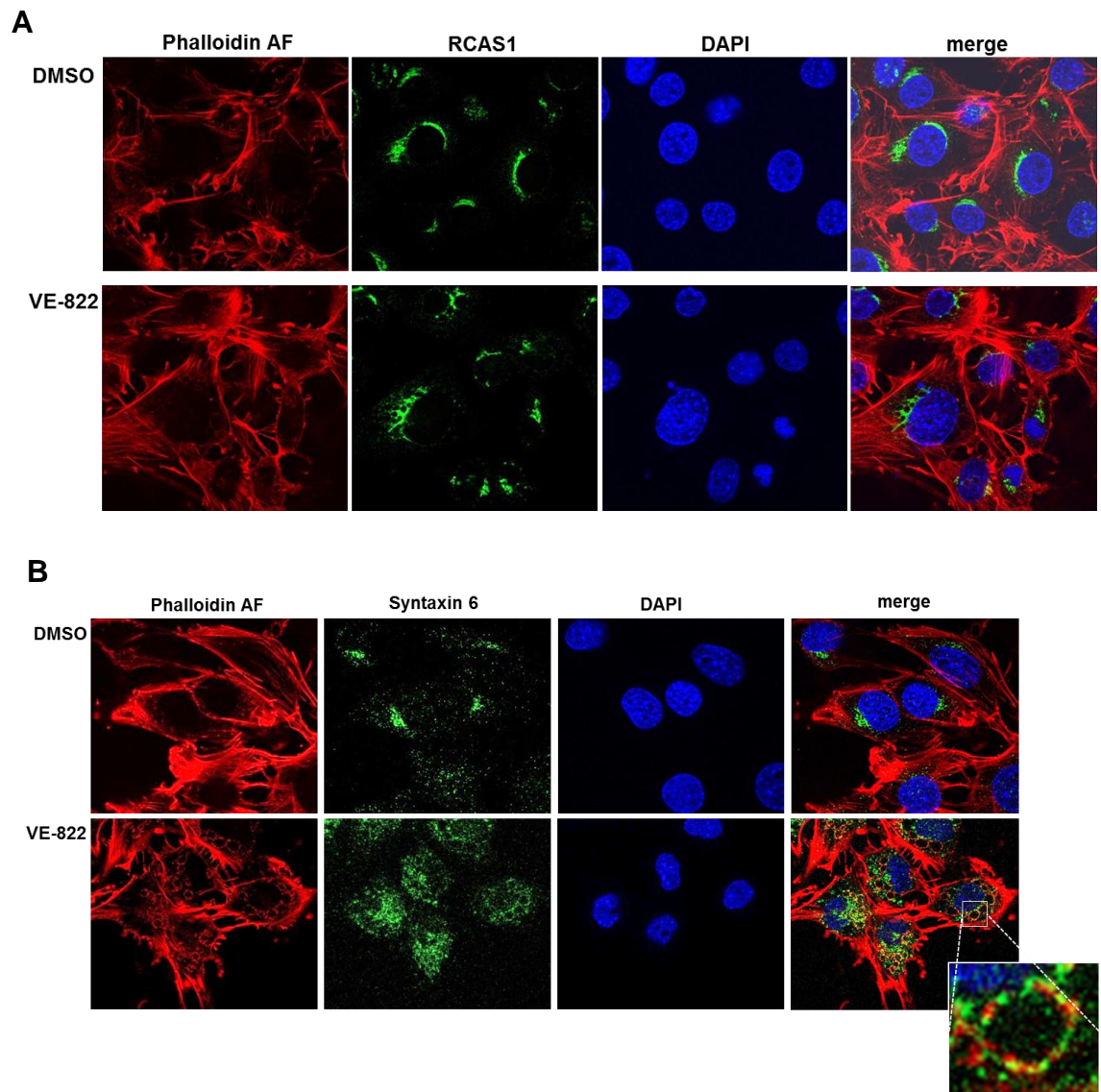


Figure 6.2.4.1. ATRi-induced vacuoles are not swollen Golgi Apparatus (GA). **A)** IF of cycling 3T3-L1 preadipocytes treated with VE-822 for 2 hrs. In untreated and VE-822-treated cells RCAS1 staining remains perinuclear and unchanged indicating ATRi treatment may not be remodelling the GA. **B)** IF of putative ATR substrate and membrane fusion protein Syntaxin 6 before and after VE-822 treatment. Following ATRi treatment, Syntaxin 6 loses perinuclear localisation and appears to localised to ATRi-induced vacuoles, indicating vacuoles could be associated with a defect in membrane fusion or vesicle trafficking. AlexaFluor-conjugated Phalloidin (red), Syntaxin 6 or RCAS1 (green) and DAPI (blue). All images representative of results obtained in at least three independent experiments.

preadipocytes RCAS1 staining appears completely perinuclear. Following 2 hrs of VE-822 treatment, RCAS1 localisation appears unchanged, and no localisation to ATRi-induced vacuoles is apparent, suggesting they have not arisen from swollen GA.

Syntaxin 6 is a vesicle- and GA-associated protein, a mediator of membrane fusion required for several vesicle-transport associated pathways ([Bock et al., 1997](#)). Interestingly, Syntaxin 6 has been recognised as a putative ATR/ATM substrate (S129) after DNA damage ([Cara et al., 2016](#); [Matsuoka et al., 2007](#)). Considering its significance as a putative ATR/ATM substrate and membrane-associated protein, I chose to further investigate the effect of ATRi treatment on Syntaxin 6 localisation. Fig 6.2.4.1.B shows in untreated 3T3-L1 preadipocytes, Syntaxin 6 is localised to the perinuclear region similarly to RCAS1 (Fig 6.2.4.1.A). Following 2 hrs VE-822 treatment, Syntaxin 6 has lost its perinuclear localisation and also appears to localise to ATRi-induced vacuoles (Fig 6.2.4.1.B, magnified section). This indicates the ATRi-induced cytoplasmic vacuolisation may be originating from aberrant processing of vesicular membranes. Organelles undergo constant remodelling as part of cellular homeostasis, and for this to occur, the appropriate provision of lipid membranes shuttled from the endomembrane system is required. Defects in vesicular transport at any stage can fundamentally shift the dynamic equilibrium required to maintain cellular homeostasis.

I hypothesised that ATRi could be causing a defect in the activity of putative substrate VPS4b (discussed in section 6.1.1), inducing the vacuolar phenotype. VPS4b is of particular interest because mutations generating defects in the ATPase activity of VPS4b result in a cytoplasmic vacuolisation phenotype ([Bishop and Woodman, 2000](#); [Scott et al., 2005](#)). Furthermore, the putative ATR/ATM phospho-site is proximal to the ATPase domain of VPS4b, suggesting potential functional relevance of this SQ motif.

To test this hypothesis, I used a site directed mutagenesis approach to generate a FLAG-tagged ATPase-defective VPS4b mutant construct (E235Q) ([Bishop and Woodman, 2000](#)) and also a phospho-mutant construct where the putative ATR phospho-site was ablated (T317A). If this site was a *bona fide* ATR target, responsible for the ATRi-induced vacuolisation, transient over-expression of the phospho-mutant would generate similar consequences to ATRi treatment.

Fig 6.2.4.2.A shows western blotting of 3T3-L1 preadipocytes transiently over-expressing FLAG-tagged VPS4b constructs, treated with or without VE-822 for 2 hrs. Fig 6.2.4.2.B shows representative brightfield microscopy images of samples over-expressing each construct, treated with VE-822 for 2 hrs. Strikingly, both WT-VPS4b and T317A-VPS4b appear to rescue the ATRi-induced vacuolar phenotype, whereas ATPase-

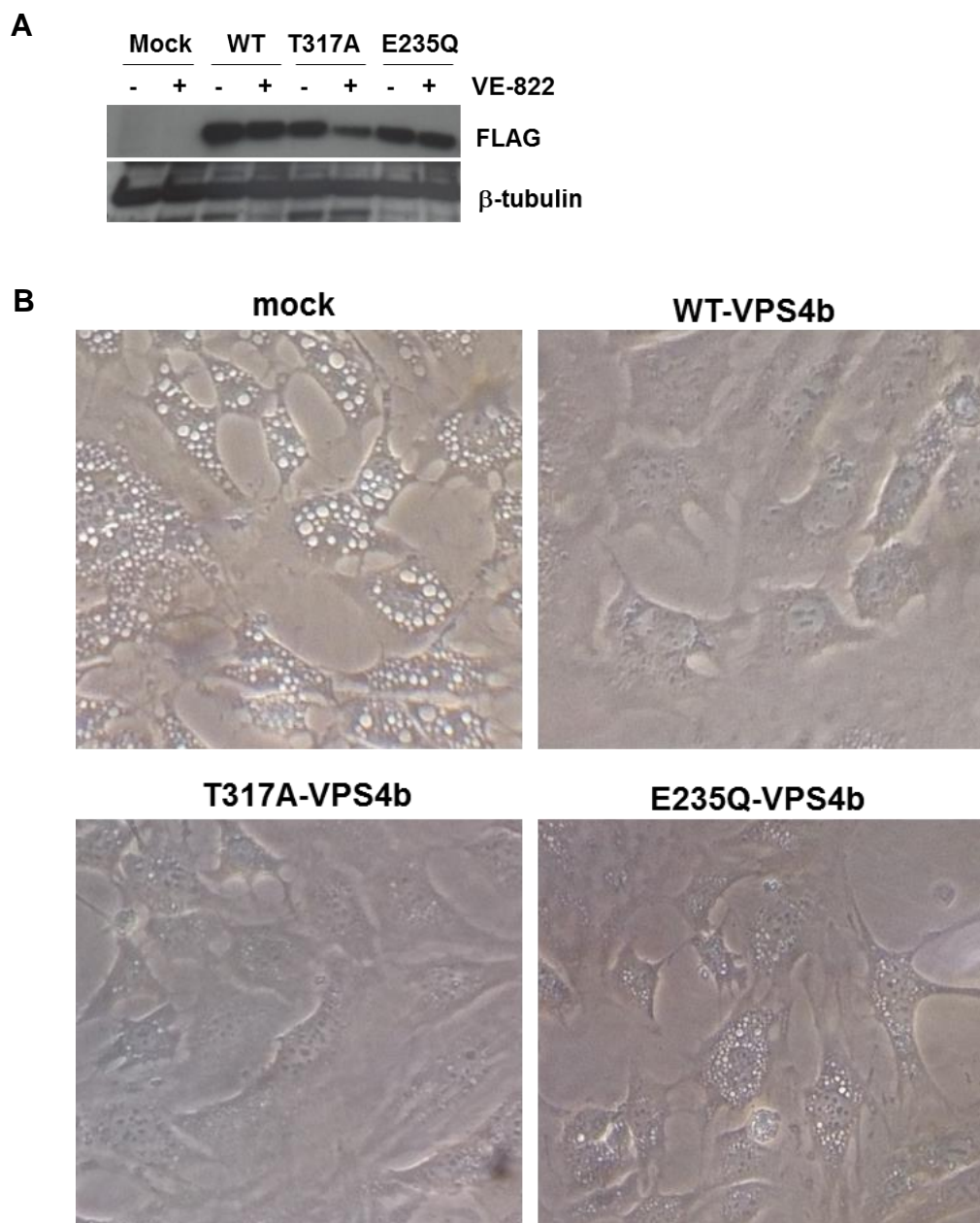


Figure 6.2.4.2. VPS4b overexpression attenuates ATRi-induced vacuolisation. A) Western blotting of 3T3-L1 preadipocytes transiently over-expressing FLAG-tagged VPS4b constructs treated with VE-822 (10 μ M, 2 hrs). β -tubulin used as loading control. **B)** Brightfield microscopy of VE-822-treated preadipocytes over-expressing VPS4b constructs. WT- and T317A-VPS4b rescue the ATRi-induced vacuolisation, whereas E235Q-VPS4b modestly alleviates this phenotype. All images representative of results obtained in at least three independent experiments.

defective mutant E235Q-VPS4b only partially diminishes this phenomenon. This suggests that shifting the dynamics of MVB transport, by saturating the cell with membrane fusion-associated protein VPS4b, has alleviated the potential block in membrane transport generated by ATRi. That both WT and phospho-mutant VPS4b constructs attenuate ATRi-induced vacuolisation suggests this putative ATR phospho-site has limited relevance in this phenotype, and perhaps furthermore, on VPS4b functionality in general.

Syntaxin 6 and VPS4b are also associated with GA-ER transport {Bock, 1997 #1305}{Obita, 2007 #1368}. Considering the limited effects of ATRi on GA-marker RCAS1, I considered that perhaps I was observing ER swelling following ATRi treatment. ER swelling has been documented in literature in response to a variety of agents, although the mechanism behind this phenomenon is poorly characterised. Further, there is wide variety in the nature of the vacuoles induced by ER swelling, which appears dependent on the inducing agent ([Shubin et al., 2016](#)). It appears the process of intracellular membrane organisation can be affected at multiple stages to induce a vacuolisation phenotype.

I used antibodies against ER membrane protein PDI to investigate if ATRi-induced vacuoles were of ER origin using IF microscopy. Fig 6.2.4.3.A shows cycling 3T3-L1 preadipocytes have punctae of PDI staining throughout the cytoplasm. Following 2 hrs VE-822 treatment, PDI is associated with the ATRi-induced vacuoles, evenly coating the membrane (Fig 6.2.4.3.A, lower panel, magnified section). This is highly indicative that ATRi treatment is inducing aberrant ER swelling. To further characterise this phenomenon I utilised antibodies against late autophagosome and endosomal protein RAB7 for IF microscopy. RAB7-positive endosomes are tightly associated with the ER ([Hyttinen et al., 2013](#); [Wang et al., 2011](#)). Fig 6.2.4.3.B (magnified section) demonstrates that following VE-822 treatment, RAB7 punctae have associated with ATRi-induced vacuoles, reinforcing the hypothesis that ATRi treatment is inducing ER swelling.

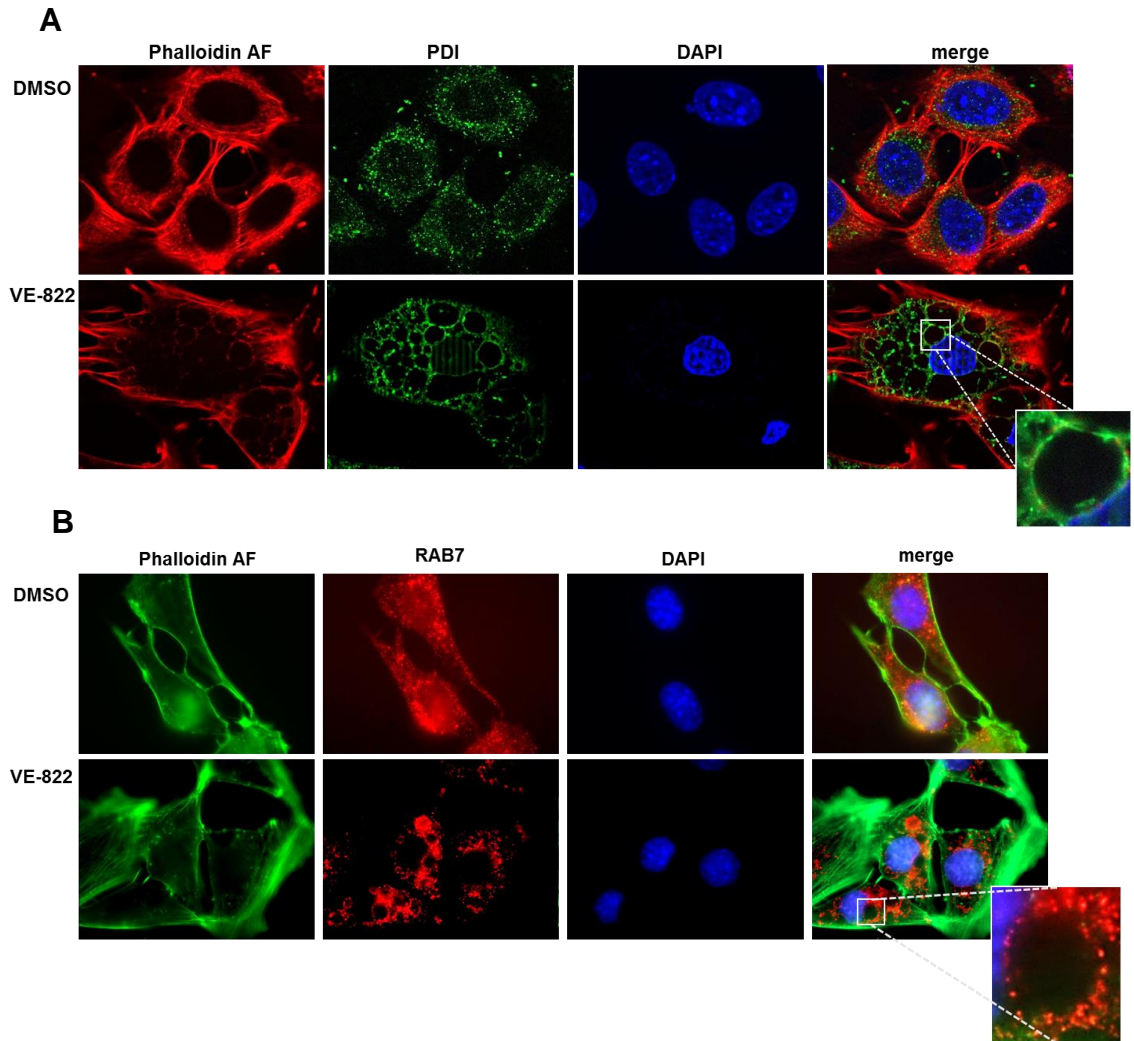


Figure 6.2.4.3. ATRi-induced vacuoles arise from swollen ER. A) IF of ER-marker PDI in cycling 3T3-L1 preadipocytes before and after treatment with VE-822 (10 μ M). Following ATRi treatment for 2 hrs, vacuoles are evenly coated in PDI staining, indicating they are swollen ER. AlexaFluor-conjugated Phalloidin (red), PDI (green) DAPI (blue). **B)** IF of late endosomal marker RAB7 (red) before and after ATRi treatment, where punctae of RAB7 localise to ATRi-induced vacuoles, reminiscent of late endosomes bound to the ER. Phalloidin (green) and DAPI (blue). All images representative of results obtained in at least three independent experiments.

6.2.5. *ATRi-induced vacuolisation is attenuated by Ca^{2+} -free media*

In chapter 4, I characterised the upregulation of the Ca^{2+} -dependent CAMKII-p38 MAPK-ATF2 axis following 24 hrs ATRi treatment. In Chapter 5, I demonstrated that ATRi-induced increased p62 expression was dependent on extracellular Ca^{2+} by utilising Ca^{2+} -free Krebs-Henseleit (KH) medium. To further characterise the ATRi-induced cytoplasmic vacuolisation, I wanted to investigate the effects of depleting extracellular Ca^{2+} . The ER

is a Ca^{2+} -sequestering organelle – perhaps the ER remodelling I have observed following ATRi could be effected by modulating the availability of extracellular Ca^{2+} .

Fig 6.2.5 shows brightfeild microscopy of cycling 3T3-L1 preadipocytes pre-cultured in DMEM or KH medium for 2 hrs, treated with or without ATRis for 15 minutes. These images correspond to the data I discussed in Fig 5.2.5, where samples were harvested after 2 hrs ATRi treatment and KH medium prevented ATRi-induced increases in p62 expression, but not ATRi-induced changes in LC3-I/II status. Culturing cells in KH medium appears to modestly reduce the volume and size of ATRi-induced vacuoles, suggesting this vacuolation process is not dependent entirely on extracellular Ca^{2+} , but can be reduced when the equilibrium of Ca^{2+} is altered.

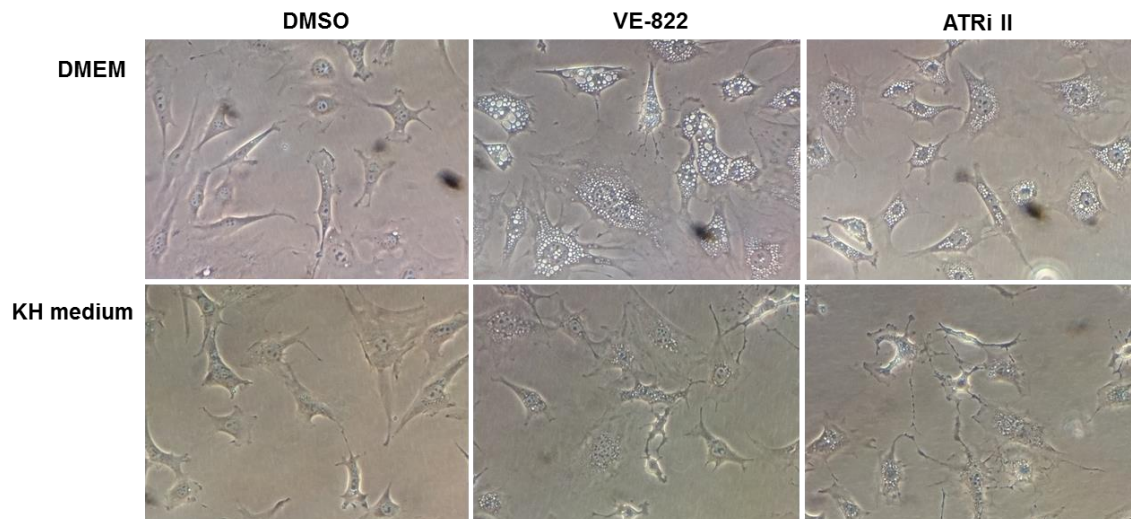


Figure 6.2.5. Treatment with Ca^{2+} -free medium reduces the appearance of ATRi-induced vacuoles. Brightfeild microscopy of cycling 3T3-L1 preadipocytes treated with or without ATRis (VE-822 and ATRi II, both 10 μM) whilst cultured in DMEM (regular) or KH (Ca^{2+} -free) medium. It is worth noting KH medium was exceptionally toxic to both samples treated with and without ATRis.

6.2.6. *ATRi treatment induces ER stress*

Considering such striking remodelling of the ER following ATRi treatment, I wanted to investigate the effects of ATRi on the ER stress response. Fig 6.2.6 shows western blotting of ER stress and UPR markers $\text{eIF}2\alpha$, ATF6 and XBP1s. In Fig 6.2.6.A, cycling 3T3-L1 preadipocytes treated with VE-822 show a small increase in BiP expression, and increased expression of the active, 50 kDa isoform of ATF6, indicating ATRi treatment is inducing increased activation and processing of ER stress protein ATF6. Fig 6.2.6.B shows

eIF2 α phosphorylation (S51) is increased following 4 hrs ATRi treatment, indicative of increased PERK activation.

IRE1 α -dependent splicing of XBP1 mRNA to generate active XBP1s also has roles in mediating specific checkpoints within the cell-cycle ([Thorpe and Schwarze, 2010](#)), so I chose to investigate potential ATRi-induced changes in XBP1s splicing in confluent 3T3-L1 preadipocytes. Using an antibody targeted to specifically the active, cleaved form of XBP1 (XBP1s), Fig 6.2.6.C shows western blotting of XBP1s following 4 hrs treatment with VE-822 or ATMi, where VE-822 treatment appears to drastically reduce XBP1s expression, indicative of IRE1 α inhibition or dysfunction following ATRi. ATMi appears to have no effect on XBP1s expression levels.

Interestingly, XBP1s has well documented roles in adipogenic differentiation – IRE1 α activity and post-transcriptional splicing of XBP1 is required for successful adipogenesis in differentiating 3T3-L1 cultures ([Sha et al., 2009](#)). I hypothesised that the profound defect in XBP1 splicing following ATRi (Fig 6.2.6.C) could perhaps cause the ATRi-induced adipogenic block I characterised in chapter 3. To investigate this, I

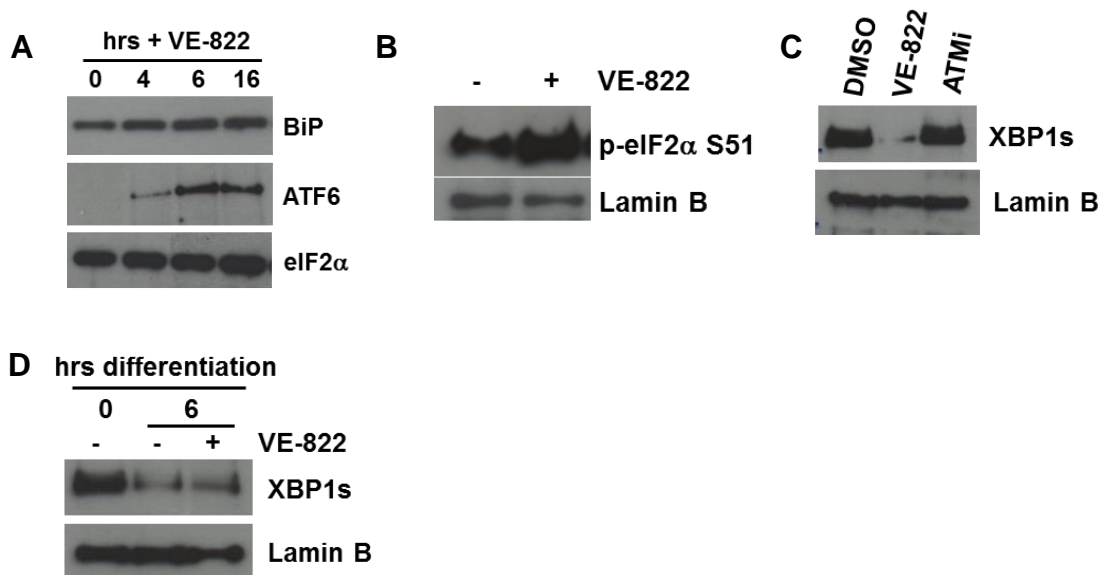


Figure 6.2.6. Acute ATRi treatment affects markers of ER stress. A) Western blotting of BiP and ATF6 in cycling 3T3-L1 preadipocytes treated with VE-822 (10 μ M). After 4 hrs of ATRi treatment, ATF6 expression is increased suggesting increased ER stress and UPR activation. eIF2 α used as loading control. **B)** Western blotting for XBP1s of confluent 3T3-L1 preadipocytes treated with VE-822 or ATMi for 4 hrs (both 10 μ M). ATMi does not affect XBP1s whereas VE-822 drastically decreases protein expression levels. Lamin B used as loading control. **C)** Western blotting of cycling RPE cells treated with VE-822 (10 μ M, 4 hrs). p-eIF2 α S51 is increased following ATRi treatment, indicative of ER stress. All images representative of results obtained in at least three independent experiments.

differentiated post-confluent 3T3-L1 preadipocytes with or without VE-822, and used western blotting to assess XBP1s expression. I chose to harvest differentiating cultures after 6 hours as literature states it is at this time that XBP1s is most required for adipogenesis ([Cho et al., 2014](#)). Fig 6.2.6.D shows that at 6 hours post induction into adipogenic differentiation, XBP1s expression has massively decreased in both untreated and VE-822-treated cultures, where VE-822 does not appear to impact XBP1s expression. This indicates that reduced IRE1 α -dependent splicing of XBP1 to XBP1s is not the cause of the ATRi-induced adipogenic block.

6.2.7. *ATR is localised to the ER*

ER-associated protein Calnexin (CANX) has been identified in several putative ATR/ATM substrate screens, although the physiological relevance of this has never been reported ([Matsuoka et al., 2007](#); [Stokes et al., 2007](#)). Considering the marked remodelling of the ER I have observed following ATRi treatment, and the precedence of ATR interactants at the ER membrane, I hypothesised that ATR could have a potential role in maintaining ER functionality. To investigate this hypothesis, initially I confirmed the existence of abundant cytoplasmic ATR and ATRIP within the 3T3-L1 preadipocyte cell line, through sub-cell fractionation and western blotting approaches (Fig 6.2.7.A).

Having confirmed cytoplasmic ATR and ATRIP, I investigated if cytoplasmic ATR was localised to the ER. To do this, I used western blotting of enriched ER extracts, fractionated from HEK293 cells. I chose not to use 3T3-L1 preadipocytes as the ER fractionation process requires >1 mg of cell pellet per sample to generate an ER-enriched protein lysate adequate for western blotting. 3T3-L1 preadipocytes must be cultured with careful consideration of their passage number, and hence cannot be grown effectively to such large volumes. HEK-293 cells however, can be continuously cultured, allowing the generation of the large cell quantities required for the ER fractionation process.

Fig 6.2.7.B shows western blotting of the ER, 'nuclear' and whole-cell lysates (WCE) generated from the ER fractionation process, where ATR appears within the enriched ER fraction at expression levels equivalent to that observed in the nuclear fraction. Interestingly, ATR localisation to the ER fraction appears unchanged following

VE-822 treatment, indicating that this localisation may be independent of ATR kinase activity. Enrichment of the ER can be gauged via the examination of several markers of cellular compartments; the absence of Lamin B in this lysate indicates there is no contamination with nuclear components; it contains luminal ER protein BiP; also the ER fraction does not appear enriched for cytoplasmic marker β -tubulin, indicating limited contamination with cytoplasmic components. The 'nuclear' fraction here however is relatively impure, as the fractionation process I utilised to enrich for the ER does not allow for equally clean enrichment of the nuclear compartment.

To further investigate the activity of ER-localised ATR, I assessed the localisation of ATRIP to the ER, and also the phospho-status of the activating ATR *trans*-autophosphorylation site T1989. Canonical activation of ATR requires ATRIP and phosphorylation of T1989. Fig 6.2.7.C shows that ATRIP localises to the ER fraction, suggesting that ATR at the ER is capable of kinase activity. Further, assessing p-ATR T1989 status indicates that ATR is activated at the ER. Together, this data is indicative of a novel localisation of kinase-active ATR-ATRIP to the ER.

Interestingly, ATM also localised to the ER fraction (Fig 6.2.7.C). The presence of ATM in my enriched ER fraction could indicate several possibilities which could be delineated with further experiments:

- 1) The ER fraction I am assessing could also contain lysosomes or other membrane-bound compartments; where a role for ATM has been characterised. Using western blotting to probe for lysosomal marker LAMP1, I could investigate if the enriched ER fraction also contains lysosomal matter, or use ATM/ATR IF to confirm ER localisation;
- 2) ATM and ATR localisation could be due the newly synthesised and folded ATM/ATR within the ER, not due to a novel role here. Using protein synthesis inhibitors I could investigate if ER ATR/ATM localisation is maintained whilst protein synthesis is blocked;
- 3) Both ATM and ATR could in fact be localised to the ER. To reinforce this hypothesis it would be necessary to rule out the 2 hypotheses above.

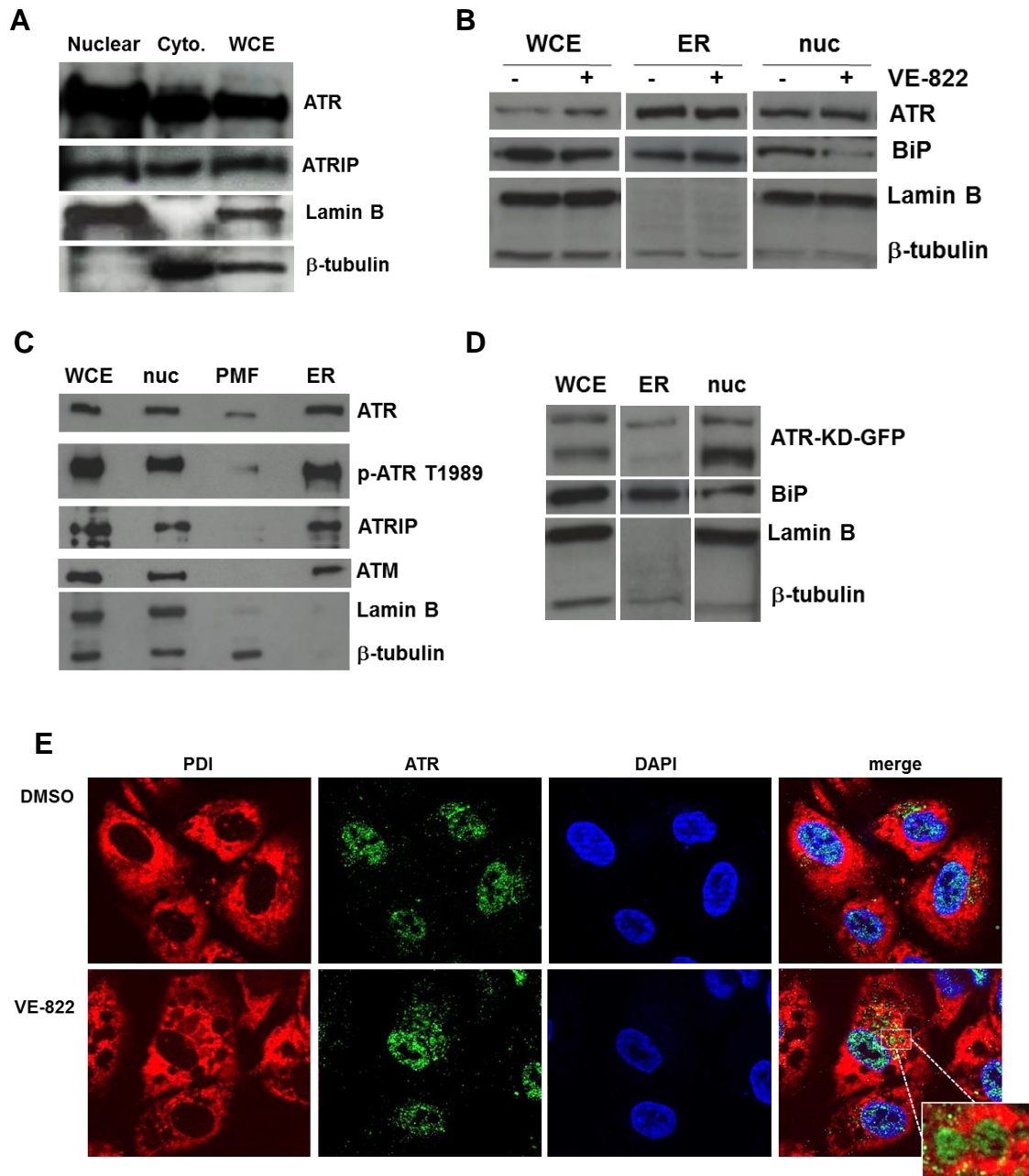


Figure 6.2.7. ATR is active at the ER. **A)** Western blotting of nuclear-cytoplasmic sub-cellular fractionation of cycling 3T3-L1 preadipocytes reveals that ATR and ATRIP are abundant within the cytoplasm. Lamin B used as control for nuclear fraction, β -tubulin used as control for cytoplasmic fraction. **B)** Western blotting of ER fractionation of HEK-293 cells before and after ATRi treatment (VE-822, 10 μ M, 2hrs) reveals cytoplasmic ATR is enriched at the ER, independently of ATRi treatment. BiP used as ER enrichment control, Lamin B as nuclear fraction control, β -tubulin as cytoplasmic fraction control. **C)** Western blotting of ER fractionation of HEK-293 cells for ATR, p-ATR T1989, ATRIP and ATM shows ATRIP is also localised to the ER and ATR appears activated. ATM appears localised to the ER also. Lamin B used as nuclear fraction control, β -tubulin as cytoplasmic control. **D)** Western blotting of ER fractionation of HEK-293 cells overexpressing a GFP-tagged KD-ATR construct. Probing for GFP reveals limited KD-ATR is localised within the ER fraction. **E)** IF of RPE cells before and after ATRi treatment. ER marker PDI (red) and ATR (green) staining demonstrates that following ATRi treatment cytoplasmic ATR appears within the ATRi-induced vacuoles. All images representative of results obtained in at least three independent experiments.

I considered that the ATR and ATM signal I observe in my ER fraction could be newly synthesised protein, undergoing folding as part of canonical ER function. ATR and ATM are large PIKKs (>270 kDa) that require chaperone-mediated folding to reach their correct conformation and tertiary structure ([Hurov et al., 2010](#); [Takai et al., 2007](#)). For this reason, newly synthesised ATR/ATM may appear within the ER for extended periods of time, unlike smaller nuclear protein Lamin B (67 kDa), which does not appear within the ER fraction at all (Fig 6.2.7.C). However, my data indicates this is not the case, as ATRIP is also abundant within my ER-enriched fraction, and like ATR, it appears at expression levels equivalent to those observed within the nuclear compartment. ATRIP is far more similar in size to Lamin B (ATRIP is ~90 kDa), suggesting that like Lamin B, it should either not require ER-mediated folding to reach its correct conformation, or, if newly synthesised ATRIP was within the ER, it would be at expression levels far lower than observed in Fig 6.2.7.C. The presence of ATRIP at the ER is perhaps indicative of a supporting role in the function of ATR at this organelle.

I next investigated if the localisation of ATR at the ER was kinase-activity independent, by overexpressing an eGFP-tagged KD-ATR construct and assessing ER localisation. Fig 6.2.7.D shows western blotting of HEK-293 cells overexpressing eGFP-tagged KD-ATR, where GFP is indicative of KD-ATR expression. Two isoforms of KD-ATR are visible, similar to the double band I observe in western blots of endogenous ATR in 3T3-L1 samples. This indicates that the difference responsible for generating two separate bands of ATR, observed via western blotting, are not dependent on the kinase activity of ATR. Fig 6.2.7.D also shows relatively low levels of GFP appear within the ER fraction, indicating KD-ATR may not be able to effectively localise to the ER. Taken with the limited effect of VE-822 of the ER localisation of endogenous ATR (Fig 6.2.7.B), this suggests that perhaps the *initial* ER localisation of ATR is kinase activity-dependent, but *maintaining* ATR at the ER is kinase-independent.

To further validate that ATR was localised to the ER, I co-stained cycling RPE cells with antibodies directed to ATR and ER-marker PDI. I utilised IF microscopy to assess the co-localisation of ATR and PDI before and after ATRi treatment. Fig 6.2.7.E shows that in untreated RPE cells, ATR does not co-localise with PDI, indicative that cytoplasmic ATR may in fact be more enriched at another organelle, for example the GA. The staining of

cytoplasmic ATR within these cells is far more reminiscent of IF of the GA marker RCAS1 (Fig 6.2.4.1.A). Following ATRi treatment, a fraction of cytoplasmic ATR appears within the ATRi-induced vacuoles.

6.2.8. *ATR kinase-dependently immunoprecipitates with CANX*

To further investigate a novel localisation of ATR at the ER, I chose to interrogate a physiological relationship between ATR and putative ATM/ATR substrate CANX. CANX is an ER-membrane protein that functions to sequester Ca^{2+} within the ER – the majority of CANX protein exists within the ER lumen, with a short tail protruding into the cytoplasm. The cytoplasmic tail of CANX is subject to modification and cleavage by several proteins, allowing CANX to transduce apoptotic signals from the cytoplasm into the ER lumen ([Takizawa et al., 2004](#)). This cytoplasmic tail of CANX contains the S/TQ motifs identified in ATM/ATR substrate screens. I hypothesised that ER-localised ATR could have a role in modulating CANX function via its cytoplasmic C-terminus tail. To investigate this, I transiently overexpressed and immunoprecipitated (IP) a FLAG-tagged CANX construct in HEK-293 cells. Following IP, I used western blotting to investigate the phospho-status of CANX S/TQ motifs before and after ATRi treatment, and further I probed for ATR within the IP extracts to investigate a potential interaction between CANX and ATR.

Fig 6.2.8 shows western blotting of CANX IP and input lysates, where FLAG indicates the expression of FLAG-CANX within total cell lysates and following IP. Anti-p-SQ/TQ antibody indicates that FLAG-CANX is phosphorylated at one or several S/TQ motifs, independently of ATRi treatment (2 hrs), suggesting the phospho-status of CANX S/TQ motifs is independent of ATR activity. Most strikingly, Fig 6.2.8 indicates that ATR can be co-precipitated with CANX, dependent on ATR kinase function. Taken together, this data suggests that there may not be a direct interaction where ATR is phosphorylating CANX, but perhaps ATR may be immunoprecipitating as part of another complex associated with ER membrane that is immunoprecipitated with CANX. This novel co-precipitation further reinforces the likelihood that ATR is localised to the ER, where no role for ATR has been characterised previously.

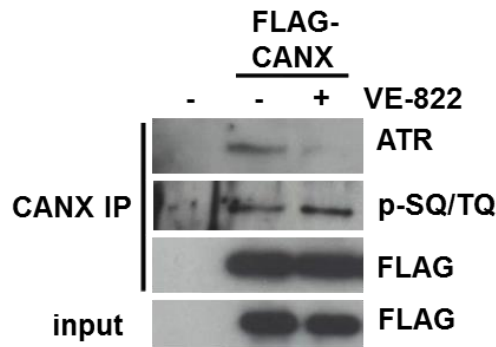


Figure 6.2.8. ATR co-precipitates with CANX. Western blotting of HEK-293 overexpressing FLAG-CANX were immunoprecipitated before and after ATRi treatment (VE-822, 4 hrs, 10 μ M) and elutured with 3X FLAG peptide. CANX IP lysates were probed for ATR, p-SQ/TQ motifs and FLAG. FLAG used as control for transfection efficiency (input) and IP efficiency (CANX IP) and as loading control. p-SQ/TQ status of CANX appears independent of VE-822 treatment, indicating these phospho-sites are ATR-independent. ATR co-precipitates with CANX in a kinase-dependent manner. Representative of results obtained in at least three independent experiments.

6.2.9. ATRi-induced vacuolisation is rescued by Obatoclax

Altering the activities of BCL-2 family members can have multiple effects on cellular homeostasis - pro-survival BCL-2 proteins have recently been investigated as novel cancer therapy targets, due to their frequent dysregulation in cancers ([Adams and Cory, 2007](#); [Schimmer et al., 2008](#)). Upregulation of pro-survival members increases sequestration of pro-apoptotic members, allowing cancerous cells the ability to evade apoptosis ([Adams and Cory, 2007](#)). Obatoclax (GX15-070) is a compound that acts as a BH3-mimetic, inhibiting autophagy and promoting pro-apoptotic pathways through the selective inhibition of pro-survival BH3 proteins such as BCL-2 ([Adams and Cory, 2007](#)). Obatoclax selectively kills cancerous cells dependent on pro-survival BH3 proteins for growth and survival ([Konopleva et al., 2008](#)). Obatoclax is in clinical trials as a novel cancer therapeutic agent, although data suggests the pro-survival pathways associated with cancer progression are more complex than initially considered, where cellular levels of other anti-apoptotic proteins must be accounted for ([Harazono et al., 2014](#)).

Interestingly, altering the BCL-2 family members BAK and BCL-XL has also been shown to induce mass cytoplasmic vacuolisation caused by ER swelling, similar to that observed following ATRis ([Klee and Pimentel-Munos, 2005](#)). Co-overexpression of BCL-XL and BAK resulted in ER swelling, through increased interaction with specifically one BH3 domain within BAK ([Zong et al., 2003](#)). BCL-XL is an antagonist of pro-apoptotic BAK, hence increased interaction with BAK results in pro-survival outcomes. For ER

swelling to occur following the increased BAK-BCL-XL interaction, unbound BID was required to induce a conformational change in ER-localised BAK. This mechanism is summarised in Fig 6.2.9.A. BAX appeared to be irrelevant in the vacuolisation phenotypes uncovered in this study, generating a novel functional divergence between the two pro-apoptotic proteins. Like almost all other published literature investigating cytoplasmic vacuolisation, the mechanism responsible for the generation of vacuoles following BAK-BCL-XL overexpression remained elusive.

I postulated that considering the existing literature characterising BID as a novel ATR interactant, perhaps BID/tBID may be associated with ATR, and ATRi was releasing BID from this association, allowing increased BID-dependent conformational change of BAK, increasing BAK-BCL-XL association, generating ATRi-induced vacuolisation (Fig 6.2.9.A). Overexpression of ATR and specifically ATR-HEAT repeats, which contain BH3-like domains, induces cytoplasmic vacuolisation ([Mori et al., 2013](#)). The literature also indicates that a potential role of ATR in the modulation of BCL-2 family members is possible. Considering the role of BCL-2 proteins in cancer progression, and their localisation to the ER, I wanted to investigate the impact of BCL-2 inhibitor Obatoclax on my ATRi-induced phenotype of mass cytoplasmic vacuolisation. I considered that due to the membrane-bound nature of CANX, ATR may be co-precipitating in a dynamic manner, through association with a different ER membrane-bound complex or BCL-2 family member, via its BH3-like domains. Perhaps ATR could also be interacting with a BCL-2 member at the ER, where ATRi was affecting this interaction generating ER swelling. If BCL-2 family members had a role in the ER swelling observed following ATRi treatment, inhibition of pro-survival BH3 proteins (BCL-2, MCL-1 and BCL-XL) with acute Obatoclax treatment could have an impact on this phenotype (Fig 6.2.9.A).

Fig 6.2.9.B shows microscopy images of cycling 3T3-L1 preadipocytes treated with VE-822 and Obatoclax for 2 hrs. Co-treatment with VE-822 and Obatoclax results in complete rescue of the ATRi-induced vacuolar phenotype. Interestingly, Obatoclax co-treatment also rescued the ATRi-induced increase in p-eIF2 α S51 (Fig 6.2.9.C), suggesting ATRi-induced ER swelling may generate the ER stress I have observed in Fig 6.2.6. This striking result further indicates a relationship between impaired ATR function and the modulation of BCL-2 family members.

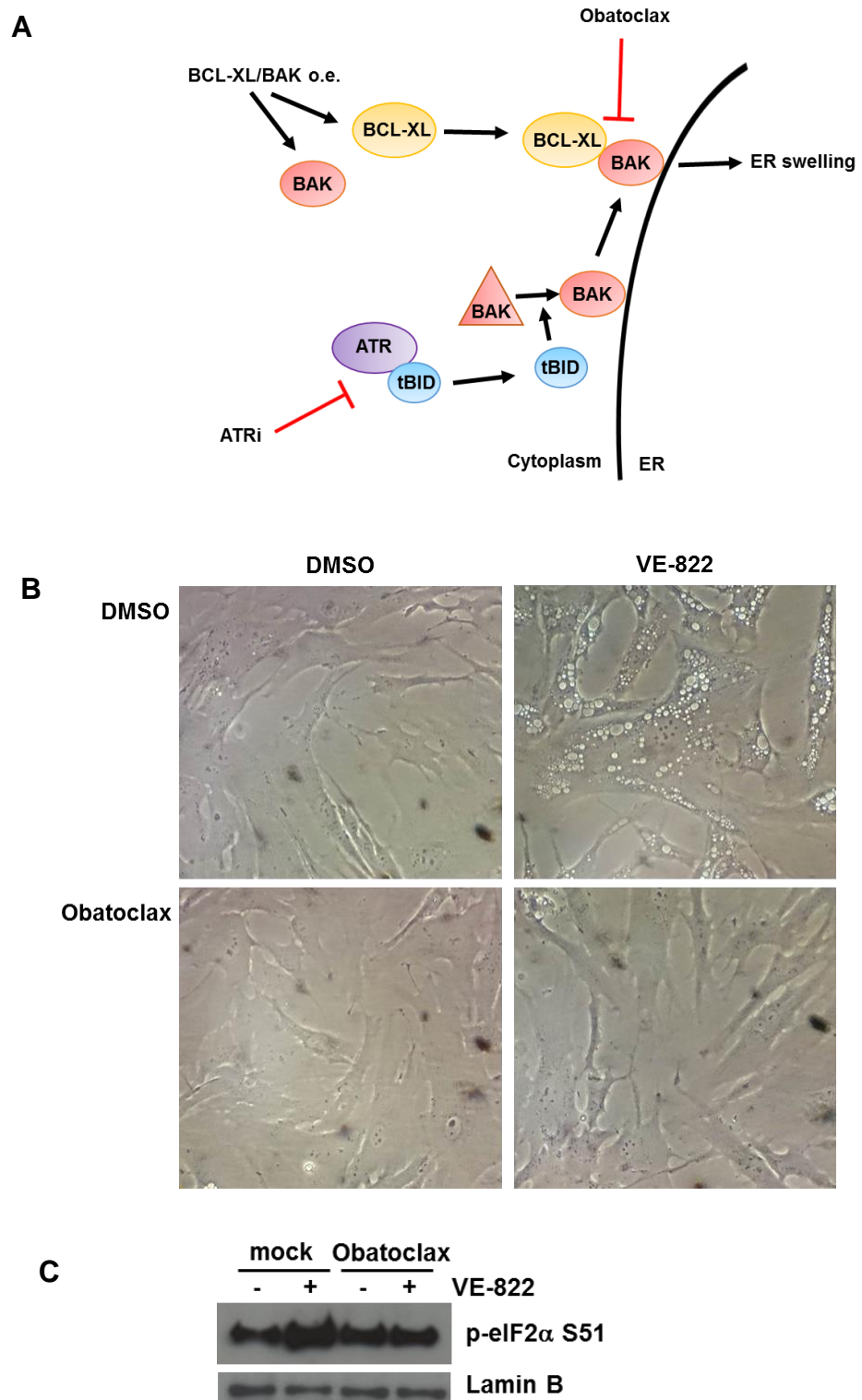


Figure 6.2.9. Obatoclox rescues ATRi-induced vacuolisation. **A)** Schematic of one proposed mechanism in which ATRi induces ER swelling via liberation of tBID from ATR, allowing induction of conformational change in BAK resulting in enhanced ER swelling-inducing BAK-BCL-XL interaction, which could be blocked by Obatoclox treatment. **B)** Microscopy of cycling 3T3-L1 preadipocytes - co-treatment with 10 μ M VE-822 and 50nM Obatoclox (both 2 hrs) prevents ATRi-induced vacuolisation. **C)** Western blotting of ER stress marker p-eIF2 α in cycling RPE cells, treated with ATRi VE-822 (10 μ M) and Obatoclox (50 nM) for 4 hrs. VE-822 treatment increased p-eIF2 α S51, a phenotype rescued by co-treatment with Obatoclox. Images representative of results obtained in at least three independent experiments.

6.3. Summary

I have shown in this chapter:

- Acute ATRi treatments and *Atr* siRNA induce conspicuous cytoplasmic vacuolisation, which appears to derive from swollen ER, where the GA does not appear to have undergone remodelling (sections 6.2.1, 6.2.2 and 6.2.4)
- ATRi treatment induces mitochondrial fission and increased mitochondrial mass (section 6.2.3)
- ATRi-induced vacuolisation can be modestly attenuated by co-culturing ATRi-treated samples in Ca^{2+} -free medium (section 6.2.5)
- At later timepoints (+4 hrs) ATRi treatment invokes the UPR (section 6.2.6)
- ATR is both cytoplasmic and nuclear, and is localised to the ER (section 6.2.7)
- ATRi-induced vacuolisation can be rescued through co-treatment with Obatoclax (section 6.2.9)

I have also investigated two putative ATR substrates associated with ER and cytoplasmic vacuolisation; CANX and VPS4b, where:

- ATR co-precipitates with ER protein CANX, an interaction that can be disrupted with ATRi (section 6.2.8)
- Overexpression of VPS4b ablates ATRi-induced vacuoles independently of its putative ATR-dependent phosphorylation at T317 (section 6.2.4)

6.4. Discussion

In this chapter, I have characterised a conspicuous cytoplasmic remodelling event following ATR inhibition. Using multiple approaches, I have demonstrated a fraction of ATR appears to localise to the ER, and ablating ATR function causes mass ER swelling and ER stress. Mitochondrial phenotypes of increased mito-fission and increased mitochondrial mass are concomitant with these ER phenotypes. In chapter 5, I observed blocked autophagy and enhanced lysosomal biogenesis after acute treatments with ATRi and *Atr* siRNA. Unaltered PGC1 α levels following ATRi suggest that the increased mitochondrial mass may be due to a block in mitophagy. Together, this data is indicative of fundamental changes in the structure and function of several cytoplasmic organelles following ATR deficiency, with detrimental effects on cellular homeostasis.

When considering these results in the context of the usage of ATRi in cancer treatment, there are potential functional significances. Tumours with increased mitochondrial dysfunction often exhibit a more aggressive phenotype ([Simonnet et al., 2002](#)) and it is conceivable that the mitochondrial dysfunction seen following impairment of the ATR signalling axis could assist cancerous cells in their metabolic shift. The defects observed in the mitochondria of ATRi-treated cells are remarkably similar to those observed in the mitochondria of cancer cells ([Simonnet et al., 2002](#)). This mitochondrial phenotype is caused by a metabolic shift to high rates of aerobic glycolysis called the 'Warburg effect' ([Hsu and Sabatini, 2008](#)). It occurs hand-in-hand with the autophagy of local cells, converting the surrounding stroma into a 'factory' for the local production of recycled nutrients ([Hsu and Sabatini, 2008](#)). The cancerous tissue capitalises on high energy nutrients and essential substrates (such as L-Lactate) to support its increase in proliferative activity ([Hsu and Sabatini, 2008](#)). The significance of the ATRi-induced mitochondrial dysfunction warrant further investigation - if ATRi therapy did not destroy all cancerous tissue *in vivo*, it may possibly fuel a more aggressive, secondary cancer. Furthermore, decreased IRE1 α activity and XBP1s splicing (which I observe following acute ATRi treatment) has recently been identified as a driver in the development of multiple myeloma ([Bujisic et al., 2017](#)).

ER stress and induction of the UPR were observed following acute ATRi treatment, although these phenotypes did not occur alongside the cytoplasmic vacuolisation. Instead, the UPR was induced after several hours of ATRi treatment. Both increased PERK-dependent phosphorylation of eIF2 α at S51 (a marker of UPR induction) and ER swelling following ATRi treatment were prevented by co-treatment with Obatoclax, indicating a relationship between ER stress/UPR induction and ER swelling following ATRi treatment, and a role for pro-survival BCL-2 family members in these ATRi-induced ER phenotypes.

I would like to present a putative hypothesis that unifies my findings regarding reduced ATR activity and ER functionality. One mechanism to induce the UPR is through dysfunction of the ERAD system. If ERAD function is compromised, the burden of unfolded proteins within the ER increases, and after some time this results in the induction of the UPR as ER stress increases ([Osłowski and Urano, 2011](#)). An ATRi-induced deficit in the ERAD pathway would explain the instant ER swelling and slightly delayed UPR induction (>4 hrs ATRi).

It is here that I would like to re-introduce the ATR substrate, DNA damage response protein and ERAD complex subunit VCP/p97. Disease-causing mutations in p97 cause inclusion body myopathy (IBM) – associated with muscle atrophy, dementia and amyotrophic lateral sclerosis ([Ching et al., 2013](#)). Ching *et al.* (2013) investigated the pathomechanistic and molecular basis of these disease-causing VCP/p97 mutations *in vitro*, revealing strikingly similar phenotypes to those that I have discovered following ATRi or *Atr* siRNA treatments of 3T3-L1 cells. Mutations in VCP/p97 induced ER swelling, UPR induction, as well as autophagic phenotypes of increased p62 and LC3-II, and reduced mTORC1 activity ([Ching et al., 2013](#)). Defects in VCP/p97 function prevent effective ERAD, resulting in UPR induction ([Wójcik et al., 2006](#)). It has been postulated that defects in VCP/p97-dependent ERAD induce ER swelling due to the build-up of aggregated and unfolded proteins within the ER lumen that cannot be effectively removed for proteasomal degradation ([Mimnaugh et al., 2006](#)).

I postulate that ATRi and *Atr* siRNA may induce cytoplasmic vacuolisation/ER swelling due to the lack of ATR-dependent phosphorylation of VCP/p97, resulting in

reduced VCP/p97 activity, reducing ERAD functionality generating ER swelling and eventual induction of the UPR. Alternatively, through an unknown mechanism, depleting ATR activity could be increasing the proteotoxic burden on ERAD. VCP/p97 has also been characterised as a substrate of AKT; I observe striking a reduction in AKT activation following acute ATRi treatments which could provide an alternative route to reduce VCP functionality ([Klein et al., 2005](#); [Vandermoere et al., 2006](#)). Furthermore, functional VCP/p97 has also been characterised as a requisite of effective mTOR activation ([Ching et al., 2013](#)) – I also observe defects in mTORC1 activity after treatment with ATRis and *Atr* siRNA.

Mimnaugh *et al.* (2006) discovered that co-treatment with proteotoxic-stress inducing drugs that increased the requirement for ERAD induced an ER swelling/vacuolisation phenotype, which could be attenuated with VCP/p97 overexpression ([Mimnaugh et al., 2006](#)). This information is relevant when considering a paper investigating the structural similarities between VPS4b and VCP/p97 ([Scott et al., 2005](#)). Scott *et al.* revealed the crystal structure of VPS4b, in which the VPS4b AAA ATPase cassette closely resembled the analogous domains in VCP/p97 (Fig 6.4.1).

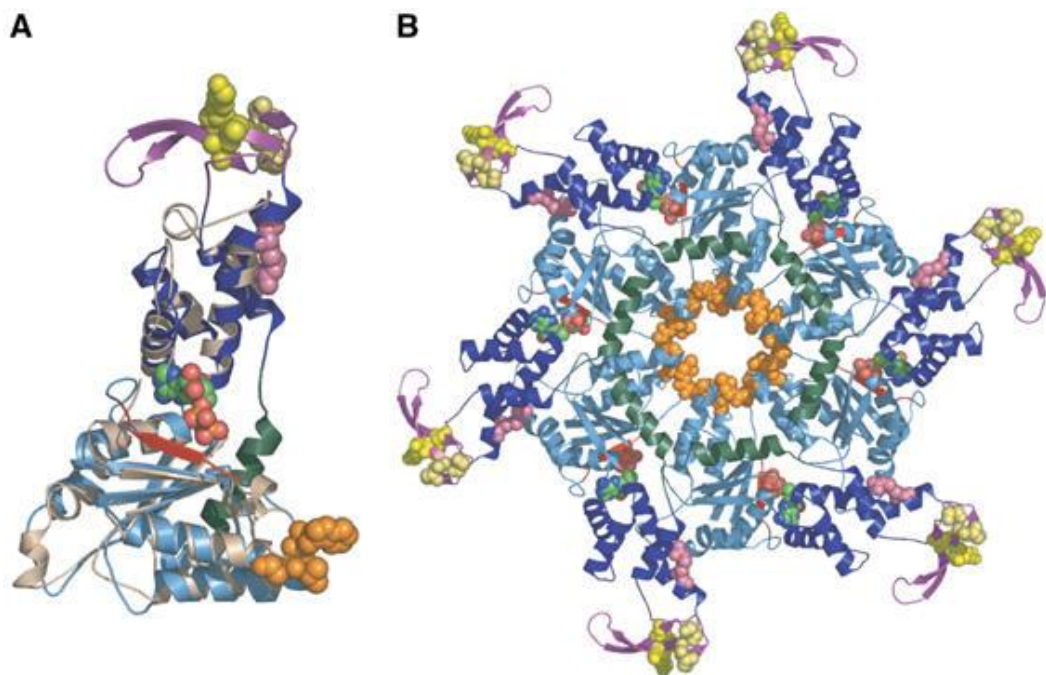


Figure 6.4.1. Structural similarities between VPS4b and p97/VCP. **A)** Overlay of VPS4b (rainbow) and p97 (beige) AAA ATPase cassettes reveals near-identical structural homology. **B)** Structure of VPS4b 123-444 ring oligomer. Taken from ([Scott et al., 2005](#))

In section 6.2.4, I reported that overexpression of WT- and phospho-mutant-VPS4b prevented ATRi-induced cytoplasmic vacuolisation in 3T3-L1 preadipocytes. I investigated VPS4b as putative ATR substrate ([Matsuoka et al., 2007](#)), concluding that the putative ATR phospho-residue on VPS4b (T317) had no functional significance in the defects I observed following ATRi. Considering the striking structural homology of VPS4b and VCP/p97 and their similar roles in the removal of protein complexes from membranes, I postulate that VPS4b overexpression might alleviate the ATRi-induced proteotoxic stress by facilitating ERAD in the absence of optimally functional VCP/p97.

How Obatoclax could prevent ATRi-induced defects in ERAD and ER swelling remains unclear. However, relationships between the BCL-2 family and ERAD pathways do exist; for example, expression of constitutively active pro-apoptotic effector BOK (BCL-2 ovarian killer) is maintained at low levels by the ERAD system; when ERAD is compromised, BOK expression increases resulting in induction of apoptosis ([Llambi et al., 2016](#)). However, BOK has been characterised as insensitive to the antagonistic effects of canonical pro-survival BCL-2 family members, suggesting Obatoclax treatment would not affect BOK activity ([Llambi et al., 2016](#)). The significance of this relationship between one BCL-2 family member and the ERAD pathway remains unclear. These putative mechanisms are summarised in Fig 6.4.2.

Furthermore, BCL-2 family member Beclin-1 has a role in early autophagy in the formation and enlongation of autophagosomes, and is inhibited by pro-apoptosis members of the BCL-2 family (discussed in section 5.1.3). As the ATRi-induced autophagic block appears at the later stages of autophagy, it is possible that alterations in Beclin-1 activity were not responsible for this effect.

As discussed in section 6.2.9 and 1.9.2, ATR can interact with BID/tBID in context dependent manners through phosphorylation or via ATRs 'BH3-like' domains. Free tBID is required to induce ER swelling that is generated by co-over-expression of BAK and BCL-XL ([Klee and Pimentel-Muñoz, 2005](#)). Another hypothesis that could explain ATRi-induced vacuolisation, is that tBID may be bound to ATR, and ATRi is liberating tBID from this interaction, allowing increased tBID-mediated conformational change of BAK, required for BCL-XL binding to induce vacuolisation. Although the mechanism behind the ATRi-induced vacuolisation is unclear, what can be ascertained is that ATRi appears

to alter the equilibrium of the BCL-2 family members, where co-treatment with a BH3 mimetic restores some level of ER functionality following ATRi treatment. At face value this appears contradictory, as ATRi treatment should liberate constitutively active, pro-apoptosis multi-region protein tBID, and Obatoclox is a pro-apoptotic, BH3-only mimetic. These putative mechanisms are also summarised in Fig 6.4.2.

A further way to dissect the mechanism of ATRi-induced cytoplasmic vacuolisation is to consider the roles of BCL-2 family members in the regulation of ER Ca^{2+} stores. Ca^{2+} -free KH medium attenuated the ATRi-induced cytoplasmic vacuolisation phenotype. The complex relationship between $[\text{Ca}^{2+}]_{\text{ER}}$ and apoptosis, and how this is modulated by multiple BCL-2 family members has been subject to extensive research, where it appears that normal $[\text{Ca}^{2+}]_{\text{ER}}$ is required for the initiation of apoptosis at the mitochondria by BAX/BAK. Additionally, pro-survival BCL-2 can function to limit $[\text{Ca}^{2+}]_{\text{ER}}$ by increasing the 'leakiness' of the ER membrane and through inhibition of IP_3Rs , to reduce the availability of Ca^{2+} required to initiate apoptosis ([Monaco et al., 2012](#);

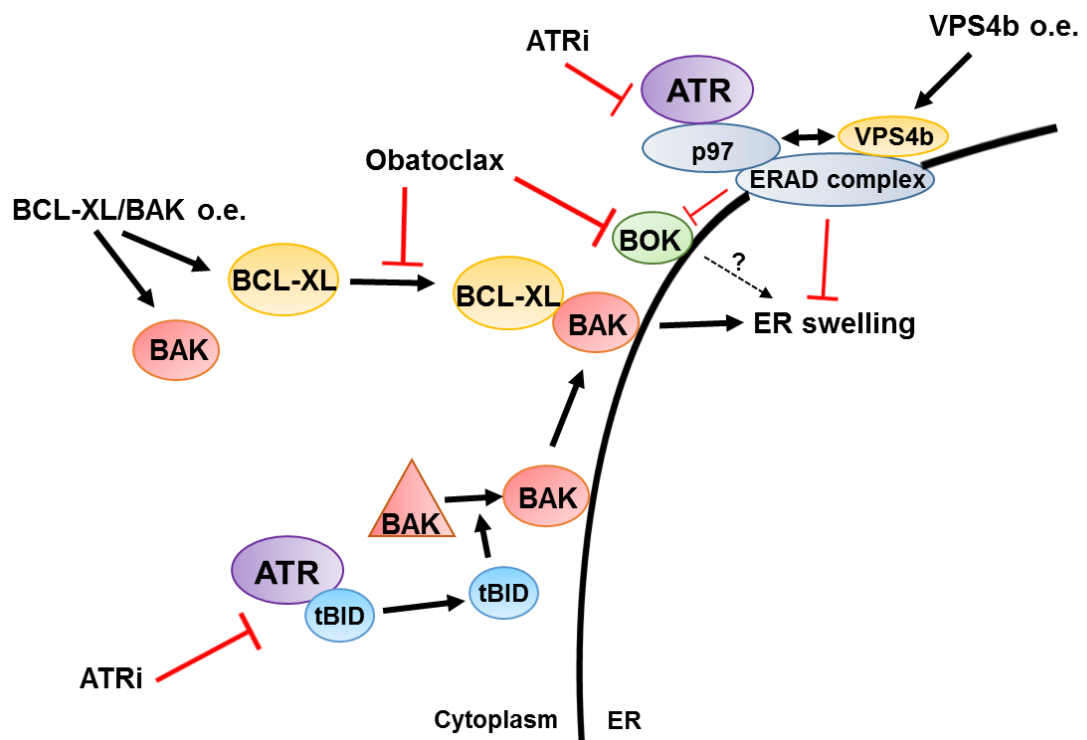


Figure 6.4.2. Schematic of putative mechanisms of ATRi-induced ER swelling. ATRi could block putative interaction with VCP/p97, compromising ERAD function, which could be rescued by overexpression of structurally homologous VPS4b. ATRi could also be liberating tBID from an ATR-tBID interaction, increasing tBID-mediated conformational changes in BAK, resulting in enhance BCL-XL-BAK interactions inducing ER swelling, similar to co-over-expression of BAK and BCL-XL. Obatoclox rescues ATRi induced ER swelling by blocking interaction between BAK and BCL-XL.

[Pinton et al., 2000](#)). Small molecule inhibitors of BCL-2 and BCL-XL have also been shown to deplete $[Ca^{2+}]_{ER}$, suggesting multifaceted roles of pro-survival BCL-2 members in $[Ca^{2+}]_{ER}$ modulation ([Gerasimenko et al., 2010](#)). Furthermore, BCL-2 has also been implicated in the regulation of cellular Ca^{2+} extrusion, where knockout of BCL-2 enhanced Ca^{2+} extrusion after a period of enhanced Ca^{2+} entry ([Ferdek et al., 2012](#)). This suggests that following inhibition of BCL-2 activity with Obatoclax, intracellular Ca^{2+} may be depleted, in a similar manner to treating cells with Ca^{2+} -free medium, linking these two treatments that attenuate ATRi-induced ER swelling.

Further understanding of the mechanism/s underlying the ATRi- and *Atr* siRNA-induced ER swelling and ER stress could have therapeutic benefits and facilitate the discovery of novel synthetic lethality approaches in the use of ATRis in cancer therapy. Existing, approved medical compounds could be utilised alongside ATRi treatments to enhance or protect against these novel ER stress- or autophagy- associated defects, selectively sensitising cancerous cells whilst reducing the therapy burden of ATRi treatment. For example, Geldanamycin interrupts HSP90 chaperone activity, increasing cell dependency on VCP/p97-mediated ERAD to clear mis-folded HSP90 clients. Geldanamycin analogues (17-DMAG) and other HSP90 inhibitors are being extensively researched as novel anti-cancer therapies. As well as investigating clinically relevant autophagy inhibitors such as hydroxychloroquine, or proteasome inhibitors such as Bortezomib, investigating the effect of ATRis and HSP90is represents a logical step in looking for novel ATRi-based synthetic lethality centred on ATRi-induced proteotoxic stress. Conversely, combination therapies must also be considered for the potentially detrimental effects on the patient – for example, although Obatoclax selectively kills cells dependent on pro-survival BCL-2 proteins, it also appears to have a cytoprotective effect on cells treated with ATRis, reducing ER swelling and ER stress.

Chapter Seven

Discussion

7.1 Summary

In this thesis, I aimed to characterise novel impacts of small molecule kinase inhibitors of ATR (ATRi) on the adipogenic differentiation of preadipocytes, as well as the impact of chronic ATRi treatment on mature, post-mitotic white adipocytes. My intended aim was to characterise a pathomechanistic link between reduced ATR function and the lipodystrophy commonly observed in mouse models of ATR deficiency and ATR-Seckel Syndrome patients. These findings potentially have significant relevance, due to the postulated use of ATRi as a novel cancer therapy, and the lipodystrophy known as cachexia observed frequently in cancers. Here I will briefly summarise my findings, before my final discussion.

7.1.1 Chapter Three

In this chapter, I investigated the effects of kinase inhibition of ATR on 3T3-L1 adipogenic differentiation. ATRi treatments throughout adipogenesis resulted in a failure to successfully differentiate, due impaired induction and expression of the master adipogenic regulator peroxisome proliferator-activated receptor γ 2 (PPAR γ 2). By assessing the S-phase kinetics of differentiating cultures treated with ATRi, I demonstrated that ATRi treatment did not impair the mitotic clonal expansion (MCE) step of adipogenic differentiation as initially hypothesised. Failure to successfully undergo adipogenesis following ATRi was concomitant with reduced mammalian target of rapamycin complex 1 (mTORC1) activity. mTORC1 is known to have dual roles in adipogenesis, where its activity either facilitates or inhibits adipogenesis, dependent on thresholds of mTORC1 activation ([Yoon et al., 2013](#); [Zhang et al., 2009](#)). Furthermore, mTORC2-dependent phosphorylation of Protein Kinase B (AKT) was decreased following ATRi, indicating that both mTORC1 and mTORC2 activity was compromised. Interestingly, transient transfection of *Atr* siRNA induced adipogenesis in post-confluent 3T3-L1 preadipocytes. Reduced ATR functionality negatively impacted on mTORC1 activity, leading me to postulate that the reduced or enhanced adipogenesis observed after ATRi and *Atr* siRNA was due to the threshold-dependent effect of reduced mTORC1 activity on adipogenesis.

7.1.2 Chapter Four

In this chapter, I investigated the effects of chronic ATRi treatment on mature, post-mitotic 3T3-L1 adipocytes. I observed profoundly decreased cellular triglyceride (TG) content, concomitant with loss of PERILIPIN A expression and markers of lipolysis and free fatty acid release (FFA). Collectively, this data is indicative of a profound loss of lipid droplet integrity. At the same time, I observed markers of white adipocyte 'browning' (UCP1, PGC1 α) and increased mitochondrial mass, indicating ATRi treatment is inducing a drastic metabolic reprogramming of white adipocytes towards energy catabolism. These results were not due to ATRi-induced enhanced replication stress, or cell cycle re-entry. The shift in lipid metabolism of mature white adipocytes following ATRi is reminiscent of that observed in cancer cachexia.

7.1.3 Chapter Five

I investigated the effects of acute ATRi treatment on the autophagy axis of 3T3-L1 preadipocytes. Acute ATRi, *Atr* siRNA and overexpression of a kinase dead (KD)-ATR construct induced a block in autophagosomal maturation, and an autophagy independent increase in sequestosome-1 (p62) expression. This result was not observed following Checkpoint kinase 1 inhibition, indicating the effects of ATRi here were not due to inhibition of the ATR-CHK1 signalling axis. Following ATRi, I also observed an increase in nuclear translocation of lysosomal biogenesis regulator transcription factor EB (TFEB). TFEB is sequestered in the cytoplasm by mTORC1-dependent phosphorylation. Following reduced mTORC1 activity, TFEB undergoes nuclear translocation to activate the lysosomal CLEAR response. This adds further functional significance to the ATRi-induced defects in mTORC1 signalling I observed in chapter three. Quite surprisingly, the impact of VE-821 treatment on p62 expression has recently been documented within the literature ([Muralidharan et al., 2017](#)).

7.1.4 Chapter Six

Here I characterised a novel conspicuous vacuolisation event in multiple cell lines, induced with several structurally dissimilar ATRis, as well as following *Atr* siRNA. Through extensive analysis, I found that ATRi-induced vacuoles were derived from the endoplasmic reticulum (ER). I characterised the ATRi-induced cytoplasmic vacuolisation

phenotype further by preventing it, utilising BH3 mimetic Obatoclax, and also with transient overexpression of vacuolar protein sorting-associated protein 4b (VPS4b). Utilising ER fractionation, immunofluorescence and over-expression of tagged ATR constructs, I characterised a novel localisation of ATR-interacting protein (ATRIP)-ATR to the ER. I also observed ER stress, and increased mitochondrial mass in 3T3-L1 preadipocytes following acute ATRi treatments, the latter being indicative of blocked mitophagy.

7.2 Discussion

Further mechanistic insight into the ATRi-induced adipogenic block can be gained through the cross-examination of results within each chapter, which I will discuss here.

7.2.1 *ER stress and adipogenesis*

ER stress activation through the protein kinase RNA-like endoplasmic reticulum kinase-eukaryotic initiation factor 2 α (PERK-eIF2 α) arm of the unfolded protein response (UPR) is also recognised as an inhibitor of adipogenesis - eIF2 α -dependent increased translation of activating transcription factor 4 (ATF4) results in increased transcription of adipogenesis-inhibitor CCAAT-enhancer-binding protein (C/EBP)-homologous protein (CHOP) ([Batchvarova et al., 1995](#)). On the other hand, X-box binding protein-1s (XBP1s), induced by the inositol-requiring enzyme 1 α (IRE1 α) arm of the UPR, is required for successful adipogenesis, due to its role in the upregulation of C/EBP family members ([Sha et al., 2009](#)).

In chapter six, I characterised activation of the UPR (increased p-eIF2 α S51 and ATF6), and decreased XBP1s following ATRi in 3T3-L1 preadipocytes. Considering the relationship between ER stress and adipogenesis, it was interesting to discover the UPR was not similarly induced following ATRi throughout 3T3-L1 adipogenesis – XBP1s expression remained equivalent in ATRi- and untreated cultures throughout (section 6.2.6). I discovered that following ATRi treatment, eIF2 α activity is also reduced throughout adipogenesis (section 3.2.4). Due to this, the relevance of the ER in the ATRi-induced adipogenic block remains unclear.

7.2.2 ER stress, autophagy and lipid metabolism

ER stress is also an established inducer of lipolysis in adipocytes ([Bogdanovic et al., 2015](#); [Deng et al., 2012](#)), where the activation of ER stress pathways underlies the pathogenesis several of metabolic syndromes ([Zha and Zhou, 2012](#)). However, it appears maintaining a balanced ER stress response is also necessary, as complete ablation of *Atf4* enhances lipogenesis and thermogenesis, resulting in lean mice ([Wang et al., 2010](#)). Investigating markers of the UPR in adipocytes could provide mechanistic insight into the metabolic phenotypes observed following chronic ATRi treatment.

In chapter five I showed that following acute ATRi treatment, lysosomal biogenesis regulator TFEB had translocated to the nucleus, indicative of increased activity and enhanced lysosomal biogenesis (section 5.2.4). In chapter four, I characterised a striking decrease in PERILIPIN A expression, and enhanced TG release and lipolysis in mature adipocytes following ATRi treatments (section 4.2.2). Interestingly, several studies have reported similar striking and rapid reduction of adipocyte PERILIPIN A expression, concomitant with enhanced lipolysis and FFA release following the enhancement of lysosome-assisted degradation pathways ([Choi et al., 2016](#); [Kaushik and Cuervo, 2015](#); [Kovsan et al., 2007](#)). The groups reported that PERILIPIN A appeared to be selectively degraded through autophagic rather than proteasomal degradation - lysosomal protease inhibitors such as leupeptin prevented PERILIPIN A degradation and attenuated the concomitant increase in lipolysis. Investigating TFEB activity or lysosomal markers in 3T3-L1 adipocytes could provide insight into why PERILIPIN A expression decreases so rapidly following ATRi. Furthermore, hydroxychloroquine (HC) is a lysosomal protease inhibitor currently in clinical trials as a novel chemotherapeutic agent. Investigating the impact of this clinically relevant lysosomal inhibitor on the ATRi-induced adipocyte phenotypes of PERILIPIN A loss and increased lipolysis could prove beneficial. Combination therapies with ATRi and HC could potentially target cancer cells exhibiting enhanced dependency on autophagic processing, through inducing an autophagic blockage at multiple nodes, whilst potentially carrying cytoprotective effects for host adipocyte metabolism, through the conservation of PERILIPIN A expression through ATRi therapy.

7.2.3 Lysosomal transport, mTOR signalling and autophagy

3T3-L1 preadipocytes failed to successfully differentiate into mature adipocytes when treated with ATRis, perhaps due to reduced activity of the mTORC1-signalling axis, required for adipogenesis. However, it was unclear how reduced ATR function had such a striking effect on the mTORC1 signalling pathway. Multiple members of the AKT-mTOR signalling axis have recently been identified as putative ATR/ATM substrates following DNA damage, including Tuberous Sclerosis Complex 1 (TSC1-S1102), Protein Kinase B (AKT3-S123) and Insulin Receptor substrate 2 (IRS2-S336) (Fig 7.2.3.1). In 3T3-L1 preadipocytes, following ATRi treatment I observed defects in both mTORC1 and mTORC2 activation, as assessed by AKT (mTORC2) and S6 (mTORC1) phosphorylation. The complex feedback mechanisms in place within mTOR-associated pathways, and the impact of ATRi on both mTORC1/2 signalling axes, renders the functional significance of these putative ATR/ATM-dependent phosphorylations difficult to predict. Furthermore,

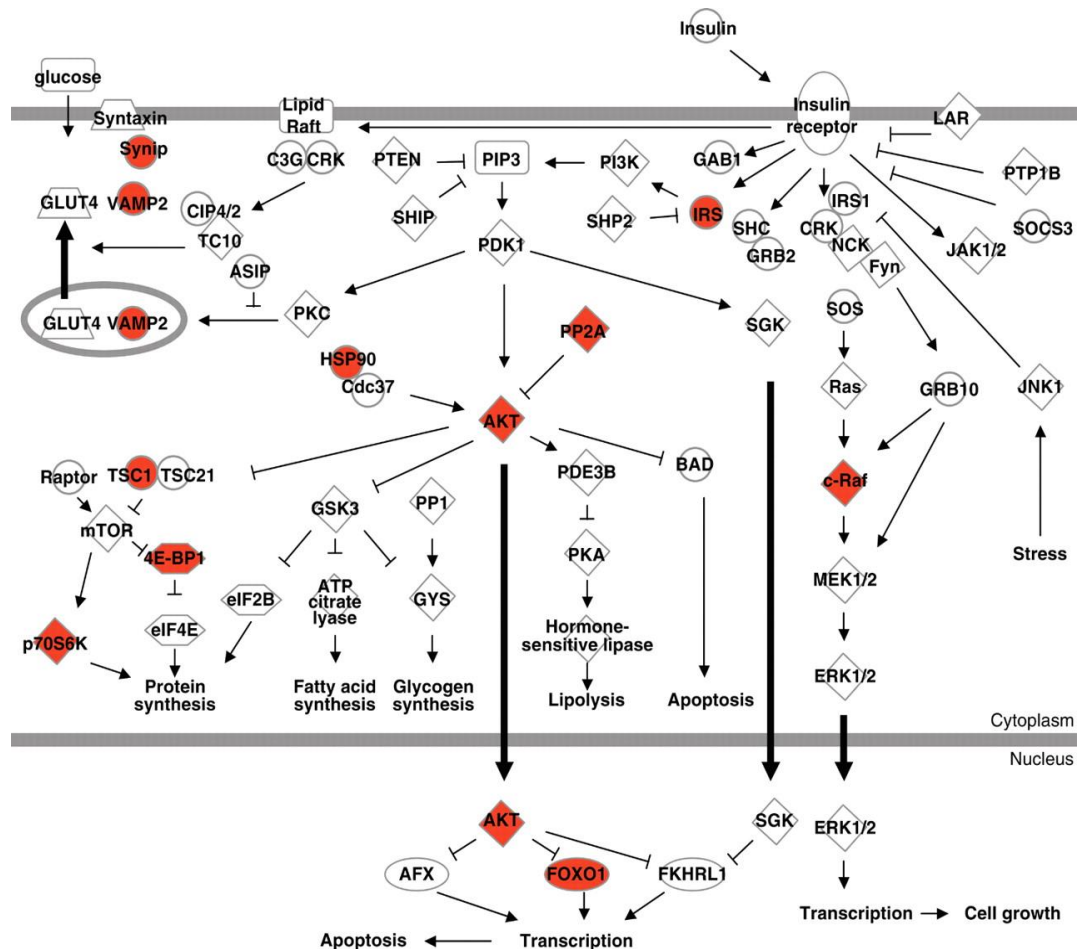


Figure 7.2.3.1. Network of putative ATR/ATM substrates involved in cell metabolism. Red colour denotes putative ATR/ATM substrates. Taken from ([Matsuoka et al., 2007](#))

their functional relevance in the ATRi-induced phenotypes of blocked autophagy and ER stress is uncertain.

Considering the volume of putative ATR/ATM substrates that have been identified within proteomic screens, it is highly likely that ATR has multiple uncharacterised targets within the cytoplasm. Reduced ATR activity may in fact impinge on several aspects of cellular function - where the phenotypes I observe following ATRi and *Atr* siRNA could be the net result of compromising multiple signalling pathways. With this in mind, I suggest a putative mechanism to coalesce several of my findings.

A requirement for mTORC1 activity is its localisation to the lysosome. For full activation of mTORC1, p62 must interact with mTORC1 at the lysosome ([Duran et al., 2011](#)). The reduced mTORC1 activity and increased p62 expression following ATRi indicates that p62 may not be effectively inducing mTORC1 activation. Additionally, mTORC1 activity is partially dependent on the dynein-driven localisation of lysosomes to the nuclear periphery – when dynein is depleted or inhibited, mTORC1 does not effectively phosphorylate S6K ([Clippinger and Alwine, 2012](#)). Maintaining the correct cellular location of organelles is an active process, requiring stable function and kinetics of both dynein and kinesin motors. Dynein function is also required to facilitate efficient and appropriate autophagy, through its control over lysosome and autophagosome localisation ([Kimura et al., 2008](#)). Disrupting dynein function results in a failure to undergo autophagosome-lysosome fusion, resulting in a block in autophagy. Following ATRi, I observed a block in autophagy at the stages of lysosomal fusion/autophagosome maturation (chapter 5), and a failure to undergo successful adipogenesis, which could be dependent on compromised mTORC1 activity (chapter 3). Compromising dynein activity can also result in these phenotypes, due to its essential role in the minus-end transport of lysosomes to the nuclear periphery.

An interaction between dynein and ATR has already been characterised within the literature (Fig 7.2.3.2), and dynein subunits have been identified previously as putative ATR/ATM substrates including DYNC1I2 T95 ([Matsuoka et al., 2007](#); [Poruchynsky et al., 2015](#)). Interestingly, p62 has recently been reported to directly interact with DYNC1I2 ([Calderilla-Barbosa et al., 2014](#)). Dynein intermediate chain subunits are essential to dynein function, playing a key role in assembly, cargo recognition and interactions with

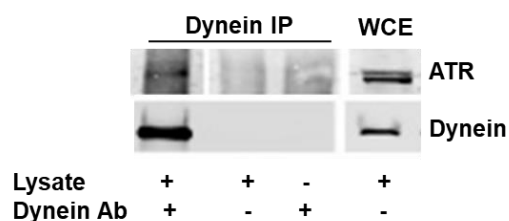


Figure 7.2.3.2 ATR coprecipitates with dynein. Modified from ([Poruchynsky et al., 2015](#))

regulatory proteins including the dynactin complex. DYNC1I2 also contributes to dynein complex localisation to the kinetochore ([Raaijmakers et al., 2013](#)), and moreover, dynein has been implicated in silencing the spindle assembly checkpoint, where a role for ATR is established ([Howell et al., 2001](#); [Kim and Burke, 2008](#); [Lawrence et al., 2015](#)).

I hypothesised that perhaps the ATRi-induced phenotypes of blocked autophagy and reduced mTORC1 activity could be linked through compromised dynein function, preventing the appropriate cellular localisation of lysosomes. Fig 7.2.3.3 shows immunofluorescence (IF) microscopy of asynchronous RPE cells stained for mTOR, before and after ATRi treatments. To characterise the loss of dynein-dependent mTOR localisation to the nuclear periphery, I utilised dynein inhibitor Ciliobrevin as a positive control. In untreated cells, mTOR appears mostly localised to the nuclear periphery. Following Ciliobrevin treatment, mTOR has lost its perinuclear localisation. Following

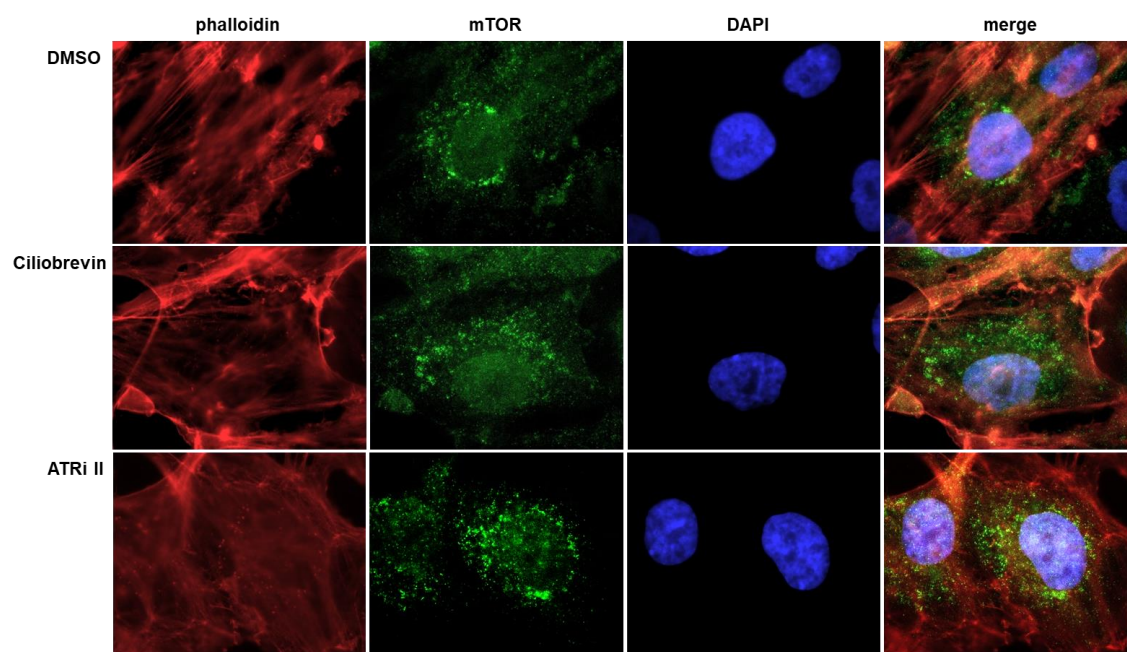


Figure 7.2.3.3. mTOR localisation is affected by ATRi. Cycling RPE cells were treated with Ciliobrevin (20 μ M, 2 hrs) or ATRi II (10 μ M, 1 hr) before analysis. mTOR is generally localised to the nuclear periphery in untreated cells. Following Ciliobrevin, this localisation is lost. Following ATRi treatment, mTOR localisation to the perinuclear region appears decreased. Images taken at 100x.

ATRi treatment, mTOR localisation at the nuclear periphery is less apparent than in untreated cells. Although this does not provide concrete evidence that ATRi-induced reduced mTOR activity is due to mislocalisation of mTOR, it justifies further investigation.

Whilst investigating the impact of ATRi treatments on post-mitotic 3T3-L1 adipocytes (chapter 4), I cultured MG63 human osteosarcoma cells with serum enriched with fatty acids (AlbuMax), forcing them to acquire lipid droplets (LDs). Following this process characterised in literature ([Ruiz-Vela et al., 2011](#)), I aimed to investigate the LD-forming capability of ATRi-treated cultures. No quantifiable difference was observed between ATRi-treated and untreated MG63 cultures in their capacity to form LDs following AlbuMax treatment (Fig 7.2.3.4.A), although IF of BODIPY 493/503-stained MG63s showed quite strikingly that LDs were localised to the cell periphery following ATRi treatments, regardless of AlbuMax treatment (Fig 7.2.3.4.B). Dynein has been postulated as a mediator of LD formation and functionality, controlling LD size, fusion, fragmentation and dispersion ([Boulant et al., 2008](#); [Zehmer et al., 2009](#)).

Additionally, the dynein complex has an essential role in primary cilia formation – where a role for ATR has been characterised within the literature ([Stiff et al., 2016](#)). Ciliopathies are a clinically heterogeneous spectrum of developmental disorders, associated with mutations in genes encoding for members of the ciliary proteome. Subsets of ciliopathies are characterised by lipodystrophy and/or obesity ([Waters and Beales, 2011](#)), and more recently, it has been postulated that the clinical manifestations of ATR-SS could be due to disorders of cilia function ([Stiff et al., 2016](#)). Further to this, Seckel Syndrome-associated genes encoding Ninein and Pericentrin (PCNT) have roles in modulating dynein functionality ([Purohit et al., 1999](#); [Redwine et al., 2017](#)).

These experiments, and precedence within the literature, provide preliminary evidence that could potentially support the putative hypothesis that ATRi is compromising dynein function via a direct or indirect mechanism. Reduced functionality of dynein following ATRi treatments could result in reduced activity of mTORC1, causing the failure to undergo adipogenic differentiation in the presence of ATRis. Further work is required to validate this putative hypothesis.

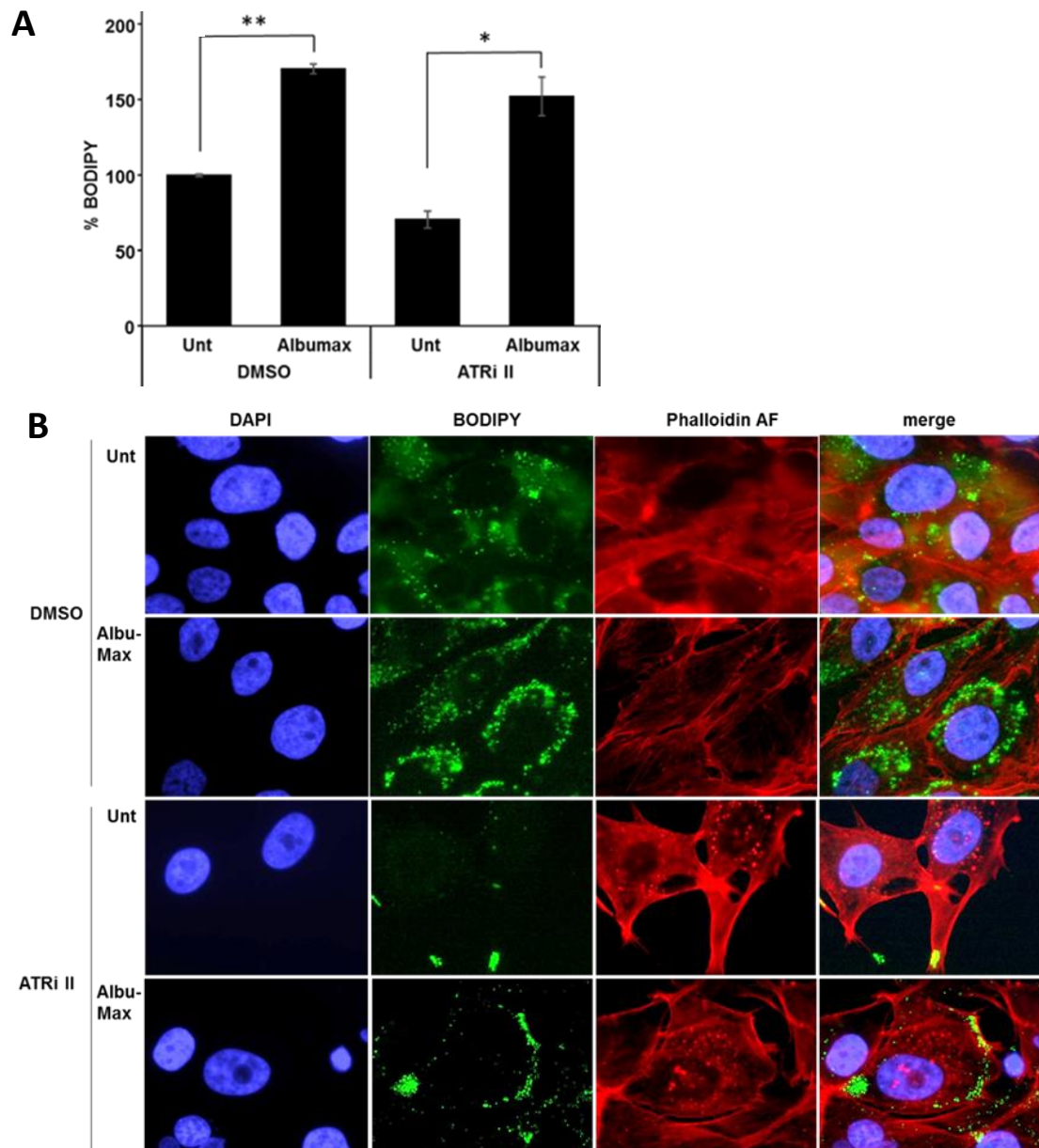


Figure 7.2.3.4. Lipid droplets re-localise to cell periphery following ATRi treatment. **A)** FACS quantification of TG content of MG63 cells treated with or without ATRi II (10 μ M, 16 hrs) and AlbuMax (1.6%, 16 hrs) shows ATRi does not affect LD formation in MG63 cells. **B)** IF microscopy corresponding to FACS analysis shows in ATRi-treated MG63 cultures, LD are localised to the cell periphery.

7.3 Concluding remarks

I have utilised clinically relevant ATRis in a model adipogenic cell culture system, to investigate a pathomechanistic link between ATR dysfunction and lipodystrophy. Lipodystrophy and/or cachexia are presentations commonly observed in congenital disorders and mouse models of ATR deficiency, presenting a potential hurdle in the therapeutic use of ATRis in cancer. The metabolic consequences of ATRi treatment could have implications for their use in cancer therapy; the browning of ATRi-treated white

adipocytes with enhanced FFA release is not dissimilar to that observed in cancer cachexia. The systemic reprogramming and browning of white adipose tissue stores is one pathomechanism behind the severe atrophy experienced by cachexic cancer patients.

On the other hand, there may also be as yet unconsidered therapeutic benefits to ATRi therapy. Investigating novel combination therapies with pre-existing medicines such as mTORC1 inhibitor rapamycin, or lysosomal protease inhibitor hydroxychloroquine, may show positive synergistic anti-cancer effects, thereby providing scope to develop novel treatment strategies whilst reducing therapy burden on the patient.

References

- Adams, J., and Cory, S. (2007). The Bcl-2 apoptotic switch in cancer development and therapy. *Oncogene* 26, 1324-1337.
- Aksamitiene, E., Kiyatkin, A., and Kholodenko, Boris N. (2012). Cross-talk between mitogenic Ras/MAPK and survival PI3K/Akt pathways: a fine balance. *Biochemical Society Transactions* 40, 139-146.
- Alcantara, D., and O'Driscoll, M. (2014). Congenital microcephaly. *American Journal of Medical Genetics Part C: Seminars in Medical Genetics* 166, 124-139.
- Alderton, G.K., Joenje, H., Varon, R., Børglum, A.D., Jeggo, P.A., and O'Driscoll, M. (2004). Seckel syndrome exhibits cellular features demonstrating defects in the ATR-signalling pathway. *Human Molecular Genetics* 13, 3127-3138.
- Altshuler-Keylin, S., Shinoda, K., Hasegawa, Y., Ikeda, K., Hong, H., Kang, Q., Yang, Y., Perera, Rushika M., Debnath, J., and Kajimura, S. (2016). Beige Adipocyte Maintenance Is Regulated by Autophagy-Induced Mitochondrial Clearance. *Cell Metabolism* 24, 402-419.
- Amaravadi, R.K., Yu, D., Lum, J.J., Bui, T., Christophorou, M.A., Evan, G.I., Thomas-Tikhonenko, A., and Thompson, C.B. (2007). Autophagy inhibition enhances therapy-induced apoptosis in a Myc-induced model of lymphoma. *Journal of Clinical Investigation* 117, 326-336.
- Anacker, D.C., Aloor, H.L., Shepard, C.N., Lenzi, G.M., Johnson, B.A., Kim, B., and Moody, C.A. (2016). HPV31 utilizes the ATR-Chk1 pathway to maintain elevated RRM2 levels and a replication-competent environment in differentiating Keratinocytes. *Virology* 499, 383-396.
- Araki, K., and Nagata, K. (2011). Protein Folding and Quality Control in the ER. *Cold Spring Harbor Perspectives in Biology* 3, a007526.
- Argiles, J.M., Busquets, S., Stemmler, B., and Lopez-Soriano, F.J. (2014). Cancer cachexia: understanding the molecular basis. *Nat Rev Cancer* 14, 754-762.
- Asano, H., Kanamori, Y., Higurashi, S., Nara, T., Kato, K., Matsui, T., and Funaba, M. (2014). Induction of Beige-Like Adipocytes in 3T3-L1 Cells. *The Journal of Veterinary Medical Science* 76, 57-64.

Axe, E.L., Walker, S.A., Manifava, M., Chandra, P., Roderick, H.L., Habermann, A., Griffiths, G., and Ktistakis, N.T. (2008). Autophagosome formation from membrane compartments enriched in phosphatidylinositol 3-phosphate and dynamically connected to the endoplasmic reticulum. *The Journal of Cell Biology* *182*, 685-701.

B'chir, W., Maurin, A.-C., Carraro, V., Averous, J., Jousse, C., Muranishi, Y., Parry, L., Stepien, G., Fafournoux, P., and Bruhat, A. (2013). The eIF2 α /ATF4 pathway is essential for stress-induced autophagy gene expression. *Nucleic Acids Research* *41*, 7683-7699.

Baenke, F., Peck, B., Miess, H., and Schulze, A. (2013). Hooked on fat: the role of lipid synthesis in cancer metabolism and tumour development. *Disease Models & Mechanisms* *6*, 1353-1363.

Bakkenist, C.J., and Kastan, M.B. (2003). DNA damage activates ATM through intermolecular autophosphorylation and dimer dissociation. *Nature* *421*, 499-506.

Ball, H.L., Myers, J.S., and Cortez, D. (2005). ATRIP Binding to Replication Protein A-Single-stranded DNA Promotes ATR-ATRIP Localization but Is Dispensable for Chk1 Phosphorylation. *Molecular Biology of the Cell* *16*, 2372-2381.

Bao, S., Tibbetts, R.S., Brumbaugh, K.M., Fang, Y., Richardson, D.A., Ali, A., Chen, S.M., Abraham, R.T., and Wang, X.-F. (2001). ATR/ATM-mediated phosphorylation of human Rad17 is required for genotoxic stress responses. *Nature* *411*, 969-974.

Barlow, C., Ribaut-Barassin, C., Zwingman, T.A., Pope, A.J., Brown, K.D., Owens, J.W., Larson, D., Harrington, E.A., Haeberle, A.-M., Mariani, J., *et al.* (2000). ATM is a cytoplasmic protein in mouse brain required to prevent lysosomal accumulation. *Proceedings of the National Academy of Sciences of the United States of America* *97*, 871-876.

Bartke, A. (2005). Minireview: Role of the Growth Hormone/Insulin-Like Growth Factor System in Mammalian Aging. *Endocrinology* *146*, 3718-3723.

Batchvarova, N., Wang, X.Z., and Ron, D. (1995). Inhibition of adipogenesis by the stress-induced protein CHOP (Gadd153). *EMBO Journal* *14*, 4654-4661.

Beijersbergen, R.L., Wessels, L.F., and Bernards, R. (2016). Synthetic Lethality in Cancer Therapeutics. *Annual Review of Cancer Biology*.

Bento, C.F., Renna, M., Ghislat, G., Puri, C., Ashkenazi, A., Vicinanza, M., Menzies, F.M., and Rubinsztein, D.C. (2016). Mammalian autophagy: How does it work? *Annual review of biochemistry* **85**, 685-713.

Berg, A.H., and Scherer, P.E. (2005). Adipose Tissue, Inflammation, and Cardiovascular Disease. *Circulation Research* **96**, 939-949.

Bernard, A., and Klionsky, D.J. (2014). Defining the membrane precursor supporting the nucleation of the phagophore. *Autophagy* **10**, 1-2.

Berridge, M.J. (2002). The endoplasmic reticulum: a multifunctional signaling organelle. *Cell Calcium* **32**, 235-249.

Berridge, M.J., Lipp, P., and Bootman, M.D. (2000). The versatility and universality of calcium signalling. *Nat Rev Mol Cell Biol* **1**, 11-21.

Berti, M., and Vindigni, A. (2016). Replication stress: getting back on track. *Nat Struct Mol Biol* **23**, 103-109.

Bertolotti, A., Zhang, Y., Hendershot, L.M., Harding, H.P., and Ron, D. (2000). Dynamic interaction of BiP and ER stress transducers in the unfolded-protein response. *Nat Cell Biol* **2**, 326-332.

Bhoumik, A., Bergami, P.L., and Ronai, Z.e. (2007). ATF2 on the Double – Activating Transcription Factor and DNA Damage Response Protein. *Pigment cell research / sponsored by the European Society for Pigment Cell Research and the International Pigment Cell Society* **20**, 498-506.

Bhoumik, A., Takahashi, S., Breitweiser, W., Shiloh, Y., Jones, N., and Ronai, Z.e. (2005). ATM-Dependent Phosphorylation of ATF2 Is Required for the DNA Damage Response. *Molecular cell* **18**, 577-587.

Bing, C., Brown, M., King, P., Collins, P., Tisdale, M.J., and Williams, G. (2000). Increased Gene Expression of Brown Fat Uncoupling Protein (UCP)1 and Skeletal Muscle UCP2 and UCP3 in MAC16-induced Cancer Cachexia. *Cancer Research* **60**, 2405-2410.

Bishop, N., and Woodman, P. (2000). ATPase-defective Mammalian VPS4 Localizes to Aberrant Endosomes and Impairs Cholesterol Trafficking. *Molecular Biology of the Cell* **11**, 227-239.

- Bjørkøy, G., Lamark, T., Brech, A., Outzen, H., Perander, M., Øvervatn, A., Stenmark, H., and Johansen, T. (2005). p62/SQSTM1 forms protein aggregates degraded by autophagy and has a protective effect on huntingtin-induced cell death. *The Journal of Cell Biology* *171*, 603-614.
- Bjørkøy, G., Lamark, T., Pankiv, S., Øvervatn, A., Brech, A., and Johansen, T. (2009). Chapter 12 Monitoring Autophagic Degradation of p62/SQSTM1. In *Methods in Enzymology* (Academic Press), pp. 181-197.
- Blüher, M., and Mantzoros, C.S. (2015). From leptin to other adipokines in health and disease: Facts and expectations at the beginning of the 21st century. *Metabolism* *64*, 131-145.
- Bock, J.B., Klumperman, J., Davanger, S., and Scheller, R.H. (1997). Syntaxin 6 functions in trans-Golgi network vesicle trafficking. *Molecular Biology of the Cell* *8*, 1261-1271.
- Boder, E., and Sedgwick, R. (1987). Ataxia–telangiectasia. In *Neurocutaneous diseases: a practical approach* (Butterworth-Heinemann), pp. 95-117.
- Bogdanovic, E., Kraus, N., Patsouris, D., Diao, L., Wang, V., Abdullahi, A., and Jeschke, M.G. (2015). Endoplasmic reticulum stress in adipose tissue augments lipolysis. *Journal of Cellular and Molecular Medicine* *19*, 82-91.
- Bos, J.L. (1989). *ras* Oncogenes in Human Cancer: A Review. *Cancer Research* *49*, 4682-4689.
- Boulant, S., Douglas, M.W., Moody, L., Budkowska, A., Targett-Adams, P., and McLauchlan, J. (2008). Hepatitis C Virus Core Protein Induces Lipid Droplet Redistribution in a Microtubule- and Dynein-Dependent Manner. *Traffic* *9*, 1268-1282.
- Boustany, R.-M.N. (2013). Lysosomal storage diseases—the horizon expands. *Nat Rev Neurol* *9*, 583-598.
- Bowers, R.R., and Lane, M.D. (2008). Wnt signaling and adipocyte lineage commitment. *Cell Cycle* *7*, 1191-1196.
- Bredemeyer, A.L., Sharma, G.G., Huang, C.-Y., Helmink, B.A., Walker, L.M., Khor, K.C., Nuskey, B., Sullivan, K.E., Pandita, T.K., Bassing, C.H., *et al.* (2006). ATM stabilizes DNA double-strand-break complexes during V(D)J recombination. *Nature* *442*, 466-470.

Bröcker, C., Engelbrecht-Vandré, S., and Ungermann, C. (2010). Multisubunit Tethering Complexes and Their Role in Membrane Fusion. *Current Biology* 20, R943-R952.

Brooks, C.L., and Gu, W. (2009). How does SIRT1 affect metabolism, senescence and cancer? *Nat Rev Cancer* 9, 123-128.

Brown, E.J., and Baltimore, D. (2000). ATR disruption leads to chromosomal fragmentation and early embryonic lethality. *Genes & Development* 14, 397-402.

Brown, N., and Costanzo, V. (2009). An ATM and ATR dependent pathway targeting centrosome dependent spindle assembly. *Cell Cycle* 8, 1997-2001.

Bruce, A.C., and Jay, L. (2015). *Cancer chemotherapy and radiation therapy*. (Oxford, UK, 'Oxford University Press').

Bryant, H.E., Schultz, N., Thomas, H.D., Parker, K.M., Flower, D., Lopez, E., Kyle, S., Meuth, M., Curtin, N.J., and Helleday, T. (2005). Specific killing of BRCA2-deficient tumours with inhibitors of poly(ADP-ribose) polymerase. *Nature* 434, 913-917.

Bucci, C., Thomsen, P., Nicoziani, P., McCarthy, J., and van Deurs, B. (2000). Rab7: A Key to Lysosome Biogenesis. *Molecular Biology of the Cell* 11, 467-480.

Bujisic, B., De Gassart, A., Tallant, R., Demaria, O., Zaffalon, L., Chelbi, S., Gilliet, M., Bertoni, F., and Martinon, F. (2017). Impairment of both IRE1 expression and XBP1 activation is a hallmark of GCB DLBCL and contributes to tumor growth. *Blood* 129, 2420-2428.

Calderilla-Barbosa, L., Seibenhener, M.L., Du, Y., Diaz-Meco, M.-T., Moscat, J., Yan, J., Wooten, M.W., and Wooten, M.C. (2014). Interaction of SQSTM1 with the motor protein dynein – SQSTM1 is required for normal dynein function and trafficking. *Journal of Cell Science* 127, 4052-4063.

Cao, Y., Jiang, X., Ma, H., Wang, Y., Xue, P., and Liu, Y. (2016). SIRT1 and insulin resistance. *Journal of Diabetes and its Complications* 30, 178-183.

Capanni, C., Mattioli, E., Columbaro, M., Lucarelli, E., Parnaik, V.K., Novelli, G., Wehnert, M., Cenni, V., Maraldi, N.M., Squarzoni, S., *et al.* (2005). Altered pre-lamin A processing is a common mechanism leading to lipodystrophy. *Human Molecular Genetics* 14, 1489-1502.

Cara, L., Baitemirova, M., Follis, J., Larios-Sanz, M., and Ribes-Zamora, A. (2016). The ATM- and ATR-related SCD domain is over-represented in proteins involved in nervous system development. *Scientific Reports* 6, 19050.

Casper, A.M., Nghiem, P., Arlt, M.F., and Glover, T.W. (2002). ATR Regulates Fragile Site Stability. *Cell* 111, 779-789.

Chakrabarti, A., Chen, A.W., and Varner, J.D. (2011). A Review of the Mammalian Unfolded Protein Response. *Biotechnology and bioengineering* 108, 2777-2793.

Charrier, J.-D., Durrant, S.J., Golec, J.M.C., Kay, D.P., Knegtel, R.M.A., MacCormick, S., Mortimore, M., O'Donnell, M.E., Pinder, J.L., Reaper, P.M., *et al.* (2011). Discovery of Potent and Selective Inhibitors of Ataxia Telangiectasia Mutated and Rad3 Related (ATR) Protein Kinase as Potential Anticancer Agents. *Journal of Medicinal Chemistry* 54, 2320-2330.

Chaudhari, N., Talwar, P., Parimisetty, A., Lefebvre d'Hellencourt, C., and Ravanian, P. (2014). A Molecular Web: Endoplasmic Reticulum Stress, Inflammation, and Oxidative Stress. *Frontiers in Cellular Neuroscience* 8, 213.

Chen, C.-F., Ruiz-Vega, R., Vasudeva, P., Espitia, F., Krasieva, T.B., de Feraudy, S., Tromberg, B.J., Huang, S., Garner, C.P., Wu, J., *et al.* (2017). ATR Mutations Promote the Growth of Melanoma Tumors by Modulating the Immune Microenvironment. *Cell Reports* 18, 2331-2342.

Chen, C.-Y., Olayioye, M.A., Lindeman, G.J., and Tang, T.K. (2006). CPAP interacts with 14-3-3 in a cell cycle-dependent manner. *Biochemical and Biophysical Research Communications* 342, 1203-1210.

Chen, H.C., and Farese, R.V. (2001). Turning WAT into BAT gets rid of fat. *Nature medicine* 7, 1102-1103.

Chen, J.-H., Zhang, P., Chen, W.-D., Li, D.-D., Wu, X.-Q., Deng, R., Jiao, L., Li, X., Ji, J., Feng, G.-K., *et al.* (2015). ATM-mediated PTEN phosphorylation promotes PTEN nuclear translocation and autophagy in response to DNA-damaging agents in cancer cells. *Autophagy* 11, 239-252.

Chen, Q., Shou, P., Zheng, C., Jiang, M., Cao, G., Yang, Q., Cao, J., Xie, N., Velletri, T., Zhang, X., *et al.* (2016). Fate decision of mesenchymal stem cells: adipocytes or osteoblasts[quest]. *Cell Death Differ* 23, 1128-1139.

Cheng, E.H.Y.A., Wei, M.C., Weiler, S., Flavell, R.A., Mak, T.W., Lindsten, T., and Korsmeyer, S.J. (2001). BCL-2, BCL-XL Sequester BH3 Domain-Only Molecules Preventing BAX- and BAK-Mediated Mitochondrial Apoptosis. *Molecular Cell* 8, 705-711.

Cheng, X.-T., Zhou, B., Lin, M.-Y., Cai, Q., and Sheng, Z.-H. (2015). Axonal autophagosomes recruit dynein for retrograde transport through fusion with late endosomes. *The Journal of Cell Biology* 209, 377-386.

Cheong, H., Lu, C., Lindsten, T., and Thompson, C.B. (2012). Therapeutic targets in cancer cell metabolism and autophagy. *Nat Biotech* 30, 671-678.

Ching, J.K., Elizabeth, S.V., Ju, J.-S., Lusk, C., Pittman, S.K., and Weihl, C.C. (2013). mTOR dysfunction contributes to vacuolar pathology and weakness in valosin-containing protein associated inclusion body myopathy. *Human Molecular Genetics* 22, 1167-1179.

Cho, Y.M., Kwak, S.-N., Joo, N.-S., Kim, D.H., Lee, A.-H., Kim, K.-S., Seo, J.B., Jeong, S.-W., and Kwon, O.-J. (2014). X-box binding protein 1 is a novel key regulator of peroxisome proliferator-activated receptor γ 2. *FEBS Journal* 281, 5132-5146.

Choi, J.-H., Lindsey-Boltz, L.A., and Sancar, A. (2009). Cooperative activation of the ATR checkpoint kinase by TopBP1 and damaged DNA. *Nucleic Acids Research* 37, 1501-1509.

Choi, M.S., Kim, H.-J., Ham, M., Choi, D.-H., Lee, T.R., and Shin, D.W. (2016). Amber Light (590 nm) Induces the Breakdown of Lipid Droplets through Autophagy-Related Lysosomal Degradation in Differentiated Adipocytes. *Scientific Reports* 6, 28476.

Cimprich, K.A., and Cortez, D. (2008). ATR: an essential regulator of genome integrity. *Nat Rev Mol Cell Biol* 9, 616-627.

Clippinger, A.J., and Alwine, J.C. (2012). Dynein mediates the localization and activation of mTOR in normal and human cytomegalovirus-infected cells. *Genes & Development* 26, 2015-2026.

Cohen, H.Y., Miller, C., Bitterman, K.J., Wall, N.R., Hekking, B., Kessler, B., Howitz, K.T., Gorospe, M., de Cabo, R., and Sinclair, D.A. (2004). Calorie Restriction Promotes Mammalian Cell Survival by Inducing the SIRT1 Deacetylase. *Science* 305, 390-392.

Coleman R. A., L.T.M., Muoio D. M. (2000). PHYSIOLOGICAL AND NUTRITIONAL REGULATION OF ENZYMES OF TRIACYLGLYCEROL SYNTHESIS. *Annual Review of Nutrition* 20, 77-103.

Contreras, C., Nogueiras, R., Diéguez, C., Medina-Gómez, G., and López, M. (2016). Hypothalamus and thermogenesis: Heating the BAT, browning the WAT. *Molecular and Cellular Endocrinology* 438, 107-115.

Cortez, D., Guntuku, S., Qin, J., and Elledge, S.J. (2001). ATR and ATRIP: Partners in Checkpoint Signaling. *Science* 294, 1713-1716.

Côté, J., Peterson, C.L., and Workman, J.L. (1998). Perturbation of nucleosome core structure by the SWI/SNF complex persists after its detachment, enhancing subsequent transcription factor binding. *Proceedings of the National Academy of Sciences of the United States of America* 95, 4947-4952.

Cotta-Ramusino, C., McDonald, E.R., Hurov, K., Sowa, M.E., Harper, J.W., and Elledge, S.J. (2011). A DNA Damage Response Screen Identifies RHINO: a 9-1-1 and TopBP1 interacting protein required for ATR signaling. *Science (New York, N.Y.)* 332, 1313-1317.

Cremona, C.A., and Behrens, A. (2014). ATM signalling and cancer. *Oncogene* 33, 3351-3360.

Cuadrado, M., Martinez-Pastor, B., Murga, M., Toledo, L.I., Gutierrez-Martinez, P., Lopez, E., and Fernandez-Capetillo, O. (2006). ATM regulates ATR chromatin loading in response to DNA double-strand breaks. *The Journal of Experimental Medicine* 203, 297-303.

D'Amours, D., Desnoyers, S., D'Silva, I., and Poirier, G.G. (1999). Poly(ADP-ribosyl)ation reactions in the regulation of nuclear functions. *Biochemical Journal* 342, 249-268.

D'Angiolella, V., Donato, V., Forrester, Frances M., Jeong, Y.-T., Pellacani, C., Kudo, Y., Saraf, A., Florens, L., Washburn, Michael P., and Pagano, M. Cyclin F-Mediated Degradation of Ribonucleotide Reductase M2 Controls Genome Integrity and DNA Repair. *Cell* 149, 1023-1034.

Dalbay, M.T., Thorpe, S.D., Connelly, J.T., Chapple, J.P., and Knight, M.M. (2015). Adipogenic Differentiation of hMSCs is Mediated by Recruitment of IGF-1r Onto the Primary Cilium Associated With Cilia Elongation. *Stem Cells (Dayton, Ohio)* 33, 1952-1961.

Darling, N.J., and Cook, S.J. (2014). The role of MAPK signalling pathways in the response to endoplasmic reticulum stress. *Biochimica et Biophysica Acta (BBA) - Molecular Cell Research* 1843, 2150-2163.

Dauber, A., LaFranchi, S.H., Maliga, Z., Lui, J.C., Moon, J.E., McDeed, C., Henke, K., Zonana, J., Kingman, G.A., Pers, T.H., *et al.* (2012). Novel Microcephalic Primordial Dwarfism Disorder

Associated with Variants in the Centrosomal Protein Ninein. *The Journal of Clinical Endocrinology and Metabolism* 97, E2140-E2151.

De Chiara, G., Marcocci, M.E., Torcia, M., Lucibello, M., Rosini, P., Bonini, P., Higashimoto, Y., Damonte, G., Armirotti, A., Amodei, S., *et al.* (2006). Bcl-2 Phosphorylation by p38 MAPK: IDENTIFICATION OF TARGET SITES AND BIOLOGIC CONSEQUENCES. *Journal of Biological Chemistry* 281, 21353-21361.

de Gonzalo-Calvo, D., López-Vilaró, L., Nasarre, L., Perez-Olabarria, M., Vázquez, T., Escuin, D., Badimon, L., Barnadas, A., Lerma, E., and Llorente-Cortés, V. (2015). Intratumor cholesteryl ester accumulation is associated with human breast cancer proliferation and aggressive potential: a molecular and clinicopathological study. *BMC Cancer* 15, 460.

de Laat, W.L., Appeldoorn, E., Sugasawa, K., Weterings, E., Jaspers, N.G.J., and Hoeijmakers, J.H.J. (1998). DNA-binding polarity of human replication protein A positions nucleases in nucleotide excision repair. *Genes & Development* 12, 2598-2609.

Del Gobbo, A., Peverelli, E., Treppiedi, D., Lania, A., Mantovani, G., and Ferrero, S. (2016). Expression of protein kinase A regulatory subunits in benign and malignant human thyroid tissues: A systematic review. *Experimental Cell Research* 346, 85-90.

Delacroix, S., Wagner, J.M., Kobayashi, M., Yamamoto, K.-i., and Karnitz, L.M. (2007). The Rad9–Hus1–Rad1 (9–1–1) clamp activates checkpoint signaling via TopBP1. *Genes & Development* 21, 1472-1477.

Deng, J., Liu, S., Zou, L., Xu, C., Bin, G., and Xu, G. (2012). Lipolysis response to endoplasmic reticulum stress in adipose cells. *Journal of Biological Chemistry*.

Denic, V., Quan, E.M., and Weissman, J.S. (2006). A Luminal Surveillance Complex that Selects Misfolded Glycoproteins for ER-Associated Degradation. *Cell* 126, 349-359.

Diao, J., Liu, R., Rong, Y., Zhao, M., Zhang, J., Lai, Y., Zhou, Q., Wilz, L.M., Li, J., Vivona, S., *et al.* (2015). ATG14 promotes membrane tethering and fusion of autophagosomes to endolysosomes. *Nature* 520, 563-566.

Ding, W.-X., Ni, H.-M., Gao, W., Chen, X., Kang, J.H., Stolz, D.B., Liu, J., and Yin, X.-M. (2009). Oncogenic transformation confers a selective susceptibility to the combined suppression of the proteasome and autophagy. *Molecular Cancer Therapeutics* 8, 2036-2045.

Distelhorst, C.W., and Bootman, M.D. (2011). Bcl-2 interaction with the inositol 1,4,5-trisphosphate receptor: role in Ca(2+) signaling and disease. *Cell calcium* 50, 234-241.

Dooley, Hannah C., Razi, M., Polson, Hannah E.J., Girardin, Stephen E., Wilson, Michael I., and Tooze, Sharon A. (2014). WIPI2 Links LC3 Conjugation with PI3P, Autophagosome Formation, and Pathogen Clearance by Recruiting Atg12–5-16L1. *Molecular Cell* 55, 238-252.

Dungrawala, H., Rose, Kristie L., Bhat, Kamakoti P., Mohni, Kareem N., Glick, Gloria G., Couch, Frank B., and Cortez, D. (2015). The Replication Checkpoint Prevents Two Types of Fork Collapse without Regulating Replisome Stability. *Molecular Cell* 59, 998-1010.

Duran, A., Amanchy, R., Linares, Juan F., Joshi, J., Abu-Baker, S., Porollo, A., Hansen, M., Moscat, J., and Diaz-Meco, Maria T. (2011). p62 Is a Key Regulator of Nutrient Sensing in the mTORC1 Pathway. *Molecular Cell* 44, 134-146.

Duursma, A.M., Driscoll, R., Elias, J.E., and Cimprich, K.A. (2013). A role for the MRN complex in ATR activation through TOPBP1 recruitment. *Molecular cell* 50, 116-122.

Dyment, D.A., Gibson, W.T., Huang, L., Bassyouni, H., Hegele, R.A., and Innes, A.M. (2014). Biallelic mutations at PPARG cause a congenital, generalized lipodystrophy similar to the Berardinelli–Seip syndrome. *European Journal of Medical Genetics* 57, 524-526.

Edmonson, J.H. (1966). Fatty acid mobilization and glucose metabolism in patients with cancer. *Cancer* 19, 277-280.

Ellgaard, L., and Ruddock, L.W. (2005). The human protein disulphide isomerase family: substrate interactions and functional properties. *EMBO Reports* 6, 28-32.

Ellison, V., and Stillman, B. (2003). Biochemical Characterization of DNA Damage Checkpoint Complexes: Clamp Loader and Clamp Complexes with Specificity for 5' Recessed DNA. *PLOS Biology* 1, e33.

Emily, H.-Y.C., Wei, M.C., Weiler, S., Flavell, R.A., Mak, T.W., Lindsten, T., and Korsmeyer, S.J. (2001). BCL-2, BCL-X L sequester BH3 domain-only molecules preventing BAX-and BAK-mediated mitochondrial apoptosis. *Molecular cell* 8, 705-711.

Engelman, J.A., Berg, A.H., Lewis, R.Y., Lin, A., Lisanti, M.P., and Scherer, P.E. (1999). Constitutively Active Mitogen-activated Protein Kinase Kinase 6 (MKK6) or Salicylate Induces Spontaneous 3T3-L1 Adipogenesis. *Journal of Biological Chemistry* 274, 35630-35638.

- Engelman, J.A., Lisanti, M.P., and Scherer, P.E. (1998). Specific Inhibitors of p38 Mitogen-activated Protein Kinase Block 3T3-L1 Adipogenesis. *Journal of Biological Chemistry* 273, 32111-32120.
- Errol, C.F., Graham, C.W., Wolfram, S., Richard, D.W., Roger, A.S., and Tom, E. (2006). *DNA Repair and Mutagenesis*, Second Edition (American Society of Microbiology).
- Falck, J., Mailand, N., Syljuasen, R.G., Bartek, J., and Lukas, J. (2001). The ATM-Chk2-Cdc25A checkpoint pathway guards against radioresistant DNA synthesis. *Nature* 410, 842-847.
- Fang, Evandro F., Scheibye-Knudsen, M., Brace, Lear E., Kassahun, H., SenGupta, T., Nilsen, H., Mitchell, James R., Croteau, Deborah L., and Bohr, Vilhelm A. (2014). Defective Mitophagy in XPA via PARP-1 Hyperactivation and NAD⁺/SIRT1 Reduction. *Cell* 157, 882-896.
- Fang, Y., Tsao, C.-C., Goodman, B.K., Furumai, R., Tirado, C.A., Abraham, R.T., and Wang, X.-F. (2004). ATR functions as a gene dosage-dependent tumor suppressor on a mismatch repair-deficient background. *The EMBO Journal* 23, 3164-3174.
- Farmer, H., McCabe, N., Lord, C.J., Tutt, A.N.J., Johnson, D.A., Richardson, T.B., Santarosa, M., Dillon, K.J., Hickson, I., Knights, C., *et al.* (2005). Targeting the DNA repair defect in BRCA mutant cells as a therapeutic strategy. *Nature* 434, 917-921.
- Farmer, S.R. (2005). Regulation of PPAR[gamma] activity during adipogenesis. *Int J Obes Relat Metab Disord* 29, S13-S16.
- Farmer, S.R. (2006). Transcriptional control of adipocyte formation. *Cell Metabolism* 4, 263-273.
- Fass, E., Shvets, E., Degani, I., Hirschberg, K., and Elazar, Z. (2006). Microtubules Support Production of Starvation-induced Autophagosomes but Not Their Targeting and Fusion with Lysosomes. *Journal of Biological Chemistry* 281, 36303-36316.
- Fearon, Kenneth C.H., Glass, David J., and Guttridge, Denis C. (2012). Cancer Cachexia: Mediators, Signaling, and Metabolic Pathways. *Cell Metabolism* 16, 153-166.
- Ferde, Pawel E., Gerasimenko, Julia V., Peng, S., Tepikin, Alexei V., Petersen, Ole H., and Gerasimenko, Oleg V. (2012). A Novel Role for Bcl-2 in Regulation of Cellular Calcium Extrusion. *Current Biology* 22, 1241-1246.
- Fernandez-Capetillo, O., Lee, A., Nussenzweig, M., and Nussenzweig, A. (2004). H2AX: the histone guardian of the genome. *DNA Repair* 3, 959-967.

Foote, K. (2015). Drugging ATR: progress in the development of specific inhibitors for the treatment of cancer. *Future Medicinal Chemistry* 7, 873-891.

Foote, K.M., Blades, K., Cronin, A., Fillery, S., Guichard, S.S., Hassall, L., Hickson, I., Jacq, X., Jewsbury, P.J., McGuire, T.M., *et al.* (2013). Discovery of 4-{4-[(3R)-3-Methylmorpholin-4-yl]-6-[1-(methylsulfonyl)cyclopropyl]pyrimidin-2-yl}-1H-indole (AZ20): A Potent and Selective Inhibitor of ATR Protein Kinase with Monotherapy in Vivo Antitumor Activity. *Journal of Medicinal Chemistry* 56, 2125-2138.

Fraldi, A., Annunziata, F., Lombardi, A., Kaiser, H.J., Medina, D.L., Spampanato, C., Fedele, A.O., Polishchuk, R., Sorrentino, N.C., Simons, K., *et al.* (2010). Lysosomal fusion and SNARE function are impaired by cholesterol accumulation in lysosomal storage disorders. *The EMBO Journal* 29, 3607-3620.

Frampton, J.E. (2015). Olaparib: A Review of Its Use as Maintenance Therapy in Patients with Ovarian Cancer. *BioDrugs* 29, 143-150.

Fu, M.-m., Nirschl, Jeffrey J., and Holzbaur, Erika L.F. (2014). LC3 Binding to the Scaffolding Protein JIP1 Regulates Processive Dynein-Driven Transport of Autophagosomes. *Developmental Cell* 29, 577-590.

Fujioka, Y., Noda, N.N., Nakatogawa, H., Ohsumi, Y., and Inagaki, F. (2010). Dimeric Coiled-coil Structure of *Saccharomyces cerevisiae* Atg16 and Its Functional Significance in Autophagy. *Journal of Biological Chemistry* 285, 1508-1515.

Fujisawa, H., Nakajima, N.I., Sunada, S., Lee, Y., Hirakawa, H., Yajima, H., Fujimori, A., Uesaka, M., and Okayasu, R. (2015). VE-821, an ATR inhibitor, causes radiosensitization in human tumor cells irradiated with high LET radiation. *Radiation Oncology (London, England)* 10, 175.

Furnari, B., Rhind, N., and Russell, P. (1997). Cdc25 Mitotic Inducer Targeted by Chk1 DNA Damage Checkpoint Kinase. *Science* 277, 1495-1497.

Gammoh, N., Florey, O., Overholtzer, M., and Jiang, X. (2013). Interaction between FIP200 and ATG16L1 distinguishes ULK1 complex-dependent and -independent autophagy. *Nat Struct Mol Biol* 20, 144-149.

Ge, X.Q., and Blow, J.J. (2010). Chk1 inhibits replication factory activation but allows dormant origin firing in existing factories. *The Journal of Cell Biology* 191, 1285-1297.

Gebauer, F., and Hentze, M.W. (2004). Molecular mechanisms of translational control. *Nat Rev Mol Cell Biol* 5, 827-835.

Gelebart, P., Opas, M., and Michalak, M. (2005). Calreticulin, a Ca^{2+} -binding chaperone of the endoplasmic reticulum. *The International Journal of Biochemistry & Cell Biology* 37, 260-266.

Gerasimenko, J., Ferdek, P., Fischer, L., Gukovskaya, A.S., and Pandol, S.J. (2010). Inhibitors of Bcl-2 protein family deplete ER Ca^{2+} stores in pancreatic acinar cells. *Pflugers Archiv* 460, 891-900.

Gesta, S., Tseng, Y.-H., and Kahn, C.R. (2007). Developmental Origin of Fat: Tracking Obesity to Its Source. *Cell* 131, 242-256.

Giam, M., Huang, D., and Bouillet, P. (2008). BH3-only proteins and their roles in programmed cell death. *Oncogene* 27, S128.

Gilad, O., Nabet, B.Y., Ragland, R.L., Schoppy, D.W., Smith, K.D., Durham, A.C., and Brown, E.J. (2010). Combining ATR Suppression with Oncogenic Ras Synergistically Increases Genomic Instability, Causing Synthetic Lethality or Tumorigenesis in a Dosage-Dependent Manner. *Cancer Research* 70, 9693-9702.

Glick, D., Barth, S., and Macleod, K.F. (2010). Autophagy: cellular and molecular mechanisms. *The Journal of pathology* 221, 3-12.

Glover, T.W., Berger, C., Coyle, J., and Echo, B. (1984). DNA polymerase α inhibition by aphidicolin induces gaps and breaks at common fragile sites in human chromosomes. *Human Genetics* 67, 136-142.

González Besteiro, M.A., and Gottifredi, V. (2015). The fork and the kinase: A DNA replication tale from a CHK1 perspective. *Mutation Research/Reviews in Mutation Research* 763, 168-180.

Graham, S.J.L., Black, M.J., Soboloff, J., Gill, D.L., Dziadek, M.A., and Johnstone, L.S. (2009). Stim1, an endoplasmic reticulum Ca^{2+} sensor, negatively regulates 3T3-L1 pre-adipocyte differentiation. *Differentiation; research in biological diversity* 77, 239-247.

Greenberg, A.S., and Obin, M.S. (2006). Obesity and the role of adipose tissue in inflammation and metabolism. *The American Journal of Clinical Nutrition* 83, 461S-465S.

Grootjans, J., Kaser, A., Kaufman, R.J., and Blumberg, R.S. (2016). The unfolded protein response in immunity and inflammation. *Nat Rev Immunol* 16, 469-484.

- Guernsey, D.L., Jiang, H., Hussin, J., Arnold, M., Bouyakdan, K., Perry, S., Babineau-Sturk, T., Beis, J., Dumas, N., Evans, S.C., *et al.* (2010). Mutations in Centrosomal Protein CEP152 in Primary Microcephaly Families Linked to MCPH4. *American Journal of Human Genetics* 87, 40-51.
- Guintini, L., Charton, R., Peyresaubes, F., Thoma, F., and Conconi, A. (2015). Nucleosome positioning, nucleotide excision repair and photoreactivation in *Saccharomyces cerevisiae*. *DNA Repair* 36, 98-104.
- Guo, C., Kumagai, A., Schlacher, K., Shevchenko, A., Shevchenko, A., and Dunphy, William G. (2015). Interaction of Chk1 with Treslin Negatively Regulates the Initiation of Chromosomal DNA Replication. *Molecular Cell* 57, 492-505.
- Halaas, J., Gajiwala, K., Maffei, M., Cohen, S., Chait, B., Rabinowitz, D., Lallone, R., Burley, S., and Friedman, J. (1995). Weight-reducing effects of the plasma protein encoded by the obese gene. *Science* 269, 543-546.
- Halaby, M.-J., Hibma, J.C., He, J., and Yang, D.-Q. (2008). ATM protein kinase mediates full activation of Akt and regulates glucose transporter 4 translocation by insulin in muscle cells. *Cellular Signalling* 20, 1555-1563.
- Halazonetis, T.D., Gorgoulis, V.G., and Bartek, J. (2008). An Oncogene-Induced DNA Damage Model for Cancer Development. *Science* 319, 1352-1355.
- Hall, A.B., Newsome, D., Wang, Y., Boucher, D.M., Eustace, B., Gu, Y., Hare, B., Johnson, M.A., Milton, S., Murphy, C.E., *et al.* (2014). Potentiation of tumor responses to DNA damaging therapy by the selective ATR inhibitor VX-970. *Oncotarget* 5, 5674-5685.
- Han, J., Murthy, R., Wood, B., Song, B., Wang, S., Sun, B., Malhi, H., and Kaufman, R.J. (2013). ER stress signalling through eIF2 α and CHOP, but not IRE1 α , attenuates adipogenesis in mice. *Diabetologia* 56, 911-924.
- Han, L., Zhou, R., Niu, J., McNutt, M.A., Wang, P., and Tong, T. (2010). SIRT1 is regulated by a PPAR γ -SIRT1 negative feedback loop associated with senescence. *Nucleic Acids Research* 38, 7458-7471.
- Hanada, T., Noda, N.N., Satomi, Y., Ichimura, Y., Fujioka, Y., Takao, T., Inagaki, F., and Ohsumi, Y. (2007). The Atg12-Atg5 Conjugate Has a Novel E3-like Activity for Protein Lipidation in Autophagy. *Journal of Biological Chemistry* 282, 37298-37302.

- Hara, T., Takamura, A., Kishi, C., Iemura, S.-i., Natsume, T., Guan, J.-L., and Mizushima, N. (2008). FIP200, a ULK-interacting protein, is required for autophagosome formation in mammalian cells. *The Journal of Cell Biology* 181, 497-510.
- Harazono, Y., Nakajima, K., and Raz, A. (2014). Why anti-Bcl-2 clinical trials fail: a solution. *Cancer metastasis reviews* 33, 285-294.
- Harms, M., and Seale, P. (2013). Brown and beige fat: development, function and therapeutic potential. *Nat Med* 19, 1252-1263.
- Hata, K., Nishimura, R., Ikeda, F., Yamashita, K., Matsubara, T., Nokubi, T., and Yoneda, T. (2003). Differential Roles of Smad1 and p38 Kinase in Regulation of Peroxisome Proliferator-activating Receptor γ during Bone Morphogenetic Protein 2-induced Adipogenesis. *Molecular Biology of the Cell* 14, 545-555.
- Hebert, D.N., Garman, S.C., and Molinari, M. (2005). The glycan code of the endoplasmic reticulum: asparagine-linked carbohydrates as protein maturation and quality-control tags. *Trends in Cell Biology* 15, 364-370.
- Heffernan, T.P., Ünsal-Kaçmaz, K., Heinloth, A.N., Simpson, D.A., Paules, R.S., Sancar, A., Cordeiro-Stone, M., and Kaufmann, W.K. (2007). Cdc7-Dbf4 and the Human S Checkpoint Response to UVC. *Journal of Biological Chemistry* 282, 9458-9468.
- Hegele, R.A. (2000). Familial Partial Lipodystrophy: A Monogenic Form of the Insulin Resistance Syndrome. *Molecular Genetics and Metabolism* 71, 539-544.
- Hetzer, M.W. (2010). The Nuclear Envelope. *Cold Spring Harbor Perspectives in Biology* 2, a000539.
- Hilton, B.A., Li, Z., Musich, P.R., Wang, H., Cartwright, B.M., Serrano, M., Zhou, X.Z., Lu, K.P., and Zou, Y. (2015). ATR Plays a Direct Antiapoptotic Role at Mitochondria Which Is Regulated by Prolyl Isomerase Pin1. *Molecular cell* 60, 35-46.
- Hirota, J., Michikawa, T., Natsume, T., Furuichi, T., and Mikoshiba, K. (1999). Calmodulin inhibits inositol 1,4,5-trisphosphate-induced calcium release through the purified and reconstituted inositol 1,4,5-trisphosphate receptor type 1. *FEBS Letters* 456, 322-326.
- Hitomi, M., Yang, K., Stacey, A.W., and Stacey, D.W. (2008). Phosphorylation of Cyclin D1 Regulated by ATM or ATR Controls Cell Cycle Progression. *Molecular and Cellular Biology* 28, 5478-5493.

Ho, A., and Dowdy, S.F. (2002). Regulation of G1 cell-cycle progression by oncogenes and tumor suppressor genes. *Current Opinion in Genetics & Development* 12, 47-52.

Ho, I.C., Kim, J.H.J., Rooney, J.W., Spiegelman, B.M., and Glimcher, L.H. (1998). A potential role for the nuclear factor of activated T cells family of transcriptional regulatory proteins in adipogenesis. *Proceedings of the National Academy of Sciences of the United States of America* 95, 15537-15541.

Hoeijmakers, J.H.J. (2009). DNA Damage, Aging, and Cancer. *New England Journal of Medicine* 361, 1475-1485.

Holohan, C., Van Schaeybroeck, S., Longley, D.B., and Johnston, P.G. (2013). Cancer drug resistance: an evolving paradigm. *Nat Rev Cancer* 13, 714-726.

Hořejší, Z., Takai, H., Adelman, C.A., Collis, S.J., Flynn, H., Maslen, S., Skehel, J.M., de Lange, T., and Boulton, S.J. (2010). CK2 Phospho-Dependent Binding of R2TP Complex to TEL2 Is Essential for mTOR and SMG1 Stability. *Molecular Cell* 39, 839-850.

Howell, B.J., McEwen, B.F., Canman, J.C., Hoffman, D.B., Farrar, E.M., Rieder, C.L., and Salmon, E.D. (2001). Cytoplasmic dynein/dynactin drives kinetochore protein transport to the spindle poles and has a role in mitotic spindle checkpoint inactivation. *The Journal of Cell Biology* 155, 1159-1172.

Hoy, A.J., Balaban, S., and Saunders, D.N. (2013). Adipocyte-Tumor Cell Metabolic Crosstalk in Breast Cancer. *Trends in Molecular Medicine* 23, 381-392.

Høyer-Hansen, M., Bastholm, L., Szyniarowski, P., Campanella, M., Szabadkai, G., Farkas, T., Bianchi, K., Fehrenbacher, N., Elling, F., Rizzuto, R., *et al.* (2007). Control of Macroautophagy by Calcium, Calmodulin-Dependent Kinase Kinase- β , and Bcl-2. *Molecular Cell* 25, 193-205.

Hsu, P.P., and Sabatini, D.M. (2008). Cancer Cell Metabolism: Warburg and Beyond. *Cell* 134, 703-707.

Hu, P., Han, Z., Couvillon, A.D., Kaufman, R.J., and Exton, J.H. (2006). Autocrine Tumor Necrosis Factor Alpha Links Endoplasmic Reticulum Stress to the Membrane Death Receptor Pathway through IRE1 α -Mediated NF- κ B Activation and Down-Regulation of TRAF2 Expression. *Molecular and Cellular Biology* 26, 3071-3084.

Huang, M., Kim, J.M., Shiotani, B., Yang, K., Zou, L., and D'Andrea, A.D. (2010). The FANCM/FAAP24 Complex is Required for the DNA Inter-strand Crosslink-Induced Checkpoint Response. *Molecular cell* 39, 259-268.

- Hurley, P.J., Wilsker, D., and Bunz, F. (2006). Human cancer cells require ATR for cell cycle progression following exposure to ionizing radiation. *Oncogene* 26, 2535-2542.
- Hurov, K.E., Cotta-Ramusino, C., and Elledge, S.J. (2010). A genetic screen identifies the Triple T complex required for DNA damage signaling and ATM and ATR stability. *Genes & Development* 24, 1939-1950.
- Hyttinen, J.M.T., Niittykoski, M., Salminen, A., and Kaarniranta, K. (2013). Maturation of autophagosomes and endosomes: A key role for Rab7. *Biochimica et Biophysica Acta (BBA) - Molecular Cell Research* 1833, 503-510.
- Iglehart, J.D., and Silver, D.P. (2009). Synthetic Lethality — A New Direction in Cancer-Drug Development. *New England Journal of Medicine* 361, 189-191.
- Jahn, R., and Scheller, R.H. (2006). SNAREs [mdash] engines for membrane fusion. *Nat Rev Mol Cell Biol* 7, 631-643.
- Jardim, M.J., Wang, Q., Furumai, R., Wakeman, T., Goodman, B.K., and Wang, X.-F. (2009). Reduced ATR or Chk1 Expression Leads to Chromosome Instability and Chemosensitization of Mismatch Repair-deficient Colorectal Cancer Cells. *Molecular Biology of the Cell* 20, 3801-3809.
- Jarrett, S.G., Wolf Horrell, E.M., Christian, P.A., Vanover, J.C., Boulanger, M.C., Zou, Y., and D’Orazio, J.A. (2014). PKA-mediated Phosphorylation of ATR Promotes Recruitment of XPA to UV-induced DNA Damage. *Molecular cell* 54, 999-1011.
- Jarrett, S.G., Wolf Horrell, E.M., and D’Orazio, J.A. (2016). AKAP12 mediates PKA-induced phosphorylation of ATR to enhance nucleotide excision repair. *Nucleic Acids Research* 44, 10711-10726.
- Jeggo, P.A., Pearl, L.H., and Carr, A.M. (2016). DNA repair, genome stability and cancer: a historical perspective. *Nat Rev Cancer* 16, 35-42.
- Jensen, B., Farach-Carson, M.C., Kenaley, E., and Akanbi, K.A. (2004). High extracellular calcium attenuates adipogenesis in 3T3-L1 preadipocytes. *Experimental Cell Research* 301, 280-292.
- Jiang, P., and Mizushima, N. (2014). Autophagy and human diseases. *Cell Res* 24, 69-79.
- Jiang, T., Harder, B., Rojo de la Vega, M., Wong, P.K., Chapman, E., and Zhang, D.D. (2015). p62 links autophagy and Nrf2 signaling. *Free Radical Biology and Medicine* 88, Part B, 199-204.

Jiang, X., Sun, Y., Chen, S., Roy, K., and Price, B.D. (2006). The FATC Domains of PIKK Proteins Are Functionally Equivalent and Participate in the Tip60-dependent Activation of DNA-PKcs and ATM. *Journal of Biological Chemistry* 281, 15741-15746.

Jossé, R., Martin, S.E., Guha, R., Ormanoglu, P., Pfister, T.D., Reaper, P.M., Barnes, C.S., Jones, J., Charlton, P., Pollard, J.R., *et al.* (2014). ATR inhibitors VE-821 and VX-970 sensitize cancer cells to topoisomerase I inhibitors by disabling DNA replication initiation and fork elongation responses. *Cancer research* 74, 6968-6979.

Jung, J.-J., Inamdar, Shivangi M., Tiwari, A., and Choudhury, A. (2012). Regulation of intracellular membrane trafficking and cell dynamics by syntaxin-6. *Bioscience Reports* 32, 383-391.

Kabeya, Y., Mizushima, N., Ueno, T., Yamamoto, A., Kirisako, T., Noda, T., Kominami, E., Ohsumi, Y., and Yoshimori, T. (2000). LC3, a mammalian homologue of yeast Apg8p, is localized in autophagosome membranes after processing, Vol 19.

Kakaroukas, A., and Jeggo, P.A. (2014). DNA DSB repair pathway choice: an orchestrated handover mechanism. *The British Journal of Radiology* 87, 20130685.

Kamphorst, J.J., Cross, J.R., Fan, J., de Stanchina, E., Mathew, R., White, E.P., Thompson, C.B., and Rabinowitz, J.D. (2013). Hypoxic and Ras-transformed cells support growth by scavenging unsaturated fatty acids from lysophospholipids. *Proceedings of the National Academy of Sciences* 110, 8882-8887.

Kampinga, H.H., and Craig, E.A. (2010). The Hsp70 chaperone machinery: J-proteins as drivers of functional specificity. *Nature reviews. Molecular cell biology* 11, 579-592.

Kang, R., Zeh, H.J., Lotze, M.T., and Tang, D. (2011). The Beclin 1 network regulates autophagy and apoptosis. *Cell Death Differ* 18, 571-580.

Kania, E., Pająk, B., and Orzechowski, A. (2015). Calcium Homeostasis and ER Stress in Control of Autophagy in Cancer Cells. *BioMed Research International* 2015, 352794.

Karanasios, E., Stapleton, E., Manifava, M., Kaizuka, T., Mizushima, N., Walker, S.A., and Ktistakis, N.T. (2013). Dynamic association of the ULK1 complex with omegasomes during autophagy induction. *Journal of Cell Science* 126, 5224-5238.

Katsura, M., Tsuruga, T., Date, O., Yoshihara, T., Ishida, M., Tomoda, Y., Okajima, M., Takaku, M., Kurumizaka, H., Kinomura, A., *et al.* (2009). The ATR-Chk1 pathway plays a role in the generation of centrosome aberrations induced by Rad51C dysfunction. *Nucleic Acids Research* 37, 3959-3968.

Kaufman, R.J., Scheuner, D., Schroder, M., Shen, X., Lee, K., Liu, C.Y., and Arnold, S.M. (2002). The unfolded protein response in nutrient sensing and differentiation. *Nat Rev Mol Cell Biol* 3, 411-421.

Kaur, J., and Debnath, J. (2015). Autophagy at the crossroads of catabolism and anabolism. *Nat Rev Mol Cell Biol* 16, 461-472.

Kaushik, S., and Cuervo, A.M. (2015). Degradation of lipid droplet-associated proteins by chaperone-mediated autophagy facilitates lipolysis. *Nature cell biology* 17, 759-770.

Kebache, S., Cardin, E., Nguyễn, D.T., Chevet, E., and Larose, L. (2004). Nck-1 Antagonizes the Endoplasmic Reticulum Stress-induced Inhibition of Translation. *Journal of Biological Chemistry* 279, 9662-9671.

Kemp, M., Spandau, D., and Travers, J. (2017a). Impact of Age and Insulin-Like Growth Factor-1 on DNA Damage Responses in UV-Irradiated Human Skin. *Molecules* 22, 356.

Kemp, M.G., Akan, Z., Yilmaz, S., Grillo, M., Smith-Roe, S.L., Kang, T.-H., Cordeiro-Stone, M., Kaufmann, W.K., Abraham, R.T., Sancar, A., *et al.* (2010). Tipin-RPA interaction mediates Chk1 phosphorylation by ATR in response to genotoxic stress. *Journal of Biological Chemistry*.

Kemp, M.G., Spandau, D.F., Simman, R., and Travers, J.B. (2017b). Insulin-like Growth Factor 1 Receptor Signaling Is Required for Optimal ATR-CHK1 Kinase Signaling in Ultraviolet B (UVB)-irradiated Human Keratinocytes. *Journal of Biological Chemistry* 292, 1231-1239.

Kerzendorfer, C., and O'Driscoll, M. (2009). Human DNA damage response and repair deficiency syndromes: Linking genomic instability and cell cycle checkpoint proficiency. *DNA Repair* 8, 1139-1152.

Kim, E.M., and Burke, D.J. (2008). DNA Damage Activates the SAC in an ATM/ATR-Dependent Manner, Independently of the Kinetochore. *PLoS Genetics* 4, e1000015.

Kim, J.B., Wright, H.M., Wright, M., and Spiegelman, B.M. (1998). ADD1/SREBP1 activates PPAR γ through the production of endogenous ligand. *Proceedings of the National Academy of Sciences of the United States of America* 95, 4333-4337.

Kim, J.E., and Chen, J. (2004). Regulation of Peroxisome Proliferator–Activated Receptor- γ Activity by Mammalian Target of Rapamycin and Amino Acids in Adipogenesis. *Diabetes* 53, 2748-2756.

Kim, S.W., Choi, J.H., Mukherjee, R., Hwang, K.-C., and Yun, J.W. (2016). Proteomic identification of fat-browning markers in cultured white adipocytes treated with curcumin. *Molecular and Cellular Biochemistry* 415, 51-66.

Kimura, S., Noda, T., and Yoshimori, T. (2008). Dynein-dependent Movement of Autophagosomes Mediates Efficient Encounters with Lysosomes. *Cell Structure and Function* 33, 109-122.

Kir, S., White, J.P., Kleiner, S., Kazak, L., Cohen, P., Baracos, V.E., and Spiegelman, B.M. (2014). Tumour-derived PTH-related protein triggers adipose tissue browning and cancer cachexia. *Nature* 513, 100-104.

Kirisako, T., Ichimura, Y., Okada, H., Kabeya, Y., Mizushima, N., Yoshimori, T., Ohsumi, M., Takao, T., Noda, T., and Ohsumi, Y. (2000). The Reversible Modification Regulates the Membrane-Binding State of Apg8/Aut7 Essential for Autophagy and the Cytoplasm to Vacuole Targeting Pathway. *The Journal of Cell Biology* 151, 263-276.

Kirkin, V., McEwan, D.G., Novak, I., and Dikic, I. (2009). A Role for Ubiquitin in Selective Autophagy. *Molecular Cell* 34, 259-269.

Klee, M., and Pimentel-Muñoz, F.X. (2005). Bcl-X(L) specifically activates Bak to induce swelling and restructuring of the endoplasmic reticulum. *The Journal of Cell Biology* 168, 723-734.

Klein, J.B., Barati, M.T., Wu, R., Gozal, D., Sachleben, L.R., Kausar, H., Trent, J.O., Gozal, E., and Rane, M.J. (2005). Akt-mediated Valosin-containing Protein 97 Phosphorylation Regulates Its Association with Ubiquitinated Proteins. *Journal of Biological Chemistry* 280, 31870-31881.

Kobayashi, M., Hayashi, N., Takata, M., and Yamamoto, K.-i. (2013). NBS1 directly activates ATR independently of MRE11 and TOPBP1. *Genes to Cells* 18, 238-246.

Kokame, K., Kato, H., and Miyata, T. (2001). Identification of ERSE-II, a New cis-Acting Element Responsible for the ATF6-dependent Mammalian Unfolded Protein Response. *Journal of Biological Chemistry* 276, 9199-9205.

Konopleva, M., Watt, J., Contractor, R., Tsao, T., Harris, D., Estrov, Z., Bornmann, W., Kantarjian, H., Viallet, J., and Samudio, I. (2008). Mechanisms of antileukemic activity of the novel Bcl-2 homology domain-3 mimetic GX15-070 (obatoclax). *Cancer research* 68, 3413-3420.

Kopecky, J., Clarke, G., Enerb, xE, ck, S., Spiegelman, B., and Kozak, L.P. (1995). Expression of the mitochondrial uncoupling protein gene from the α 2 gene promoter prevents genetic obesity. *The Journal of Clinical Investigation* 96, 2914-2923.

Kornberg, R.D., and Lorch, Y. (1999). Twenty-Five Years of the Nucleosome, Fundamental Particle of the Eukaryote Chromosome. *Cell* 98, 285-294.

Kotsantis, P., Silva, L.M., Irmscher, S., Jones, R.M., Folkes, L., Gromak, N., and Petermann, E. (2016). Increased global transcription activity as a mechanism of replication stress in cancer. *Nature Communications* 7, 13087.

Kouroku, Y., Fujita, E., Tanida, I., Ueno, T., Isoai, A., Kumagai, H., Ogawa, S., Kaufman, R.J., Kominami, E., and Momoi, T. (2006). ER stress (PERK//eIF2[α] phosphorylation) mediates the polyglutamine-induced LC3 conversion, an essential step for autophagy formation. *Cell Death Differ* 14, 230-239.

Kovsan, J., Ben-Romano, R., Souza, S.C., Greenberg, A.S., and Rudich, A. (2007). Regulation of Adipocyte Lipolysis by Degradation of the Perilipin Protein: NELFINAVIR ENHANCES LYSOSOME-MEDIATED PERILIPIN PROTEOLYSIS. *Journal of Biological Chemistry* 282, 21704-21711.

Kraft, C., Peter, M., and Hofmann, K. (2010). Selective autophagy: ubiquitin-mediated recognition and beyond. *Nat Cell Biol* 12, 836-841.

Kraus, N.A., Ehebauer, F., Zapp, B., Rudolphi, B., Kraus, B.J., and Kraus, D. (2016). Quantitative assessment of adipocyte differentiation in cell culture. *Adipocyte* 5, 351-358.

Krejci, L., Altmannova, V., Spirek, M., and Zhao, X. (2012). Homologous recombination and its regulation. *Nucleic Acids Research* 40, 5795-5818.

Kuljis, R.O., Xu, Y., Aguila, M.C., and Baltimore, D. (1997). Degeneration of neurons, synapses, and neuropil and glial activation in a murine Atm knockout model of ataxia–telangiectasia. *Proceedings of the National Academy of Sciences* 94, 12688-12693.

Kumagai, A., and Dunphy, W.G. (2000). Claspin, a Novel Protein Required for the Activation of Chk1 during a DNA Replication Checkpoint Response in *Xenopus* Egg Extracts. *Molecular Cell* 6, 839-849.

Kumagai, A., Lee, J., Yoo, H.Y., and Dunphy, W.G. (2006). TopBP1 Activates the ATR-ATRIP Complex. *Cell* 124, 943-955.

- Kumar, A., Mazzanti, M., Mistrik, M., Kosar, M., Beznoussenko, Galina V., Mironov, Alexandre A., Garrè, M., Parazzoli, D., Shivashankar, G.V., Scita, G., *et al.* (2014). ATR Mediates a Checkpoint at the Nuclear Envelope in Response to Mechanical Stress. *Cell* **158**, 633-646.
- Kunkel, G.T., Maceyka, M., Milstien, S., and Spiegel, S. (2013). Targeting the sphingosine-1-phosphate axis in cancer, inflammation and beyond. *Nat Rev Drug Discov* **12**, 688-702.
- Kuwana, T., Bouchier-Hayes, L., Chipuk, J.E., Bonzon, C., Sullivan, B.A., Green, D.R., and Newmeyer, D.D. (2005). BH3 domains of BH3-only proteins differentially regulate Bax-mediated mitochondrial membrane permeabilization both directly and indirectly. *Molecular cell* **17**, 525-535.
- Lamb, C.A., Yoshimori, T., and Tooze, S.A. (2013). The autophagosome: origins unknown, biogenesis complex. *Nat Rev Mol Cell Biol* **14**, 759-774.
- Lamb, H.K., Mee, C., Xu, W., Liu, L., Blond, S., Cooper, A., Charles, I.G., and Hawkins, A.R. (2006). The Affinity of a Major Ca²⁺ Binding Site on GRP78 Is Differentially Enhanced by ADP and ATP. *Journal of Biological Chemistry* **281**, 8796-8805.
- Laplante, M., Horvat, S., Festuccia, W.T., Birsoy, K., Prevorsek, Z., Efeyan, A., and Sabatini, D.M. (2012). DEPTOR cell-autonomously promotes adipogenesis and its expression is associated with obesity. *Cell metabolism* **16**, 202-212.
- Laplante, M., and Sabatini, D.M. (2012). mTOR signaling in growth control and disease. *Cell* **149**, 274-293.
- Laplante, M., and Sabatini, D.M. (2013). Regulation of mTORC1 and its impact on gene expression at a glance. *Journal of Cell Science* **126**, 1713-1719.
- Lass, A., Zimmermann, R., Oberer, M., and Zechner, R. (2011). Lipolysis – A highly regulated multi-enzyme complex mediates the catabolism of cellular fat stores. *Progress in Lipid Research* **50**, 14-27.
- Lavin, M.F. (2008). Ataxia-telangiectasia: from a rare disorder to a paradigm for cell signalling and cancer. *Nat Rev Mol Cell Biol* **9**, 759-769.
- Lavin, M.F., and Shiloh, Y. (1997). The genetic defect in ataxia-telangiectasia. *Annual review of immunology* **15**, 177-202.

Lawrence, K.S., Chau, T., and Engebrecht, J. (2015). DNA Damage Response and Spindle Assembly Checkpoint Function throughout the Cell Cycle to Ensure Genomic Integrity. *PLOS Genetics* *11*, e1005150.

Lee, C.-K., Shibata, Y., Rao, B., Strahl, B.D., and Lieb, J.D. (2004). Evidence for nucleosome depletion at active regulatory regions genome-wide. *Nat Genet* *36*, 900-905.

Lee, E.K., Jeong, J.U., Chang, J.W., Yang, W.S., Kim, S.B., Park, S.K., Park, J.S., and Lee, S.K. (2012). Activation of AMP-Activated Protein Kinase Inhibits Albumin-Induced Endoplasmic Reticulum Stress and Apoptosis through Inhibition of Reactive Oxygen Species. *Nephron Experimental Nephrology* *121*, e38-e48.

Lee, J.-E., and Ge, K. (2014). Transcriptional and epigenetic regulation of PPAR γ expression during adipogenesis. *Cell & Bioscience* *4*, 29.

Lee, K., Tirasophon, W., Shen, X., Michalak, M., Prywes, R., Okada, T., Yoshida, H., Mori, K., and Kaufman, R.J. (2002). IRE1-mediated unconventional mRNA splicing and S2P-mediated ATF6 cleavage merge to regulate XBP1 in signaling the unfolded protein response. *Genes & Development* *16*, 452-466.

Lee, M.-J., Wu, Y., and Fried, S.K. (2010). Adipose tissue remodeling in pathophysiology of obesity. *Current opinion in clinical nutrition and metabolic care* *13*, 371-376.

Lee, M.Y., Kong, H.J., and Cheong, J. (2001). Regulation of Activating Transcription Factor-2 in Early Stage of the Adipocyte Differentiation Program. *Biochemical and Biophysical Research Communications* *281*, 1241-1247.

Lei, K., and Davis, R.J. (2003). JNK phosphorylation of Bim-related members of the Bcl2 family induces Bax-dependent apoptosis. *Proceedings of the National Academy of Sciences of the United States of America* *100*, 2432-2437.

Lempiäinen, H., and Halazonetis, T.D. (2009). Emerging common themes in regulation of PIKKs and PI3Ks. *The EMBO Journal* *28*, 3067-3073.

Lewis, K.A., Bakkum-Gamez, J., Loewen, R., French, A.J., Thibodeau, S.N., and Cliby, W.A. (2007). Mutations in the ataxia telangiectasia and rad3-related-checkpoint kinase 1 DNA damage response axis in colon cancers. *Genes, Chromosomes and Cancer* *46*, 1061-1068.

- Lewis, K.A., Mullany, S., Thomas, B., Chien, J., Loewen, R., Shridhar, V., and Cliby, W.A. (2005). Heterozygous ATR Mutations in Mismatch Repair–Deficient Cancer Cells Have Functional Significance. *Cancer Research* 65, 7091-7095.
- Li, G., Mongillo, M., Chin, K.-T., Harding, H., Ron, D., Marks, A.R., and Tabas, I. (2009a). Role of ERO1- α –mediated stimulation of inositol 1,4,5-triphosphate receptor activity in endoplasmic reticulum stress–induced apoptosis. *The Journal of Cell Biology* 186, 783-792.
- Li, H., Rao, A., and Hogan, P.G. Interaction of calcineurin with substrates and targeting proteins. *Trends in Cell Biology* 21, 91-103.
- Li, J., Han, Y.R., Plummer, M.R., and Herrup, K. (2009b). Cytoplasmic ATM in Neurons Modulates Synaptic Function. *Current Biology* 19, 2091-2096.
- Lim, D.-S., Kirsch, D.G., Canman, C.E., Ahn, J.-H., Ziv, Y., Newman, L.S., Darnell, R.B., Shiloh, Y., and Kastan, M.B. (1998). ATM binds to β -adaptin in cytoplasmic vesicles. *Proceedings of the National Academy of Sciences of the United States of America* 95, 10146-10151.
- Linhart, H.G., Ishimura-Oka, K., DeMayo, F., Kibe, T., Repka, D., Poindexter, B., Bick, R.J., and Darlington, G.J. (2001). C/EBP α is required for differentiation of white, but not brown, adipose tissue. *Proceedings of the National Academy of Sciences* 98, 12532-12537.
- Liu, H., Cheng, E.H.-Y., and Hsieh, J.J.-D. (2007). Bimodal degradation of MLL by SCF^{Skp2} and APC^{Cdc20} assures cell cycle execution: a critical regulatory circuit lost in leukemogenic MLL fusions. *Genes & Development* 21, 2385-2398.
- Liu, K., Paik, J.C., Wang, B., Lin, F.-T., and Lin, W.-C. (2006a). Regulation of TopBP1 oligomerization by Akt/PKB for cell survival. *The EMBO Journal* 25, 4795-4807.
- Liu, Y. (2006). Fatty acid oxidation is a dominant bioenergetic pathway in prostate cancer. *Prostate Cancer Prostatic Dis* 9.
- Liu, Y., Bertram, C.C., Shi, Q., and Zinkel, S.S. (2011). Proapoptotic Bid mediates the Atr-directed DNA damage response to replicative stress. *Cell Death and Differentiation* 18, 841-852.
- Liu, Y., Rusinol, A., Sinensky, M., Wang, Y., and Zou, Y. (2006b). DNA damage responses in progeroid syndromes arise from defective maturation of prelamin A. *Journal of Cell Science* 119, 4644-4649.

Livingstone, M., Ruan, H., Weiner, J., Clauser, K.R., Strack, P., Jin, S., Williams, A., Greulich, H., Gardner, J., Venere, M., *et al.* (2005). Valosin-Containing Protein Phosphorylation at Ser⁷⁸⁴ in Response to DNA Damage. *Cancer Research* 65, 7533-7540.

Llambi, F., Wang, Y.-M., Victor, B., Yang, M., Schneider, D.M., Gingras, S., Parsons, M.J., Zheng, J.H., Brown, S.A., Pelletier, S., *et al.* (2016). BOK Is a Non-Canonical BCL-2 Family Effector of Apoptosis Regulated by ER-Associated Degradation. *Cell* 165, 421-433.

Lo, Kinyui A., and Sun, L. (2013). Turning WAT into BAT: a review on regulators controlling the browning of white adipocytes. *Bioscience Reports* 33, e00065.

Lovejoy, C.A., Xu, X., Bansbach, C.E., Glick, G.G., Zhao, R., Ye, F., Sirbu, B.M., Titus, L.C., Shyr, Y., and Cortez, D. (2009). Functional genomic screens identify CINP as a genome maintenance protein. *Proceedings of the National Academy of Sciences of the United States of America* 106, 19304-19309.

Lu, Z., Luo, R.Z., Lu, Y., Zhang, X., Yu, Q., Khare, S., Kondo, S., Kondo, Y., Yu, Y., Mills, G.B., *et al.* (2008). The tumor suppressor gene ARHI regulates autophagy and tumor dormancy in human ovarian cancer cells. *The Journal of Clinical Investigation* 118, 3917-3929.

Lumsden, J.M., McCarty, T., Petiniot, L.K., Shen, R., Barlow, C., Wynn, T.A., Morse, H.C., Gearhart, P.J., Wynshaw-Boris, A., Max, E.E., *et al.* (2004). Immunoglobulin Class Switch Recombination Is Impaired in *Atm*-deficient Mice. *The Journal of Experimental Medicine* 200, 1111-1121.

Luu, Y.K., Pessin, J.E., Judex, S., Rubin, J., and Rubin, C.T. (2009). Mechanical signals as a non-invasive means to influence mesenchymal stem cell fate, promoting bone and suppressing the fat phenotype. *IBMS BoneKEy* 6, 132-149.

Maier, B., Gluba, W., Bernier, B., Turner, T., Mohammad, K., Guise, T., Sutherland, A., Thorner, M., and Scrable, H. (2004). Modulation of mammalian life span by the short isoform of p53. *Genes & Development* 18, 306-319.

Majewski, F., Goecke, T., and Opitz, J.M. (1982). Studies of microcephalic primordial dwarfism I: Approach to a delineation of the seckel syndrome. *American Journal of Medical Genetics* 12, 7-21.

Manju, K., Muralikrishna, B., and Parnaik, V.K. (2006). Expression of disease-causing lamin A mutants impairs the formation of DNA repair foci. *Journal of Cell Science* 119, 2704-2714.

Maréchal, A., and Zou, L. (2013). DNA Damage Sensing by the ATM and ATR Kinases. *Cold Spring Harbor Perspectives in Biology* 5, a012716.

- Matsunaga, K., Morita, E., Saitoh, T., Akira, S., Ktistakis, N.T., Izumi, T., Noda, T., and Yoshimori, T. (2010). Autophagy requires endoplasmic reticulum targeting of the PI3-kinase complex via Atg14L. *The Journal of Cell Biology* 190, 511-521.
- Matsuoka, S., Ballif, B.A., Smogorzewska, A., McDonald, E.R., Hurov, K.E., Luo, J., Bakalarski, C.E., Zhao, Z., Solimini, N., Lerenthal, Y., *et al.* (2007). ATM and ATR Substrate Analysis Reveals Extensive Protein Networks Responsive to DNA Damage. *Science* 316, 1160-1166.
- Mattson, M.P., and Chan, S.L. (2003). Calcium orchestrates apoptosis. *Nat Cell Biol* 5, 1041-1043.
- Medina-Gomez, G., Gray, S.L., Yetukuri, L., Shimomura, K., Virtue, S., Campbell, M., Curtis, R.K., Jimenez-Linan, M., Blount, M., Yeo, G.S.H., *et al.* (2007). PPAR gamma 2 Prevents Lipotoxicity by Controlling Adipose Tissue Expandability and Peripheral Lipid Metabolism. *PLOS Genetics* 3, e64.
- Mekahli, D., Bultynck, G., Parys, J.B., De Smedt, H., and Missiaen, L. (2011). Endoplasmic-Reticulum Calcium Depletion and Disease. *Cold Spring Harbor Perspectives in Biology* 3, a004317.
- Mimnaugh, E.G., Xu, W., Vos, M., Yuan, X., and Neckers, L. (2006). Endoplasmic Reticulum Vacuolization and Valosin-Containing Protein Relocalization Result from Simultaneous Hsp90 Inhibition by Geldanamycin and Proteasome Inhibition by Velcade. *Molecular Cancer Research* 4, 667-681.
- Mizushima, N., and Komatsu, M. (2011). Autophagy: Renovation of Cells and Tissues. *Cell* 147, 728-741.
- Mizushima, N., Noda, T., Yoshimori, T., Tanaka, Y., Ishii, T., George, M.D., Klionsky, D.J., Ohsumi, M., and Ohsumi, Y. (1998). A protein conjugation system essential for autophagy. *Nature* 395, 395-398.
- Mizushima, N., Yamamoto, A., Hatano, M., Kobayashi, Y., Kabeya, Y., Suzuki, K., Tokuhi, T., Ohsumi, Y., and Yoshimori, T. (2001). Dissection of Autophagosome Formation Using Apg5-Deficient Mouse Embryonic Stem Cells. *The Journal of Cell Biology* 152, 657-668.
- Mizushima, N., and Yoshimori, T. (2007). How to Interpret LC3 Immunoblotting. *Autophagy* 3, 542-545.
- Mleczak, A., Millar, S., Tooze, S.A., Olson, M.F., and Chan, E.Y.W. (2013). Regulation of autophagosome formation by Rho kinase. *Cellular Signalling* 25, 1-11.

- Mokrani-Benhelli, H., Gaillard, L., Biasutto, P., Le Guen, T., Touzot, F., Vasquez, N., Komatsu, J., Conseiller, E., Picard, C., Gluckman, E., *et al.* (2013). Primary Microcephaly, Impaired DNA Replication, and Genomic Instability Caused by Compound Heterozygous ATR Mutations. *Human Mutation* 34, 374-384.
- Monaco, G., Decrock, E., Akl, H., Ponsaerts, R., Vervliet, T., Luyten, T., De Maeyer, M., Missiaen, L., Distelhorst, C.W., De Smedt, H., *et al.* (2012). Selective regulation of IP(3)-receptor-mediated Ca(2+) signaling and apoptosis by the BH4 domain of Bcl-2 versus Bcl-Xl. *Cell Death and Differentiation* 19, 295-309.
- Mordes, D.A., and Cortez, D. (2008). Activation of ATR and related PIKKs. *Cell cycle (Georgetown, Tex.)* 7, 2809-2812.
- Mordes, D.A., Glick, G.G., Zhao, R., and Cortez, D. (2008). TopBP1 activates ATR through ATRIP and a PIKK regulatory domain. *Genes & Development* 22, 1478-1489.
- Mori, C., Yamaguchi, Y., Teranishi, M., Takanami, T., Nagase, T., Kanno, S., Yasui, A., and Higashitani, A. (2013). Over-expression of ATR causes autophagic cell death. *Genes to Cells* 18, 278-287.
- Moss, B. (2013). Poxvirus DNA Replication. *Cold Spring Harbor Perspectives in Biology* 5.
- Moss, J., Tinline-Purvis, H., Walker, C.A., Folkes, L.K., Stratford, M.R., Hayles, J., Hoe, K.-L., Kim, D.-U., Park, H.-O., Kearsey, S.E., *et al.* (2010). Break-induced ATR and Ddb1–Cul4(Cdt2) ubiquitin ligase-dependent nucleotide synthesis promotes homologous recombination repair in fission yeast. *Genes & Development* 24, 2705-2716.
- Mowers, E.E., Sharifi, M.N., and Macleod, K.F. (2017). Autophagy in cancer metastasis. *Oncogene* 36, 1619-1630.
- Mueller, E., Drori, S., Aiyer, A., Yie, J., Sarraf, P., Chen, H., Hauser, S., Rosen, E.D., Ge, K., Roeder, R.G., *et al.* (2002). Genetic Analysis of Adipogenesis through Peroxisome Proliferator-activated Receptor γ Isoforms. *Journal of Biological Chemistry* 277, 41925-41930.
- Muller, P.A.J., and Vousden, K.H. (2013). p53 mutations in cancer. *Nat Cell Biol* 15, 2-8.
- Müller, T.D., Lee, S.J., Jastroch, M., Kabra, D., Stemmer, K., Aichler, M., Abplanalp, B., Ananthakrishnan, G., Bhardwaj, N., Collins, S., *et al.* (2013). p62 Links β -adrenergic input to mitochondrial function and thermogenesis. *The Journal of Clinical Investigation* 123, 469-478.

- Murga, M., Bunting, S., Montana, M.F., Soria, R., Mulero, F., Canamero, M., Lee, Y., McKinnon, P.J., Nussenzweig, A., and Fernandez-Capetillo, O. (2009). A mouse model of ATR-Seckel shows embryonic replicative stress and accelerated aging. *Nat Genet* 41, 891-898.
- Murphy, D.J., and Vance, J. (1999). Mechanisms of lipid-body formation. *Trends in Biochemical Sciences* 24, 109-115.
- Nagano, A., and Arahata, K. (2000). Nuclear envelope proteins and associated diseases. *Current Opinion in Neurology* 13, 533-539.
- Nair, U., Yen, W.-L., Mari, M., Cao, Y., Xie, Z., Baba, M., Reggiori, F., and Klionsky, D.J. (2012). A role for Atg8–PE deconjugation in autophagosome biogenesis. *Autophagy* 8, 780-793.
- Nakamura, S., and Yoshimori, T. (2017). New insights into autophagosome–lysosome fusion. *Journal of Cell Science* 130, 1209-1216.
- Nam, E.A., and Cortez, D. (2011). ATR signalling: more than meeting at the fork. *Biochemical Journal* 436, 527-536.
- Nam, E.A., Zhao, R., Glick, G.G., Bansbach, C.E., Friedman, D.B., and Cortez, D. (2011). Thr-1989 Phosphorylation Is a Marker of Active Ataxia Telangiectasia-mutated and Rad3-related (ATR) Kinase. *The Journal of Biological Chemistry* 286, 28707-28714.
- Neal, J.W., and Clipstone, N.A. (2002). Calcineurin Mediates the Calcium-dependent Inhibition of Adipocyte Differentiation in 3T3-L1 Cells. *Journal of Biological Chemistry* 277, 49776-49781.
- Neal, J.W., and Clipstone, N.A. (2003). A Constitutively Active NFATc1 Mutant Induces a Transformed Phenotype in 3T3-L1 Fibroblasts. *Journal of Biological Chemistry* 278, 17246-17254.
- Nebenführ, A. (2002). Vesicle traffic in the endomembrane system: a tale of COPs, Rabs and SNAREs. *Current Opinion in Plant Biology* 5, 507-512.
- Neese, R.A., Misell, L.M., Turner, S., Chu, A., Kim, J., Cesar, D., Hoh, R., Antelo, F., Strawford, A., McCune, J.M., *et al.* (2002). Measurement in vivo of proliferation rates of slow turnover cells by (2)H(2)O labeling of the deoxyribose moiety of DNA. *Proceedings of the National Academy of Sciences of the United States of America* 99, 15345-15350.

Nghiem, P., Park, P.K., Kim, Y.-s., Vaziri, C., and Schreiber, S.L. (2001). ATR inhibition selectively sensitizes G1 checkpoint-deficient cells to lethal premature chromatin condensation. *Proceedings of the National Academy of Sciences* 98, 9092-9097.

Nguyễn, D.T., Kebache, S., Fazel, A., Wong, H.N., Jenna, S., Emadali, A., Lee, E.-h., Bergeron, J.J.M., Kaufman, R.J., Larose, L., *et al.* (2004). Nck-dependent Activation of Extracellular Signal-regulated Kinase-1 and Regulation of Cell Survival during Endoplasmic Reticulum Stress. *Molecular Biology of the Cell* 15, 4248-4260.

Niida, H., Katsuno, Y., Banerjee, B., Hande, M.P., and Nakanishi, M. (2007). Specific Role of Chk1 Phosphorylations in Cell Survival and Checkpoint Activation. *Molecular and Cellular Biology* 27, 2572-2581.

Nixon, R.A. (2013). The role of autophagy in neurodegenerative disease. *Nat Med* 19, 983-997.

O'Driscoll, M., Ruiz-Perez, V.L., Woods, C.G., Jeggo, P.A., and Goodship, J.A. (2003). A splicing mutation affecting expression of ataxia-telangiectasia and Rad3-related protein (ATR) results in Seckel syndrome. *Nat Genet* 33, 497-501.

O'Driscoll, M. (2009). Mouse models for ATR deficiency. *DNA Repair* 8, 1333-1337.

O'Driscoll, M., Gennery, A.R., Seidel, J., Concannon, P., and Jeggo, P.A. (2004). An overview of three new disorders associated with genetic instability: LIG4 syndrome, RS-SCID and ATR-Seckel syndrome. *DNA Repair* 3, 1227-1235.

O'Driscoll, M., and Jeggo, P.A. (2003). Clinical Impact of ATR Checkpoint Signalling Failure in Humans. *Cell Cycle* 2, 193-194.

Oakes, S.A., Opferman, J.T., Pozzan, T., Korsmeyer, S.J., and Scorrano, L. (2003). Regulation of endoplasmic reticulum Ca²⁺ dynamics by proapoptotic BCL-2 family members. *Biochemical Pharmacology* 66, 1335-1340.

Obita, T., Saksena, S., Ghazi-Tabatabai, S., Gill, D.J., Perisic, O., Emr, S.D., and Williams, R.L. (2007). Structural basis for selective recognition of ESCRT-III by the AAA ATPase Vps4. *Nature* 449, 735-739.

Ogden, C.L., Carroll, M.D., Curtin, L.R., McDowell, M.A., Tabak, C.J., and Flegal, K.M. (2006). Prevalence of overweight and obesity in the united states, 1999-2004. *JAMA* 295, 1549-1555.

Ogi, T., Walker, S., Stiff, T., Hobson, E., Limsirichaikul, S., Carpenter, G., Prescott, K., Suri, M., Byrd, P.J., Matsuse, M., *et al.* (2012). Identification of the First ATRIP–Deficient Patient and Novel Mutations in ATR Define a Clinical Spectrum for ATR–ATRIP Seckel Syndrome. *PLoS Genetics* 8, e1002945.

Ohsumi, Y. (2014). Historical landmarks of autophagy research. *Cell Res* 24, 9-23.

Oishi, Y., Manabe, I., Tobe, K., Tsushima, K., Shindo, T., Fujiu, K., Nishimura, G., Maemura, K., Yamauchi, T., Kubota, N., *et al.* (2005). Krüppel-like transcription factor KLF5 is a key regulator of adipocyte differentiation. *Cell Metabolism* 1, 27-39.

Ojha, S., Budge, H., and Symonds, M.E. (2014). Adipocytes in Normal Tissue Biology A2 - McManus, Linda M. In *Pathobiology of Human Disease*, R.N. Mitchell, ed. (San Diego: Academic Press), pp. 2003-2013.

Okamoto, K. (2011). Mitochondria breathe for autophagy. *The EMBO Journal* 30, 2095-2096.

Okamura, M., Inagaki, T., Tanaka, T., and Sakai, J. (2010). Role of histone methylation and demethylation in adipogenesis and obesity. *Organogenesis* 6, 24-32.

Osowski, C.M., and Urano, F. (2011). Measuring ER stress and the unfolded protein response using mammalian tissue culture system. *Methods in enzymology* 490, 71-92.

Palmieri, M., Impey, S., Kang, H., di Ronza, A., Pelz, C., Sardiello, M., and Ballabio, A. (2011). Characterization of the CLEAR network reveals an integrated control of cellular clearance pathways. *Human Molecular Genetics* 20, 3852-3866.

Papp, S., Dziak, E., Michalak, M., and Opas, M. (2003). Is all of the endoplasmic reticulum created equal? The effects of the heterogeneous distribution of endoplasmic reticulum Ca(2+)-handling proteins. *The Journal of Cell Biology* 160, 475-479.

Parenti, G., Andria, G., and Ballabio, A. (2015). Lysosomal storage diseases: from pathophysiology to therapy. *Annual review of medicine* 66, 471-486.

Parray, H.A., and Yun, J.W. (2016). Cannabidiol promotes browning in 3T3-L1 adipocytes. *Molecular and Cellular Biochemistry* 416, 131-139.

- Patrick, S.M., Oakley, G.G., Dixon, K., and Turchi, J.J. (2005). DNA Damage Induced Hyperphosphorylation of Replication Protein A. 2. Characterization of DNA Binding Activity, Protein Interactions, and Activity in DNA Replication and Repair(). *Biochemistry* *44*, 8438-8448.
- Peasland, A., Wang, L.Z., Rowling, E., Kyle, S., Chen, T., Hopkins, A., Cliby, W.A., Sarkaria, J., Beale, G., Edmondson, R.J., *et al.* (2011). Identification and evaluation of a potent novel ATR inhibitor, NU6027, in breast and ovarian cancer cell lines. *Br J Cancer* *105*, 372-381.
- Peirce, V., Carobbio, S., and Vidal-Puig, A. (2014). The different shades of fat. *Nature* *510*, 76-83.
- Periasamy, M., and Kalyanasundaram, A. (2007). SERCA pump isoforms: Their role in calcium transport and disease. *Muscle & Nerve* *35*, 430-442.
- Perry, J., and Kleckner, N. (2003). The ATRs, ATMs, and TORs Are Giant HEAT Repeat Proteins. *Cell* *112*, 151-155.
- Petruzzelli, M., Schweiger, M., Schreiber, R., Campos-Olivas, R., Tsoi, M., Allen, J., Swarbrick, M., Rose-John, S., Rincon, M., Robertson, G., *et al.* A Switch from White to Brown Fat Increases Energy Expenditure in Cancer-Associated Cachexia. *Cell Metabolism* *20*, 433-447.
- Picard, F., Kurtev, M., Chung, N., Topark-Ngarm, A., Senawong, T., Machado de Oliveira, R., Leid, M., McBurney, M.W., and Guarente, L. (2004). Sirt1 promotes fat mobilization in white adipocytes by repressing PPAR- γ . *Nature* *429*, 771-776.
- Pinton, P., Ferrari, D., Magalhães, P., Schulze-Osthoff, K., Di Virgilio, F., Pozzan, T., and Rizzuto, R. (2000). Reduced Loading of Intracellular Ca^{2+} Stores and Downregulation of Capacitative Ca^{2+} Influx in Bcl-2–Overexpressing Cells. *The Journal of Cell Biology* *148*, 857-862.
- Ploegh, H.L. (2007). A lipid-based model for the creation of an escape hatch from the endoplasmic reticulum. *Nature* *448*, 435-438.
- Polak, P., Cybulski, N., Feige, J.N., Auwerx, J., Rüegg, M.A., and Hall, M.N. (2008). Adipose-Specific Knockout of raptor Results in Lean Mice with Enhanced Mitochondrial Respiration. *Cell Metabolism* *8*, 399-410.
- Pope, B.D., Warren, C.R., Parker, K.K., and Cowan, C.A. Microenvironmental Control of Adipocyte Fate and Function. *Trends in Cell Biology* *26*, 745-755.

Poruchynsky, M.S., Komlodi-Pasztor, E., Trostel, S., Wilkerson, J., Regairaz, M., Pommier, Y., Zhang, X., Kumar Maity, T., Robey, R., Burotto, M., *et al.* (2015). Microtubule-targeting agents augment the toxicity of DNA-damaging agents by disrupting intracellular trafficking of DNA repair proteins. *Proceedings of the National Academy of Sciences of the United States of America* 112, 1571-1576.

Postigo, A., Ramsden, A.E., Howell, M., and Way, M. (2017). Cytoplasmic ATR Activation Promotes Vaccinia Virus Genome Replication. *Cell Reports* 19, 1022-1032.

Poulos, S.P., Dodson, M.V., and Hausman, G.J. (2010). Cell line models for differentiation: preadipocytes and adipocytes. *Experimental Biology and Medicine* 235, 1185-1193.

Powell, S.N., and Kachnic, L.A. (2003). Roles of BRCA1 and BRCA2 in homologous recombination, DNA replication fidelity and the cellular response to ionizing radiation. *Oncogene* 22, 5784-5791.

Prevo, R., Fokas, E., Reaper, P.M., Charlton, P.A., Pollard, J.R., McKenna, W.G., Muschel, R.J., and Brunner, T.B. (2012). The novel ATR inhibitor VE-821 increases sensitivity of pancreatic cancer cells to radiation and chemotherapy. *Cancer Biology & Therapy* 13, 1072-1081.

Prusty, D., Park, B.-H., Davis, K.E., and Farmer, S.R. (2002). Activation of MEK/ERK Signaling Promotes Adipogenesis by Enhancing Peroxisome Proliferator-activated Receptor γ (PPAR γ) and C/EBP α Gene Expression during the Differentiation of 3T3-L1 Preadipocytes. *Journal of Biological Chemistry* 277, 46226-46232.

Purohit, A., Tynan, S.H., Vallee, R., and Doxsey, S.J. (1999). Direct Interaction of Pericentrin with Cytoplasmic Dynein Light Intermediate Chain Contributes to Mitotic Spindle Organization. *The Journal of Cell Biology* 147, 481-492.

Pylayeva-Gupta, Y., Grabocka, E., and Bar-Sagi, D. (2011). RAS oncogenes: weaving a tumorigenic web. *Nat Rev Cancer* 11, 761-774.

Qiang, L., Wang, L., Kon, N., Zhao, W., Lee, S., Zhang, Y., Rosenbaum, M., Zhao, Y., Gu, W., Farmer, Stephen R., *et al.* (2012). Brown Remodeling of White Adipose Tissue by SirT1-Dependent Deacetylation of Ppar γ . *Cell* 150, 620-632.

Qiu, B., Ackerman, D., Sanchez, D.J., Li, B., Ochocki, J.D., Grazioli, A., Bobrovnikova-Marjon, E., Diehl, J.A., Keith, B., and Simon, M.C. (2015). HIF2 α -Dependent Lipid Storage Promotes Endoplasmic Reticulum Homeostasis in Clear-Cell Renal Cell Carcinoma. *Cancer Discovery* 5, 652-667.

Qiu, Z., Wei, Y., Chen, N., Jiang, M., Wu, J., and Liao, K. (2001). DNA Synthesis and Mitotic Clonal Expansion Is Not a Required Step for 3T3-L1 Preadipocyte Differentiation into Adipocytes. *Journal of Biological Chemistry* 276, 11988-11995.

Qu, X., Yu, J., Bhagat, G., Furuya, N., Hibshoosh, H., Troxel, A., Rosen, J., Eskelinen, E.-L., Mizushima, N., Ohsumi, Y., *et al.* (2003). Promotion of tumorigenesis by heterozygous disruption of the beclin 1 autophagy gene. *Journal of Clinical Investigation* 112, 1809-1820.

Qvist, P., Huertas, P., Jimeno, S., Nyegaard, M., Hassan, M.J., Jackson, S.P., and Børglum, A.D. (2011). CtIP Mutations Cause Seckel and Jawad Syndromes. *PLOS Genetics* 7, e1002310.

Raaijmakers, J.A., Tanenbaum, M.E., and Medema, R.H. (2013). Systematic dissection of dynein regulators in mitosis. *The Journal of Cell Biology* 201, 201-215.

Raffaello, A., Mammucari, C., Gherardi, G., and Rizzuto, R. (2016). Calcium at the Center of Cell Signaling: Interplay between Endoplasmic Reticulum, Mitochondria, and Lysosomes. *Trends in Biochemical Sciences* 41, 1035-1049.

Ragland, R.L., Arlt, M.F., Hughes, E.D., Saunders, T.L., and Glover, T.W. (2009). Mice hypomorphic for Atr have increased DNA damage and abnormal checkpoint response. *Mammalian Genome* 20, 375-385.

Rahman, K. (2007). Studies on free radicals, antioxidants, and co-factors. *Clinical Interventions in Aging* 2, 219-236.

Ramm, G., Slot, J.W., James, D.E., and Stoorvogel, W. (2000). Insulin Recruits GLUT4 from Specialized VAMP2-carrying Vesicles as well as from the Dynamic Endosomal/Trans-Golgi Network in Rat Adipocytes. *Molecular Biology of the Cell* 11, 4079-4091.

Rashid, H.-O., Yadav, R.K., Kim, H.-R., and Chae, H.-J. (2015). ER stress: Autophagy induction, inhibition and selection. *Autophagy* 11, 1956-1977.

Rautureau, G.J.P., Day, C.L., and Hinds, M.G. (2010). Intrinsically Disordered Proteins in Bcl-2 Regulated Apoptosis. *International Journal of Molecular Sciences* 11, 1808-1824.

Ravikumar, B., Acevedo-Arozena, A., Imarisio, S., Berger, Z., Vacher, C., O'Kane, C.J., Brown, S.D.M., and Rubinsztein, D.C. (2005). Dynein mutations impair autophagic clearance of aggregate-prone proteins. *Nat Genet* 37, 771-776.

- Ravikumar, B., Moreau, K., Jahreiss, L., Puri, C., and Rubinsztein, D.C. (2010). Plasma membrane contributes to the formation of pre-autophagosomal structures. *Nat Cell Biol* 12, 747-757.
- Reaper, P.M., Griffiths, M.R., Long, J.M., Charrier, J.-D., MacCormick, S., Charlton, P.A., Golec, J.M.C., and Pollard, J.R. (2011). Selective killing of ATM- or p53-deficient cancer cells through inhibition of ATR. *Nat Chem Biol* 7, 428-430.
- Redwine, W.B., DeSantis, M.E., Hollyer, I., Htet, Z.M., Tran, P.T., Swanson, S.K., Florens, L., Washburn, M.P., and Reck-Peterson, S.L. (2017). The Human Cytoplasmic Dynein Interactome Reveals Novel Activators Of Motility. *bioRxiv*.
- Reggiori, F., Tucker, K.A., Stromhaug, P.E., and Klionsky, D.J. (2004). The Atg1-Atg13 Complex Regulates Atg9 and Atg23 Retrieval Transport from the Pre-Autophagosomal Structure. *Developmental Cell* 6, 79-90.
- Rigamonti, A., Brennand, K., Lau, F., and Cowan, C.A. (2011). Rapid Cellular Turnover in Adipose Tissue. *PLoS ONE* 6, e17637.
- Rivera-Calzada, A., López-Perrote, A., Melero, R., Boskovic, J., Muñoz-Hernández, H., Martino, F., and Llorca, O. (2015). Structure and Assembly of the PI3K-like Protein Kinases (PIKKs) Revealed by Electron Microscopy. *AIMS Biophysics* 2, 36-57.
- Robak, T. (2015). Bortezomib in the treatment of mantle cell lymphoma. *Future Oncology* 11, 2807-2818.
- Roczniak-Ferguson, A., Petit, C.S., Froehlich, F., Qian, S., Ky, J., Angarola, B., Walther, T.C., and Ferguson, S.M. (2012). The Transcription Factor TFEB Links mTORC1 Signaling to Transcriptional Control of Lysosome Homeostasis. *Science Signaling* 5, ra42-ra42.
- Rodbell, M. (1966). The Metabolism of Isolated Fat Cells: IV. REGULATION OF RELEASE OF PROTEIN BY LIPOLYTIC HORMONES AND INSULIN. *Journal of Biological Chemistry* 241, 3909-3917.
- Rodriguez, A., Durán, A., Selloum, M., Champy, M.-F., Diez-Guerra, F.J., Flores, J.M., Serrano, M., Auwerx, J., Diaz-Meco, M.T., and Moscat, J. (2006). Mature-onset obesity and insulin resistance in mice deficient in the signaling adapter p62. *Cell Metabolism* 3, 211-222.
- Ron, D., and Habener, J.F. (1992). CHOP, a novel developmentally regulated nuclear protein that dimerizes with transcription factors C/EBP and LAP and functions as a dominant-negative inhibitor of gene transcription. *Genes & Development* 6, 439-453.

Rosenfeld, M.R., Ye, X., Supko, J.G., Desideri, S., Grossman, S.A., Brem, S., Mikkelsen, T., Wang, D., Chang, Y.C., Hu, J., *et al.* (2014). A phase I/II trial of hydroxychloroquine in conjunction with radiation therapy and concurrent and adjuvant temozolomide in patients with newly diagnosed glioblastoma multiforme. *Autophagy* 10, 1359-1368.

Roux, P.P., and Blenis, J. (2004). ERK and p38 MAPK-Activated Protein Kinases: a Family of Protein Kinases with Diverse Biological Functions. *Microbiology and Molecular Biology Reviews* 68, 320-344.

Rubinson, E.H., Metz, A.H., O'Quin, J., and Eichman, B.F. (2008). A New Protein Architecture for Processing Alkylation Damaged DNA: The Crystal Structure of DNA Glycosylase AlkD. *Journal of molecular biology* 381, 13-23.

Ruiz-Vela, A., Aguilar-Gallardo, C., Martínez-Arroyo, A.M., Soriano-Navarro, M., Ruiz, V., and Simón, C. (2011). Specific Unsaturated Fatty Acids Enforce the Transdifferentiation of Human Cancer Cells toward Adipocyte-like Cells. *Stem Cell Reviews and Reports* 7, 898-909.

Rundle, S., Bradbury, A., Drew, Y., and Curtin, N. (2017). Targeting the ATR-CHK1 Axis in Cancer Therapy. *Cancers* 9, 41.

Rusten, T.E., and Stenmark, H. (2010). p62, an autophagy hero or culprit? *Nat Cell Biol* 12, 207-209.

Ruzankina, Y., Pinzon-Guzman, C., Asare, A., Ong, T., Pontano, L., Cotsarelis, G., Zediak, V.P., Velez, M., Bhandoola, A., and Brown, E.J. (2007). Deletion of the Developmentally Essential Gene ATR in Adult Mice Leads to Age-Related Phenotypes and Stem Cell Loss. *Cell Stem Cell* 1, 113-126.

Ruzankina, Y., Schoppy, D.W., Asare, A., Clark, C.E., Vonderheide, R.H., and Brown, E.J. (2009a). Tissue regenerative delays and synthetic lethality in adult mice after combined deletion of Atr and Trp53. *Nat Genet* 41, 1144-1149.

Ruzankina, Y., Schoppy, D.W., Asare, A., Clark, C.E., Vonderheide, R.H., and Brown, E.J. (2009b). Tissue regenerative delays and synthetic lethality in adult mice upon combined deletion of ATR and p53. *Nature genetics* 41, 1144-1149.

Rysman, E., Brusselmans, K., Scheys, K., Timmermans, L., Derua, R., Munck, S., Van Veldhoven, P.P., Waltregny, D., Daniëls, V.W., Machiels, J., *et al.* (2010). *De novo* Lipogenesis Protects Cancer Cells from Free Radicals and Chemotherapeutics by Promoting Membrane Lipid Saturation. *Cancer Research* 70, 8117-8126.

Salma, N., Xiao, H., Mueller, E., and Imbalzano, A.N. (2004). Temporal recruitment of transcription factors and SWI/SNF chromatin-remodeling enzymes during adipogenic induction of the peroxisome proliferator-activated receptor gamma nuclear hormone receptor. *Mol Cell Biol* 24.

Sanchez-Wandelmer, J., Ktistakis, N.T., and Reggiori, F. (2015). ERES: sites for autophagosome biogenesis and maturation? *Journal of Cell Science* 128, 185-192.

Satir, P., Pedersen, L.B., and Christensen, S.T. (2010). The primary cilium at a glance. *Journal of Cell Science* 123, 499-503.

Schimmer, A.D., O'Brien, S., Kantarjian, H., Brandwein, J., Cheson, B.D., Minden, M.D., Yee, K., Ravandi, F., Giles, F., and Schuh, A. (2008). A phase I study of the pan bcl-2 family inhibitor obatoclax mesylate in patients with advanced hematologic malignancies. *Clinical Cancer Research* 14, 8295-8301.

Schmidt, T.I., Kleylein-Sohn, J., Westendorf, J., Le Clech, M., Lavoie, S.B., Stierhof, Y.-D., and Nigg, E.A. (2009). Control of Centriole Length by CPAP and CP110. *Current Biology* 19, 1005-1011.

Schoppy, D.W., Ragland, R.L., Gilad, O., Shastri, N., Peters, A.A., Murga, M., Fernandez-Capetillo, O., Diehl, J.A., and Brown, E.J. (2012). Oncogenic stress sensitizes murine cancers to hypomorphic suppression of ATR. *The Journal of Clinical Investigation* 122, 241-252.

Schröder, M., and Kaufman, R.J. (2005). The mammalian unfolded protein response. *Annu. Rev. Biochem.* 74, 739-789.

Scott, A., Chung, H.-Y., Gonciarz-Swiatek, M., Hill, G.C., Whitby, F.G., Gaspar, J., Holton, J.M., Viswanathan, R., Ghaffarian, S., Hill, C.P., *et al.* (2005). Structural and mechanistic studies of VPS4 proteins. *The EMBO Journal* 24, 3658-3669.

Scott, C.C., Vacca, F., and Gruenberg, J. (2014). Endosome maturation, transport and functions. *Seminars in Cell & Developmental Biology* 31, 2-10.

Scott, K., Hayden, P.J., Will, A., Wheatley, K., and Coyne, I. (2016). Bortezomib for the treatment of multiple myeloma. *Cochrane Database of Systematic Reviews*.

Seibenhener, M.L., Babu, J.R., Geetha, T., Wong, H.C., Krishna, N.R., and Wooten, M.W. (2004). Sequestosome 1/p62 Is a Polyubiquitin Chain Binding Protein Involved in Ubiquitin Proteasome Degradation. *Molecular and Cellular Biology* 24, 8055-8068.

- Sekulić, A., Hudson, C.C., Homme, J.L., Yin, P., Otterness, D.M., Karnitz, L.M., and Abraham, R.T. (2000). A Direct Linkage between the Phosphoinositide 3-Kinase-AKT Signaling Pathway and the Mammalian Target of Rapamycin in Mitogen-stimulated and Transformed Cells. *Cancer Research* 60, 3504-3513.
- Seo, J., Fortuno, E.S., Suh, J.M., Stenesen, D., Tang, W., Parks, E.J., Adams, C.M., Townes, T., and Graff, J.M. (2009). Atf4 Regulates Obesity, Glucose Homeostasis, and Energy Expenditure. *Diabetes* 58, 2565-2573.
- Sepa-Kishi, D.M., and Ceddia, R.B. (2016). Exercise-mediated effects on white and brown adipose tissue plasticity and metabolism. *Exercise and sport sciences reviews* 44, 37-44.
- Sethi, J.K., and Vidal-Puig, A.J. (2007). Thematic review series: Adipocyte Biology. Adipose tissue function and plasticity orchestrate nutritional adaptation. *Journal of Lipid Research* 48, 1253-1262.
- Settembre, C., Zoncu, R., Medina, D.L., Vetrini, F., Erdin, S., Erdin, S., Huynh, T., Ferron, M., Karsenty, G., Vellard, M.C., *et al.* (2012). A lysosome-to-nucleus signalling mechanism senses and regulates the lysosome via mTOR and TFEB. *The EMBO Journal* 31, 1095-1108.
- Sha, H., He, Y., Chen, H., Wang, C., Zenno, A., Shi, H., Yang, X., Zhang, X., and Qi, L. (2009). The IRE1 α -XBP1 Pathway of the Unfolded Protein Response is Required for Adipogenesis. *Cell metabolism* 9, 556-564.
- Shamas-Din, A., Kale, J., Leber, B., and Andrews, D.W. (2013). Mechanisms of Action of Bcl-2 Family Proteins. *Cold Spring Harbor Perspectives in Biology* 5, a008714.
- Shamu, C.E., and Walter, P. (1996). Oligomerization and phosphorylation of the Ire1p kinase during intracellular signaling from the endoplasmic reticulum to the nucleus. *The EMBO Journal* 15, 3028-3039.
- Shen, J., Chen, X., Hendershot, L., and Prywes, R. (2002). ER Stress Regulation of ATF6 Localization by Dissociation of BiP/GRP78 Binding and Unmasking of Golgi Localization Signals. *Developmental Cell* 3, 99-111.
- Shepherd, P.R., Gnudi, L., Tozzo, E., Yang, H., Leach, F., and Kahn, B.B. (1993). Adipose cell hyperplasia and enhanced glucose disposal in transgenic mice overexpressing GLUT4 selectively in adipose tissue. *Journal of Biological Chemistry* 268, 22243-22246.

Showkat, M., Beigh, M.A., and Andrabi, K.I. (2014). mTOR Signaling in Protein Translation Regulation: Implications in Cancer Genesis and Therapeutic Interventions. *Molecular Biology International* 2014, 14.

Shubin, A.V., Demidyuk, I.V., Komissarov, A.A., Rafieva, L.M., and Kostrov, S.V. (2016). Cytoplasmic vacuolization in cell death and survival. *Oncotarget* 7, 55863-55889.

Sibanda, B.L., Chirgadze, D.Y., and Blundell, T.L. (2010). Crystal Structure of DNA-PKcs Reveals a Large Open-Ring Cradle Comprised of HEAT Repeats. *Nature* 463, 118-121.

Sieber, M., and Baumgrass, R. (2009). Novel inhibitors of the calcineurin/NFATc hub - alternatives to CsA and FK506? *Cell Communication and Signaling : CCS* 7, 25-25.

Simonnet, H., Alazard, N., Pfeiffer, K., Gallou, C., Bérout, C., Demont, J., Bouvier, R., Schägger, H., and Godinot, C. (2002). Low mitochondrial respiratory chain content correlates with tumor aggressiveness in renal cell carcinoma. *Carcinogenesis* 23, 759-768.

Sims Iii, R.J., Nishioka, K., and Reinberg, D. (2003). Histone lysine methylation: a signature for chromatin function. *Trends in Genetics* 19, 629-639.

Singh, R., Kaushik, S., Wang, Y., Xiang, Y., Novak, I., Komatsu, M., Tanaka, K., Cuervo, A.M., and Czaja, M.J. (2009a). Autophagy regulates lipid metabolism. *Nature* 458, 1131-1135.

Singh, R., Xiang, Y., Wang, Y., Baikati, K., Cuervo, A.M., Luu, Y.K., Tang, Y., Pessin, J.E., Schwartz, G.J., and Czaja, M.J. (2009b). Autophagy regulates adipose mass and differentiation in mice. *The Journal of Clinical Investigation* 119, 3329-3339.

Sinha, S., and Levine, B. (2008). The autophagy effector Beclin 1: a novel BH3-only protein. *Oncogene* 27, S137-S148.

Sirbu, B.M., and Cortez, D. (2013). DNA Damage Response: Three Levels of DNA Repair Regulation. *Cold Spring Harbor Perspectives in Biology* 5.

Sivasubramaniam, S., Sun, X., Pan, Y.-R., Wang, S., and Lee, E.Y.H.P. (2008). Cep164 is a mediator protein required for the maintenance of genomic stability through modulation of MDC1, RPA, and CHK1. *Genes & Development* 22, 587-600.

Slobodkin, M.R., and Elazar, Z. (2013). The Atg8 family: multifunctional ubiquitin-like key regulators of autophagy. *Essays In Biochemistry* 55, 51-64.

- Smith, M.H., Ploegh, H.L., and Weissman, J.S. (2011). Road to Ruin: Targeting Proteins for Degradation in the Endoplasmic Reticulum. *Science* 334, 1086-1090.
- Smyth, J.T., Hwang, S.-Y., Tomita, T., DeHaven, W.I., Mercer, J.C., and Putney, J.W. (2010). Activation and regulation of store-operated calcium entry. *Journal of Cellular and Molecular Medicine* 14, 2337-2349.
- Soliman, G.A., Acosta-Jaquez, H.A., and Fingar, D.C. (2010). mTORC1 Inhibition via Rapamycin Promotes Triacylglycerol Lipolysis and Release of Free Fatty Acids in 3T3-L1 Adipocytes. *Lipids* 45, 1089-1100.
- Song, C., Wang, Q., Song, C., Lockett, S.J., Colburn, N.H., Li, C.-C.H., Wang, J.M., and Rogers, T.J. (2015). Nucleocytoplasmic Shuttling of Valosin-Containing Protein (VCP/p97) Regulated by Its N domain and C-terminal Region. *Biochimica et biophysica acta* 1853, 222-232.
- Spalding, K.L., Arner, E., Westermark, P.O., Bernard, S., Buchholz, B.A., Bergmann, O., Blomqvist, L., Hoffstedt, J., Naslund, E., Britton, T., *et al.* (2008). Dynamics of fat cell turnover in humans. *Nature* 453, 783-787.
- Spiegelman, B.M., Hu, E., Kim, J.B., and Brun, R. (1997). PPAR γ and the control of adipogenesis. *Biochimie* 79, 111-112.
- Stenmark, H. (2009). Rab GTPases as coordinators of vesicle traffic. *Nat Rev Mol Cell Biol* 10, 513-525.
- Stiff, T., Casar Tena, T., O'Driscoll, M., Jeggo, P.A., and Philipp, M. (2016). ATR promotes cilia signalling: links to developmental impacts. *Human Molecular Genetics* 25, 1574-1587.
- Stiff, T., Reis, C., Alderton, G.K., Woodbine, L., O'Driscoll, M., and Jeggo, P.A. (2005). Nbs1 is required for ATR-dependent phosphorylation events. *The EMBO Journal* 24, 199-208.
- Stokes, M.P., Rush, J., MacNeill, J., Ren, J.M., Sprott, K., Nardone, J., Yang, V., Beausoleil, S.A., Gygi, S.P., Livingstone, M., *et al.* (2007). Profiling of UV-induced ATM/ATR signaling pathways. *Proceedings of the National Academy of Sciences* 104, 19855-19860.
- Stolz, A., Ernst, A., and Dikic, I. (2014). Cargo recognition and trafficking in selective autophagy. *Nat Cell Biol* 16, 495-501.
- Strzyz, P. (2016). Lipid metabolism: Lipid droplet growth in brown fat. *Nat Rev Mol Cell Biol* 17, 3-3.

- Subramanian, V., Rothenberg, A., Gomez, C., Cohen, A.W., Garcia, A., Bhattacharyya, S., Shapiro, L., Dolios, G., Wang, R., Lisanti, M.P., *et al.* (2004). Perilipin A Mediates the Reversible Binding of CGI-58 to Lipid Droplets in 3T3-L1 Adipocytes. *Journal of Biological Chemistry* 279, 42062-42071.
- Sulli, G., Di Micco, R., and di Fagagna, F.d.A. (2012). Crosstalk between chromatin state and DNA damage response in cellular senescence and cancer. *Nat Rev Cancer* 12, 709-720.
- Sun, Q., Westphal, W., Wong, K.N., Tan, I., and Zhong, Q. (2010). Rubicon controls endosome maturation as a Rab7 effector. *Proceedings of the National Academy of Sciences* 107, 19338-19343.
- Sun, Y., Xu, Y., Roy, K., and Price, B.D. (2007). DNA Damage-Induced Acetylation of Lysine 3016 of ATM Activates ATM Kinase Activity. *Molecular and Cellular Biology* 27, 8502-8509.
- Sztalryd, C., Xu, G., Dorward, H., Tansey, J.T., Contreras, J.A., Kimmel, A.R., and Londos, C. (2003). Perilipin A is essential for the translocation of hormone-sensitive lipase during lipolytic activation. *The Journal of Cell Biology* 161, 1093-1103.
- Taccioli, G.E., Amatuucci, A.G., Beamish, H.J., Gell, D., Xiang, X.H., Arzayus, M.I.T., Priestley, A., Jackson, S.P., Rothstein, A.M., Jeggo, P.A., *et al.* (1998). Targeted Disruption of the Catalytic Subunit of the DNA-PK Gene in Mice Confers Severe Combined Immunodeficiency and Radiosensitivity. *Immunity* 9, 355-366.
- Takai, H., Wang, R.C., Takai, K.K., Yang, H., and de Lange, T. (2007). Tel2 Regulates the Stability of PI3K-Related Protein Kinases. *Cell* 131, 1248-1259.
- Takenouchi, T., Takayama, Y., and Takezawa, T. (2004). Co-treatment with dexamethasone and octanoate induces adipogenesis in 3T3-L1 cells. *Cell Biology International* 28, 209-216.
- Takizawa, T., Tatematsu, C., Watanabe, K., Kato, K., and Nakanishi, Y. (2004). Cleavage of Calnexin Caused by Apoptotic Stimuli: Implication for the Regulation of Apoptosis. *The Journal of Biochemistry* 136, 399-405.
- Tanaka, A., Weinell, S., Nagy, N., O'Driscoll, M., Lai-Cheong, Joey E., Kulp-Shorten, Carol L., Knable, A., Carpenter, G., Fisher, Sheila A., Hiragun, M., *et al.* (2012). Germline Mutation in ATR in Autosomal-Dominant Oropharyngeal Cancer Syndrome. *American Journal of Human Genetics* 90, 511-517.
- Tang, Q.-Q., Grønborg, M., Huang, H., Kim, J.-W., Otto, T.C., Pandey, A., and Lane, M.D. (2005). Sequential phosphorylation of CCAAT enhancer-binding protein β by MAPK and glycogen synthase

kinase 3β is required for adipogenesis. *Proceedings of the National Academy of Sciences of the United States of America* *102*, 9766-9771.

Tang, Q.-Q., Otto, T.C., and Lane, M.D. (2003). Mitotic clonal expansion: A synchronous process required for adipogenesis. *Proceedings of the National Academy of Sciences* *100*, 44-49.

Tang, Q.Q., and Lane, M.D. (2012). Adipogenesis: From Stem Cell to Adipocyte. *Annual Review of Biochemistry* *81*, 715-736.

Tang, Y., Qian, S.-W., Wu, M.-Y., Wang, J., Lu, P., Li, X., Huang, H.-Y., Guo, L., Sun, X., Xu, C.-J., *et al.* (2016). BMP4 mediates the interplay between adipogenesis and angiogenesis during expansion of subcutaneous white adipose tissue. *Journal of Molecular Cell Biology* *8*, 302-312.

Tarnopolsky, M.A., Rennie, C.D., Robertshaw, H.A., Fedak-Tarnopolsky, S.N., Devries, M.C., and Hamadeh, M.J. (2007). Influence of endurance exercise training and sex on intramyocellular lipid and mitochondrial ultrastructure, substrate use, and mitochondrial enzyme activity. *American Journal of Physiology - Regulatory, Integrative and Comparative Physiology* *292*, R1271-R1278.

Tauchi-Sato, K., Ozeki, S., Houjou, T., Taguchi, R., and Fujimoto, T. (2002). The Surface of Lipid Droplets Is a Phospholipid Monolayer with a Unique Fatty Acid Composition. *Journal of Biological Chemistry* *277*, 44507-44512.

Taylor, A.M.R., Groom, A., and Byrd, P.J. (2004). Ataxia-telangiectasia-like disorder (ATLD)—its clinical presentation and molecular basis. *DNA Repair* *3*, 1219-1225.

Taylor, A.M.R., Lam, Z., Last, J.I., and Byrd, P.J. (2015). Ataxia telangiectasia: more variation at clinical and cellular levels. *Clinical Genetics* *87*, 199-208.

Tchkonia, T., Morbeck, D.E., Von Zglinicki, T., Van Deursen, J., Lustgarten, J., Scrable, H., Khosla, S., Jensen, M.D., and Kirkland, J.L. (2010). Fat tissue, aging, and cellular senescence. *Aging Cell* *9*, 667-684.

Thorpe, J.A., and Schwarze, S.R. (2010). IRE1 α controls cyclin A1 expression and promotes cell proliferation through XBP-1. *Cell Stress & Chaperones* *15*, 497-508.

Thumm, M., Egner, R., Koch, B., Schlumpberger, M., Straub, M., Veenhuis, M., and Wolf, D.H. (1994). Isolation of autophagocytosis mutants of *Saccharomyces cerevisiae*. *FEBS Letters* *349*, 275-280.

- Tivey, H.S.E., Rokicki, M.J., Barnacle, J.R., Rogers, M.J., Bagley, M.C., Kipling, D., and Davis, T. (2013). Small Molecule Inhibition of p38 MAP Kinase Extends the Replicative Life Span of Human ATR-Seckel Syndrome Fibroblasts. *The Journals of Gerontology Series A: Biological Sciences and Medical Sciences* 68, 1001-1009.
- Toledo, L.I., Murga, M., Zur, R., Soria, R., Rodriguez, A., Martinez, S., Oyarzabal, J., Pastor, J., Bischoff, J.R., and Fernandez-Capetillo, O. (2011). A cell-based screen identifies ATR inhibitors with synthetic lethal properties for cancer-associated mutations. *Nat Struct Mol Biol* 18, 721-727.
- Tontonoz, P., Hu, E., Graves, R.A., Budavari, A.I., and Spiegelman, B.M. (1994). mPPAR gamma 2: tissue-specific regulator of an adipocyte enhancer. *Genes & Development* 8, 1224-1234.
- Trenz, K., Errico, A., and Costanzo, V. (2008). Plx1 is required for chromosomal DNA replication under stressful conditions. *The EMBO journal* 27, 876-885.
- Trinh, A.T., Kim, S.H., Chang, H.-y., Mastrocola, A.S., and Tibbetts, R.S. (2013). Cyclin-dependent Kinase 1-dependent Phosphorylation of cAMP Response Element-binding Protein Decreases Chromatin Occupancy. *Journal of Biological Chemistry* 288, 23765-23775.
- Tsoli, M., Moore, M., Burg, D., Painter, A., Taylor, R., Lockie, S.H., Turner, N., Warren, A., Cooney, G., Oldfield, B., *et al.* (2012). Activation of Thermogenesis in Brown Adipose Tissue and Dysregulated Lipid Metabolism Associated with Cancer Cachexia in Mice. *Cancer Research* 72, 4372-4382.
- Tsukada, M., and Ohsumi, Y. (1993). Isolation and characterization of autophagy-defective mutants of *Saccharomyces cerevisiae*. *FEBS Letters* 333, 169-174.
- Tsukiyama-Kohara, K., Poulin, F., Kohara, M., DeMaria, C.T., Cheng, A., Wu, Z., Gingras, A.-C., Katsume, A., Elchebly, M., Spiegelman, B.M., *et al.* (2001). Adipose tissue reduction in mice lacking the translational inhibitor 4E-BP1. *Nat Med* 7, 1128-1132.
- Tyner, S.D., Venkatachalam, S., Choi, J., Jones, S., Ghebranious, N., Igelmann, H., Lu, X., Soron, G., Cooper, B., Brayton, C., *et al.* (2002). p53 mutant mice that display early ageing-associated phenotypes. *Nature* 415, 45-53.
- Ünsal-Kaçmaz, K., Makhov, A.M., Griffith, J.D., and Sancar, A. (2002). Preferential binding of ATR protein to UV-damaged DNA. *Proceedings of the National Academy of Sciences of the United States of America* 99, 6673-6678.

Urano, F., Wang, X., Bertolotti, A., Zhang, Y., Chung, P., Harding, H.P., and Ron, D. (2000). Coupling of Stress in the ER to Activation of JNK Protein Kinases by Transmembrane Protein Kinase IRE1. *Science* 287, 664-666.

Vail, G., Cheng, A., Han, Y.R., Zhao, T., Du, S., Loy, M.M.T., Herrup, K., and Plummer, M.R. (2016). ATM protein is located on presynaptic vesicles and its deficit leads to failures in synaptic plasticity. *Journal of Neurophysiology* 116, 201-209.

Valdés-Sánchez, L., De la Cerda, B., Diaz-Corrales, F.J., Massalini, S., Chakarova, C.F., Wright, A.F., and Bhattacharya, S.S. (2013). ATR localizes to the photoreceptor connecting cilium and deficiency leads to severe photoreceptor degeneration in mice. *Human Molecular Genetics* 22, 1507-1515.

Van Petegem, F. (2012). Ryanodine Receptors: Structure and Function. *Journal of Biological Chemistry* 287, 31624-31632.

Vandermoere, F., El Yazidi-Belkoura, I., Slomianny, C., Demont, Y., Bidaux, G., Adriaenssens, E., Lemoine, J., and Hondemarck, H. (2006). The Valosin-containing Protein (VCP) Is a Target of Akt Signaling Required for Cell Survival. *Journal of Biological Chemistry* 281, 14307-14313.

Vávrová, J., Zárbynická, L., Lukášová, E., Řezáčová, M., Novotná, E., Šinkorová, Z., Tichý, A., Pejchal, J., and Ďurišová, K. (2013). Inhibition of ATR kinase with the selective inhibitor VE-821 results in radiosensitization of cells of promyelocytic leukaemia (HL-60). *Radiation and Environmental Biophysics* 52, 471-479.

Vaz, B., Halder, S., and Ramadan, K. (2013). Role of p97/VCP (Cdc48) in genome stability. *Frontiers in Genetics* 4, 60.

Vendetti, F.P., Lau, A., Schamus, S., Conrads, T.P., O'Connor, M.J., and Bakkenist, C.J. (2015). The orally active and bioavailable ATR kinase inhibitor AZD6738 potentiates the anti-tumor effects of cisplatin to resolve ATM-deficient non-small cell lung cancer in vivo. *Oncotarget* 6, 44289-44305.

Vignard, J., Mirey, G., and Salles, B. (2013). Ionizing-radiation induced DNA double-strand breaks: A direct and indirect lighting up. *Radiotherapy and Oncology* 108, 362-369.

von Haehling, S., and Anker, S.D. (2014). Prevalence, incidence and clinical impact of cachexia: facts and numbers—update 2014. *Journal of Cachexia, Sarcopenia and Muscle* 5, 261-263.

Walker, J.R., Corpina, R.A., and Goldberg, J. (2001). Structure of the Ku heterodimer bound to DNA and its implications for double-strand break repair. *Nature* 412, 607-614.

- Walther, T.C., and Farese, R.V. (2012). Lipid Droplets And Cellular Lipid Metabolism. *Annual review of biochemistry* *81*, 687-714.
- Wang, C., Huang, Z., Du, Y., Cheng, Y., Chen, S., and Guo, F. (2010). ATF4 regulates lipid metabolism and thermogenesis. *Cell Res* *20*, 174-184.
- Wang, G.-X., Zhao, X.-Y., and Lin, J.D. (2015). The brown fat secretome: metabolic functions beyond thermogenesis. *Trends in Endocrinology & Metabolism* *26*, 231-237.
- Wang, T., Ming, Z., Xiaochun, W., and Hong, W. (2011). Rab7: Role of its protein interaction cascades in endo-lysosomal traffic. *Cellular Signalling* *23*, 516-521.
- Wang, W. (2007). Emergence of a DNA-damage response network consisting of Fanconi anaemia and BRCA proteins. *Nat Rev Genet* *8*, 735-748.
- Wang, W., and Seale, P. (2016). Control of brown and beige fat development. *Nat Rev Mol Cell Biol* *17*, 691-702.
- Wang, X., and Ron, D. (1996). Stress-induced phosphorylation and activation of the transcription factor CHOP (GADD153) by p38 MAP kinase. *Science* *272*, 1347-1349.
- Wang, X., Zou, L., Lu, T., Bao, S., Hurov, K.E., Hittelman, W.N., Elledge, S.J., and Li, L. (2006). Rad17 Phosphorylation Is Required for Claspin Recruitment and Chk1 Activation in Response to Replication Stress. *Molecular Cell* *23*, 331-341.
- Wang, Y., Shen, J., Arenzana, N., Tirasophon, W., Kaufman, R.J., and Prywes, R. (2000). Activation of ATF6 and an ATF6 DNA binding site by the ER stress response. *Journal of Biological Chemistry*.
- Warburg, O. (1956). On the Origin of Cancer Cells. *Science* *123*, 309-314.
- Waters, A.M., and Beales, P.L. (2011). Ciliopathies: an expanding disease spectrum. *Pediatric Nephrology (Berlin, Germany)* *26*, 1039-1056.
- Wei, F., Yan, J., and Tang, D. (2011). Extracellular Signal-Regulated Kinases Modulate DNA Damage Response - A Contributing Factor to Using MEK Inhibitors in Cancer Therapy. *Current Medicinal Chemistry* *18*, 5476-5482.

Wei, M.C., Zong, W.-X., Cheng, E.H.-Y., Lindsten, T., Panoutsakopoulou, V., Ross, A.J., Roth, K.A., MacGregor, G.R., Thompson, C.B., and Korsmeyer, S.J. (2001). Proapoptotic BAX and BAK: a requisite gateway to mitochondrial dysfunction and death. *Science* 292, 727-730.

Wei, Y., Pattingre, S., Sinha, S., Bassik, M., and Levine, B. (2008). JNK1-Mediated Phosphorylation of Bcl-2 Regulates Starvation-Induced Autophagy. *Molecular Cell* 30, 678-688.

Welihinda, A.A., and Kaufman, R.J. (1996). The Unfolded Protein Response Pathway in *Saccharomyces cerevisiae*: OLIGOMERIZATION AND TRANS-PHOSPHORYLATION OF Ire1p (Ern1p) ARE REQUIRED FOR KINASE ACTIVATION. *Journal of Biological Chemistry* 271, 18181-18187.

Welte, Michael A. (2015). Expanding Roles for Lipid Droplets. *Current Biology* 25, R470-R481.

Westermann, B. (2012). Bioenergetic role of mitochondrial fusion and fission. *Biochimica et Biophysica Acta (BBA) - Bioenergetics* 1817, 1833-1838.

Westphal, D., Dewson, G., Czabotar, P.E., and Kluck, R.M. (2011). Molecular biology of Bax and Bak activation and action. *Biochimica et Biophysica Acta (BBA) - Molecular Cell Research* 1813, 521-531.

White, E. (2015). The role for autophagy in cancer. *The Journal of Clinical Investigation* 125, 42-46.

Williams, D.B. (2006). Beyond lectins: the calnexin/calreticulin chaperone system of the endoplasmic reticulum. *Journal of Cell Science* 119, 615-623.

Williams, R.A.M., Smith, T.K., Cull, B., Mottram, J.C., and Coombs, G.H. (2012). ATG5 Is Essential for ATG8-Dependent Autophagy and Mitochondrial Homeostasis in *Leishmania major*. *PLoS Pathogens* 8, e1002695.

Willis, S.N., Chen, L., Dewson, G., Wei, A., Naik, E., Fletcher, J.I., Adams, J.M., and Huang, D.C. (2005). Proapoptotic Bak is sequestered by Mcl-1 and Bcl-xL, but not Bcl-2, until displaced by BH3-only proteins. *Genes & development* 19, 1294-1305.

Wójcik, C., Rowicka, M., Kudlicki, A., Nowis, D., McConnell, E., Kujawa, M., and DeMartino, G.N. (2006). Valosin-containing Protein (p97) Is a Regulator of Endoplasmic Reticulum Stress and of the Degradation of N-End Rule and Ubiquitin-Fusion Degradation Pathway Substrates in Mammalian Cells. *Molecular Biology of the Cell* 17, 4606-4618.

Wold, M.S. (1997). Replication protein A: a heterotrimeric, single-stranded DNA-binding protein required for eukaryotic DNA metabolism. *Annual review of biochemistry* 66, 61-92.

Wong, P.-M., Puente, C., Ganley, I.G., and Jiang, X. (2013). The ULK1 complex. *Autophagy* 9, 124-137.

Worman, H.J., and Bonne, G. (2007). "Laminopathies:" a wide spectrum of human diseases. *Experimental cell research* 313, 2121-2133.

Wright, D.C., Geiger, P.C., Han, D.-H., Jones, T.E., and Holloszy, J.O. (2007). Calcium Induces Increases in Peroxisome Proliferator-activated Receptor γ Coactivator-1 α and Mitochondrial Biogenesis by a Pathway Leading to p38 Mitogen-activated Protein Kinase Activation. *Journal of Biological Chemistry* 282, 18793-18799.

Wu, J., Boström, P., Sparks, Lauren M., Ye, L., Choi, Jang H., Giang, A.-H., Khandekar, M., Virtanen, Kirsi A., Nuutila, P., Schaart, G., *et al.* (2012). Beige Adipocytes Are a Distinct Type of Thermogenic Fat Cell in Mouse and Human. *Cell* 150, 366-376.

Xie, Z., and Klionsky, D.J. (2007). Autophagosome formation: core machinery and adaptations. *Nat Cell Biol* 9, 1102-1109.

Xu, N., Hegarat, N., Black, E.J., Scott, M.T., Hochegger, H., and Gillespie, D.A. (2010). Akt/PKB suppresses DNA damage processing and checkpoint activation in late G2. *The Journal of Cell Biology* 190, 297-305.

Xu, N., Lao, Y., Zhang, Y., and Gillespie, D.A. (2012). Akt: A Double-Edged Sword in Cell Proliferation and Genome Stability. *Journal of Oncology* 2012, 951724.

Yamamoto, H., Kakuta, S., Watanabe, T.M., Kitamura, A., Sekito, T., Kondo-Kakuta, C., Ichikawa, R., Kinjo, M., and Ohsumi, Y. (2012). Atg9 vesicles are an important membrane source during early steps of autophagosome formation. *The Journal of Cell Biology* 198, 219-233.

Yan, W., Frank, C.L., Korth, M.J., Sopher, B.L., Novoa, I., Ron, D., and Katze, M.G. (2002). Control of PERK eIF2 α kinase activity by the endoplasmic reticulum stress-induced molecular chaperone P58(IPK). *Proceedings of the National Academy of Sciences of the United States of America* 99, 15920-15925.

Yang, D.-Q., Halaby, M.-J., Li, Y., Hibma, J.C., and Burn, P. (2011a). Cytoplasmic ATM protein kinase: an emerging therapeutic target for diabetes, cancer and neuronal degeneration. *Drug Discovery Today* 16, 332-338.

Yang, D.-Q., and Kastan, M.B. (2000a). Participation of ATM in insulin signalling through phosphorylation of eIF-4E-binding protein 1. *Nat Cell Biol* 2, 893-898.

- Yang, D.Q., and Kastan, M.B. (2000b). Participation of ATM in insulin signalling through phosphorylation of eIF-4E-binding protein 1. *Nature Cell Biology* 2, 893-898.
- Yang, T.T.C., Xiong, Q., Enslen, H., Davis, R.J., and Chow, C.W. (2002). Phosphorylation of NFATc4 by p38 mitogen-activated protein kinases. *Molecular and Cellular Biology* 22, 3892-3904.
- Yang, Z.J., Chee, C.E., Huang, S., and Sinicrope, F.A. (2011b). The Role of Autophagy in Cancer: Therapeutic Implications. *Molecular cancer therapeutics* 10, 1533-1541.
- Ye, Y., Shibata, Y., Kikkert, M., van Voorden, S., Wiertz, E., and Rapoport, T.A. (2005). Recruitment of the p97 ATPase and ubiquitin ligases to the site of retrotranslocation at the endoplasmic reticulum membrane. *Proceedings of the National Academy of Sciences of the United States of America* 102, 14132-14138.
- Yeh, W.C., Bierer, B.E., and McKnight, S.L. (1995). Rapamycin inhibits clonal expansion and adipogenic differentiation of 3T3-L1 cells. *Proceedings of the National Academy of Sciences of the United States of America* 92, 11086-11090.
- Yen, W.-L., Legakis, J.E., Nair, U., and Klionsky, D.J. (2007). Atg27 Is Required for Autophagy-dependent Cycling of Atg9. *Molecular Biology of the Cell* 18, 581-593.
- Yi, C., Tong, J., Lu, P., Wang, Y., Zhang, J., Sun, C., Yuan, K., Xue, R., Zou, B., Li, N., *et al.* (2017). Formation of a Snf1-Mec1-Atg1 Module on Mitochondria Governs Energy Deprivation-Induced Autophagy by Regulating Mitochondrial Respiration. *Developmental Cell* 41, 59-71.e54.
- Yoo, H.Y., Kumagai, A., Shevchenko, A., Shevchenko, A., and Dunphy, W.G. (2007). Ataxia-telangiectasia Mutated (ATM)-dependent Activation of ATR Occurs through Phosphorylation of TopBP1 by ATM. *Journal of Biological Chemistry* 282, 17501-17506.
- Yoo, H.Y., Shevchenko, A., Shevchenko, A., and Dunphy, W.G. (2004). Mcm2 is a direct substrate of ATM and ATR during DNA damage and DNA replication checkpoint responses. *Journal of Biological Chemistry* 279, 53353-53364.
- Yoon, M.-S., Zhang, C., Sun, Y., Schoenherr, C.J., and Chen, J. (2013a). Mechanistic target of rapamycin controls homeostasis of adipogenesis. *Journal of Lipid Research* 54, 2166-2173.
- Yoon, M.S., Zhang, C., Sun, Y., Schoenherr, C.J., and Chen, J. (2013b). Mechanistic target of rapamycin controls homeostasis of adipogenesis. *Journal of Lipid Research* 54, 2166-2173.

- Yoshimura, S.H., and Hirano, T. (2016). HEAT repeats – versatile arrays of amphiphilic helices working in crowded environments? *Journal of Cell Science* 129, 3963-3970.
- You, Z., Chahwan, C., Bailis, J., Hunter, T., and Russell, P. (2005). ATM Activation and Its Recruitment to Damaged DNA Require Binding to the C Terminus of Nbs1. *Molecular and Cellular Biology* 25, 5363-5379.
- Youle, R.J., and Strasser, A. (2008). The BCL-2 protein family: opposing activities that mediate cell death. *Nature reviews Molecular cell biology* 9, 47-59.
- Yu, J.S.L., and Cui, W. (2016). Proliferation, survival and metabolism: the role of PI3K/AKT/mTOR signalling in pluripotency and cell fate determination. *Development* 143, 3050-3060.
- Yu, K., Mo, D., Wu, M., Chen, H., Chen, L., Li, M., and Chen, Y. (2014). Activating transcription factor 4 regulates adipocyte differentiation via altering the coordinate expression of CCATT/enhancer binding protein β and peroxisome proliferator-activated receptor γ . *FEBS Journal* 281, 2399-2409.
- Yue, S., Li, J., Lee, S.-Y., Lee, Hyeon J., Shao, T., Song, B., Cheng, L., Masterson, Timothy A., Liu, X., Ratliff, Timothy L., *et al.* (2014). Cholesteryl Ester Accumulation Induced by PTEN Loss and PI3K/AKT Activation Underlies Human Prostate Cancer Aggressiveness. *Cell Metabolism* 19, 393-406.
- Zalckvar, E., Berissi, H., Mizrachy, L., Idelchuk, Y., Koren, I., Eisenstein, M., Sabanay, H., Pinkas-Kramarski, R., and Kimchi, A. (2009). DAP-kinase-mediated phosphorylation on the BH3 domain of beclin 1 promotes dissociation of beclin 1 from Bcl-X_L and induction of autophagy. *EMBO reports* 10, 285-292.
- Zanchetti, A., Rosei, E.A., Dal Palù, C., Leonetti, G., Magnani, B., and Pessina, A. (1998). The Verapamil in Hypertension and Atherosclerosis Study (VHAS): Results of long-term randomized treatment with either verapamil or chlorthalidone on carotid intima-media thickness. *Journal of hypertension* 16, 1667-1676.
- Zechner, R., Zimmermann, R., Eichmann, Thomas O., Kohlwein, Sepp D., Haemmerle, G., Lass, A., and Madeo, F. (2012). FAT SIGNALS - Lipases and Lipolysis in Lipid Metabolism and Signaling. *Cell Metabolism* 15, 279-291.
- Zehmer, J.K., Huang, Y., Peng, G., Pu, J., Anderson, R.G.W., and Liu, P. (2009). A role for lipid droplets in inter-membrane lipid traffic. *Proteomics* 9, 914-921.

Zha, B.S., and Zhou, H. (2012). ER Stress and Lipid Metabolism in Adipocytes. *Biochemistry Research International* 2012, 9.

Zhang, H.H., Huang, J., Düvel, K., Boback, B., Wu, S., Squillace, R.M., Wu, C.-L., and Manning, B.D. (2009a). Insulin Stimulates Adipogenesis through the Akt-TSC2-mTORC1 Pathway. *PLoS ONE* 4, e6189.

Zhang, J.-W., Klemm, D.J., Vinson, C., and Lane, M.D. (2004a). Role of CREB in Transcriptional Regulation of CCAAT/Enhancer-binding Protein β Gene during Adipogenesis. *Journal of Biological Chemistry* 279, 4471-4478.

Zhang, J., Fu, M., Cui, T., Xiong, C., Xu, K., Zhong, W., Xiao, Y., Floyd, D., Liang, J., Li, E., *et al.* (2004b). Selective disruption of PPAR γ 2 impairs the development of adipose tissue and insulin sensitivity. *Proceedings of the National Academy of Sciences of the United States of America* 101, 10703-10708.

Zhang, J., Tripathi, D.N., Jing, J., Alexander, A., Kim, J., Powell, R.T., Dere, R., Tait-Mulder, J., Lee, J.-H., Paull, T.T., *et al.* (2015). ATM functions at the peroxisome to induce pexophagy in response to ROS. *Nat Cell Biol* 17, 1259-1269.

Zhang, Y.-W., Jones, T.L., Martin, S.E., Caplen, N.J., and Pommier, Y. (2009b). Implication of Checkpoint Kinase-dependent Up-regulation of Ribonucleotide Reductase R2 in DNA Damage Response. *The Journal of Biological Chemistry* 284, 18085-18095.

Zhu, D., Shi, S., Wang, H., and Liao, K. (2009). Growth arrest induces primary-cilium formation and sensitizes IGF-1-receptor signaling during differentiation induction of 3T3-L1 preadipocytes. *Journal of Cell Science* 122, 2760-2768.

Zimmermann, R., Strauss, J.G., Haemmerle, G., Schoiswohl, G., Birner-Gruenberger, R., Riederer, M., Lass, A., Neuberger, G., Eisenhaber, F., Hermetter, A., *et al.* (2004). Fat Mobilization in Adipose Tissue Is Promoted by Adipose Triglyceride Lipase. *Science* 306, 1383-1386.

Zinkel, S.S., Hurov, K.E., Ong, C., Abtahi, F.M., Gross, A., and Korsmeyer, S.J. (2005). A Role for Proapoptotic BID in the DNA-Damage Response. *Cell* 122, 579-591.

Zoico, E., Darra, E., Rizzatti, V., Budui, S., Franceschetti, G., Mazzali, G., Rossi, A.P., Fantin, F., Menegazzi, M., Cinti, S., *et al.* (2016). Adipocytes WNT5a mediated dedifferentiation: a possible target in pancreatic cancer microenvironment. *Oncotarget* 7, 20223-20235.

Zong, W.-X., Li, C., Hatzivassiliou, G., Lindsten, T., Yu, Q.-C., Yuan, J., and Thompson, C.B. (2003). Bax and Bak can localize to the endoplasmic reticulum to initiate apoptosis. *The Journal of Cell Biology* *162*, 59-69.

Zou, L., and Elledge, S.J. (2003). Sensing DNA Damage Through ATRIP Recognition of RPA-ssDNA Complexes. *Science* *300*, 1542-1548.

Zou, Y., Liu, Y., Wu, X., and Shell, S.M. (2006). Functions of Human Replication Protein A (RPA): From DNA Replication to DNA Damage and Stress Responses. *Journal of cellular physiology* *208*, 267-273.

Zweytick, D., Athenstaedt, K., and Daum, G. (2000). Intracellular lipid particles of eukaryotic cells. *Biochimica et Biophysica Acta (BBA) - Reviews on Biomembranes* *1469*, 101-120.